Performance-based design of self-compacting fibre reinforced concrete

Performance-based design of self-compacting fibre reinforced concrete

Proefschrift

ter verkrijging van de graad van doctor
aan de Technische Universiteit Delft,
op gezag van de Rector Magnificus prof.dr.ir. J.T. Fokkema,
voorzitter van het College voor Promoties,
in het openbaar te verdedigen

op vrijdag 4 juni 2004 om 10.30 uur

door

Steffen GRÜNEWALD

Diplom-Ingenieur
(Technische Universiteit Darmstadt, Duitsland)
geboren te Rheinfelden (Duitsland).

Dit proefschrift is goedgekeurd door de promotor:

Prof.dr.ir. J.C. Walraven

Samenstelling promotiecommissie:

Rector Magnificus,	Technische Universiteit Delft, voorzitter.
Prof.dr.ir. J.C. Walraven,	Technische Universiteit Delft, promotor.
Prof.dr.ir. P.J.M. Bartos,	Universiteit van Paisley, Schotland.
Prof.dr.ir. D.A. Hordijk,	Technische Universiteit Eindhoven.
Prof.ir. G.J. Maas,	Technische Universiteit Eindhoven.
Prof.dr.ir. K. van Breugel,	Technische Universiteit Delft.
Prof.dr.ir. L. Vandewalle,	Katholieke Universiteit Leuven, België.
Dr.ir. C. van der Veen,	Technische Universiteit Delft.
Prof.ir. L.A.G. Wagemans,	Technische Universiteit Delft, reservelid.

Published and distributed by: DUP Science

DUP Science is an imprint of
Delft University Press
P.O. Box 98
2600 MG Delft
The Netherlands
Telephone: + 31 15 2785678
Telefax: + 31 15 2785706
E-mail: info@library.tudelft.nl

ISBN: 90-407-2487-3

Keywords:
bending behaviour, mixture composition, self-compacting fibre reinforced concrete

Copyright © 2004 by S. Grünewald

All rights reserved. No part of the material protected by this copyright notice may be reproduced or utilized in any form or by any means, electronic or mechanical, including photocopying, recording or by any information storage and retrieval system, without written permission from the publisher: Delft University Press.

Printed in the Netherlands

Summary

Performance-based design of self-compacting fibre reinforced concrete

The development of self-compacting concrete (SCC) marks an important milestone in improving the product quality and efficiency of the building industry. SCC homogenously spreads due to its own weight, without any additional compaction energy and does not entrap air. SCC improves the efficiency at the construction sites, enhances the working conditions and the quality and the appearance of concrete. Fibres bridge cracks and retard their propagation. They contribute to an increased energy absorption compared with plain concrete. Self-compacting fibre reinforced concrete (SCFRC) combines the benefits of SCC in the fresh state and shows an improved performance in the hardened state compared with conventional concrete due to the addition of the fibres. Due to its special characteristics new fields of application can be explored.

This thesis provides tools and models to optimise SCFRC in the fresh and the hardened state. Relevant literature and the experience gained during the experiments are summarised; various experimental studies were performed. The objectives of this research project were to optimise SCFRC in the fresh and the hardened state and to model the behaviour in order to provide reliable design tools; mainly steel fibres were applied. SCFRC can be optimised for various purposes: to apply the highest possible fibre content, to obtain the highest performance-cost ratio, to design the granular skeleton for the highest packing density or to produce with the lowest possible material costs. The effect of the production process on the characteristics of SCFRC was also studied.

To introduce into the theoretical background of SCFRC in the fresh state, selected literature on SCC, especially with regard to the packing density and the effects of the fibres on workability is reviewed. Test methods are described; previous experience with SCC and fibre reinforced concrete (FRC) in the fresh state and approaches to model the behaviour are summarised.

The packing density of the aggregates and the fibres of SCFRC determine the amount of cement paste that is required to fill the interstices of the granular skeleton. In order to predict the packing density of the granular skeleton, the 'Compressible Packing Model' was used and calibrated with the applied materials. Predictions from five approaches to include the steel fibres were compared with results of experiments to obtain the best accuracy. The accuracy of the predictions depends on the composition of the aggregates. The simulations had an average error close to 2% for optimised mixtures with aggregates up to 8 or 16 mm; predictions of the packing density of mixtures with smaller maximum aggregate sizes were less accurate.

Sixteen stable SCCs at defined characteristics in the fresh state were used to study the effect of the type and the content of the steel fibres; in total 121 mixtures were tested.

The maximum aggregate size of the reference mixtures was 4, 8 or 16 mm; the volumes of the paste as well as the sand to total aggregate contents were varied. The fibres affect the characteristics of SCC in the fresh state: the slump flow decreases and the yield value, the plastic viscosity (the resistance to flow) and the bar spacing required to avoid blocking increase compared with a reference SCC. For each reference mixture and the applied fibre type the maximum fibre content was determined. Due to the higher density of the steel fibres, segregation might occur even when the aggregates are homogenously distributed. Based on experimental results, models were developed, which quantify the effect of the steel fibres and with which key characteristics of SCFRC in the fresh state can be predicted. Criteria are proposed to design and to characterise SCFRC; basic principles to optimise SCFRC are described.

SCFRC was also tested in the hardened state. A summary of the literature discusses mechanical characteristics of conventional and self-compacting concrete reinforced with steel fibres and the effect of the orientation and the distribution of the fibres.

Bending tests were performed on seventeen optimised mixtures, which were selected from the studies on the characteristics in the fresh state. The mixtures differed in the compressive strength class, the type and the content of the steel fibres and the manner of manufacturing of the specimens. The variation of the maximum flexural strength was in each case below 12%, which is significantly lower with what is usually obtained for steel fibre reinforced concrete (SFRC). The comparison of the bending behaviour of SCFRC and SFRC indicated significant differences concerning the performance and the variation in the test response: SCFRC performed much better. Two additional studies were performed to determine the origin of the differences. First, the orientation numbers of fibres of the cross-sections of the beams were determined by an image analysis. The fibres in SCFRC were found to be more favourably aligned into the direction of the flow. Second, a comparison between the pull-out behaviour of single fibres from SCC and conventional concrete showed that in most cases higher pull-out forces were obtained with SCC. The single fibre pull-out test might give a better indication of the actual performance of a fibre in SCC than in conventional concrete. Entrapped air and neighbouring fibres affect the performance of a fibre in SFRC more than in SCFRC.

By applying the multi-layer procedure of Hordijk an inverse analysis of the bending tests was performed. Based on the experimental results of the bending tests a combined stress-strain/stress-crack width model for SCFRC in tension was developed. The model was calibrated with results from fifteen mixtures, which contained hooked-end steel fibres. The proposed stress-strain/stress-crack width model distinguishes three tensile regions: the elastic and the reduced elastic strain ranges and a softening branch. The difference between results of simulations with the combined tensile model and experimental results is in average below 8%.

Three full-scale applications with SCFRC are discussed: sheet piles, tunnel segments and large beams. The focus of these studies was on the orientation and the distribution of the steel fibres. Different techniques were applied to quantify 'orientation'. SCFRC was found to be an inhomogeneous material; the fibres are rarely randomly oriented. The preferred orientation of the fibres can be considered as a benefit or, the opposite as

an intrinsic weakness of SCFRC. The studies on sheet piles and tunnel segments demonstrated that applications with SCFRC can be economical, offer products with interesting characteristics and present innovative solutions. The production process is an important factor, which affects the performance of SCFRC.

Steffen Grünewald, Delft University of Technology

Samenvatting

Prestatie-gericht ontwerpen van zelfverdichtend vezelbeton

De ontwikkeling van zelfverdichtend beton (ZVB) is een belangrijke stap om de productkwaliteit en de effectiviteit van de bouwindustrie te verbeteren. ZVB vloeit homogeen door zijn eigen gewicht zonder toevoeging van verdichtingsenergie en sluit daarbij geen lucht in. ZVB verhoogt de effectiviteit op de bouwplaats, verbetert de arbeidsomstandigheden, de kwaliteit en het uiterlijk van het beton. Vezels overbruggen scheuren en vertragen de scheurgroei. In vergelijking met conventioneel beton verhogen ze de breukenergie. Zelfverdichtend vezelbeton (ZVVB) combineert de voordelen van ZVB in de vloeibare fase en geeft een betere kwaliteit in de verharde toestand omdat het vezels bevat. Door de bijzondere eigenschappen kunnen nieuwe toepassingen ontwikkeld worden.

Dit proefschrift biedt hulpmiddelen en modellen om ZVVB in de vloeibare en de verharde toestand te optimaliseren. Relevante literatuur en ervaringen die gedurende de experimenten zijn opgedaan zijn samengevat; verscheidene experimentele studies zijn uitgevoerd. De doelstellingen van dit onderzoeksproject waren het optimaliseren van ZVVB in de vloeibare en de verharde fase en het modelleren van het gedrag om betrouwbare hulpmiddelen voor het ontwerpen ervan te ontwikkelen. In hoofdzaak zijn staalvezels toegepast. ZVVB kan voor verschillende doeleinden geoptimaliseerd worden: het hoogst mogelijke vezelgehalte, de hoogste prestatie-kosten verhouding, het ontwerpen van het korrelskelet voor de hoogste pakking of het met zo laag mogelijk materiaalkosten produceren. De invloed van het productieproces op de eigenschappen van ZVVB werd ook onderzocht.

Om een overzicht van de theoretische achtergrond van ZVVB in de vloeibare fase te geven is literatuur geselecteerd op het gebied van ZVB, in het bijzonder met betrekking tot de pakking en de invloed van vezels op de verwerkbaarheid. Testmethodes zijn beschreven en voorafgaande ervaringen met ZVB en vezelversterkt beton (VVB) in de vloeibare fase en modellen om het gedrag te voorspellen, zijn samengevat.

De pakking van de toeslag en de vezels in ZVVB bepaalt de hoeveelheid cementlijm die nodig is om de holle ruimte van het korrelskelet op te vullen. Om de pakking te voorspellen is het 'Compressible Packing Model' toegepast en met de gebruikte materialen gekalibreerd. Om de grootst mogelijke nauwkeurigheid te verkrijgen zijn de uitkomsten van vijf methodes, om de staalvezels in de simulaties mee te nemen, met resultaten van experimenten vergeleken. De nauwkeurigheid van de voorspellingen hangt van de samenstelling van de toeslag af. De voorspellingen voor geoptimaliseerde mengsels hadden een gemiddelde afwijking van ongeveer 2% bij een maximale diameter van de toeslag van 8 of 16 mm. Voorspellingen van de pakking van mengsels met een kleinere maximale korreldiameter waren minder nauwkeurig.

Zestien stabiele ZVB mengsels met gedefinieerde eigenschappen in de vloeibare fase zijn op de invloed van het type en de hoeveelheid staalvezels onderzocht; in totaal zijn

121 mengsels beproefd. De maximale diameters van de toeslag van de referentie mengsels waren 4, 8 of 16 mm; de volumes cementlijm en zand van het totale gehalte aan toeslag werden gevarieerd. De vezels beïnvloeden de eigenschappen van ZVB in de vloeibare fase: de vloeimaat wordt kleiner, de afschuifspanning, de plastische viscositeit (de weerstand tegen het vloeien) en de wapeningsafstand vereist om het blokkeren te vermijden worden groter in vergelijking met een referentie ZVB. Het maximale vezelgehalte werd bepaald voor ieder referentiemengsel en type vezel. Vanwege de hogere volumieke massa van de staalvezels kan ontmenging optreden ook al is de toeslag homogeen verdeeld. Op basis van experimentele resultaten zijn modellen ontwikkeld die het effect van de vezels kwantificeren en waarmee de belangrijkste karakteristieken van ZVVB in de vloeibare fase voorspeld kunnen worden. Eisen zijn geformuleerd om ZVVB te ontwerpen en te karakteriseren; de voorwaarden voor het kunnen optimaliseren zijn beschreven.

ZVVB werd ook in de verharde toestand beproefd. Een samenvatting van de literatuur beschrijft mechanische eigenschappen van conventioneel en zelfverdichtend beton gewapend met staalvezels en het effect van de oriëntatie en de verdeling van de vezels.

Buigproeven zijn uitgevoerd op zeventien geoptimaliseerde mengsels die uit de studies naar eigenschappen in de vloeibare fase gekozen zijn. De verschillen tussen deze mengsels waren de sterkteklasse, het type en de hoeveelheid staalvezels en de manier van het storten van de proefstukken. De variatie in de maximale buigtreksterkte was kleiner dan 12%, wat duidelijk lager is dan hetgeen voor staalvezelversterkt beton (SVB) gevonden wordt. De vergelijking van het buiggedrag van ZVVB en SVB liet duidelijke verschillen met betrekking tot de prestatie en de variatie in het testresultaat zien: ZVVB presteerde veel beter. Twee aanvullende studies werden verricht om de oorsprong van de verschillen te achterhalen. Ten eerste zijn de oriëntatiegetallen van vezels in de dwarsdoorsneden van de balkjes bepaald door middel van beeldanalyse. De vezels in ZVVB waren meer in de stroomrichting georiënteerd. Ten tweede liet een vergelijking van het uittrekgedrag van enkele vezels uit ZVB en conventioneel beton zien dat in de meeste gevallen hogere uittrekkrachten voor ZVB behaald werden. De uittrekproef met een enkele vezel geeft misschien een betere indruk van het werkelijke gedrag van een vezel in ZVB dan in conventioneel beton. Ingesloten lucht en nabij gelegen vezels beïnvloeden namelijk het gedrag van een enkele vezel in SVB meer dan in ZVVB.

Een inverse analyse van de balkproefjes is uitgevoerd met de 'multi-layer procedure' van Hordijk. Op basis van de experimentele resultaten van de buigproeven is een gecombineerd spanning-rek/spanning-scheuropening model voor ZVVB onder trek ontwikkeld. Het model is gekalibreerd met resultaten van vijftien mengsels waaraan staalvezels met eindhaakjes toegevoegd zijn. Het voorgestelde spanning-rek/spanning-scheuropening model maakt onderscheid tussen drie verschillende trekgebieden: de elastische en de gereduceerd elastische rek gebieden en een dalende tak. Het verschil tussen de resultaten van simulaties met het gecombineerde model en experimentele resultaten is gemiddeld kleiner dan 8%.

Drie toepassingen met ZVVB zijn besproken: damwanden, tunnelsegmenten en grote balken. In deze studies lag de nadruk op onderzoek naar de oriëntatie en de verdeling van de staalvezels. Verschillende methodes zijn toegepast om de oriëntatie te

kwantificeren. ZVVB kan als een inhomogeen materiaal beschouwd worden; de vezels zijn zelden in alle richtingen gelijk georiënteerd. De voorkeursoriëntatie van de vezels kan een voordeel zijn, maar kan ook als minpunt van ZVVB gezien worden. De studies op damwanden en tunnelsegmenten toonden aan dat toepassingen met ZVVB economisch kunnen zijn, producten met interessante eigenschappen mogelijk maken en innovatieve oplossingen kunnen zijn. Het productieproces is een belangrijke factor die de prestatie van ZVVB beïnvloedt.

Steffen Grünewald, TU Delft

Acknowledgements

This thesis is the result of a research project carried out at the Section of Structural and Building Engineering of the Delft University of Technology. The Dutch Technology Foundation STW and the Priority Program Materials (PPM) - research program 'Cement-Based Materials' (grant number 4010 III) - funded the project.

I want to thank my supervisor Joost Walraven for initiating an interesting and innovative research project. I appreciate the opportunities I got and the space to develop both a new material and myself. Developing a new material often requires innovative approaches; with great personal interest and support Joost Walraven realised them. He contributed with valuable comments to the outcome of this research project.

An essential part of this research project was to carry out experiments, which finally allowed testing self-compacting fibre reinforced concrete in full-scale applications. This work would not have been possible without the support of my colleagues of the Concrete Structures Group and of partners from industry. I want to thank Albert Bosman for his expert execution of the bending tests, Galia Pelova and Takehiko Midorikawa for interesting discussions, René v.d. Baars, Ton Blom, Erik Horeweg and Ron Mulder for their help and ideas about carrying out tests on SCFRC, Theo Steijn for preparing excellent drawings. Thanks also to Wim Jansze, Martin Langbroek, Dirk Nemegeer, Bas Obladen and Willem Zegwaard for their interest, support and effort to realise applications with SCFRC. The members of the STW/PPM committee contributed with valuable remarks and ideas to obtain the final result of this research project as presented here. The discussions with René Braam, Joop Den Uijl, Alain Kooiman, Eleni Lappa, Ivan Markovic, Petra Schumacher and Cor van der Veen contributed to the direction and the results of this project. I also want to thank Dirk Maroske, Bas Obladen and my colleagues of the Concrete Structures Group for reading preliminary versions of this thesis.

Besides work I had a good time with roommates and colleagues from the Concrete Structures Group, who shared with me their views and enjoyed our 'stortborrels'. Doing research in the Netherlands was an interesting opportunity and experience. I want to thank my parents, family and friends for the support they provided. Doing a PhD is not solely a thing of business; everyone who supported me contributed to the outcome of this work.

Steffen Grünewald

Table of contents

Chapter 1:
Introduction
1.1 Scope of the research……...1
1.2 Research objective……...2
1.3 Research strategy……2
1.4 Outline of the thesis……3

Part I: SCFRC in the fresh state

Chapter 2: SCC as a suspension
2.1 Introduction…… 5
2.2 Characterisation of SCC……5
2.2.1 Segregation resistance……6
2.2.2 Filling ability……6
2.2.3 Passing ability……6
2.3 Rheology as a tool to characterise SCC……6
2.3.1 Introduction to Rheology……6
2.3.2 Rheology of SCC…… 8
2.4 Design methods for SCC…… 9
2.4.1 Japanese design method……10
2.4.2 Risk of blocking (CBI-method)……10
2.5 Modelling the behaviour of SCC in the fresh state……12
2.5.1 Layer models……12
2.5.2 Packing model……15
2.6 Concluding remarks……16

Chapter 3: Effect of fibres on the behaviour of concrete in the fresh state
3.1 Introduction……19
3.2 Characteristics of the fibres……19
3.3 Conventional concrete and fibres……20
3.4 SCC and fibres……25
3.5 Concluding remarks…… 26

Chapter 4: Predicting the packing density of the granular skeleton
4.1 Introduction…… 27
4.2 Parameters affecting the packing density……27
4.3 Compressible Packing Model (CPM)……29
4.3.1 Wall-effects……30
4.3.2 Approaches to include steel fibres into the CPM……31
4.4 Experimental set-up…… 33
4.4.1 Types of steel fibres used in experiments……33
4.4.2 Applied compaction methods……34
4.5 Packing density: experimental results and predictions……35
4.5.1 Wall-effect of the steel fibres……36
4.5.2 K-index of the applied compaction method……38
4.5.3 Experimental packing density of steel fibres and aggregates…… 39
4.5.4 Five approaches to include steel fibres into the CPM…… 40
4.6 Concluding remarks…… 45

Chapter 5: Experimental parameter studies on SCFRC in the fresh state
5.1 Introduction…… 47
5.2 Methods and materials…… 47
5.2.1 Experimental program……48
5.2.2 Aggregate preparation……49
5.2.3 Mixing procedures……50
5.2.4 Evaluation methods for SCC and SCFRC……50
5.2.5 Paste characteristics……53
5.3 Design criteria for SCFRC…… 54
5.4 Test results: SCC and SCFRC in the fresh state……56
5.4.1 Characteristics of the reference SCCs…… 56
5.4.2 SCFRC – slump flow……58
5.4.3 SCFRC – yield value……59
5.4.4 SCFRC – plastic viscosity…… 60
5.4.5 SCFRC – passing ability……60
5.4.6 SCFRC – maximum fibre content…… 61
5.4.7 SCFRC – segregation resistance……62
5.5 Concluding remarks…… 63

Chapter 6: Modelling SCFRC in the fresh state: From individual components to an optimised mixture composition
6.1 Introduction…… 65
6.2 Modelling of characteristics of SCC in the fresh state…… 65
6.2.1 Characterisation of the components of SCC……65
6.2.2 Characteristics of the reference mixtures……68
6.3 Effect of the steel fibres on the characteristics of SCC…… 72
6.3.1 Effect of the fibres on the slump flow……72
6.3.2 Effect of the fibres on the yield value……75
6.3.3 Effect of the fibres on the plastic viscosity…… 77
6.3.4 Passing ability of SCFRC…… 80
6.3.5 Maximum fibre content of SCFRC……85
6.4 Examples of predictions of characteristics in the fresh state…… 88
6.5 Optimisation of SCFRC…… 89
6.6 Concluding remarks…… 90

Part II: SCFRC in the hardened state

Chapter 7: Cement-based fibre reinforced matrices in the hardened state
7.1 Introduction…… 91
7.2 Characteristics in the hardened state……92
7.2.1 Single fibre pull-out test……92
7.2.2 Tensile behaviour of SFRC……94
7.2.3 Compressive behaviour of SFRC……95
7.2.4 Bending behaviour of SFRC……96
7.2.5 Effect of the fibres on other mechanical characteristics…… 97
7.3 Orientation and distribution of the fibres…… 98
7.3.1 Orientation numbers: 1D, 2D and 3D…… 98
7.3.2 Distribution of the fibres……100
7.3.3 Influence of the production method……101
7.4 Orientation and distribution of the fibres: case studies…… 101

7.5 Concluding remarks…… 102

Chapter 8: The effect of steel fibres on characteristics of SCC in the hardened state
8.1 Introduction……..103
8.2 Three-point bending tests……... 103
8.2.1 Specimens for bending tests……104
8.2.2 Results of the bending tests……107
8.2.3 Comparing SCFRC and SFRC……...110
8.3 Fibre orientation in small beams…… 111
8.3.1 Analysis of a cross-section by image analysis……111
8.3.2 Results of the image analysis…….. 112
8.4 Single fibre pull-out tests……113
8.4.1 Experimental set-up……113
8.4.2 Results of single fibre pull-out tests……115
8.5 Concluding remarks…… 119

Chapter 9: Modelling the bending behaviour of SCFRC
9.1 Introduction…… 121
9.2 Development of a tensile model for SCFRC……121
9.2.1 Stress-crack width approach……... 122
9.2.2 Inverse modelling……123
9.2.3 Multi-layer procedure…….. 124
9.3 Model 'Kooiman' – a bilinear stress-crack width relation for SFRC……126
9.4 Modelling the bending behaviour of SCFRC…… 128
9.4.1 A combined stress-strain/stress-crack width model……... 128
9.4.2 Simulations with the combined tensile model…….. 130
9.4.3 Kooiman's model: Input parameters for SCFRC…….. 131
9.4.4 Input parameters of the combined tensile model…… 134
9.4.5 Accuracy check…… 140
9.5 Discussion of the proposed tensile model…… 141
9.6 Concluding remarks…… 144

Part III: Applications of SCFRC

Chapter 10: Case studies on SCFRC
10.1 Introduction…….. 147
10.2 Case study 1: Sheet piles……147
10.2.1 Experimental set-up……147
10.2.2 Mixture optimisation……149
10.2.3 Performance of the sheet piles……150
10.3 Case study 2: Tunnel segments…….. 151
10.3.1 Introduction……..151
10.3.2 Experimental set-up……151
10.3.3 Characteristics of the cylinders in the hardened state…….. 155
10.4 Case study 3: Large beams…… 158
10.4.1 Experimental set-up……158
10.4.2 Orientation of the fibres due to the flow…… 159
10.5 How the flow orients the fibres……161
10.6 Concluding remarks……162

Part IV: Final remarks

Chapter 11: Conclusions and future perspectives
11.1 Conclusions……..163
11.2 Future perspectives…… 165

References

Appendices: overview

Appendices

Notations and symbols

Curriculum vitae

Chapter 1:

Introduction

1.1 Scope of the research

The development of self-compacting concrete (SCC) marks a huge step towards improved efficiency and working conditions on construction sites and in the prefab-industry. A low degree of automation of the concrete industry, the shortcoming of labourers and durability problems of concrete forced Japanese researchers to think about the future; as a consequence, SCC was developed [Okamura et al., 1993]. SCC homogenously spreads due to its own weight only, without any additional compaction energy, and spreads without entrapping air. Filling ability, segregation resistance and passing ability are the key characteristics of SCC. While the worst part of the placement, i.e. vibrating the concrete, is eliminated, also other improvements are achieved, e.g. shorter casting periods, a more esthetical concrete surface appearance and improved characteristics in the hardened state. Dense reinforcement configurations, remote casting and architectural concrete are applications tailored for SCC.

Brittle cementitious materials like concrete and mortar can benefit from an addition of fibres: Fibres bridge cracks and retard their propagation. They contribute to an increased energy absorption compared with plain concrete. Fibres improve the properties of cementitious materials whenever its intrinsic brittleness limits a possible application. Steel fibres have been applied to replace bar reinforcement, to decrease the width of cracks and to improve the tensile strength or the post-cracking behaviour.

Casting concrete segments with self-compacting fibre reinforced concrete (SCFRC) facilitates the production process. The easiest way to produce a concrete element is to prepare a mould, to cast the concrete and finish it; no placement of bar reinforcement or vibration is necessary. SCFRC combines the benefits of SCC in the fresh state and shows an improved performance in the hardened state due to the addition of the fibres. The workability is improved compared with fibre reinforced concrete (FRC).

SCFRC is a tailor-made type of concrete. The fibres affect the characteristics of SCC in the fresh and the hardened state. Design tools to predict characteristics and to optimise the mixture composition of SCFRC reduce the number of 'trial and error' experiments and indicate possibilities and limits. Optimised SCFRC might be an alternative for either typical SCC- or FRC-applications; due to its special characteristics new fields of application can be explored.

1.2 Research objective

The objectives of this research project were to optimise SCFRC in the fresh and the hardened state and to model the behaviour in order to provide reliable design tools. SCFRC can be optimised for various purposes: to apply the highest possible fibre content, to obtain the highest performance-cost ratio, to design the granular skeleton for the highest packing density or to produce with the lowest possible material costs. This thesis discusses the mixture design as well as material properties and provides tools to design SCFRC mixtures for defined performance and purposes. The research was split into three parts: the fresh as well as the hardened state of SCFRC and the influence of the production process.

First, fibres are known to negatively affect workability; the effect of the fibres on the key characteristics of SCC (filling ability, segregation resistance and passing ability) had to be quantified. Consequently, the question arose whether the mixture composition of SCC has to be different in case steel fibres are added and if so, how to compose optimised SCFRC.

Second, the orientation and the distribution of the fibres might be affected by the flow and the bond behaviour of steel fibres embedded in SCC might be different compared with conventional concrete: The performance of SCFRC in the hardened state also might deviate from that of conventional steel fibre reinforced concrete (SFRC). Bending tests were carried out to quantify the effect of the steel fibres on the post-cracking behaviour of SCFRC.

Finally, the production process is an important factor, once SFRC becomes self-compacting. Full-scale tests were conducted to study the performance of SCFRC: optimised mixtures were applied and the influence of the casting method on the fresh and the hardened state was studied.

1.3 Research strategy

The strategy to investigate SCFRC can be divided into four parts:

First, experimental and numerical studies were performed on the effect of steel fibres on the packing density of the granular skeleton. To simulate the packing density the Compressible Packing Model [De Larrard, 1999] was applied, and its input parameters were experimentally obtained.

Second, a preliminary study on the effect of steel fibres on characteristics of SCC in the fresh state was carried out from which design criteria were derived. Based on those criteria, reference mixtures without fibres at defined characteristics in the fresh state were composed and used as a reference; the effects of the type and the content of the steel fibres on the key characteristics of SCC were studied.

Third, bending tests were performed; optimised mixtures from the studies on SCFRC in the fresh state were tested. The flow and the walls caused the fibres to orient; this effect was quantified by means of an image analysis. A comparative study on the single fibre pull-out behaviour of SCC and conventional concrete was performed to quantify the differences.

Finally, three full-scale tests were carried out at the Delft University of Technology or in cooperation with partners from industry. These projects were sheet piles, tunnel segments and large beams. The main focus of these studies was on how the production process affects the orientation of the fibres.

1.4 Outline of the thesis

This thesis is split into four parts; Fig. 1.1 shows its components. The numbers presented in parenthesis stand for the number of the chapter. Part I deals with the optimisation of SCFRC in the fresh state. The focus of part II is on the behaviour of SCFRC in the hardened state. In part III, three applications of SCFRC are discussed. Part IV ends the thesis with general conclusions and future perspectives.

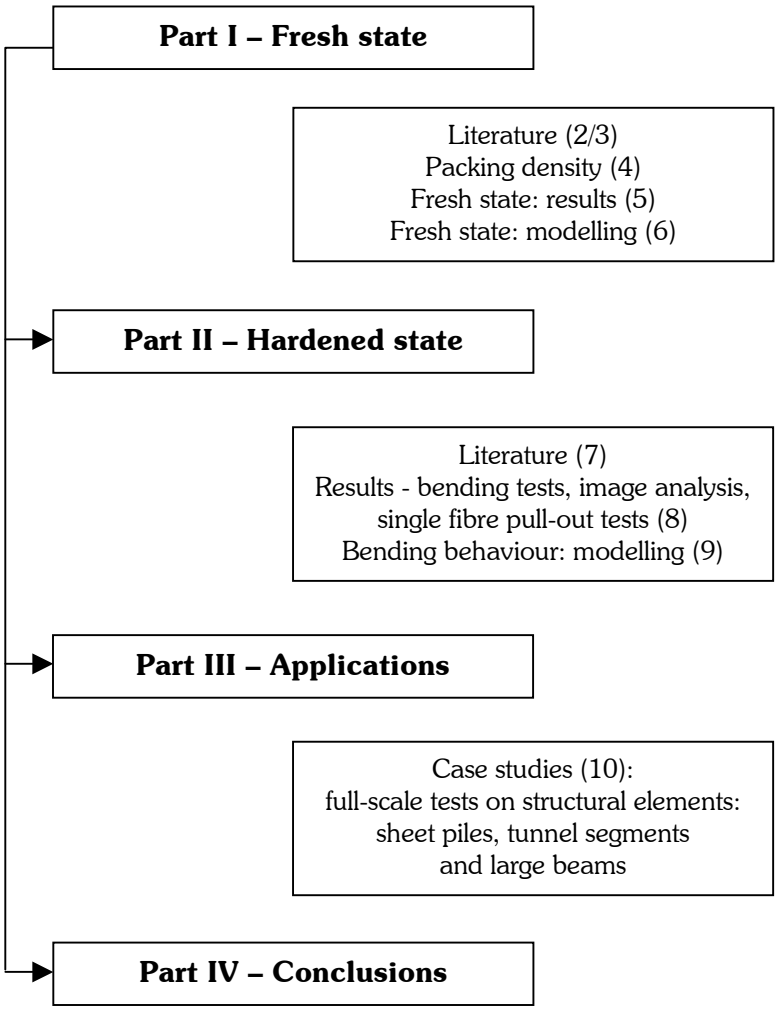


Fig. 1.1 Optimisation of SCFRC – overview of the four parts of the thesis

Part I consists of five chapters (Chapters 2-6). In Chapter 2, the literature on SCC in the fresh state is reviewed. This chapter aims at providing a theoretical background on SCC, describes test methods, and summarises approaches to compose and to model SCC.

In Chapter 3, the effect of fibres in general and steel fibres in particular on the workability of cement-based composites is discussed. Recommendations provide an indication about the maximum fibre content and the affecting parameters on workability.

Chapter 4 describes experimental studies that were carried out into the packing density and the optimisation of the granular skeleton (aggregates and steel fibres). The 'Compressible Packing Model' was applied to predict the packing density. Different approaches to include the fibres are compared; the accuracy of the predictions is discussed.

In Chapter 5, three parameter studies on the effect of the type and the content of the steel fibres on the key characteristics of SCC in the fresh state are described. From these studies optimised mixtures were chosen for tests into the behaviour of SCFRC in the hardened state.

Chapter 6 provides models to predict the behaviour of SCFRC in the fresh state and to compose it for defined purposes.

Part II (Chapters 7-9) describes studies on SCFRC in the hardened state and is subdivided into three chapters. Related literature is summarised, tests on SCFRC in the hardened state are described and a model is presented to predict the bending behaviour of hardened SCFRC.

Chapter 7 reviews literature about the effect of steel fibres on characteristics of cement-based materials in the hardened state.

Chapter 8 reports about results of bending tests, an image analysis and single fibre pull-out tests; differences between SCC and conventional concrete are pointed out.

Chapter 9 presents the analysis of bending tests with 17 optimised SCFRC mixtures. An inverse analysis was applied: a combined stress-strain/crack width relation for SCFRC in tension is proposed.

Part III (Chapter 10) summarises results and experiences gained from three case studies. Optimised mixtures were applied to produce sheet piles and tunnel segments; the influence of the production process was studied. In addition, large beams were cast; the focus of this study was on the orientation of the fibres due to the flow of the concrete.

Part IV (Chapter 11), presents the final conclusions and lists recommendations for future research on the optimisation and application of SCFRC.

Chapter 2:

SCC as a suspension

2.1 Introduction

This chapter reviews literature about SCC in the fresh state: its characteristics, common test methods and available models that describe its behaviour in the fresh state.

SCC contains cement, filler and aggregates in a wide range of sizes; it can be considered as a suspension of solid particles. Fibres differ from these solids due to their dimensions, shape and surface characteristics. To provide a theoretical background of the models on SCFRC, which are included in Chapter 6, four aspects of SCC in the fresh state are discussed in this chapter: First, rheology is an useful approach to characterise SCC; an introduction to rheology is presented. Second, empirical test methods to determine the three key characteristics of SCC are discussed. These characteristics are filling ability, passing ability and segregation resistance. Third, general principles to optimise the mixture composition are summarised. Finally, models are surveyed that describe characteristics of SCC.

2.2 Characterisation of SCC

The development of SCC in Japan was initiated due to a shortcoming of labourers, the wish to eliminate vibrating the concrete and to limit the number of defects due to bad construction. To homogeneously fill a mould, SCC has to fulfil high demands with regard to filling ability, passing ability and segregation resistance. Driven by its own weight, the concrete has to fill a mould completely without leaving entrapped air even in the presence of dense steel bar reinforcement. The components have to be homogeneously distributed during the flow and at rest. Clustering of the aggregates in the vicinity of reinforcement (blocking) and separation of water or paste affect the characteristics of SCC in the hardened state. Several authors report on the development and examples of applications of SCC in the Netherlands [Bennenk, 2000/2001; De Jong, 1998; Obladen, 2002; Oude Kempers, 1999; Takada, 2004; Van Aalst et al., 1996; Van Halderen; 1995; Walraven, 1998; Walraven et al., 1999]. Various test methods have been applied to detect the key characteristics of SCC; a single, practicable and reliable test method for SCC is not yet available. Test methods to design SCC for quality control have been described and discussed by e.g. Bartos et al. [2000], EFNARC [2001] and RILEM [2000]. It is still unclear whether the proposed criteria for test methods guarantee a satisfying performance at the construction site. The

appearance of the surface skin and the number of air entrapments also determine the quality of SCC; often it is required to carry out full-scale tests to study the interactions of the production process, the surface of the mould and the formwork oil. Appendix A presents the test methods for SCC and SCFRC, which were applied in this study. Additional characteristics of SCC in the fresh state like pumpability, finishability, plastic settlement and washout resistance are not discussed in this thesis.

2.2.1 Segregation resistance

The segregation resistance is the resistance of the components of SCC to migration or separation. Particles having a relatively high density or a low surface-volume ratio are more prone to segregation. The segregation resistance of SCC can be different under static (at rest) and dynamic (during the flow) conditions. Slightly segregating mixtures result in very smooth, fault-free surfaces, since the cement paste segregates at the walls of the formwork. Common test methods to determine segregation resistance are: Settlement Column test, Sieve Stability test, Penetration apparatus, V-funnel, Orimet and visual observations (e.g. on the slump flow spread).

2.2.2 Filling ability

Without vibrating the concrete, SCC has to fill any space within the formwork; it has to flow in horizontal and vertical directions without keeping air entrapped inside the concrete or at the surface. The driving forces of this process are the weight of the concrete and the casting energy. Examples of test methods for filling ability are: slump flow, the flow times T_{50} and T_{60}, V-funnel, Orimet, U-Box and L-Box.

2.2.3 Passing ability

Passing ability is required to guarantee a homogenous distribution of the components of SCC in the vicinity of obstacles. The minimum bar distance to avoid blocking depends on the flowability of SCC, on the maximum aggregate size, the paste content and the distribution and the shape of the aggregates. To optimise SCC for one specific application, testing requires an instrument with the possibility to vary the bar spacing. Test methods for determining the passing ability are: the J-ring in combination with the slump flow, L-Box, U-Box, V-funnel, Orimet and filling vessel test.

2.3 Rheology as a tool to characterise SCC

2.3.1 Introduction to Rheology

Rheology is the science of the deformation and flow of matter and it is concerned with the relationships between stress, strain, rate of strain and time [Tattersall & Banfill,

1983]. Rheometry is the notation for measuring rheology. SCC is a suspension of solid materials of rather deviating sizes in water; rheological measurements provide fundamental insight into the effect of the mixture composition, the interaction of the components and the flow behaviour. Different types of viscometers have been applied in concrete technology in order to determine its characteristics in the fresh state. Available commercial concrete viscometers are the BML-Viscometer [Wallevik, 2000], the BTRHEOM [De Larrard et al., 1998], the UBC-Rheometer, [Beaupré, 1994] and the MK-Apparatus [Tattersall, 1991].

Flow curves

A suspension responds with a deformation or strain when loaded with a force. Time- and shear-dependent phenomena affect the rheological characteristics of cement-based matrices:

- The characteristics of a cement paste change in time due to the agglomeration of particles, the breakdown of a structure and the progress of the hydration of cement.
- Interparticle forces cluster small grains; dependent on the applied shear rate equilibrium is obtained.
- Plasticisers and superplasticisers disperse cement and powder clusters and decrease the porosity of the granular skeleton.

The 'Newtonian model' (Equation 2.1) states a linear relation between the shear stress τ and the rate of shear deformation. The higher the rate of shear deformation, the higher the shear resistance, reflected by the shear stress τ. A constant factor, which is defined as the plastic viscosity, links both parameters.

$$\tau = \mu \cdot \dot{\gamma} \tag{2.1}$$

where: τ = shear stress [Pa]
μ = plastic viscosity [Pa·s]
$\dot{\gamma}$ = shear rate [1/s]

The 'Bingham model' (Equation 2.2) describes the flow behaviour of suspensions more generally. To initiate the flow a minimum shear stress τ_0 (yield value) has to be surpassed. Beyond this threshold, the shear stress is linearly related with the increase of the rate of deformation. The Bingham model reduces to the Newtonian model in case the yield value is zero.

$$\tau = \tau_0 + \mu \cdot \dot{\gamma} \tag{2.2}$$

where: τ_0 = yield value [Pa]

Shear-dependent behaviour

Shear-thickening as well as shear-thinning may take place, which is characterised by an overproportional, or a sub-proportional increase of the shear resistance at increasing rate of deformation respectively. Shear-thinning is the result of the orientation of long components, stretching or deformation of the solids or the distribution of agglomerations, which are clustered due to surface forces at a lower shear rate. Shear-thickening can be the result of a redistribution of the solids. The 'Herschel-Bulkley model' (Equation 2.3) modifies the Bingham model by taking into account the shear-dependency of the plastic viscosity. A fluid with an exponent $e>1$ is called shear-thickening (shear-thinning: $e<1$).

$$\tau = \tau_0 + \mu \cdot \dot{\gamma}^e \qquad (2.3)$$

where: e = exponent of Herschel-Bulkley model [-]

Time-dependent behaviour

At a constant shear rate, a structure of particles may build-up or breaks down: the response is time-dependent. Thixotropic materials undergo a structural breakdown while being deformed, whereas the structure rebuilds at rest. Anti-thixotropic behaviour characterises materials that build-up while being deformed, and break down during rest.

2.3.2 Rheology of SCC

SCC has been applied in a wide range of compositions. Fig. 2.1 (grey areas) shows that their characteristics in the fresh state are also rather different.

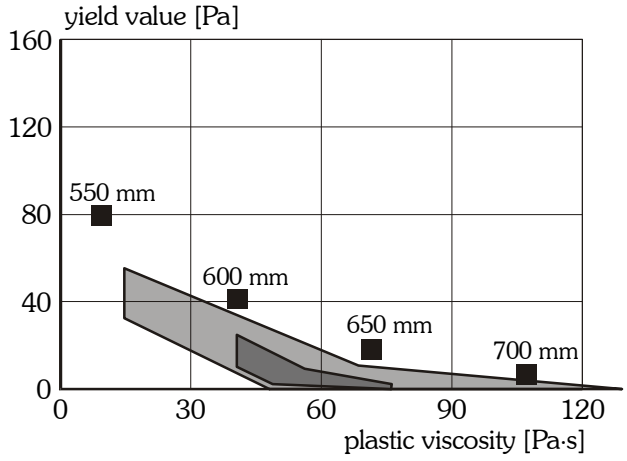


Fig. 2.1 Target range for SCC and the related minimum slump flow [after: Nielsson & Wallevik, 2003]

Rheological measurements on SCC resulted in ranges of plastic viscosities of 7-160 Pa·s and yield values from 0-60 Pa [Wallevik, 2003]. The dark grey region marks the target area of SCC concerning the yield value and the plastic viscosity, which is the result of measurements executed with the BML-Viscometer [Níelsson & Wallevik, 2003]. The minimum slump flow to achieve SCC is also included in Fig. 2.1.

The Bingham model describes the flow behaviour of SCC best [Wallevik, 2000]. De Larrard et al. [1998] obtained flow curves from SCC with the BTRHEOM that were described best by the Herschel-Bulkley model, which indicated SCC to be shear-thickening. Shear-dependency of SCC might be observed in case particles orientate or components segregate during the measurement. In case equilibrium is not reached the measured torque is higher compared with that in the equilibrium state [Wallevik, 2000]. The number and the nature of contact points (due to friction) between the grains govern the yield value. The role of the liquid phase is to create distance between the solids [De Larrard, 1999]. SCC with a negligible yield value (<10 Pa) shows Newtonian flow behaviour [Wallevik, 2003]. The plastic viscosity is mainly affected by the dissipation of the liquid phase [De Larrard, 1999]. The thixotrophic behaviour of SCC affects the formwork pressure [Billberg, 2003].

SCC can be realised with different design approaches: some of them are connected with rheological considerations [Wallevik, 2003].

- *High yield value (lattice effect):* A SCC having a high yield value (up to 60 Pa, [Wallevik, 2003]) can be obtained by optimising the composition and the content of the aggregates or by composing the paste to counteract segregation.
- *High plastic viscosity:* An increased content of the powders (reduces the water to powder ratio) and adding superplasticiser characterises the powder-type SCC; the plastic viscosity falls in the upper range of Fig. 2.1. A viscosity agent increases the plastic viscosity and decreases the sensitivity to changes in the mixture composition.
- *Thixotrophic SCC:* The rebuilding of the structure of the cement paste counteracts segregation once SCC is in rest.

2.4 Design methods for SCC

SCC was first developed in Japan. To optimise it, different design approaches are followed in other countries. First, superplasticiser and cement are the most expensive components; research often focuses on reducing the paste content. The aggregate skeleton might be optimised to obtain a high packing density. Reducing the coarse aggregate content, decreasing the maximum aggregate size and adding round instead of crushed aggregate are common concepts to optimise the granular skeleton. Second, cement has been replaced by adding water and a viscosity agent and/or fillers. Third, adding air entrainer increases the paste content. Fourth, the production process and design of the concrete elements offer a potential for further optimisation.

2.4.1 Japanese design method

The Japanese design approach [Okamura & Ouchi, 1999] is relatively work-intensive, but provides a fundamental understanding of the interaction of the components of SCC. Their method is to optimise SCC on three different levels: performing paste tests, optimising the mortar phase, and finally adjusting SCC on the concrete level. Self-compactability is obtained even in heavily reinforced sections. Fig. 2.2 illustrates the Japanese approach. The packing density of the coarse aggregates (<20 mm) has to be determined, 50% of this volume is appropriate for SCC. The remaining part, the mortar phase, is composed of 40 Vol.-% sand (<5 mm) and 60 Vol.-% cement paste (<0.09 mm).

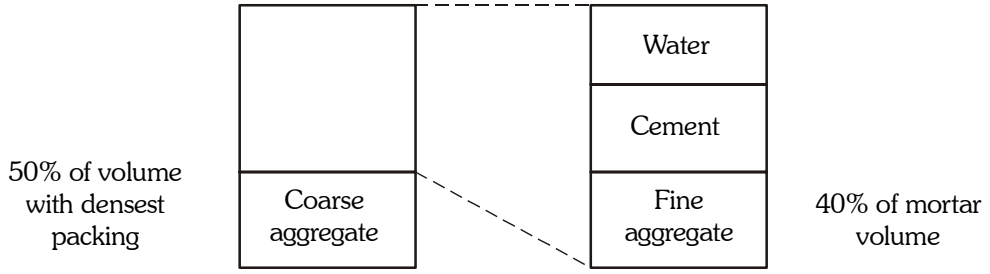


Fig. 2.2 Components of SCC according to the Japanese approach [after: Okamura & Ouchi, 1999]

In order to take the characteristics of deviating materials into account, empirical tests have to be carried out on three levels [Takada et al., 1997]. First, the level of cement paste is considered and the porosity of the granular skeleton of cement and fillers is determined. At this stage, the water demand of the powders has to be determined by flow tests at different water contents. Second, cement paste lubricates small aggregates in mortar. At this stage, a superplasticiser is added to decrease the water demand and to determine its effect in combination with powders. The contents of water and superplasticiser have to be adjusted to obtain a defined mortar spread of 245 mm and a flow-time of about 10 s. Finally, the content and the maximum size of coarse aggregates are chosen to pass the reinforcement at a specified bar spacing. To fulfil the design criteria, the contents of water and superplasticiser are adjusted.

2.4.2 Risk of blocking (CBI-method)

Following the approach of Bui [1994] on passing ability, the Swedish Cement and Concrete Research Institute (CBI) proposed a design method for SCC. This approach takes into account the void content of the aggregates, the effect of the aggregates on passing ability (risk of blocking) and the characteristics of fine mortar [Petersson et al., 1998]. The effect of a single sized fraction on the passing ability was experimentally studied with the L-box. Bartos et al. [2000] describe the L-box and the measurement procedure. The blocking criterion is 0.8 (ratio of the heights inside the column and at the end of the L-box); the bar spacing of the L-box is 34 mm. Fig. 2.3 shows the relative effect of the aggregates on the passing ability of SCC (n_{abi}) related to the ratio of the bar

spacing c divided by the diameter of the aggregate fraction D_{af}. The curves of Fig. 2.3 are recalculated from experiments [Petersson, 2003]. The equivalent diameter D_{af} of an aggregate fraction can be calculated with Equation 2.4:

$$D_{af} = M_{i-1} + ¾ (M_i - M_{i-1}) \quad (2.4)$$

where: M_i = upper sieve dimension of aggregate [mm]
M_{i-1} = lower sieve dimension of aggregate [mm]

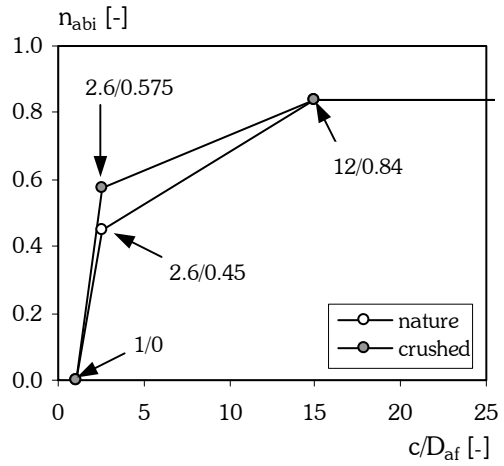


Fig. 2.3 Relation between the ratio of the clear bar spacing c to fraction diameter of the aggregates and the blocking volume ratio

Similar to the Miner-rule on fatigue, the contribution of each aggregate fraction is accumulated with Equation 2.5. The 'risk of blocking' has to remain below 1. Once the content and the composition of the aggregates is known, the paste composition has to be chosen in order to fulfil the design requirements for SCC in the fresh and the hardened state.

Risk of blocking:
$$\sum_{i=1}^{n} \frac{n_{ai}}{n_{abi}} = \sum_{i=1}^{n} \frac{V_{ai}}{V_{abi}} \leq 1 \quad (2.5)$$

where: n_{ai} = aggregate contribution of group i to blocking [-]
n_{abi} = blocking volume ratio of group i [-]; $n_{abi} = V_{abi} / V_t$
V_t = total volume of the concrete mix [m^3]
V_{ai} = aggregate volume of group i [m^3]
V_{abi} = blocking volume of aggregate group i [m^3]

Simulations with the CBI-model and Swedish aggregates showed that the passing ability determines self-compactability at relevant gravel to total aggregate ratios (>20%) [Petersson et al., 1998]. The paste content of SCC has to be higher than the content that would be necessary to fill the interstices of the aggregates (>31 Vol.-%). Rheological parameter studies were performed on fine mortar to extend their model and to reduce the number of experiments to obtain optimised SCC [Billberg, 1999]. The link between characteristics of fine mortar and SCC is difficult to establish: verification tests on SCC still have to be carried out to fulfil the criteria for SCC.

2.5 Modelling the behaviour of SCC in the fresh state

SCC is a suspension of solid particles of rather different sizes in water. The behaviour of cement and fillers is different from that of the aggregates; attractive and repulsive forces determine the degree of agglomeration. Superplasticisers are usually applied in SCC, which significantly affects the structure of the powders. A superplasticiser disperses cement flocks and increases the packing density. SCC might be distinguished on two levels: first, all solids (powders and aggregates) are suspended by water and second, aggregates are lubricated by cement paste. The interstices of the granular skeleton have to be filled. An excess of the fluid reduces the friction by separating the solids with a small layer of either water or cement paste. Fig. 2.4 shows the formation of layers of cement paste around aggregates. The thickness of the paste layer can be best related to the diameter of the grains [Oh et al., 1999]. An excess of paste has to be added to keep the solid particles on distance and to reduce the friction between the aggregates. The cement paste thus has a filling, a binding and a smearing action. For the calculation of the layer thickness the correct surface area has to be taken into account. The ratio of surface area to volume increases the more the solids deviate from the round shape.

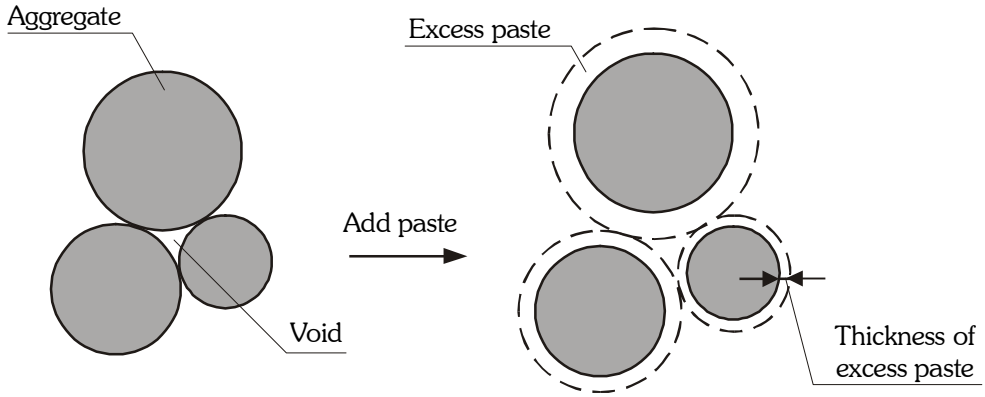


Fig. 2.4 Excess paste layer around aggregates
[after: Oh et al., 1999]

2.5.1 Layer models

Kennedy [1940] states that the consistency of concrete depends on two factors: First, the amount of excess paste to fill the voids in-between the aggregates and second, on the consistency of the paste itself. Because the composition and the surface characteristics of the aggregates are not constant, empirical tests have to be carried out to determine a relationship between these parameters and the consistency of the concrete. According to Kennedy, concrete becomes workable when the content of cement paste exceeds the volume required to fill the voids; a lubricating layer reduces the friction between the aggregates.

Corrected water and paste layer thicknesses

Krell [1985] studied the effect of the aggregate grading and the distribution of cement on the flow diameter (Fig. 2.5: parameter o), which was determined by applying the German flow test, in order to predict the behaviour of fresh concrete. No superplasticiser was applied in his study. He calculated both the layer thicknesses of the paste around aggregates (particles > 0.125 mm) and of water around the powders. Fig. 2.5 shows that the flow spread was larger at increasing water or paste layer thicknesses, which he assumed to be constant around all particles. Krell calculated an equivalent diameter for powders and aggregates, which might be different even when the specific surface area of the granular skeleton would be the same. The decrease of the water layer thickness due to the formation of reaction products and its effect on the flow also was studied. In order to obtain the same paste layer thickness for the same consistency it was required to apply a correction. A second correction was required to compensate for the deviating distributions of the powders. With the model, the flow spread could be predicted for concrete mixtures, but it was not accurate for mortars. At a given layer thickness the flow of a mortar usually was overpredicted.

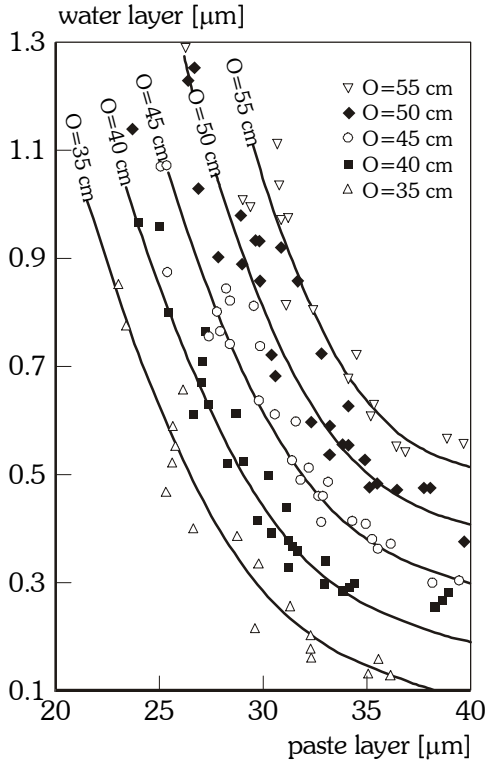


Fig. 2.5 Relation between the flow diameter and the corrected water and paste layer thicknesses [after: Krell, 1985]

The model of Krell aimed at predicting the flow diameter of the German flow test, which is not a useful test method for SCC. A drawback of the model is the assumption of a constant layer thickness around the solids; a correction is required in case the grading or the maximum size of the solids is varied.

Relative paste layer thickness

Oh et al. [1999] modelled characteristics of SCC in the fresh state by applying the 'relative' paste layer thickness (Fig. 2.4) and related it to the diameter of the aggregates (Equation 2.6). They found that the relative plastic viscosity and the relative yield value were better correlated to this factor compared with the constant but absolute layer thickness. Both numbers were determined with a cylindrical rheometer. They varied the content of the aggregates, whereas their distribution was kept the same. Four different pastes were tested. The void content, the surface area including a shape factor and the diameter of the aggregates were taken into account for the calculation of the relative paste layer thickness.

$$\Gamma = \frac{P_e}{\sum_{i=1}^{n} n_i \cdot s_i \cdot D_{pi}} \qquad (2.6)$$

where: Γ = relative thickness of the surrounding fluid [-]
P_e = excess paste volume [mm^3]
n_i = number of aggregates of group i [-]
s_i = surface area of the aggregate grains in group i [mm^2]
D_{pi} = diameter of grain group i [mm]

Both the characteristics of cement paste and the relative layer thickness affect the characteristics of SCC in the fresh state. The model of Oh et al. [1999] does not take the characteristics of the cement paste into account. Due to different paste properties their measurements scatters around the predicted values.

Water layer thickness

Maeyama et al. [1998] report on the effect of the composition of the cement paste on the characteristics of SCC and proposed the water layer model. The absolute thickness of the water layer was obtained from the size distribution of the powders. They defined the 'flocculation number', which takes into account the degree of flocculation of different powder types (Fig. 2.6). Tests on mortar showed that the water layer thickness was about the same, in case the mortar flow and the flow time were the same. Concrete tests showed the applicability of the model; the composition and the content of the aggregates were kept constant. Their conclusion was that at a given theoretical paste layer thickness the water layer thickness has to be constant in order to obtain the same mortar flow. Once the flocculation number of a combination of powders was known, the water content of SCC could be calculated.

In order to include the effect of the distribution and the content of the aggregates into the water layer model, Midorikawa et al. [2001] carried out a second study on the water layer thickness. One type of cement was applied. With the assumption that the water layer thickness was always 15 μm (all mixtures had resulted in the same mortar flow-time and spread), the flocculation number of the mortars was calculated. At increasing

sand content in the mortar the contents of water and superplasticiser also increased, whereas the flocculation number decreased.

The superplasticiser content alters the state of flocculation and significantly affects the packing density. The flocculation number is not a constant number. The use of superplasticisers complicates the application of the water layer model. The link between the dosage and the type of superplasticiser, the combination of the powders and the required water layer thickness at a given content and composition of the aggregates is not yet established.

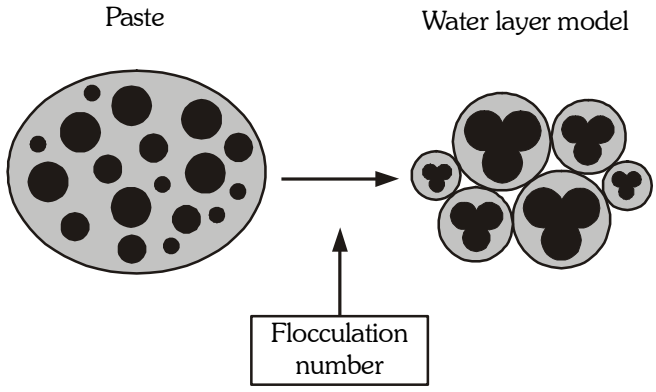


Fig. 2.6 Water layer around flocculated powder grains [after: Maeyama et al., 1998]

2.5.2 Packing model

Sedran [1999] and De Larrard [1999] describe models to estimate the yield value and the plastic viscosity of SCC, which were derived from the packing concept. The packing density is a characteristic of the granular skeleton, which takes into account the packing process, the distribution and the shape of the grains and the degree of agglomeration of the powders. Predictions with the 'Compressible Packing Model (CPM)' were the basis to develop their models. The theoretical background on packing density and the CPM is summarised in Chapter 4.

Plastic viscosity

The normalised solid concentration, which is the content of the solids (powders and aggregates) divided by the packing density, was the single factor that affected the plastic viscosity [De Larrard, 1999]. From a series of 78 mixtures, Equation 2.7 was obtained (error: 61 Pa·s):

$$\mu = \exp\left[26.75 \cdot \left(\frac{\phi}{\phi^*}\right) - 0.7448\right] \qquad (2.7)$$

where: μ = plastic viscosity [Pa·s]
ϕ = solid content [-]
ϕ^* = packing density, space occupied by the solids [-]

Yield value

The number of contact points affects the yield value; the effect of the grains is more pronounced the smaller they are [De Larrard, 1999]. The addition of a superplasticiser significantly affects the yield value. The following model (Equation 2.8) is proposed to predict the yield value:

$$\tau_0 = \exp\left(2.537 + \sum_{aggregate}[0.736 - 0.216\log(d_i)]K_i' + [0.224 + 0.910\cdot(1 - P/P^*)^3]\cdot K_c'\right) \qquad (2.8)$$

where: τ_0 = yield value [Pa]
d_i = geometrical diameter of grain group i [mm]
K_i' = contribution of grain fraction i to the compaction index [-]
P/P^* = content superplasticiser compared with the saturation dosage [-]
K_c' = contribution of cement (or powders) to the compaction index [-]

Both models allow predicting the plastic viscosity and the yield value once preliminary tests on cement paste have been carried out; SCC can be composed on a spreadsheet. The yield value is very sensitive to the addition of superplasticiser; the dosage of superplasticiser affects the packing density of the paste.

2.6 Concluding remarks

This chapter discussed selected literature on SCC in the fresh state. The key characteristics of SCC are filling ability, passing ability and segregation resistance. Rheological and empirical test methods were presented to determine these key characteristics. At this time, no single test method is available that is able to define self-compactability with one single criterion. Several models were summarised that aim at describing the characteristics of SCC. Essentially, two types of models were developed: layer and packing models, which distinguish water and cement paste as the suspending medium. The CBI-approach [Petersson et al., 1998] on passing ability allows composing the granular skeleton.

Krell [1985] concluded from his analysis that both the thickness of the water and the paste layers affect the flow diameter. A thicker water layer compensates for a smaller paste thickness. Oh et al. [1999] found that a relative rather than a constant paste layer thickness results in better predictions of characteristics of SCC in the fresh state. The characteristics of the paste can be predicted by applying the 'flocculation number', which depends on the dosage of the superplasticiser [Midorikawa et al., 2001]. Sedran [1999] successfully predicted the yield value and the plastic viscosity of SCC by applying packing concepts. The mechanisms that affect the key characteristics of SCC are not yet fully understood. An adequate prediction of the paste composition for

defined characteristics decreases the number of experiments to obtain optimised SCC. The link between the dosage and the type of superplasticiser at a given combination of powders and the characteristics of cement paste as well as of SCC is not established; it is still necessary to conduct additional tests to determine the interaction of the components.

Chapter 3:

Effect of fibres on the behaviour of concrete in the fresh state

3.1 Introduction

This chapter presents an overview of relevant literature on parameters affecting the characteristics of fibre reinforced concrete and SCFRC in the fresh state. The mixture composition of fibre reinforced concrete often is a compromise between the requirements on the fresh and the hardened state. The shape of the fibres differs from that of the aggregates; due to the long elongated shape and/or a higher surface area the workability of concrete is affected. The practical fibre content is limited: a sudden decrease of workability occurs at a certain fibre content, which depends on the mixture composition and the applied fibre type. The affecting parameters on the behaviour of concrete in the fresh state were varied in several experimental studies to find their effect on the key characteristics of SCC.

3.2 Characteristics of the fibres

Fibres have been added to cementitious materials in order to improve the characteristics in the hardening or the hardened state. The steel fibre is the most common fibre type in the building industry; plastic, glass and carbon fibres contribute to a smaller part to the market. The fibre type, the mixture composition, the mixing process and the compaction technique determine the maximum fibre content. To optimise the performance of a single fibre, fibres need to be homogeneously distributed; clustering of fibres has to be counteracted.

Fibres differ in a wide range of materials and characteristics. Their effect on workability is mainly due to four reasons: First, the shape of the fibres is more elongated compared with aggregates; the surface area at the same volume is higher. Second, stiff fibres change the structure of the granular skeleton, while flexible fibres fill the space between them. Stiff fibres push apart particles that are relatively large compared with the fibre length. The porosity of the granular skeleton increases. Third, surface characteristics of fibres differ from that of cement and aggregates, e.g. plastic fibres might be hydrophilic or hydrophobic. Finally, steel fibres often are deformed (e.g. have hooked ends or are wave-shaped) to improve the anchorage between a fibre and the surrounding matrix. The friction between hooked-end steel fibres and aggregates is higher compared with straight steel fibres.

3.3 Conventional concrete and fibres

Steel fibre reinforced concrete (SFRC) appears stiffer (lower slump) compared with conventional concrete without fibres even when the workability (judged by any test using vibration) is the same [Johnston, 2001]. SFRC tends to 'hang' together. Vibration is encouraged to increase the density, to decrease the air void content and to improve the bond with reinforcement bars. In spite of a stiff appearance, a well-adjusted fibre mixture can be pumpable [ACI 544, 1993]. The size of the fibres relative to that of the aggregates determines their distribution (Fig. 3.1). To be effective in the hardened state it is recommended to choose fibres not shorter than the maximum aggregate size [Johnston, 1996; Vandewalle, 1993]. Usually, the fibre length is 2-4 times that of the maximum aggregate size. It is recommended to reduce to volume of coarse aggregates by 10% compared with plain concrete to facilitate pumping. The initial slump of plain concrete should be 50-75 mm more than the desired final slump; to obtain it a superplasticiser rather than excess water should be added [Johnston, 2001].

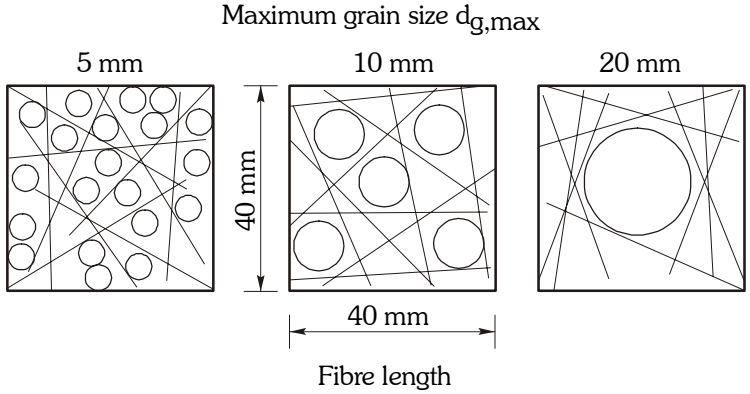


Fig. 3.1 Effect of the aggregate size on the fibre distribution [after: Johnston, 1996]

The size, the shape and the content of the coarse aggregates as well as the geometry and the volume fraction of steel fibres affect the workability of concrete [Swamy, 1975]. At a given fibre diameter and volume fraction, compactability was linearly related with the aspect ratio (L_f/d_f) of the fibres. The relative fibre to coarse aggregate volume and the 'balling up' phenomenon govern the maximum possible content of steel fibres [Swamy & Mangat, 1974]. Fig. 3.2 shows how the maximum content of the steel fibres decreases at increasing coarse aggregate content. The maximum fibre content is the critical fibre content at which the compactability drastically decreases. Steel fibres with a length of 25 mm (d_f: 0.25 mm) and single sized aggregates (crushed aggregate) with a maximum aggregate size of 10 mm were applied in their investigation. Fibre balling already might occur before the fibres are included into the concrete. The more fibres the mixture contains the more likely the occurrence of fibre balling; a maximum of 2 Vol.-% of steel fibres (1 Vol.-% at a high aspect ratio) is considered as a maximum [ACI 544, 1993].

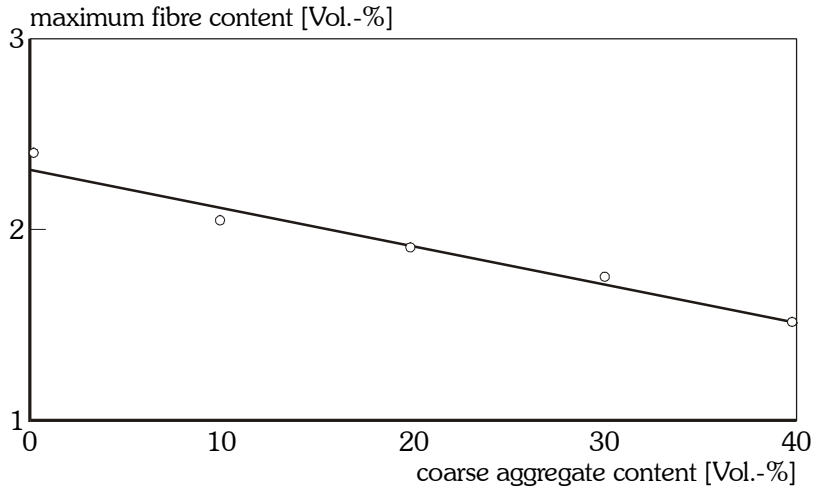


Fig. 3.2 Effect of the coarse aggregate content on the maximum content of steel fibres [after: Swamy & Mangat, 1974]

Edgington et al. [1978] performed tests on the effect of the aspect ratio (L_f/d_f) and the fibre concentration on the Vebe-time. Mixtures without fibres were used as a reference. The reference mortar contained aggregates with a maximum size of 5 mm. Fig. 3.3 presents the results of this study. To obtain the same Vebe-time the maximum fibre volume fraction had to be decreased, the higher the aspect ratio was.

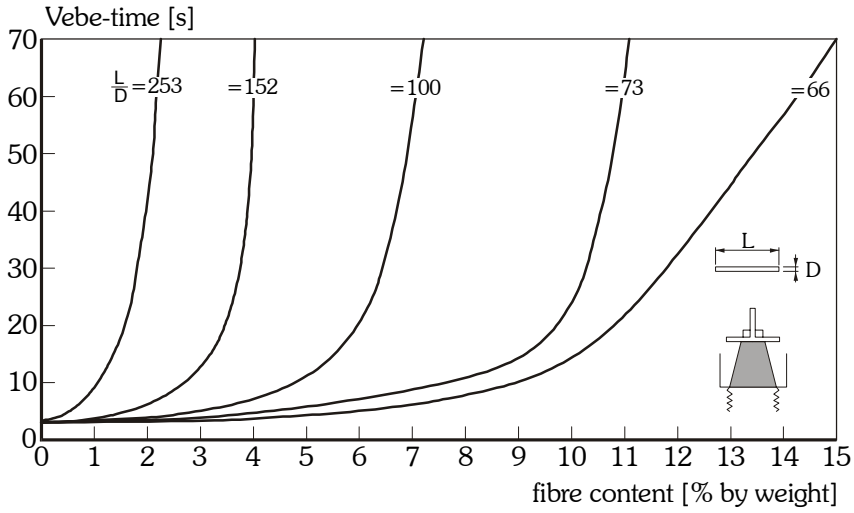


Fig. 3.3 Effect of the type and the content of the steel fibres on the Vebe-time of fibre reinforced mortar [after: Edgington et al., 1978]

In the same study, different reference mixtures were tested [Edgington et al., 1978], which differed in the maximum aggregate size (20, 10, 5 mm and cement paste). One type of steel fibre was applied; the aspect ratio was kept constant at 100 (Fig. 3.4).

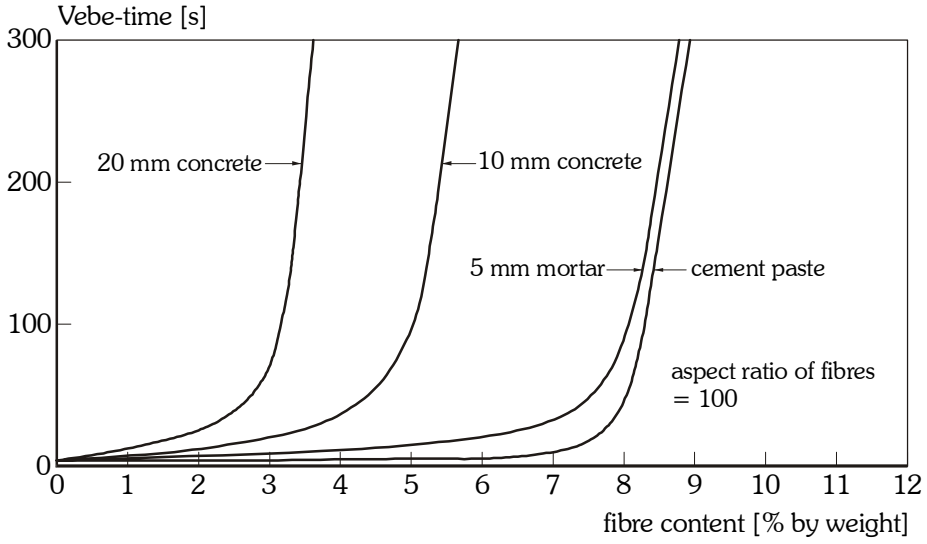


Fig. 3.4 Effect of the mixture composition and the fibre content on the Vebe-time [after: Edgington et al., 1978]

The larger the maximum aggregate size the higher the Vebe-time was for a certain steel fibre content (Fig. 3.4). The difference between the cement paste and a 5 mm-mortar was rather small; the aggregates were relatively small compared with the fibre length. An increase of the maximum aggregate size usually implies that the aggregate content is higher, since less paste is required to fill the interstices of the granular skeleton.

Narayanan & Kareem-Palanjian [1982] found that the 'optimum fibre content' increased at increasing percentage sand of total aggregate; both parameters were linearly correlated. The 'optimum fibre content' was defined as the content of the steel fibres beyond which fibre balling took place. The maximum aggregate size of the coarse aggregates was 14 mm (sand: 3 mm). Different steel fibre types with lengths between 25-43 mm were tested. The established relation was independent of the ratios of aggregate to cement and water to cement, which means that balling occurred at a given fibre content no matter what was the composition of the concrete.

Rossi & Harrouche [1990] proposed a design method to optimise the granular skeleton of fibre reinforced concrete that was based on the Baron-Lesage method. They made two assumptions: First, the most workable concrete is obtained in case the granular skeleton is optimised. Second, the first holds true independently of the nature or volume of the cement paste. The characteristics of FRC in the fresh state were determined with the LCL-Workabilitymeter; the flow-time was determined by applying external vibration. Fig. 3.5 shows the general effect of the variation of the granular skeleton on the flow-time; the content and the composition of the paste were kept constant. The optimum sand content depends on the type and the content of the steel fibres.

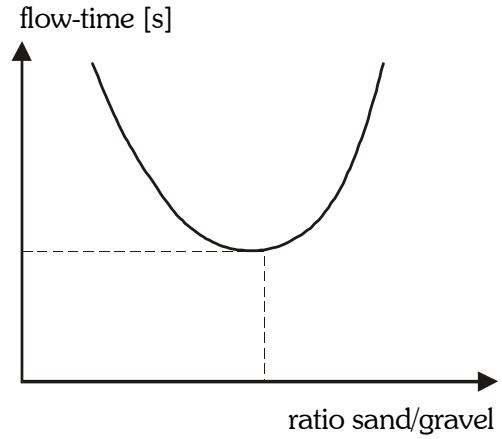


Fig. 3.5 Fibre reinforced concrete - optimisation of the granular skeleton [after: Rossi & Harrouche, 1990]

Hoy [1998] performed experimental and numerical studies on the packing density of the granular skeleton of SFRC. To include steel fibres into the Solid Suspension Model (SSM), which is a packing program developed by De Larrard & Sedran [1994], various methods were tested. Hoy assumed that the most workable mixture would be that with the highest packing density. He obtained the optimum composition of the granular skeleton from simulations with the SSM. Input parameters of simulations were the characteristics of the components (steel fibres, sand and coarse aggregate). Fig. 3.6 shows results of a numerical parameter study. The higher the content of the steel fibres the higher was the required optimum sand content. At a defined content of the steel fibres, the sand to total aggregate ratio had to be higher the higher the aspect ratio was. Practical considerations limit the applicability of Fig. 3.6; steel fibre contents larger than 2.0 Vol.-% cause a significant decrease of workability.

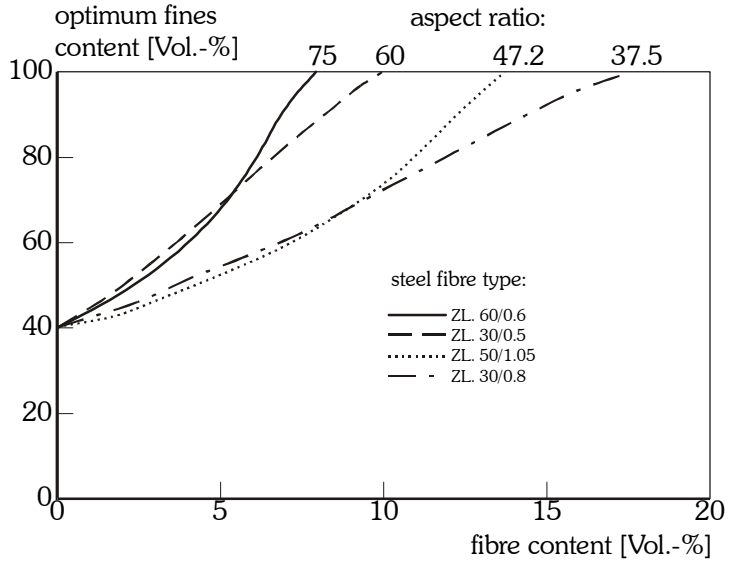


Fig. 3.6 Theoretical effect of the type and the content of the steel fibres on the optimum sand content [after: Hoy, 1998]

Fibre producers provide guidance for composing SFRC. Table 3.1 recommends the maximum fibre content, which depends on the fibre type, the maximum aggregate size and whether SFRC has to be pumped or not.

Table 3.1 Maximum content of steel fibres in concrete
[Dramix product information; after: Kooiman, 1996]

L_f/d_f	*60*	*75*	*100*
$d_{g,max}$	*Normal (Pumping)*	*Normal (Pumping)*	*Normal (Pumping)*
[mm]	*[kg/m³]*	*[kg/m³]*	*[kg/m³]*
4	160 (120)	125 (95)	95 (70)
8	125 (95)	100 (75)	75 (55)
16	85 (65)	70 (55)	55 (40)
32	50 (40)	40 (30)	30 (25)

The effect of flexible fibres differs from that of stiff fibres; they fill the interstices between the aggregates rather than pushing the aggregates apart. The surface area of flexible fibres often is much higher compared with that of the steel fibres. Plastic fibres having the same surface area might affect the workability to different degrees; the fibres might be either hydrophobic or hydrophilic. The flow of cement-based matrices also depends on the surface area of the fibres. Fig. 3.7 shows a linear correlation between the flow spread and the fibre content (specific surface area) of a carbon fibre reinforced paste [Ando et. al., 1990].

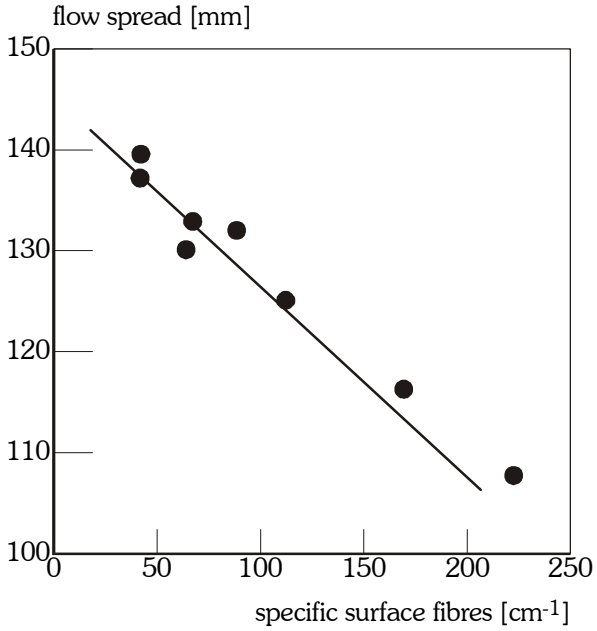


Fig. 3.7 Effect of the specific surface area of carbon fibres on the flow spread of fibre reinforced paste [after: Ando et. al., 1990]

3.4 SCC and fibres

Characteristics in the fresh state

SCFRC can maintain self-compactability in spite of the addition of the fibres. Groth [2000a] performed parameter studies on the effect of steel fibres on the characteristics of SCC in the fresh state (slump flow, flow-time T_{50} and J-ring test). To determine the effect of the fibres, tests were also carried out with SCC without fibres. The higher the fibre factor [$V_f \cdot L_f/d_f$], the more the slump flow decreased. The flow-time T_{50} was higher with steel fibres compared to a reference SCC. The degree to which the steel fibres affected the slump flow and T_{50} depended on the mixture composition of the SCC without fibres. Khayat & Roussel [1999] tested SCFRC with the IBB-Rheometer; the applied fibre contents were 0.5 and 1.0 Vol.-%. The relative plastic viscosity increased and the filling degree of the filling vessel decreased at increasing fibre content. Ambroise et al. [1999] tested a viscosity-agent type SCFRC with 1.0 Vol.-% of long steel fibres (aspect ratio: 81, length: 50 mm steel fibres). Higher contents of short steel fibres have been added to self-compacting mortar [Sato et al., 2000; Markovic et al., 2003]. Nemegeer [1999] reports on a study on the passing ability of SCFRC; the J-ring in combination with the slump flow test was used to determine the bar spacing required to avoid blocking. A bar spacing of about two times the fibre length was required to avoid blocking. Groth [2000b] proposed a guideline for hooked-end steel fibres with circular cross-sections (Table 3.2) to avoid blocking of SCFRC, which is independent of the composition of SCFRC.

Table 3.2 Recommendation on the normalised bar spacing to avoid blocking of SCFRC [after: Groth, 2000b]

c/L_f [-]	L_f/d_f [-]	Max. m_f [kg/m³]
≥ 3	80	30
	65	60
≥ 2	65	30
	45	60
≥ 1.5	45	30

The effect of two types of polypropylene fibres (L_f: 12 mm, V_f: 0.2 Vol.-%) on the characteristics of SCC in the fresh state was studied by Grünewald & Walraven [2000], which were a monofilament and a fibrillated fibre type. SCC remained self-compacting with the fibrillated type (d_f=60 μm); the slump flow decreased from 710 to 620 mm, while the filling degree (U-Box test) was only slightly affected. The monofilament type (d_f=18 μm) significantly decreased the slump flow to 440 mm due to the higher surface area.

Orientation and distribution of the fibres

The orientation and the distribution of the fibres affect the performance and the variation of characteristics of SCFRC in the hardened state. Petersson [1998] reports on

a study on the distribution of steel fibres in the L-Box; X-ray photographs were taken from cross-sections of the hardened concrete. The conclusions were that the fibres were remarkably well distributed, although a slightly increased segregation of fibres was observed compared to the coarse aggregates. The fibres were oriented to some degree into the flow direction; this effect was more pronounced for longer fibres. Nemegeer [1999] concluded that the flow orients the fibres and commonly applied contents of steel fibres have little influence on the characteristics of SCC. The bending performance of SCFRC was equal to or better than what would be expected for SFRC at the same strength class and at the same type and content of the steel fibres [Nemegeer, 1999], which might be contributed to the pronounced orientation of the fibres into the direction of the principal tensile stress.

3.5 Concluding remarks

This chapter discussed the effect of the type and the content of the fibres and the mixture composition on the characteristics of plain concrete and SCC in the fresh state. The mix design of FRC is a compromise between the desired performance in the hardened state and the demands on workability in the fresh state; the fibre content has to remain within practicable limits. Few studies and applications on SCFRC are reported in literature: the applied fibre contents were within the range normally used in FRC. The limit of how many fibres can be added and what parameters affect this limit is unknown.

The mix design of FRC often is based on some rules of thumb: increase the paste content, the dosage of superplasticiser and the content of the fine aggregates at increasing aspect ratio and fibre volume. Rossi & Harrouche [1990] and Hoy [1998] approached the mix design of fibre reinforced matrices on a more systematic manner: they optimised the granular skeleton. Besides the granular skeleton, the content and the characteristics of the paste have to be taken into account to link workability and the mixture composition. This link is not yet established for FRC and SCFRC. A homogenous distribution and orientation of fibres in FRC is often assumed but rarely investigated. The requirement on the key characteristics of SCC remains the same for SCFRC; the optimisation of SCFRC can be done from different points of view: e.g. passing ability, post-cracking behaviour, compressive strength class and costs.

Chapter 4:

Predicting the packing density of the granular skeleton

4.1 Introduction

Chapter 4 reports on the background and on experimental and numerical studies on packing density. After a brief introduction into the literature and a description of the Compressible Packing Model (CPM), experimental as well as numerical results are discussed. The porosity of the granular skeleton (aggregates and steel fibres) determines how much paste is required to fill its interstices. Two questions are discussed in this chapter: How to decrease the porosity as much as possible and how to predict it. Experimental studies were performed, which aimed at optimising the granular skeleton. Results of packing experiments are compared with numerical predictions of the CPM. The required input parameters to conduct simulations with the CPM are experimentally determined. Five approaches are compared to include the fibres into the CPM; the accuracy of the predictions is calculated. The approach with the best accuracy is applied to predict the packing density of SCFRC.

4.2 Parameters affecting the packing density

The bulk density divided by the density of the solids is defined as the packing density [Hoy, 1998]. The packing density (PD) can be calculated with Equation 4.1; the required parameters are the density and the weight of the solids filled into a container of a specified volume. The porosity is the volume of interstices within the granular skeleton (1-PD).

$$PD = \frac{\frac{W_B}{Vol_C}}{\rho} \qquad (4.1)$$

where: PD = packing density [-]
W_B = weight of solids in a container [kg]
Vol_C = volume of the container [dm^3]
ρ = mean specific gravity of the solids [kg/dm^3]

Cumberland & Crawford [1987], German [1989] and Gray [1968] reviewed affecting parameters on packing density; Milewski [1973] and Yu & Zou [1998] discussed the effect of non-spherical particles on it. According to Gray [1968], the particles' characteristics, the container, the way of deposition and the treatment after deposition affect the porosity of the granular skeleton (Table 4.1).

Table 4.1 Affecting parameters on the packing density [after: Gray, 1968]

Particle	*Container*	*Deposition*	*After deposition*
Shape	Shape	Intensity	Vibratory compaction
Absolute size	Size	Velocity of deposition	Pressure compaction
Size distribution	Elasticity	Method	
Mass	Surface properties		
Elasticity			
Resilience			
Surface properties			

Concrete contains particles of different shapes. The porosity of the granular skeleton is low since particles in a wide range of sizes (cement and aggregates) are applied in concrete. Very small particles (e.g. micro- or nanosilica) widen the grading curve even more, but significantly increase the total surface area. The water demand depends on the interstices of the granular skeleton, the size, the shape and the content of each aggregate fraction. Surface forces affect the packing density of very small particles; frictional forces dominate the interaction between larger particles. Dispersed particles pack tighter compared with the same particles when agglomerated. To decrease the porosity of the granular skeleton of very fine particles, plasticisers and superplasticisers are applied. They disperse the cement and the fillers. The fewer interstices the aggregate skeleton contains, the less paste is required to fill them. The excess of the paste surrounds the solids and decreases the friction. Except of the surplus of paste, workability also depends on the characteristics of the cement paste and the surface characteristics of the aggregates.

Dependent on the origin of the aggregates (sea, river or crushed), their shape and surface characteristics might be rather different; cements and fillers also differ on these aspects. According to Wadell [1935], sphericity gives an indication of the shape and the surface characteristics of solids and is defined as the surface area of a sphere having the same volume as the particle divided by the surface area of the particle (Equation 4.2).

$$\psi = \left(\frac{d_v}{d_s} \right)^2 \tag{4.2}$$

where: ψ = sphericity [-]
d_v = diameter of a sphere having the same volume as the particle [mm]
d_s = diameter of a sphere having the same surface area as the particle [mm]

4.3 Compressible Packing Model (CPM)

The aim of developing the Compressible Packing Model (CPM) was to predict the packing density of polydisperse mixtures of grains; De Larrard [1999] presents the model in full detail. According to De Larrard, the error in absolute value is 0.77% for rounded grains and 1.77% for crushed aggregates. The model was validated with data from literature and results of experiments from different laboratories.

Based on the residual packing density (the virtual packing density of a single sized fraction), the interaction of smaller and larger particles is accounted for. Virtual means a degree of packing that is non-accessible in experiments; the grains have to be placed by hand into the optimum position. The interaction of a grain with larger particles results in a wall-effect, smaller particles exert a loosening-effect. The effect of the interactions between grains is assumed to be additive; no interaction between both effects was taken into account. For each fraction (i) a mixed residual packing density of this fraction can be calculated by applying Equation 4.3. The lowest number of all fractions results in the 'true' virtual packing density of the polydisperse mixture. The geometrical diameter ($d_g=(M_i \cdot M_{i-1})^{0.5}$) was applied as the equivalent diameter of each single size fraction [De Larrard, 1999].

$$\gamma_i = \frac{\beta_i}{1-\sum_{j=1}^{i-1}\left[1-\beta_i+b_{ij}\cdot\beta_i\left(1-\frac{1}{\beta_j}\right)\right]\cdot y_j-\sum_{j=i+1}^{n}\left[1-a_{ij}\cdot\frac{\beta_i}{\beta_j}\right]\cdot y_j};\ \gamma = Minimum(\gamma_i) \qquad (4.3)$$

where:
- γ_i = virtual packing density of a polydisperse mix (group i dominant) [-]
- β_i, β_j = residual packing density of a monodisperse mix of group i (j) [-]
- a_{ij} = loosening effect of grains of group j on group i [-]
- b_{ij} = wall-effect of grains of group j on group i [-]
- y_j = volume fraction group j relative to the total solid volume [-]
- γ = virtual packing density of a polydisperse mix [-]

The parameters a (loosening-effect, Equation 4.4) and b (wall-effect, Equation 4.5) of Equation 4.3 were experimentally determined and depend on the ratio of diameters of two different grain fractions [De Larrard, 1999].

$$a_{ij} = \sqrt{1-\left(1-\frac{d_j}{d_i}\right)^{1.02}} \qquad (4.4)$$

$$b_{ij} = 1-\left(1-\frac{d_i}{d_j}\right)^{1.50} \qquad (4.5)$$

where:
- d_i = geometrical diameter of grain group i [mm]; $d_i > d_j$
- d_j = geometrical diameter of grain group j [mm]

The actual packing density of the granular skeleton depends on the method of depositing the grains and the treatment after depositing (Table 4.1). The higher the applied level of energy transferred to the grains the higher the actual packing density becomes with the residual packing density as the upper limit. The effect of the packing method is taken into account for the CPM by the compaction index K (Equation 4.6). K needs to be experimentally determined for the deposition method under consideration.

$$K = \sum_{i=1}^{n} K_i = \sum_{i=1}^{n} \frac{\frac{y_j}{\beta_i}}{\frac{1}{\Phi} - \frac{1}{\gamma_i}} \qquad (4.6)$$

where: K = compaction index [-]
K_i = contribution of grain group i to the compaction index [-]
y_j = volume fraction group j relative to the total solid volume [-]
β_i = residual packing density of a monodisperse mix of group i [-]
Φ = solid volume of a granular mix, in a unit total volume [-]
γ_i = virtual packing density of a polydisperse mix (group i dominant) [-]

4.3.1 Wall-effects

A cylindrical container was applied to determine the packing density. Its size affects the packing density, which is due to the varying percentage of the volume perturbed by the walls compared with the unperturbed volume. The porosity of the granular skeleton of the bulk is lower compared with that of the disturbed area. Ben-Aïm [1970] limited the effect of a wall on the packing density of aggregates to a distance of half the diameter of a grain. The packing density of the disturbed area close to the walls decreases with a factor k_W. He proposed 0.88 for round and 0.73 for crushed aggregates respectively. Equation 4.7 describes the effect of a wall on the mean (actual) packing density:

$$\overline{\alpha} = (1 - v_p) \cdot \alpha + v_p \cdot k_W \cdot \alpha \qquad (4.7)$$

where: $\overline{\alpha}$ = mean packing density (affected by the container size) [-]
v_p = perturbed volume in a container [Vol.-%]
α = unperturbed packing density [-]
k_W = wall-effect aggregates [-]

Hoy [1998] investigated the effect of walls on the packing density of steel fibres by performing tests with two containers of different volumes. He found about the same packing density with steel fibres (L_f=30 mm) and container volumes of 2.7 and 7.0 litres. He assumed that fibres align more parallel to the walls with decreasing size of the container, which compensates for the increased perturbed volume of the smaller container. In his calculations he did not adjust the experimental packing density of the fibres for a wall-effect.

4.3.2 Approaches to include steel fibres into the CPM

Concept of the 'perturbed zone'

De Larrard [1999] proposed a method to include stiff steel fibres into the CPM-model. The perturbed volume of each grain fraction around the fibres was calculated by an inverse analysis from experiments of Bartos & Hoy [1996]. Subtracting half of the diameter of the grain fraction i under consideration of the fibre length, the length of a cylindrical or a rectangular volume v_p of a single fibre is obtained (Fig. 4.1). To calculate the volume v_P, this length is multiplied with the sum of the diameter of the fibre and the diameter of the grain times a fitting factor k_F. The best estimation of k_F was 0.065. The mean packing density can be calculated with Equation 4.8:

$$\overline{\alpha} = (1 - \phi_f - N_{sf} \cdot v_p) \cdot \alpha \qquad (4.8)$$

where: $\overline{\alpha}$ = mean packing density (affected by the container size) [-]
ϕ_f = percentage of fibres of the granular skeleton [-]
N_{sf} = number of steel fibres [-]
v_p = perturbed volume in a container [Vol.-%]
α = unperturbed packing density [-]

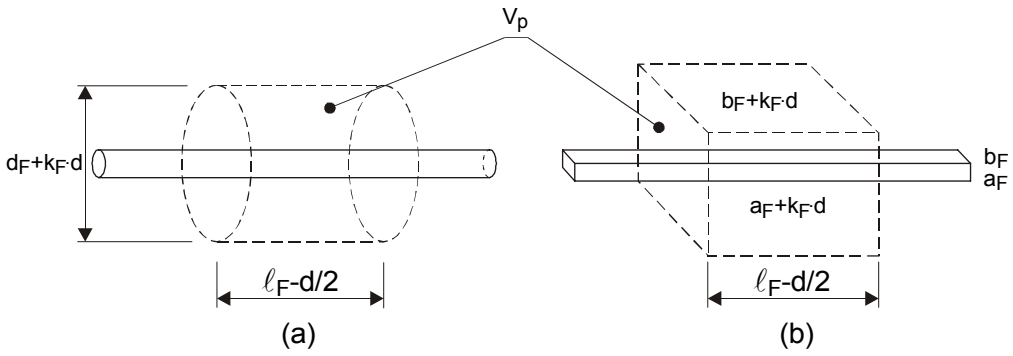


Fig. 4.1 Principle of the perturbed zone: wall-effect of grains around fibres [after: De Larrard, 1999]

Good predictions were obtained for stiff steel fibres up to an aspect ratio of 60; the accuracy was worse with flexible fibres (e.g. polypropylene fibres) or for stiff fibres at higher aspect ratios [De Larrard, 1999].

Concept of the 'equivalent packing diameter'

According to Yu & Zou [1998], the initial packing density of irregular particles depends on the shape and the size of the grains and the applied compaction energy. Yu et al. [1993] proposed the concept of the 'equivalent packing diameter' to include non-spherical particles into numerical simulations. Their approach was to relate the shape and the dimension of a non-spherical particle to the diameter of a fictitious sphere having an equivalent diameter that does not result in a change of the packing density

when combined with a spherical grain of the same diameter. The following equations were proposed to calculate the equivalent packing diameter:

Cylindrical shape [Yu et al., 1993]:

$$d_p = (3.1781 - 3.6821 \cdot \frac{1}{\psi} + 1.5040 \cdot \frac{1}{\psi^2}) \cdot d_v \quad (4.9)$$

Convex shape [Yu & Zou, 1998]:

$$d_p = \frac{d_v}{\psi^{2.785} \cdot \exp[2.946 \cdot (1-\psi)]} \quad (4.10)$$

where: d_p = equivalent packing diameter [mm]
ψ = sphericity [-]

The parameters ψ (sphericity, Equation 4.11) and d_V (volume diameter, Equation 4.12) of a fibre only depend on its dimensions. Sphericity is the 'ratio of the surface area of the sphere, having the same volume as the particle, to its actual surface area; the volume diameter is the 'diameter of a sphere having the same volume as the particle' [Yu et al., 1993].

Sphericity (ψ): $$\psi = 2.621 \cdot \frac{(L_f / d_f)^{2/3}}{1 + 2 \cdot (L_f / d_f)} \quad (4.11)$$

Volume diameter (d_v): $$d_V = 1.145 \cdot (L_f / d_f)^{1/3} \cdot d_f \quad (4.12)$$

where: d_f = fibre diameter [mm]
L_f = fibre length [mm]

To optimise SFRC, Hoy [1998] applied Yu's approach (Equation 4.9) in combination with an earlier version of the CPM, the 'Solid Suspension Model', which was developed by De Larrard & Sedran [1994]. In the study on SCFRC, the CPM was applied to calculate the packing density of the granular skeleton (aggregates and steel fibres). Hoy [1998] mentioned that the predictions are only of interest up to practical fibre contents; beyond these limits, the mixtures are not workable anymore. In order to determine the maximum fibre content of SCFRC, experimental studies were carried out with fibre contents close to the threshold (Chapters 5 and 6). Clustering of fibres counteracts the flow of SCC. Predictions with the CPM become less meaningful and probably less accurate beyond this threshold.

Three steps have to be followed to determine the packing density of mono- and polydisperse groups of grains or fibres for CPM simulations [De Larrard, 1999]. The appropriate K-index of the chosen compaction method is obtained with Equation 4.6;

the virtual packing density of a polydisperse mixture (γ) can be calculated with Equation 4.3. The packing density increases with each step ($\overline{\alpha} < \alpha < \beta$). The three steps are:

1) Determination of the packing density by an experiment (excl. wall-effect)

- of a single aggregate fraction ($\overline{\alpha}$), a granular mixture ($\overline{\Phi}$) or fibres

2) Adjustment of the experimental packing density (incl. wall-effect)

- of a single aggregate fraction (α), a granular mixture (Φ) or fibres (Equations 4.7 or 4.8 have to be applied)

3) Virtual adjusted packing density (includes the compaction method; K-index)

- calculation of the virtual packing density under consideration of Equation 4.13; the result is the residual packing density (β) of a fraction or a granular mixture of Equation 4.3.

4.4 Experimental set-up

4.4.1 Types of steel fibres used in experiments

The length and the weight of 48 fibres of one fibre type were determined. An 'equivalent fibre diameter' [CUR-Recommendation 35, 1994] was calculated with the assumption that the fibres are straight and round. Table 4.2 shows the characteristics of the applied steel fibres (first index: L_f/d_f; second index: L_f). The fibres differ in several ways; steel fibres with deviating minimum tensile strengths were applied. The Eurosteel 50/50 steel fibre is round and wave-shaped. The Harex 01/32-fibres are milled chips and are cut from steel. They are twisted and deformed at the ends. Dramix OL13/0.16 and Dramix OL6/0.16 steel fibres are straight without any deformation. The other fibre types are deformed at their ends (hooked ends) and, as Table 4.2 shows, some are glued in bundles to avoid fibre clustering during the mixing stage.

Table 4.2 Characteristics of the applied steel fibres

Fibre type	L_f	*Equivalent* d_f	*Aspect ratio* (L_f/d_f)	*Glued in bundles*	*Minimum tens. strength*
first index: L_f/d_f; second index: L_f	*[mm]*	*[mm]*	*[-]*		*[MPa]*
Dramix BP 80/60 C	61.06	0.713	85.66	Yes	2000
Dramix BN 80/60 C	57.94	0.761	76.10	Yes	1100
Dramix BN 45/50 L	51.09	1.063	48.08	-	1000
Eurosteel 50/50	47.77	1.043	45.81	-	-[2]
Dramix BN 65/40 C	41.24	0.635	64.94	Yes	1000
Harex 01/32	32.40	0.987	32.82	-	< 980
Dramix BP 80/30 C	30.48	0.388	78.50	Yes	2300
Dramix BN 45/30 L	28.80	0.621	46.34	-	1000
Harex 65/20	20.20	0.314	64.30	-	-[2]
Dramix OL 13/0.16[1]	13	0.16	81.25	-	2000
Dramix OL 6/0.16[1]	6	0.16	37.50	-	2000

[1]straight fibres: producer's information [2]no data available

4.4.2 Applied compaction methods

Aggregate fractions of the same batch were used throughout the research project on SCFRC; the composition of the sand and the coarse aggregates was kept constant. The composition was based on Vol.-%. The aggregates were dried in an oven at 105°C for 24 hours. In advance, the packing density was roughly estimated and the quantity of each fraction and/or steel fibres (with 15% surplus) was weighted out for the test. The aggregates were carefully mixed by hand for at least 60 s. The fibres were added and remixed for further 60 s or until they appeared homogenously distributed. Hoy [1998] also applied hand mixing in his experiments; it is questionable whether mixing in a mixer will produce a better distribution in case fibres are added; fibres also might bend due to the mixing process.

Compaction method: steel fibres and aggregates (standard)

Compaction is more effective on the packing density of fibres and irregular aggregates than on spherical particles [Hoy, 1998]. At a low compaction level the porosity between the fibres is high; the change in packing density is relatively larger at increasing compacting level compared with round grains. Hoy performed experiments according to the British Standard [BS 812: Part 2, 1975]. He found that the variation of this method was lower compared to pouring or vibrating. Still, the single results of his measurement showed significant scatter; to minimise the scatter a higher level of compaction energy was adopted. The applied compaction method was the following: First, a container (volume: 8.67 litres; to measure the Vebe-time) was filled in three equal layers; each layer was tamped 30 times by a rod. The falling height of the rod was 50 mm. This compaction method is similar to that of British Standard [BS 812: Part 2, 1975]; the size of the container differed. Next, two additional minutes of vibration (Vebe-instrument) with a compression force of 14 kg were applied. The weight was imposed by a second container (container: NEN 5961, 1988), which covered the complete surface. The surplus of solids was removed by striking up the top with the rod. The fibres (tests with fibres alone) were carefully removed by hand not to disturb the packing.

Compaction method: wall-effect steel fibres

In BS 812: Part 2 [1975], the number of blows with the rod is related to the size of the container, which has to be chosen in accordance with the maximum size of the aggregates. In order to determine the wall-effect at deviating containers sizes, the same compaction energy has to be applied. It is questionable whether the number of rod blows is comparable for different container sizes, even when the number of blows would be different. For this reason, another compaction method was chosen: Two different containers were used; the heights of the containers were about the same (Table 4.3).

Table 4.3 Dimensions of the containers to determine the wall-effect of the steel fibres

	Big container	*Small container*
Height [mm]	192	212
Diameter [mm]	239.7	185.6
Volume [dm^3]	8.67	5.73

The fibres were filled into the container without adding any compaction energy (max. falling height: 100 mm). Both containers were vibrated (Vebe-instrument) for two minutes; no weight was placed on the top of the containers. The smaller container was fixed inside the larger container to transmit the vibrations. During vibration, sufficient surplus of the fibres was added to keep the container filled. The surplus of fibres to the volume of the container was carefully removed by hand in order to keep the structure of the fibres as undisturbed as possible.

Compaction method: cement paste

A centrifuge (producer: Dumee, Jouan: E82N) was applied to compact the solids and to determine the surplus of water, which allowed calculating the packing density of the paste. After mixing the paste, four plastic beakers were filled; centrifuging was carried out for 10 minutes at 4000 rounds per minute. The surplus of water was removed with a pipette after the test; the weight of the beakers before and after centrifuging was determined. Considering the water surplus and the composition of the cement paste the packing density was calculated. The results on the packing density of cement paste are listed in Appendix F (Table F1).

4.5 Packing density: experimental results and predictions

The CPM is a tool to determine the packing density of spherical grains with sufficient accuracy [De Larrard, 1999]. In order to make the CPM applicable for SCFRC, four studies were carried out:

- *Wall-effect of the steel fibres:* The fibres are large compared with the diameter of the aggregate fractions; walls might have an even more significant effect on the 'initial packing density of the particles' compared with the aggregates.
- *K-index of the applied compaction method:* The applied compaction method affects the packing of fibres [Gray, 1968]. The energy applied to compact the granular skeleton in this study was intermediate between that of Hoy [1998] and De Larrard [1999]; the compacting index of the chosen method had to be experimentally determined.
- *Experimental packing density of steel fibres and aggregates:* The packing densities of each aggregate fraction and almost all fibre types were determined.

- *Five approaches to include the steel fibres into the CPM-model:* The accuracy of five approaches was determined and compared with the experimental packing density.

4.5.1 Wall-effect of the steel fibres

The K-Index links the actual with the virtual packing density of a monodisperse fraction and indicates the compaction level (Equation 4.13). De Larrard [1999] proposed K-indices for different compaction levels: pouring resulted in a K-index of 4.1, sticking with a rod in 4.5 and vibration in a K-index of 4.75. According to De Larrard [1999], the compaction index K of a monodisperse fraction links the virtual and the actual packing densities by Equation 4.13; the virtual packing density of the fibres becomes:

$$K = \frac{1}{\beta / \Phi - 1} \qquad \text{Reformulated: } \beta = \Phi \cdot (1 + 1/K) \qquad (4.13)$$

where: K = compaction index [-]
β = virtual packing density of a monodisperse mix [-]
Φ = solid volume of a granular mix, in a unit total volume [-]

With the assumption that the compaction index (K) of the tests with two different containers was the same (compaction method: wall-effect steel fibres), the wall-effect of the fibres was calculated. The virtual packing density (Equation 4.13: β) is the same in both containers but unknown. The actual packing density was replaced by the mean packing density of each container, which is affected by the walls of the container (Equation 4.7). The influencing area within which the fibres disturb the packing density was assumed to be the complete fibre length; the top and the bottom of the container were assumed to be walls, too. With the previous assumptions a single equation was obtained with two unknown parameters: the wall-effect and the virtual packing density.

A numerical solution was obtained with the Excel-solver and the criterion that the virtual packing density had to be the maximum; Appendix C (Table C1) summarises the results. Fig. 4.2 shows the wall-effect of steel fibres (k_{SF}) within an area of one fibre length (Dramix 45/50 was not tested).

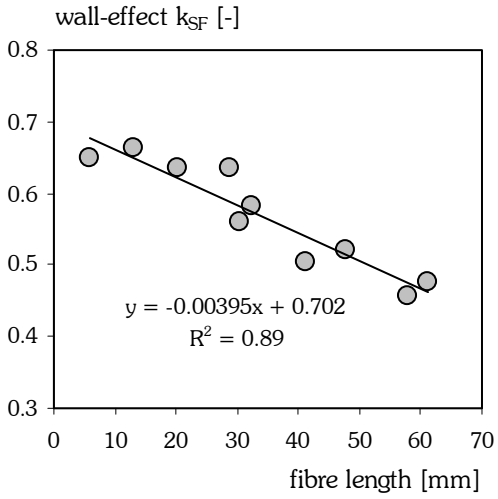


Fig. 4.2 Effect of the fibre length on the wall-effect k_{SF} (influence length = L_f)

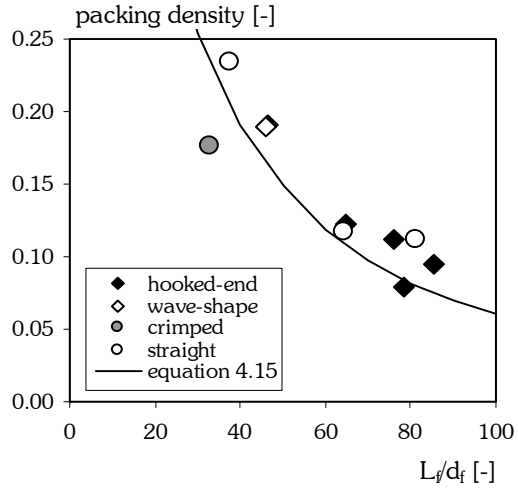


Fig. 4.3 Effect of the aspect ratio on the virtual, undisturbed or dense (Equation 4.15) packing density of steel fibres

The longer the fibre the higher the porosity is within the disturbed area. Fig. 4.3 shows the related maximum (virtual) packing density. The packing density decreased at increasing aspect ratio. The milled Harex 01/32 fibre deviated from other types of steel fibres, due to its irregular shape. The wall-effect k_{SF} of steel fibres within an area of one fibre length can be approximated with Equation 4.14 (Fig. 4.2):

$$k_{SF} = 0.702 - 0.00395 \cdot L_f \tag{4.14}$$

where: k_{SF} = wall-effect of a steel fibre (experimental result) [-]
L_f = fibre length [mm]

Zou & Yu [1996] suggested a formula to approximate the experimental (dense) packing density of cylinders (Equation 4.15). Fig. 4.3 compares analytical and numerical results.

$$\ln \varepsilon_{Od,cyl} = \Psi^{6.74} \cdot \exp[8.00 \cdot (1 - \Psi)] \cdot \ln 0.36 \tag{4.15}$$

where: $\varepsilon_{0d,cyl}$ = dense (experimental) packing density of fibres [-]
ψ = sphericity [-]

Equation 4.15 might be applied to approximate the virtual packing density of steel fibres, but it slightly underestimates the results of the analysis. Equation 4.15 is an approximation of experimental data, while the data points of Fig. 4.3 are virtual packing densities (solver solutions). Fig. 4.4 shows the packing density as a function of sphericity. The highest packing density is achieved with particles that are almost spherical.

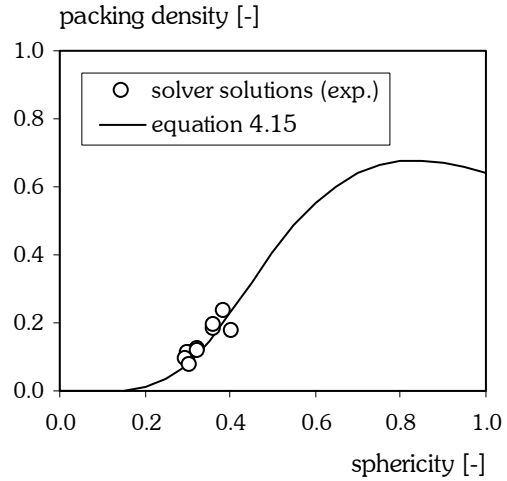


Fig. 4.4 Virtual packing density (solver solutions) versus predictions obtained with Equation 4.15

4.5.2 K-index of the applied compaction method

The composition of the applied aggregates and the packing density of each fraction are summarised in Table 4.4. The aggregates originated from the Netherlands (river and crushed). The sand grains (0.125-4 mm) were rounder compared with the coarse aggregates, this fact is reflected by the packing density of the fraction itself. The initial packing density of each aggregate fraction (Table 4.4) and the type of steel fibre were determined in experiments and were input parameters for the CPM. The wall-effect of the aggregates and the fibres and the maximum (virtual) packing density are further input parameters.

Table 4.4 Packing density and distribution of the aggregate fractions

Fractions	*0.125-0.25*	*0.25-0.5*	*0.5-1.0*	*1.0-2.0*	*2.0-4.0*	*4.0-8.0*	*8.0-16.0*	*4/16 crushed*
Packing density	0.611	0.653	0.653	0.642	0.648	0.630	0.631	0.624
Sand	9.3%	30.2%	30.2%	18.6%	11.7%	-	-	-
Coarse aggregate	-	-	-	-	-	35.1%	64.9%	-

To determine the compaction index K (Equation 4.6), the fraction 1-2 mm was used as the reference fraction. The content of the 1-2 mm fraction was successively replaced by aggregates of other fractions (in steps of 10 Vol.-%). Three series of tests were carried out: with 0.5-1, 2-4 and 4-8 mm fractions. The packing density was determined according to the standard compaction method. The K-index that fitted the results best was 3.6 and was lower compared with what De Larrard [1999] recommended for this compaction level (4.5-4.75). He found a higher compaction index, in spite of lower initial packing densities of the aggregate fractions. A lower K-index indicates that the applied compaction process was less effective in compacting the granular skeleton. As was discussed by Hoy [1998], the shape of a particle also determines the sensitivity towards a specific compacting method. Appendix B provides an overview on results of

the study on the K-index. The mean error of the three series for this K-index was 0.46-0.62%, with a maximum error of 0.81-1.18%.

4.5.3 Experimental packing density of steel fibres and aggregates

The content sand of total aggregate was varied from 0-100 Vol.-% and different types and contents of the steel fibres were tested. The applied fibre contents were 1.5 and 3.0 Vol.-% of the granular skeleton. It was not possible to test 3 Vol.-% for fibres having an aspect ratio of 60 or higher since fibre clustering counteracted a homogenous distribution of the fibres. Fig. 4.5 shows the effect of different sand contents and fibre types (at 1.5 Vol.-%) on the packing density. The average of three measurements and the variation are summarised in Appendix C (Tables C4-6).

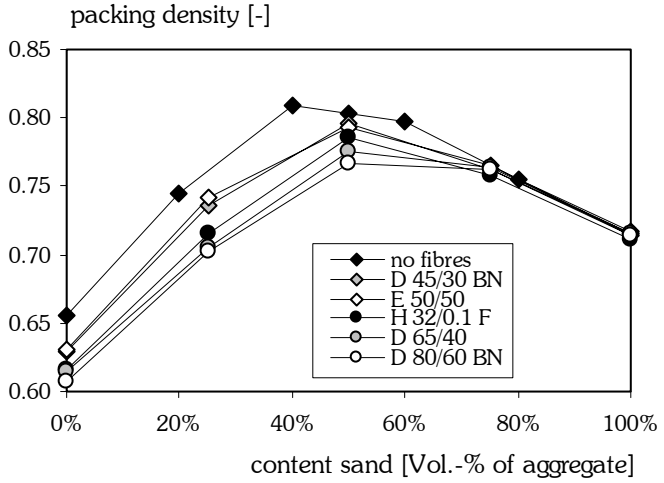


Fig. 4.5 Effect of the sand content and the type of the steel fibres (at 1.5 Vol.-%) on packing density

The actual fibre content in SCC at 1.5 Vol.-% of the granular skeleton is lower, since SCC also contains paste: assuming a paste content of 38 Vol.-% the content of steel fibres equals 0.93 Vol.-%. The effect on the packing density was remarkable even at low fibre contents; more paste has to be added to compensate for the addition of the fibres. The higher the aspect ratio and the lower the content of sand the more pronounced the effect on packing density is. At sand contents of 75 Vol.-%, about the same packing density was found for different types of steel fibres. The relative size between the fibre and the aggregates also affects the packing density. The maximum decreases and shifts towards higher sand contents. To compensate for the effect of the fibres the mixture composition has to be adjusted by increasing the content of grains that are relatively small compared with the fibre length. The same result was numerically obtained by Hoy (Fig. 3.6). Fig. 4.5 shows that the maximum was in the range of sand to total aggregate contents of 50-75 Vol.-%; 57 and 68 Vol.-% were tested at different paste contents in parameter studies on SCFRC (Chapter 5.2.1).

Experiments were also carried out with coarse aggregates and steel fibres. Fig. 4.6 shows the decrease of the packing density at increasing fibre content (round aggregates: 4-16 mm). The fibre content was increased in steps of 0.5 Vol.-% (1.0 Vol.-% for fibre contents > 2.0 Vol.-%). The degree to which the packing density decreased depended on the aspect ratio of the fibres. Each point represents the average of three measurements; the results are summarised in Appendix C (Tables C2-3).

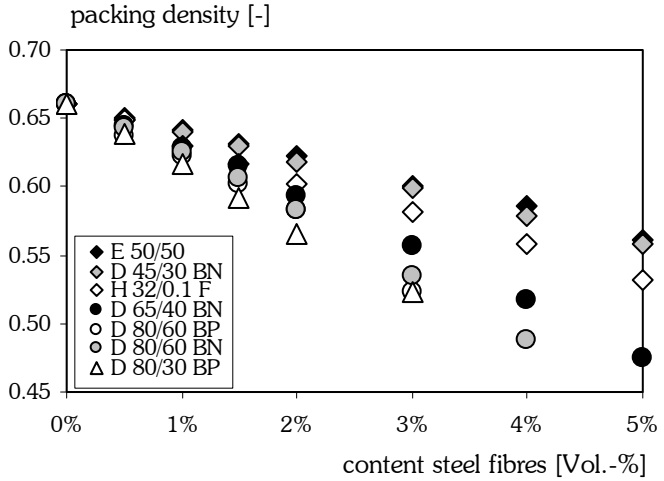


Fig. 4.6 Packing density of coarse aggregates (4-16 mm) and different types and contents of steel fibres

Not all fibre types could be tested up to 5 Vol.-% due to the clustering of the fibres during mixing and shovelling. It was observed that at a defined fibre content clustering occurred no matter what the composition of the aggregates was. The rigid structure of the fibres counteracts the flow (Fig. 4.7).

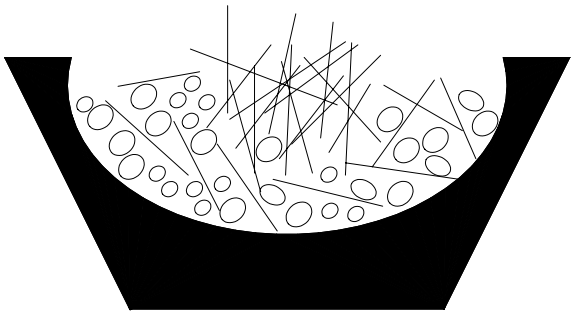


Fig. 4.7 Formation of a stiff structure of fibres and aggregates

4.5.4 Five approaches to include steel fibres into the CPM

In order to check the accuracy of the CPM to predict the packing density of SCFRC, two series of experiments were compared with simulations: First, the packing density of the aggregates and the steel fibres of eight optimised mixtures (for bending tests, Chapter 8) was determined. The approach with the best accuracy was chosen for further

simulations. Second, mixtures with sand, coarse aggregates and steel fibres at 1.5 and 3.0 Vol.-% (Appendix C, Tables C4-6) were used to determine the accuracy of the predictions. Whether or not the wall-effect is included affects the virtual packing density of a single fraction or fibres; the higher the virtual packing density of a single fraction the higher the virtual packing density of the mixture becomes. In order to compare experiments and simulations, the wall-effect has to be excluded, which lowers the virtual packing density of each component and of the mixture. The factor k_W (Chapter 4.3.1) was set 1.0 in all cases, the factor k_{SF} was 1.0 (=excl. wall-effect) or was taken equal to the experimental result (=incl. wall-effect, Fig. 4.2). Five approaches are compared to include the fibres:

- *A1: Model Yu 1 (Equation 4.9, cylinders), experimental PD, excl. wall-effect:*

The packing density of the fibres was obtained from packing experiments (K=3.6). The equivalent packing diameter (Equation 4.9) was calculated. No wall-effect (k_{SF}=1.0) was included for the estimation of the virtual packing density, which means that the experimental result was not adjusted for the wall-effect.

- *A2: Model Yu 1 (Equation 4.9, cylinders), analytical PD, incl. wall-effect:*

Equation 4.9 (model Yu 1) was adopted; the maximum (virtual) packing density of each fibre type was applied (numerical solution from solver of the study on the wall-effect). No adjustment for the effect of the walls was made.

- *A3: Model Yu 1 (Equation 4.9, cylinders), experimental. PD, incl. wall-effect:*

The virtual packing density of the steel fibres was calculated from the experimental packing density under consideration of the wall-effect (experimental results: Fig. 4.2) and the applied compaction process (K=3.6).

- *A4: Model Yu 2 (Equation 4.10, convex shape), experimental PD, excl. wall-effect:*

Equation 4.10 was applied to include the fibres into the CPM. The experimental packing density (K=3.6) was not adjusted for the wall-effect of the container (k_{SF}=1.0).

- *A5: Model De Larrard (k_F = 0.065), concept 'perturbed zone':*

De Larrard [1999] proposed the concept of the perturbed zone to include steel fibres into the CPM, which takes into account the wall-effect of each fibre in the vicinity of an aggregate grain.

Fig. 4.8 shows the experimental packing density of mixtures 1-7 (Table 4.5) compared with simulations of the CPM and for five different approaches to include the fibres. The packing density of mixture 8 was much lower (0.657) and is excluded from Fig. 4.8. Mixtures 1-7 are concretes ($d_{g,max}$=8 or 16 mm), while mixture 8 is a mortar ($d_{g,max}$=1 mm).

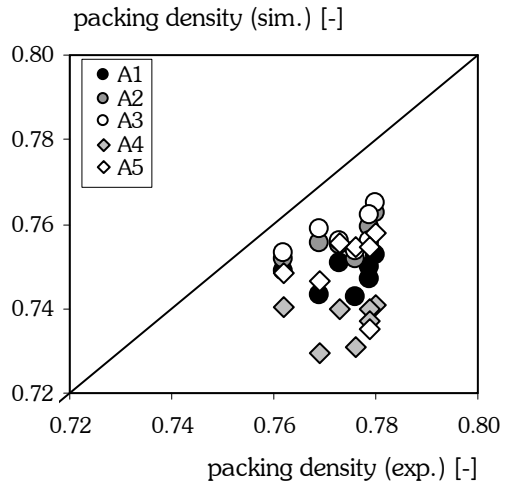


Fig. 4.8 Five approaches to include the steel fibres into the CPM: experiments versus simulations

All simulations on the packing density of mixtures 1-7 underestimated the experimental results. Table 4.5 shows the deviation of the simulations from the experimental results. The compositions of mixtures of Table 4.5 are summarised by Appendix D (Table D2).

Table 4.5 Comparison of five approaches to include steel fibres into the CPM (deviation of experimental results and simulations)

Mix No.	*Mixture (Table 8.1)*	*Fibre type*	*V_f [kg/m^3]*	*Exper. PD*	*A1*	*A2*	*A3*	*A4*	*A5*
					error (experiment-simulation)				
PD 1	3/9	D 65/40	100	0.769	0.026	0.014	0.010	0.040	0.023
PD 2	2/8	D 80/30	60	0.776	0.033	0.024	0.022	0.045	0.021
PD 3	1/7/11	D 80/60 BP	60	0.780	0.027	0.017	0.015	0.039	0.022
PD 4	4/10/12	D 45/30	140	0.779	0.032	0.024	0.023	0.039	0.044
PD 5	13	D 80/60 BP	60	0.779	0.029	0.020	0.017	0.042	0.025
PD 6	5	D 80/30	40	0.773	0.022	0.018	0.017	0.033	0.018
PD 7	6	H 65/20	60	0.762	0.013	0.010	0.009	0.022	0.014
PD 8	14	OL 13/0.16	125	0.657	-0.021	-0.028	-0.027	0.001	-0.004
		Mean error (mix 1-8)			*0.025*	*0.019*	*0.018*	*0.033*	*0.021*
		Mean error (mix 1-7)			*0.026*	*0.018*	*0.016*	*0.037*	*0.024*

Approach A3 (Model Yu 1, Equation 4.9, cylinders, exp. PD, incl. wall-effect) was closest to the experimental results; the results of approach A2 were close to that of A3. Since all approaches underestimated the experimental packing density of mixtures 1-7, the approach that gave the highest virtual packing density of the fibres resulted in the best accuracy. The mean error of mixtures 1-7 was 0.018 with an average variation of 2.1% (mixtures 1-8: 0.019 and 2.3%).

Hoy [1998] concluded from experiments with containers of different sizes that no wall-effect has to be taken into account since the packing density in a small container was the same as in a large container. This might, however, be the result of different levels of compaction. In contrast to the results of Hoy, higher packing densities were obtained in a larger container, which is reflected in the wall-effect (Fig. 4.2). The walls increased the

porosity in case only fibres were tested. In contrast, such an increase of porosity was not observed once the fibres were mixed with aggregates. The aggregates completely filled the space between the walls and the fibres. To take this fact into account, the experimental packing density of the fibres must be adjusted for the wall-effect, which increases the virtual packing density. The effect of including the walls is reflected by the improvement of the accuracy from approach A1 to A3. In the following, approach A3 is applied to predict the packing density of the granular skeleton of SCFRC.

Further investigation on the accuracy of predictions for approach A3

The packing density of a second series of mixtures was determined and compared with predictions of the CPM in combination with approach A3. The applied sand to total aggregate contents were 100, 75, 50, 25 and 0%. Table 4.6 shows a summary of the mean and the maximum errors of the predictions. Appendix C (Table C5-6) presents the results of simulations with the CPM and experiments.

Table 4.6 Mean and maximum errors (in average) of the CPM predictions and approach A3 (experimental data, incl. wall-effect)

Fibre	V_f	*Mean error*		*Maximum error*	
type	*[Vol.-%]*	*error*	*deviation*	*error*	*deviation*
D 45/30	1.5	0.012	1.7%	0.020	3.1%
	3.0	0.016	2.3%	0.029	4.0%
ES 50/50	1.5	0.015	2.1%	0.031	4.9%
	3.0	0.022	3.3%	0.047	7.8%
H 32/0.1	1.5	0.013	1.9%	0.021	3.2%
	3.0	0.012	1.8%	0.018	3.1%
D 65/40	1.5	0.017	2.5%	0.032	5.2%
D 80/60	1.5	0.022	3.4%	0.047	7.7%
Mean error		*0.016*	*2.4%*	*0.031*	*4.9%*

The mean of the predictions was about the same as for the mixtures for the bending tests (Table 4.5). Hoy [1998] found that the 'Solid Suspension Model' overestimates the packing density of fibres with sand or coarse aggregates, whereas it underestimates it at 50% sand to total aggregate. The accuracy of the prediction thus depends on the composition of the aggregates. Fig. 4.9 shows the comparison between the experimental and numerical results on the packing density. The CPM slightly underestimate the packing density at high packing densities (Fig. 4.9), while it overestimates it in case fewer fractions were applied (sand or coarse aggregates). Mixture 8 contained only three fractions, and the packing density was overestimated. Therefore, the accuracy of the predictions for mortars with fibres is expected to be worse.

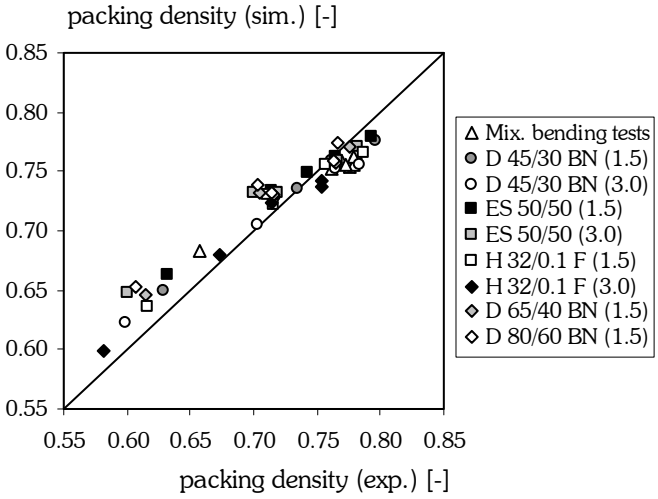


Fig. 4.9 Experimental and numerical results (for approach A3) on the packing density of the granular skeleton (fibre content in Vol.-%)

The sand to total aggregate ratio of mixtures with a maximum aggregate size of 16 mm (mixtures 1-5) was 68 Vol.-%. Table 4.7 shows the results at sand to total aggregate ratios of 50 and 75 Vol.-%; the accuracy of the predictions improved at 75 Vol.-%.

Table 4.7 Comparison of simulations (with approach A3) and experimental results on the packing density at sand to total aggregate contents of 50 and 75 Vol.-%

Fibre		*- at 50% sand -*			*- at 75% sand -*		
type	*[Vol.-%]*	*exp.*	*difference*	*error*	*exp.*	*difference*	*error*
D45/30	1.5	0.7962	0.020	2.5%	0.7616	0.002	0.3%
	3.0	0.7843	0.029	3.7%	0.7644	0.013	1.6%
ES 50/50	1.5	0.7931	0.014	1.7%	0.7647	0.002	0.3%
	3.0	0.7815	0.011	1.4%	0.7656	0.007	0.9%
H 32/0.1	1.5	0.7863	0.021	2.7%	0.7575	0.002	0.3%
	3.0	0.7543	0.017	2.3%	0.7538	0.011	1.5%
D 65/40	1.5	0.7760	0.006	0.7%	0.7640	0.006	0.8%
D 80/60	1.5	0.7670	0.007	0.9%	0.7630	0.004	0.5%
Mean			*0.016*	*2.0%*		*0.006*	*0.8%*

The mean error was 2.0% at 50 Vol.-%, while it was 0.8% at 75 Vol.-%. The mean error of the CPM-model without steel fibres according to De Larrard [1999] was 0.77% for round aggregates and 1.77 % for crushed aggregates. The CPM and approach A3 were applied to predict the packing density of the granular skeleton of SCFRC. The paste surplus of SCFRC with a maximum aggregate size of 8 or 16 mm was slightly overestimated and underestimated for mortar mixtures. The prediction of the packing density of mortars with fibres is less accurate.

4.6 Concluding remarks

The packing density (the complement of the porosity) of a granular skeleton determines the amount of cement paste that is required to fill the interstices. Any surplus of paste contributes to a better workability by reducing the friction between fibres and aggregates. Minimising the porosity also reduces material costs and affects paste-related aspects of concrete like shrinkage. Steel fibres increase the porosity of the granular skeleton; the degree of the increase depends on the relative size of the aggregate grains to the fibre length. In order to predict the packing density of the granular skeleton, the Compressible Packing Model (CPM) was applied. Five approaches were tested and compared with results of experiments to obtain the best accuracy. To apply the CPM, the initial packing density of the components, the wall-effect of the fibres and the compaction index of the chosen compaction method were determined. The accuracy of the predictions depends on the composition of the aggregates. The simulations had an average error close to 2% for optimised mixtures with aggregates up to 8 or 16 mm; predictions of the packing density of mixtures with smaller maximum aggregate sizes are less accurate.

Chapter 5:

Experimental parameter studies on SCFRC in the fresh state

5.1 Introduction

This chapter describes three experimental parameter studies on the characteristics of SCFRC in the fresh state. The type and the content of the steel fibres was varied; self-compacting mixtures without fibres were used as a reference. Criteria have been proposed to design and judge the self-compactability of SCFRC. A study was carried out to determine design criteria and the effect of the fibres on filling ability, passing ability and segregation resistance of SCC; the applicability of test methods was investigated. The fibre contents were varied in order to find the maximum possible fibre content. Besides a preliminary study, two additional studies were conducted, one with self-compacting mortars and short steel fibres and one on SCC to optimise the mixture composition for SCFRC. This chapter presents the experimental set-up, the compositions of the reference mixtures, the applied fibre types and contents, mixing procedures and test methods. It also includes design criteria and characteristics of SCC and SCFRC in the fresh state.

5.2 Methods and materials

Three parameter studies were performed to determine the effect of different types and contents of the steel fibres on the characteristics of SCC in the fresh state.

- *Preliminary study (PS, 31 mixtures):* Four reference SCC mixtures were composed according to the Japanese design method (Chapter 2.4.1) and tested. The sand content of mortar was constant at 40 Vol.-%, whereas the paste content was varied. The maximum aggregate size was 16 mm.

- *Optimisation study (OS, 65 mixtures):* Based on the preliminary study on the granular skeleton (Chapter 4.5.3), nine reference mixtures were composed. They differed in the sand to total aggregate content, the composition of the cement paste and the maximum aggregate size.

- *Mortar study (MS, 25 mixtures):* Three reference mortars at defined characteristics in the fresh state and different aggregate contents were applied to

determine the characteristics of different types, contents and combinations of short steel fibres (fibre lengths: 6 and 13 mm).

5.2.1 Experimental program

Reference SCC mixtures

Table 5.1 shows the composition (in Vol.-%) of sixteen self-compacting mixtures without steel fibres. The target slump flow of the mixtures of series PS/OS was 710±20 mm (mixture PS1: 743 mm); the V-funnel flow-time was 10±2 s. Several mixtures of series OS (paste content of 39.0 Vol.-% or $d_{g,max}$= 8 mm) were composed to achieve a shorter flow-time (9±1 s) to compensate for the smaller impact of the aggregates on the flow-time. The size of the V-funnel applied to test mixtures of series PS differed from that of series OS/MS; Appendix A (Figs. A2-3) shows both V-funnels. The target flow-time (mortar funnel) of series MS was 10±2 s. The criterion for the mortar flow of series MS was 245±20 mm.

Table 5.1 Mixture composition of 16 self-compacting reference mixtures (in Vol.-%)

No.	*Mixture coding*	*Fine aggregates (0.125-4 mm)*	*Coarse aggregates (4-16 mm)*	*Paste content (<0.125 mm)*	*Compressive strength class*
	Preliminary study				
1	PS 1, 37.2/35.1	23.40	39.50	35.10	B45
2	PS 2, 40.2/36.9	24.59	36.52	36.89	B45
3	PS 3, 43.9/38.9	25.95	33.13	38.92	B45
4	PS 4, 47.9/41.0	27.31	29.72	40.97	B45
	Optimisation study				
5	OS 1-57.0/36.5	35.10	26.40	36.50	B65
6	OS 2-57.0/39.0	33.63	25.37	39.00	B65
7	OS 3-68.0/36.5	41.82	19.68	36.50	B65
8	OS 4-68.0/39.0	40.12	18.88	39.00	B65
9	OS 5-68.0/34.0	43.52	20.48	34.00	B45
10	OS 6-68.0/36.5	41.82	19.68	36.50	B45
11	OS 7-68.0/39.0	40.12	18.88	39.00	B45
12	OS 8-70.0/37.7	42.21	18.09 (4-8 mm)	37.70	B65
13	OS 9-70.0/40.0	40.60	17.40 (4-8 mm)	40.00	B65
	Mortar study				
14	MS 1-40	40.0	-	60.0	B65
15	MS 2-50	50.0	-	50.0	B65
16	MS 3-55	55.0	-	45.0	B65

The composition of the pastes and the aggregates are summarised in Appendix D (Table D1); the characteristics of the applied materials are shown in Appendix E. The following parameters were varied: the type and the content of the steel fibres, the maximum aggregate size as well as the content and the composition of the granular skeleton. The target compressive strength of series PS and OS5-7 was B45; this was B65 for series OS1-4 and OS8-9. The compressive strength was not a design parameter of series MS. The air content of series OS/PS was assumed to be 2.0 Vol.-% (series MS: 0 Vol.-%) for the design of the mixtures. It was concluded from packing experiments (Chapter 4.5.3) that the maximum packing density is in the range of the ratios sand to

total aggregate of 50-75 Vol.-%: ratios of 57 and 68 Vol.-% were tested. The content and the composition of the cement paste differed. The maximum aggregate size of series PS1-4 and OS1-7 was 16 mm (OS8-9: 8 mm; MS1-3: 4 mm). The ratio sand to total aggregate of series OS8-9 was kept constant at 70 Vol.-%.

SCC with steel fibres

Each reference mixture was considered to be stable. The fibre contents of series PS/OS were increased in steps of 20 kg/m^3 (series MS: 0.5 Vol.-%) to determine the maximum fibre content of each reference mixture and the applied fibre type. Table 5.2 shows the test program; each mixture was tested once. In total 121 mixtures were tested; 16 mixtures contained no fibres. Depending on the response of the previous mixture, it was decided whether to increase or decrease the fibre amount. The changing flow patterns were studied around the threshold of the maximum fibre content (Chapter 5.3). With this test set-up it was possible to determine the limit of every mixture. In order to adjust the mixture composition for the addition of the fibres, their volume was replaced against the same volume of the coarse aggregates (series PS), against aggregates (the ratio sand to total aggregate was kept constant) for series OS and against fine aggregates for the series MS respectively.

Table 5.2 Applied types and contents of the steel fibres (series PS/OS: kg/m^3; series MS: Vol.-%)

Fibre type	*D-45/30*	*ES-50/50*	*D-65/40*	*D-80/60 BN*	
Series PS (kg/m^3)					
PS 1, 37.2/35.1	40/60/80	-	-	20/40	
PS 2, 40.2/36.9	80/100	60/80	40/60	40/60	
PS 3, 43.9/38.9	80/100/120	60/80/100	40/60/80	40/60/80	
PS 4, 47.9/41.0	100/120	-	-	-	
Fibre type	*D-45/30*	*D-65/40*	*D-80/30 BP*	*D-80/60 BP*	*H-65/20*
Series OS (kg/m^3)					
OS 1-57.0/36.5	80/100	-	40/60	40/60	-
OS 2-57.0/39.0	120/140	-	60/80	40/60	-
OS 3-68.0/36.5	120/140	-	40/60	40/60	-
OS 4-68.0/39.0	120/140/160	100/120	60/80	60/80	-
OS 5-68.0/34.0	100/120	-	40/60	40/60	-
OS 6-68.0/36.5	120/140	-	60/80	40/60	-
OS 7-68.0/39.0	120/140	80/100	60/80	60/80	-
OS 8-70.0/37.7	-	-	20/40	-	40/60
OS 9-70.0/40.0	-	-	40/60	-	40/60/80
Fibre type	*D-OL6*	*D-OL13*	D-OL6+OL13	*D-OL6+OL13*	*D-OL6+OL13*
Series MS (Vol.-%)					
MS 1-40	1.0/3.0/4.0/5.0	1.5/2.0/3.0	1.5+1.5	2.0+0.5	2.0+1.0
MS 2-50	3.0/4.0	1.0/1.5/2.0	1.5+1.5	2.0+0.5	2.0+1.0
MS 3-55	1.5/3.0	1.0/1.5	-	-	-

5.2.2 Aggregate preparation

Sand (0.125-4 mm) and coarse aggregates (4-16 mm) were combined from fractions, which were delivered in plastic bags and were from the same stock. The aggregates (round) origin from Dutch rivers. The aggregates were prewetted to avoid mixture

stiffening due to the absorption of water directly after mixing. To assure stable moisture conditions of the aggregates within the container the following procedures were applied:

The coarse aggregates of series PS were kept under water for 24 hours and were refilled into another container. In order to realise a constant water surplus of aggregates throughout the container, another method was applied for series OS. The coarse aggregates were stored on a sieve in a plastic container and had to remain under water for 24 hours. Through an opening gap below the sieve the water was allowed to drain between the aggregates. The tap was closed once the water stopped to drain and the upper side was sealed with a cover and an extra plastic foil.

The sand fractions were premixed; water (2.2% by weight of the fine aggregate) was added during the mixing process. The prewetting of the fine aggregates was also necessary to avoid the segregation of especially the finest fractions from the bulk.

5.2.3 Mixing procedures

A forced pan type of mixer (Zyklos) with a maximum capacity of 120 litres was used (series PS/OS). The volume of a batch with fibres was kept constant at 40 litres. A smaller forced pan type of mixer (Zyklos) with a maximum capacity of 25 litres was used to prepare mixtures of series MS. The volume of each batch was 16 litres. Fig. 5.1 shows the mixing procedure.

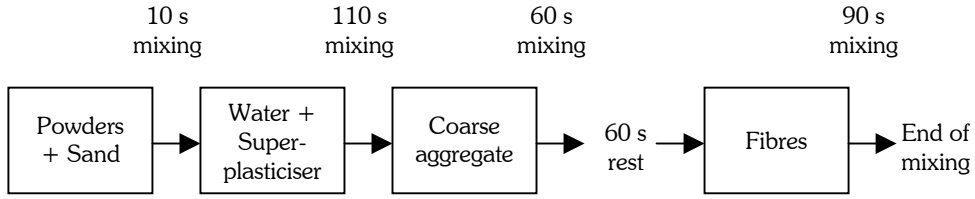


Fig. 5.1 Mixing procedure for SCFRC (Zyklos mixers)

5.2.4 Evaluation methods for SCC and SCFRC

Rheological measurements

The BML-Viscometer (Fig. 5.2) is a coaxial cylindrical viscometer, with which the rheological characteristics of coarse particle suspensions like mortar and concrete can be measured [Wallevik, 2000]. It consists of a system of inner and outer cylinders. An electric motor controls the speed of the outer cylinder, whereas the inner cylinder registers the torque by the use of a load cell.



Fig. 5.2 BML-Viscometer

The rotation velocity of the outer cylinder was increased up to its maximum. Once it was reached, the velocity was decreased. Table 5.3 presents the settings of the measurements. Rheological measurements were carried out with mixtures of series OS.

Table 5.3 Test set-up of measurements with the BML-Viscometer (series OS)

Experimental set-up BML-Viscometer	
Radius inner cylinder [cm]	10.0
Radius outer cylinder [cm]	14.7
Height inner cylinder [cm]	20.0
Max. rotation velocity [rps]	0.39
Min. rotation velocity [rps]	0.03
Number of measuring points	7
Number points/measurement	50
Transient interval [s]	0.4
Sampling interval [s]	2.0

Filling ability (slump flow, flow-time T_{50})

The slump flow test was applied to determine the filling ability of SCFRC (Appendix A, Fig. A11). After keeping a waiting period of 30 s, the Abrams' cone was lifted. The 'slump flow' is the mean diameter of the two measured diameters (the largest and the one perpendicular to it). The time of the flow front to first reach a prescribed circle of 500 mm (T_{50}) after lifting the cone was also recorded. The stopwatch was started once the concrete started to flow.

Filling ability (V-funnel, Fibre funnel, Mortar funnel)

The rate of deformation through a funnel depends on three key characteristics of SCC. In case blocking and segregation do not occur, the flow-time is related to the plastic viscosity [Níelsson & Wallevik, 2003]. Preliminary tests with the V-funnel indicated that long steel fibres might cause blocking; a larger funnel was used to test SCFRC. Each

funnel test was carried out twice; a rest of 30 s was kept before the outlet was opened. The applied funnels are presented by Appendix A (Figs. A1-4).

Segregation resistance (wash-out test)

Fig. 5.3 shows the principle of the test on the static segregation resistance of series OS. Directly after mixing, a sample of about 5 litres was put into a plastic beaker. After a rest of 15 min, the content was refilled into smaller beakers as shown by Fig. 5.3.

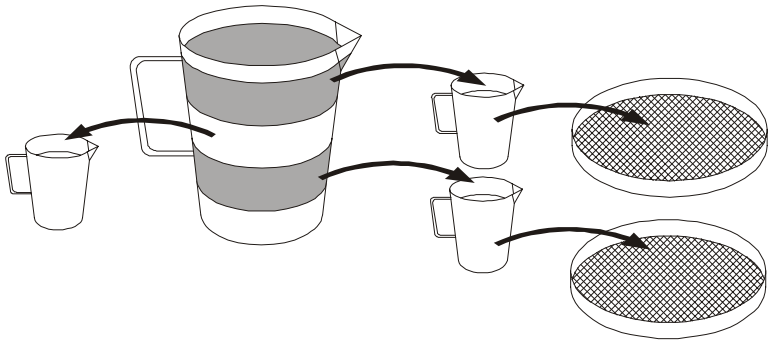


Fig. 5.3 Test set-up segregation resistance

The middle layer was removed, while the remaining samples were washed out on a sieve of 4 mm. The aggregates and the fibres were dried in an oven for 24 hours at 105°C; the fibres were separated from the aggregates with a magnet. The segregation indices (SI) were separately calculated for coarse aggregates and steel fibres according to Equation 5.1.

$$\text{Segregation index (SI)} = weight\frac{lower}{lower + upper}\ layer \qquad (5.1)$$

Passing ability (slump flow test with J-ring)

The size, the content and the shape of the solids affect the flow of SCC through obstacles. The long elongated shape of steel fibres mainly determines the passing ability [Nemegeer, 1999/2001]. Since the length of fibres differs, most common test methods for passing ability are not applicable for SCFRC. A J-ring with seventy-two drilled holes (Appendix A; Figs. A6-7) was used to vary the distance of the bars. The diameter of the J-ring was 300 mm (distance of the centres of the holes). The applied bars are smooth, are made from stainless steel and have a diameter of 16 mm. Blocking is defined to occur in case the difference between the heights of the concrete directly in- and outside of the J-ring (Δh) is at least 10 mm. The height difference is measured at four points (rotation of 90°); the smallest and the largest differences are omitted. The bar spacing of the J-ring was varied three times in order to obtain one height difference above and below the criterion for blocking (10 mm). The bar spacings of the J-ring were 36, 49, 62, 74, 87, 99, 111 and 122 mm.

Passing ability (Filling vessel test, U-box)

The filling vessel test (Appendix A, Fig. A5) simulates practice-alike casting conditions and was used to test the passing ability of the reference mixtures of series PS/OS. A filling degree of more than 90% indicates a SCC [Takada et al., 1997]. Since it is not possible to vary the bar spacing, the filling vessel test is not applicable for SCFRC. The U-Box (Appendix A, Fig. A8) is a test method to determine the passing ability of SCC. Depending on the required level of self-compactability, different bar spacing can be applied. A minimum filling height of at least 300 mm is required for SCC.

Test methods for SCC and SCFRC

The applied test methods are summarised in Table 5.4. The order in which the tests were performed is the same as Table 5.4 lists. The slump flow test being the first test was carried out directly after mixing. If possible, different tests were carried out at the same time to shorten the testing period.

Table 5.4 Applied test methods for SCC and SCFRC in the fresh state

Test method	*SCC series PS/OS*	*SCFRC series PS/OS*	*SCC/SCFRC series MS*
Slump flow / T_{50}	X	X	X
Segregation test	X (only OS)	X (only OS)	-
Air content[1]	X	X	X
V-funnel	X	-	X
Fibre funnel	X	X	-
BML-Viscometer	X (only OS)	X (only OS)	-
J-ring	X	X	X
Filling vessel test	X	-	-
U-box	X	-	-

[1]NEN 5961, 1988

5.2.5 Paste characteristics

The pastes of the reference SCCs were tested on their characteristics in the fresh state by applying the following test methods: centrifuging (Chapter 4.4.2), mini-slump test (Appendix A, Fig. A9) and the flow-time through a mortar funnel (Appendix A, Fig. A1). The composition of the paste was kept the same as in SCC. Two litres of cement paste were prepared in a small Hobart mixer, according to the following mixing procedure:

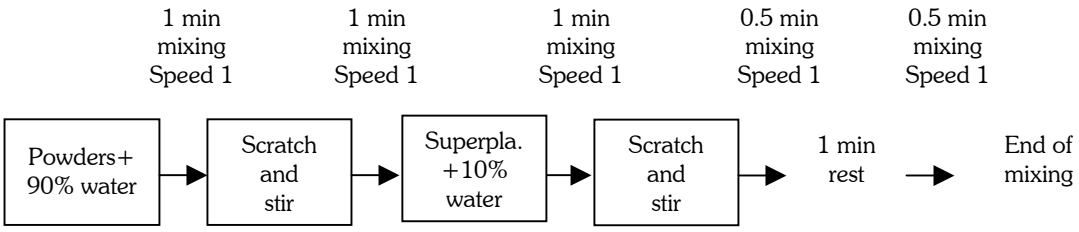


Fig. 5.4 Mixing procedure for cement paste (Hobart mixer)

Directly after mixing, the centrifuge was started to determine the surplus of water and the packing density of the paste. Eight minutes after mixing, which was about half of the time to perform the tests on characteristics of SCFRC in the fresh state, the paste was stirred up by hand (ten times). Directly after remixing, the mini-slump test was carried out (dimensions of the cone: upper/lower diameter: 20/37 mm; height: 57 mm). Ten minutes after mixing, the mortar funnel was filled (after remixing the paste ten times) and the flow-test was performed twice; the average of both measurements is the 'flow-time'.

5.3 Design criteria for SCFRC

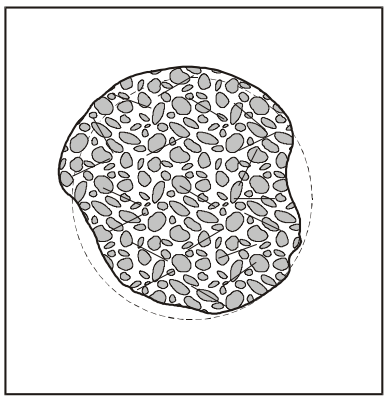
The first experience with SCC in the Netherlands was made with the Japanese design method [Okamura & Ouchi, 1999]. Four reference mixtures (PS1-4) were composed according to this approach [Grünewald & Walraven, 2001a], which were designed as powder-type SCCs with zero yield value, a high plastic viscosity and applicable in the most dense reinforcement configurations. Three main conclusions were drawn from this study: First, a slump flow slightly higher than 700 mm allowed to add reasonable fibre contents; still a minimum of about 600 mm was required for SCFRC. Second, the steel fibres did not segregate due to the high plastic viscosity of SCC. The slump flow decreased and T_{50} increased at increasing fibre content. Finally, close to the threshold of 600 mm three distinguished flow patterns indicated whether the maximum fibre content was exceeded.

From the preliminary study the following design criteria were proposed [Grünewald & Walraven, 2001c]:

- Slump flow > 600 mm (reference mixtures of series PS/OS: 710 ± 20 mm)
- No segregation of the fibres
  - judged by their distribution in the mixer
- Homogenous distribution of SCC on the flow table
  - uniform distribution of the fibres/aggregates/cement paste
  - round shape of the flow spread

Mixtures with a slump flow close to 600 mm filled the moulds of small beams for bending tests in spite of the decrease of filling ability (smaller slump flow and higher T_{50} flow-time). Measurements with the BML-Viscometer indicated that a slump flow close to 600 mm often coincides with a sharp increase of the yield value. The slump flow test did not indicate this change; more information about the flow behaviour was obtained from the appearance of the flow spread. The following visual observations gave a good indication whether a mixture was self-compacting. It should be kept in mind that the clustering of fibres significantly affects the magnitude and the variation of characteristics of SCFRC in the hardened state. The following flow patterns indicated that the maximum fibre content of SCC was surpassed:

A: Fibres having a high surface area

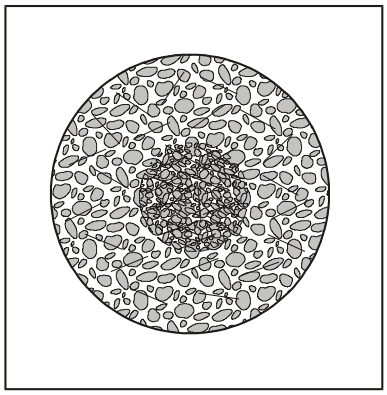


In case the matrix is sufficiently cohesive, fibre types with a high surface area decrease the filling ability of SCFRC. The fibres are homogeneously distributed but the shape of the flow is not round. Such a SCFRC is not expected to fill a mould homogeneously; a high content of entrapped air is transported. This flow pattern often coincides with a flow spread smaller than 600 mm.

(Example: Dramix 80/30 BP)

Fig. 5.5 Obstruction of the free flow

B: Long fibres

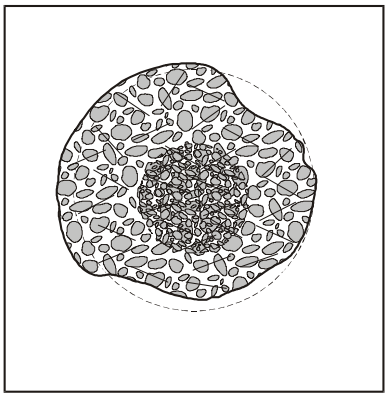


This flow pattern can be observed in two cases: First, the mixture is not stable, the fibres segregate or second, the maximum content of long fibres is surpassed. In the latter case this flow pattern was observed even when the fibres did not segregate in the mixer. This flow pattern coincides with a large slump flow, since the flow is barely obstructed by the fibres.

(Example: Dramix 80/60 BN)

Fig. 5.6 Clustering of fibres and/or aggregates, which barely affects the slump flow

C: Combination of A and B (low to intermediate aspect ratios; L_f/d_f: 45-65)



The flow patterns of A and B are combined. The free flow is obstructed and a cluster of fibres and/or aggregates remains in the centre of the flow table.

(Example: Dramix 65/40 BN)

Fig. 5.7 Clustering and obstruction of the free flow

Flow patterns A-C were not observed at fibre contents below the maximum fibre content; the fibres affected the slump flow, but were homogeneously distributed. Once the maximum is exceeded any adjustment of the paste (water or superplasticiser) increases the separation between matrix and fibres. Large slump flows (close to that of the reference mixture without fibres) at high fibre contents indicate a lack of stability. SCFRC with high fibre contents has to be balanced to avoid flow patterns A (low filling ability) and B (clustering and segregation of the fibres) to occur.

5.4 Test results: SCC and SCFRC in the fresh state

The characteristics of SCC and SCFRC in the fresh state are listed in Appendix G. In the following, a selection of the results will be presented in order to highlight important conclusions. Models to predict the characteristics of SCFRC are presented in Chapter 6. Grünewald & Walraven [2000, 2001a/b, 2003] provide a more detailed discussion of the test results.

5.4.1 Characteristics of the reference SCCs

Table 5.5 summarises the results of sixteen reference SCCs mixtures without fibres. All mixtures were stable and excellently self-compacting; the filling degrees (filling vessel test) of all mixtures from series OS/PS were higher than 90%.

Table 5.5 Test results: 16 self-compacting reference mixtures in the fresh state

Test response	*Slump flow*	*Yield value*	*Plastic viscosity*	T_{50}	*V-funnel*	*Fibre funnel*	*Filling vessel test*	*SI-index*
	[mm]	*[Pa]*	*[Pa·s]*	*[s]*	*[s]*	*[s]*	*[%]*	*[-]*
Series PS								
PS 1, 37.2/35.1	718	-	-	2.4	8.6	5.1	91.1	-
PS 2, 40.2/36.9	708	-	-	3.3	10.8	4.5	97.6	-
PS 3, 43.9/38.9	716	-	-	4.2	9.5	5.7	97.7	-
PS 4, 47.9/41.0	743	-	-	3.5	10.2	4.5	98.9	-
Series OS								
OS 1-57.0/36.5	703	-32.7	69.2	1.9	10.5	3.2	93.8	0.48
OS 2-57.0/39.0	693	-26.5	59.4	2.1	9.0	3.2	90.4	0.52
OS 3-68.0/36.5	730	-0.2	87.9	2.1	10.2	2.9	93.0	0.51
OS 4-68.0/39.0	725	-11.9	56.0	2.6	8.9	2.9	93.9	0.50
OS 5-68.0/34.0	698	-38.3	97.6	3.3	10.5	2.9	95.8	0.51
OS 6-68.0/36.5	728	31.4	81.0	3.0	11.9	2.9	98.8	0.49
OS 7-68.0/39.0	720	18.9	62.2	2.7	9.3	3.2	97.8	0.50
OS 8-70.0/37.7	690	4.9	71.3	2.0	8.12	2.4	91.3	0.50
OS 9-70.0/40.0	693	-6.4	57.5	2.4	8.12	2.6	91.3	0.50
Series MS								
MS 1-40	830 / 265[1]	-	-	1.2	6.1	8.5[2]	-	-
MS 2-50	865 / 266[1]	-	-	1.6	6.4	8.5[2]	-	-
MS 3-55	800 / 244[1]	-	-	2.0	6.0	11.2[2]	-	-

[1] Mortar flow spread [2] Flow-time mortar funnel

The dimensions of the V-funnel applied for series PS are according to EFNARC [2001]; series OS/MS were tested with a V-funnel according to CUR-Recommendation 93 [2002]. After performing the test with the BML-Viscometer it was checked whether equilibrium was obtained for at least one third of all data points. An analysis indicated that the steady state was achieved for all mixtures at the four lowest rotation speeds. These four points were used to calculate the yield value and the plastic viscosity according to the 'Bingham model' (R^2 was greater than 0.98 in all cases). The J-ring test was performed with all mixtures. The height difference at a bar distance of 36 mm was less than 10 mm in most cases (mixture PS1: 49 mm). The filling height of the U-Box of all mixtures of series PS/OS was higher than 300 mm. The segregation index of series OS was close to 0.5; no coarse aggregate segregation was observed.

Characteristics in the fresh state in time

Two types of superplasticisers were applied to obtain stable characteristics within the period of testing since various tests had to be carried out. Once the combination of powders was chosen to achieve the required strength class, the combination of superplasticisers was fixed. Mortar tests (sand content: 40 Vol.-%) were performed once a reference mixture fulfilled the design criteria (Chapter 5.3) on SCC to control the change of the characteristics in time. Appendix A (Fig. A10) shows the mortar flow cone. The mortars were tested 10 and 30 minutes after mixing. The mortar flow spread decreased with a maximum of 16 mm (Fig. 5.8), the flow-time increased with a maximum of 1.0 s (Fig. 5.9). The characteristics of the pastes of SCFRC in the fresh state were also determined. The packing density, the results of the mini-slump flow and the mortar funnel tests of the paste of the reference mixtures are given in Appendix F.

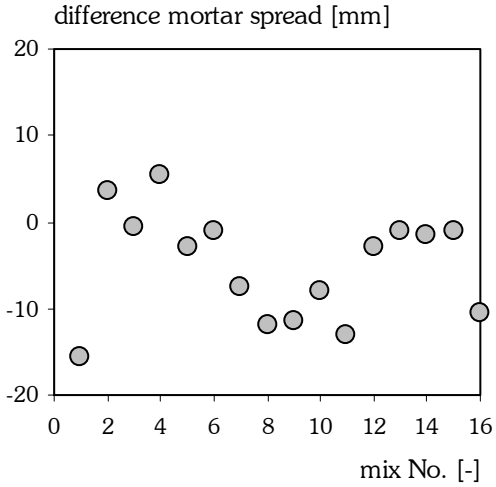


Fig. 5.8 Difference of the mortar flow of sixteen references mixtures (measured 10 and 30 minutes after mixing)

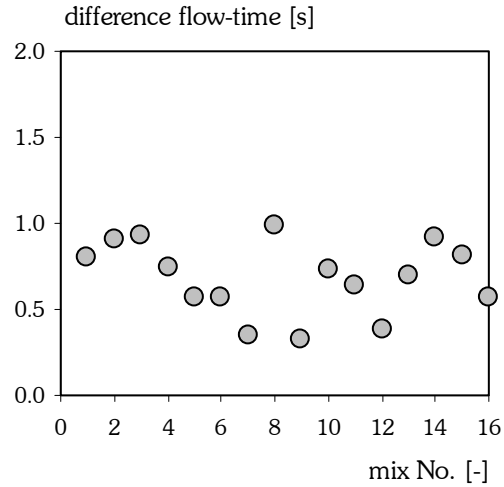


Fig. 5.9 Difference of the mortar flow-time of sixteen references mixtures (measured 10 and 30 minutes after mixing)

5.4.2 SCFRC - slump flow

Groth & Nemegeer [1999] applied the fibre factor ($V_f \cdot L_f/d_f$) to describe the effect of different types and contents of steel fibres on the slump flow. Fig. 5.10 shows the decrease of the slump flow at increasing fibre factor for series PS; the slump flow of the reference mixtures was in the range of 708-743 mm. The more fibres were added and the higher their aspect ratio was, the more the slump flow decreased compared with a reference SCC without fibres. Once the maximum fibre content is surpassed, the degree to which the slump flow is affected depends on the fibre type (Chapter 5.3). The fibre factor does not take deviating flow patterns into account. In order to be able to add high fibre contents the slope should be as low as possible, whereas the slump flow of the reference mixture should be as large as possible. Segregation of the fibres has to be counteracted. Some mixtures of series OS were adjusted for higher fibre contents. Fig. 5.11 shows that the slope of a linear regression line decreases for series OS4 (68/39.0) compared with series OS3 (68/36.5) and series OS8 (70/37.7); at the same fibre content a higher slump flow was achieved. Series OS4 resulted in the lowest slope of series PS/OS.

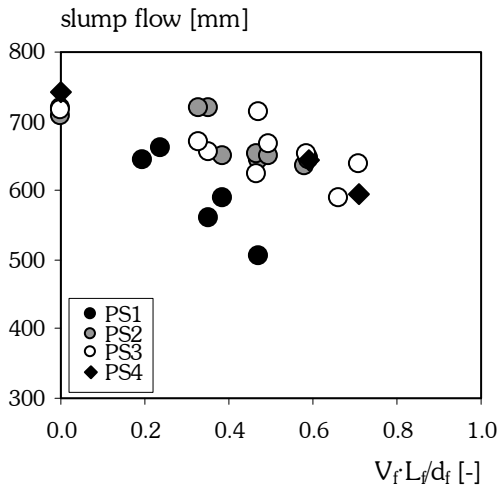


Fig. 5.10 Effect of the fibre factor and the mixture composition on the slump flow of series PS1-4

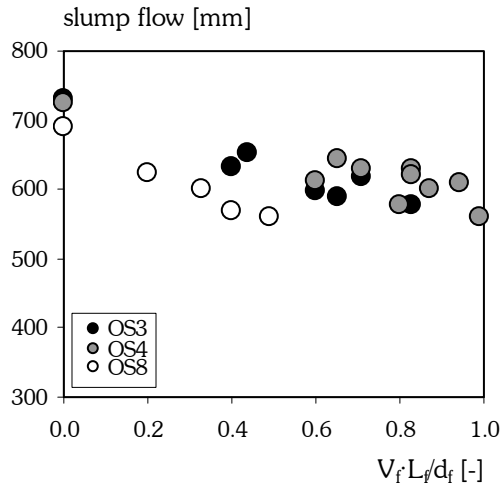


Fig. 5.11 Effect of the fibre factor and the mixture composition on the slump flow of series OS3/4/8

The target mortar flow spread without fibres was 245 mm (series MS: slump flow~800 mm) (Fig. 5.12). Short fibres (6 and/or 13 mm) were tested with a maximum aggregate size of 4 mm. The paste content of mixtures MS1-3 differed, whereas the composition of the aggregates was the same. The lower the aggregate content the higher the fibre factor at which a slump flow of 600 mm was surpassed. Curves rather than straight lines were obtained: higher fibre volumes had an overproportional effect on the slump flow reduction. These results support the concept of the maximum fibre content: once it is surpassed, the slump flow decreases quickly.

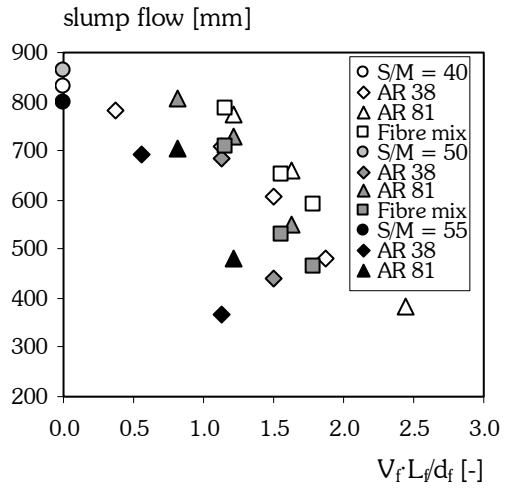


Fig. 5.12 Effect of the fibre factor and the mixture composition on the slump flow (series MS; aspect ratio (AR) = L_f/d_f)

5.4.3 SCFRC - yield value

Rheological measurements were conducted with the BML-Viscometer. Fig. 5.13 relates the slump flow of mixtures of series OS1-9 with the yield value. The slump flow is not correlated with the yield value once the maximum fibre content is surpassed.

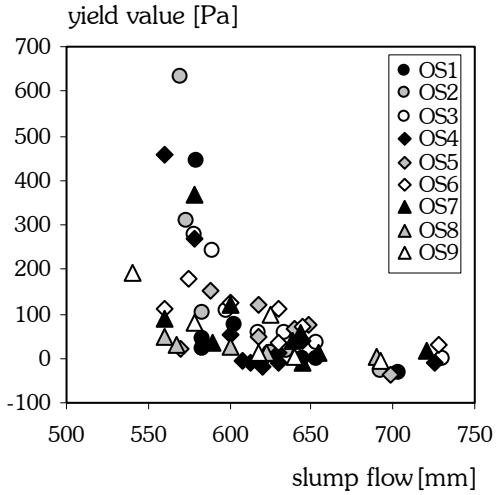


Fig. 5.13 Rheological measurements on SCFRC (series OS): slump flow versus yield value

A sudden increase of the yield value was found for some mixtures (e.g. OS4), whereas a smooth increase characterised other mixtures (e.g. OS9). The degree to which the yield value increased at decreasing slump flow depends on the reference mixture. Visual observations provide additional information about the flow behaviour. The yield values of SCC without fibres were close to zero (Table 5.5). According to Wallevik [2003], the maximum yield value of SCC is 60 Pa. The yield values of SCFRC at slump flows larger than 600 mm was close to or lower than 100 Pa; below 600 mm they often were much

higher. The increase of the yield value beyond a threshold of 600 mm is overproportional and corresponds with the clustering of the fibres.

5.4.4 SCFRC - plastic viscosity

Fig. 5.14 shows the plastic viscosity (the slope of the Bingham model) of mixtures of series OS related to the fibre factor. The plastic viscosity increased due to the addition of the fibres, the degree to which depended on the composition of the reference mixture. SCFRC, which was self-compacting and fulfilled all design criteria, was found up to a plastic viscosity of 270 Pa·s. The plastic viscosity increased with a factor of 3 compared with the reference mixture. The higher resistance of SCFRC was also experienced during remixing the concrete by hand. The higher resistance promotes the formation of layers in case SCFRC has to be cast in several batches.

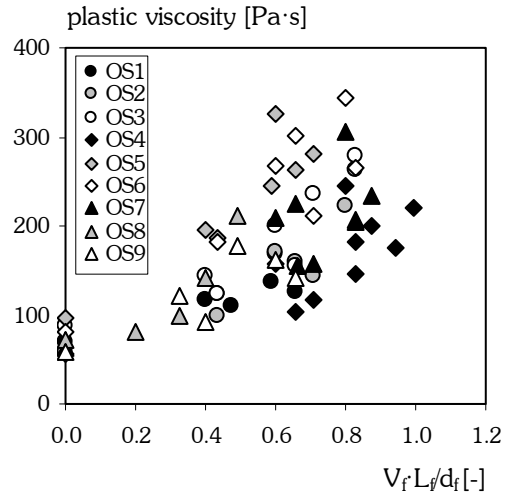


Fig. 5.14 Effect of the fibre factor and the mixture composition on the plastic viscosity (series OS)

5.4.5 SCFRC - passing ability

Dependent of the type and the content of the steel fibres, the required bar spacing of SCFRC to avoid blocking might be much larger. Groth advised a factor 3 (bar spacing to fibre length) for 30 kg/m^3 of 60 mm steel fibres, which is 180 mm (Table 3.2). Table 5.6 shows the results of J-ring tests for series PS1-4. The results in parenthesis represent mixtures that were not considered to be self-compacting. The bar spacings for 'blocking' and 'non-blocking' of series PS/OS/MS are summarised in Appendix G.

Table 5.6 Required bar spacings (c_{NB}) for non-blocking of series PS (in mm)

Steel fibre content	*0 [kg/m³]*	*20 [kg/m³]*	*40 [kg/m³]*	*60 [kg/m³]*	*80 [kg/m³]*	*100 [kg/m³]*	*120 [kg/m³]*
Series PS 1	49						
Dramix - 45/30 RL	-	-	87	(99)	(87)	-	-
Dramix - 80/60 RC	-	99	(111)	-	-	-	-
Series PS 2	36						
Dramix - 45/30 RL	-	-	-	-	74	(87)	-
Eurosteel 50/50	-	-	-	74	(99)	-	-
Dramix - 65/40 RC	-	-	74	99	-	-	-
Dramix - 80/60 RC	-	-	87	(111)	-	-	-
Series PS 3	36						
Dramix - 45/30 RL	-	-	-	-	62	74	(87)
Eurosteel 50/50	-	-	-	74	87	(99)	-
Dramix - 65/40 RC	-	-	74	87	(99)	-	-
Dramix - 80/60 RC	-	-	62	(122)	(122)	-	-
Series PS 4	36						
Dramix - 45/30 RL	-	-	-	-	-	74	(87)

5.4.6 SCFRC - maximum fibre content

The fibre content was increased in steps of 20 kg/m³ (series MS: 0.5 Vol.-%) until the maximum content was surpassed (criteria: Chapter 5.3). The maximum fibre content of one fibre type depends on the characteristics and the composition of the reference SCC. Table 5.7 summarises the maximum fibre contents of mixtures of series PS/OS/MS.

Table 5.7 Maximum fibre content of SCFRC (series OS/PS: kg/m³, series MS: Vol.-%)

Fibre type	*D-45/30*	*ES-50/50*	*D-65/40*	*D-80/60 BN*	
Series PS (kg/m³)					
PS 1, 37.2/35.1	40	-	-	20	
PS 2, 40.2/36.9	80	60	60	40	
PS 3, 43.9/38.9	100	80	60	40	
PS 4, 47.9/41.0	100	-	-	-	
Fibre type	*D-45/30*	*D-65/40*	*D-80/30 BP*	*D-80/60 BP*	*H-65/20*
Series OS (kg/m³)					
OS 1-57.0/36.5	80	-	40	40	-
OS 2-57.0/39.0	120	-	60	40	-
OS 3-68.0/36.5	120	-	40	40	-
OS 4-68.0/39.0	140	100	60	60	-
OS 5-68.0/34.0	100	-	40	40	-
OS 6-68.0/36.5	120	-	60	40	-
OS 7-68.0/39.0	120	80	60	60	-
OS 8-70.0/37.7	-	-	20	-	40
OS 9-70.0/40.0	-	-	40	-	60
Fibre type	*D-OL6*	*D-OL13*	D-OL6+OL13	*D-OL6+OL13*	*D-OL6+OL13*
Series MS (Vol.-%)					
MS 1-40	4.0	2.0	-	2.0+0.5	2.0+1.0
MS 2-50	3.0	1.5	-	2.0+0.5	-
MS 3-55	1.5	1.0	-	-	-

The highest fibre contents of long steel fibres (at least 20 mm) were found for series OS4. Higher maximum fibre contents (fibre lengths: 6 and 13 mm) were found for series MS. The higher the paste content the more the relative thickness of the paste layer

increased, which provides 'space' to the fibres. An upper limit fibre content (the fibres cluster no matter what the composition is) was found for Dramix 80/60 BP; 80 kg/m^3 of this fibre type caused fibre clustering without any interaction of the aggregates.

5.4.7 SCFRC - segregation resistance

The static segregation resistance of series OS was separately determined for coarse aggregates and steel fibres. A sieve of 4 mm was applied to wash out the concrete. Fig. 5.15 presents the segregation index SI (Equation 5.1); a higher SI-index indicates a higher proneness to segregation. A SI-index of 0.54 coincident with 85% in the upper layer compared to the lower layer.

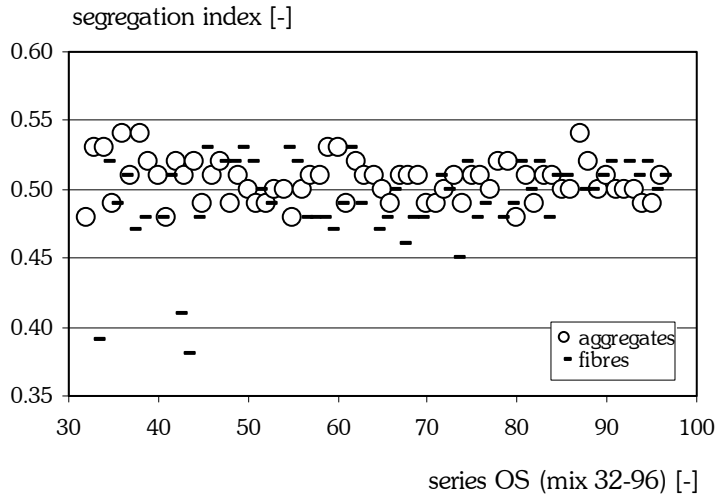


Fig. 5.15 Segregation index (SI) of coarse aggregates (>4 mm) and steel fibres (series OS)

Aggregates and fibres did not segregate (SI ~0.50); in case differences were found they were small. The fibres did not segregate more. A low segregation index (close to 0.4) indicates that more fibres were found in the upper layer. In case fibres are relatively large compared with the diameter of the beaker problems with refilling the concrete might occur.

The smaller the diameter of an aggregate the larger is its specific surface area. Fig. 5.16 shows a geometrical consideration on segregation resistance. The weighed surface area (divided by the density) between fibres and an aggregate fraction decreases the smaller the diameter of a fraction is. The segregation resistance of the steel fibres relative to the aggregates decreases: a stable distribution of the coarsest aggregates might not be a adequate criterion. The segregation resistance of fibres in mortars should be controlled by an additional test.

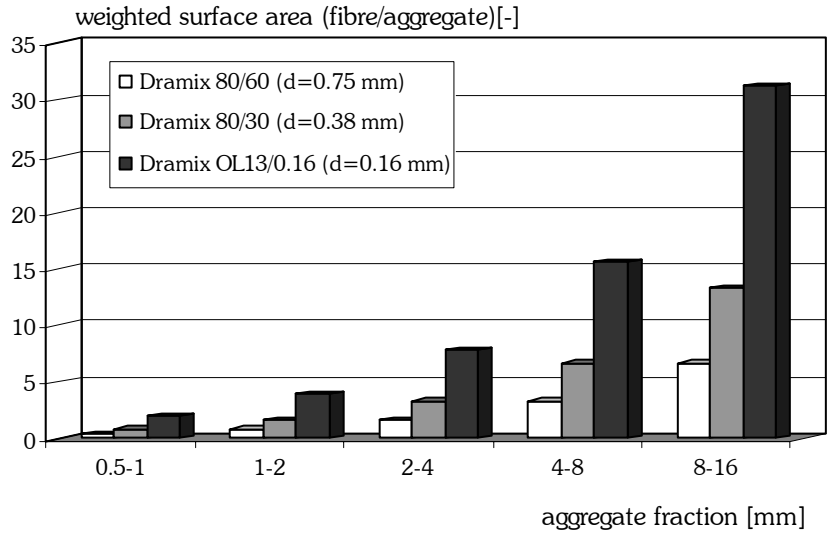


Fig. 5.16 Change of the ratio of the weighed surface areas of steel fibres and aggregates (normalised by the density) and for different aggregate sizes

5.5 Concluding remarks

This chapter presented results of three parameter studies on the characteristics of SCFRC in the fresh state. The experimental set-up was described, design criteria for SCFRC were proposed and test results of SCC and SCFRC presented.

Sixteen stable SCCs at defined characteristics in the fresh state were used to study the effect of the type and the content of the steel fibres; in total 121 mixtures were tested. The fibres affect the characteristics of SCC in the fresh state: the slump flow decreases and the yield value, the plastic viscosity and the bar spacing to avoid blocking increase compared with a reference SCC. The degree to which the key characteristics are affected depends on the mixture composition, which provides the opportunity to optimise SCFRC. Segregation resistance is the most important characteristic of SCFRC; the thicker the fibre the more it is prone to segregation. Segregation tests on SCFRC with a maximum aggregate size of 8 and 16 mm indicated that fibres are stable in case the coarse aggregates were also homogeneously distributed. Mixtures with a smaller maximum aggregate size might be prone to segregation. Especially at high fibre contents the balance between stability and filling ability becomes the most important design issue. The maximum fibre content is the amount of one fibre type, at which SCC still is self-compacting; the composition and the characteristics of SCC determine it. Visual observations on the slump flow test provide additional information concerning the maximum fibre content.

Chapter 6:

Modelling SCFRC in the fresh state: From individual components to an optimised mixture composition

6.1 Introduction

The previous chapter discussed the results of three parameter studies on the characteristics of SCFRC in the fresh state. Based on these results, design tools for performance-based SCFRC are developed; this chapter describes the analysis and the models.

The components of SCFRC have to be homogeneously distributed; sinking of particles, fibre clustering or blocking have to be counteracted. The fibre content has to remain below a maximum, which depends on the fibre type and the mixture composition. Chapter 6 consists of four parts: First, a characterisation of the components of SCC is presented and how their properties are related to the performance of SCC in the fresh state. These components are the granular skeleton (aggregates and steel fibres) and the paste. Second, models on the characteristics of SCC without fibres in the fresh state are described. Third, models are developed, which allow predicting characteristics of SCFRC in the fresh state. Finally, the CBI-approach 'risk of blocking' is applied and altered to determine the required bar spacing for non-blocking and the maximum fibre content.

6.2 Modelling of characteristics of SCC in the fresh state

6.2.1 Characterisation of the components of SCC

The behaviour of SCC in the fresh state depends on the characteristics of both the granular skeleton and the paste. Oh et al. [1999] proposed the relative paste layer thickness and improved the model of Krell [1985], who calculated constant layer thicknesses of water and paste. To calculate the absolute layer thickness a correction is required in case the grading of the solids differs. The interaction between a superplasticiser and the powders is difficult to predict without testing the paste. De Larrard [1999] proposed to apply the normalised solid concentration, which is the

content of solids divided by the packing density. In the following, the concepts of the relative layer thickness and of the normalised solid content are compared. The relative layer thickness is calculated with Equation 6.1. The relative water layer thickness takes into account the size and the distribution of the powders, while the relative paste layer thickness considers aggregates and fibres. The surface area of the fibres was related to their diameter. The surplus of the suspending medium was calculated with Equation 6.2 (for a m^3). The packing density of aggregates and fibres was obtained from CPM simulations (cement paste: experimental by centrifuging).

$$\Gamma = \frac{V_e}{Grains\sum_{i=1}^{n} n_{g,i} \cdot s_{g,i} \cdot d_{g,i} + Fibres\sum_{i=1}^{n} n_{f,i} \cdot s_{f,i} \cdot d_{f,i}} \tag{6.1}$$

where:
- Γ = relative thickness of the surrounding fluid [-]
- V_e = volume of excess fluid to surround the grains [mm^3]
- $n_{i,g}$ = number of grains of group i [-]
- $s_{g,i}$ = surface area of grain of group i corrected by the sphericity factor [mm^2]
- $d_{g,i}$ = diameter of grain group i [mm]
- $n_{i,f}$ = number of fibres of type i [-]
- $s_{f,i}$ = surface area of a single fibre of type i [mm^2]
- $d_{f,i}$ = equivalent diameter of fibre i [mm]

with:
$$V_e = V_{fluid} - \left(\frac{V_{solid}}{PD_g} - V_{solid}\right) \tag{6.2}$$

where:
- V_e = volume of excess fluid to surround the grains [Vol.-%]
- V_{fluid} = volume of fluid [paste (incl. air) or water (excl. air)] [Vol.-%]
- PD = packing density [-]; PD_g: aggregates; PD_p: paste
- V_{solid} = solid content [Vol.-%]

Fig. 6.1 compares the relative paste layer thickness with the normalised solid content of the aggregates of reference mixtures without fibres. A high correlation indicates that both parameters describe the same characteristic of the granular skeleton. The relation for mixtures with a maximum aggregate size of 4 mm was slightly different from that for maximum aggregate sizes of 8 or 16 mm; the packing density affects both parameters differently. Fig. 6.2 relates the relative water layer thickness to the normalised solid content of the paste. The relative layer thickness also depends on a factor to correct the surface area (the solids are not perfectly round). The correction factor thus affects the relation between both parameters. The following factors were applied: round aggregates: 1.08 [Oh et al., 1999], fly ash: 1.14 and cement: 1.33 [Saak, 2000]. The smallest sieve size of the powders was 1.8 µm ; 3.9-11.2% of the powders passed it. The cement particles are assumed to be fully dispersed.

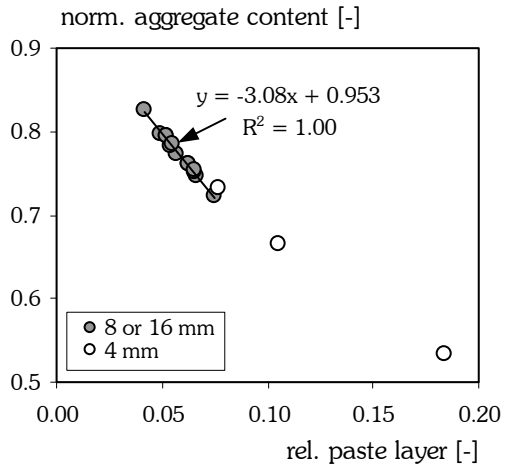


Fig. 6.1 Relative paste layer thickness versus the normalised aggregate content

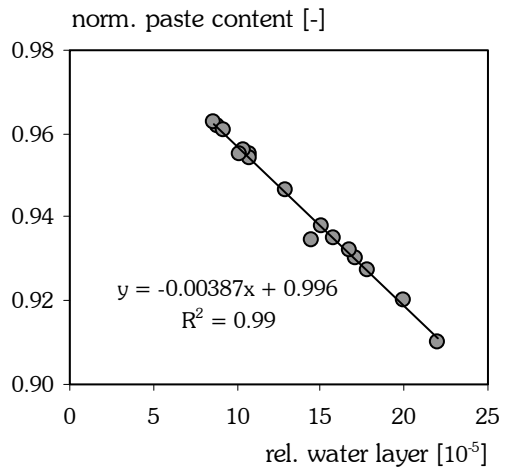


Fig. 6.2 Relative water layer thickness versus the normalised paste content

The normalised solid content was calculated from the mixture composition; the packing density was either predicted or measured. The relative layer thickness can be transferred into the normalised solid content with Equation 6.3 (for paste around aggregates) and with Equation 6.4 (for water around powder grains).

$$\left(\frac{\phi}{\phi^*}\right)_g = -3.08 \cdot RPL + 0.953 \qquad (R^2=1.00) \qquad (6.3)$$

where: ϕ = solid content [-]
ϕ^* = packing density, space occupied by the solids [-]
$(\phi/\phi^*)_g$ = normalised solid content (fibres and aggregates)[-]
RPL = relative paste layer thickness [-]

$$\left(\frac{\phi}{\phi^*}\right)_p = -3.87 \cdot 10^{-3} \cdot RWL + 0.996 \qquad (R^2=0.99) \qquad (6.4)$$

where: $(\phi/\phi^*)_p$ = normalised paste content [-]
RWL = relative water layer thickness [-]

More parameters are required to calculate the relative layer thickness: the packing density, the content and the grading of the solids and the shape factor. The concept of the relative layer thickness includes more uncertainties. The characteristics of the granular skeleton are summarised in Appendix G (paste: Appendix F).

Several tests were performed with the pastes of the sixteen reference mixtures, whereas their composition was kept exactly the same as for the tests on SCC. Appendix F summarises the characteristics of the pastes in the fresh state. The relative water layer thickness is correlated with the paste flow-time (Fig. 6.3). De Larrard [1999] found that the normalised solid content is correlated with the plastic viscosity. The flow-time gives an indication of the plastic viscosity and the normalised solid content is correlated with

the relative layer thickness (Fig. 6.3). In contrast, the relation between the relative water layer thickness and the mini-slump flow is not unique, but depends on the composition of the powders (Fig. 6.4). All mini-slump flows are in the range of 110-160 mm; a linear relation is found for each powder combination (Fig. 6.4). The composition of the powders of series OS was slightly different for one strength class (OS 1-4, 5-7 and 8-9); their composition was altered to compensate for a varying water demand, different paste contents and aggregate distributions.

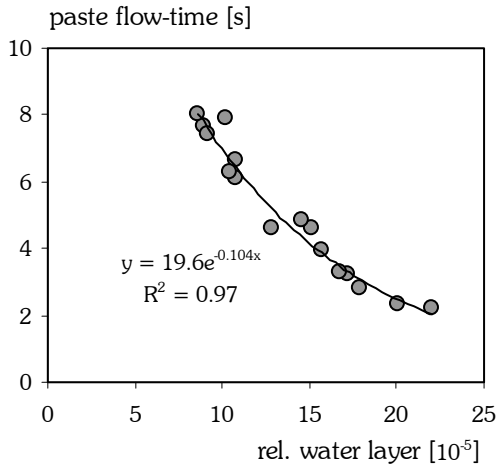


Fig. 6.3 Relation between the relative water layer thickness and the paste flow-time of sixteen pastes of the reference SCCs

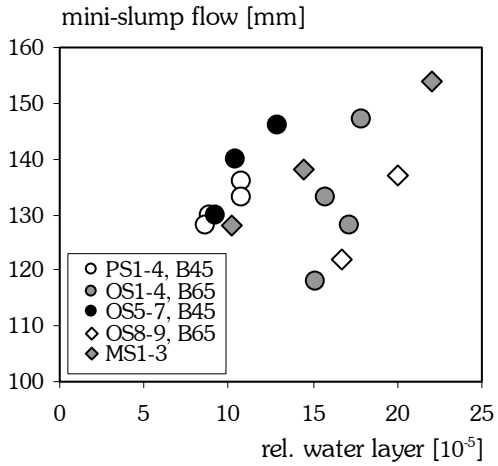


Fig. 6.4 Relation between the relative water layer thickness and the mini-slump flow of sixteen pastes of the reference SCCs

6.2.2 Characteristics of the reference mixtures

Fig. 6.5 compares the relative paste and water layer thicknesses of the reference mixtures of series PS/OS/MS. The relation depends on the combination of the powders and the maximum aggregate size; a similarity with the model of Krell [1985] to predict the flow spread (German flow) is obtained (Fig. 2.5): to obtain the same slump or mortar flow spread, a lower relative paste layer thickness was compensated for by a higher relative water layer thickness or vice versa. A correction is required to determine a unique relation between both characteristics. The relative water layer thickness is not sufficient to describe the effect of cement paste on the slump flow. The paste flow time, which is related to the relative water layer thickness, also does not provide this information. Smeplass & Mørtsell [2001] draw the same conclusion from their experiments. They proposed the 'particle matrix model' as a tool to design SCC. In their approach, the matrix (particles < 0.125 mm) is characterised by a flow-resistance ratio (flow-time), which is determined with the FlowCyl. They expected the same slump flow in case the content and the distribution of the aggregates and the flow-resistance ratio of cement paste of different compositions are the same. Their experiments could not confirm this assumption. They concluded that the flow-resistance ratio does not reflect the difference of the slump flows.

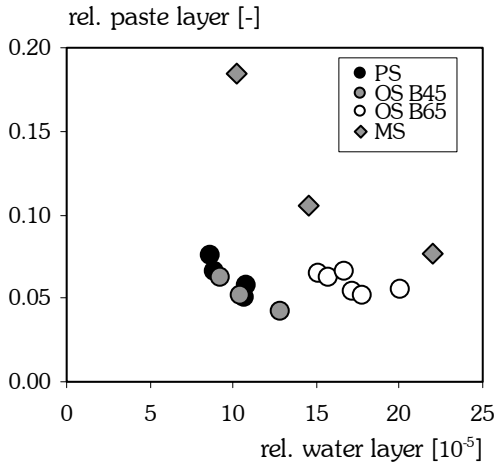


Fig. 6.5 Relation between the relative layer thicknesses of water and paste of sixteen reference mixtures

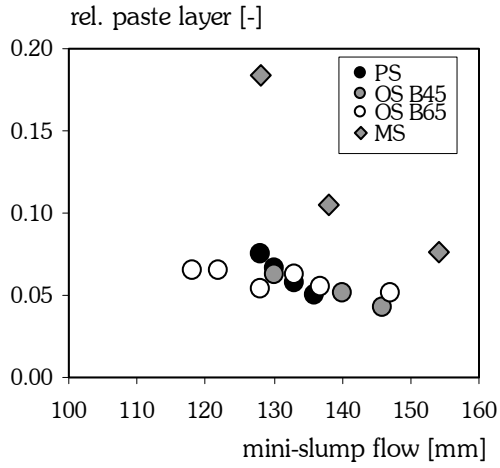


Fig. 6.6 Relation between the mini-slump flow and the relative paste layer thickness of sixteen reference mixtures

A better correlation was found between the relative paste layer thickness and the mini-slump flow (Fig. 6.6). The mini-slump flow is a characteristic of the paste, which is related to the slump flow of SCC. The slump flow could not be described solely by geometrical characteristics and the contents of the aggregates and the powders. A more detailed discussion of the paste characteristics of SCC is presented by Grünewald & Walraven [2004].

Slump flow and yield value of SCC

Fig. 6.7 relates the measurements on the slump flow and the yield value of the reference mixtures of series OS. The yield value of the reference mixtures was close to zero. The yield value was negative in some cases, which is not possible from the physical point of view and is rather the consequence of the experimental set-up and/or the analysis of the measurements with the Bingham model.

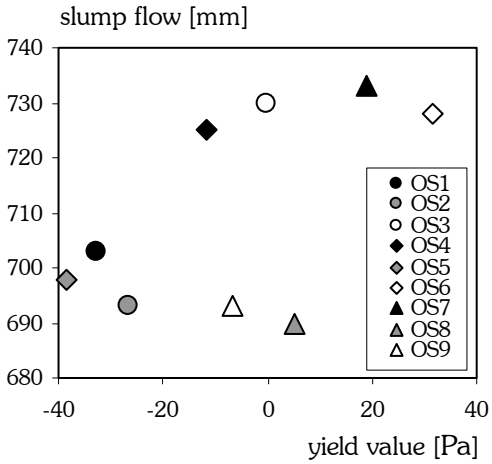


Fig. 6.7 Yield values and slump flows of the reference mixtures (series OS)

The slump flows and the yield values of mixtures of series OS are about the same (the range of yield values of various types of concretes is much broader). In order to predict the slump flow and the yield value, a single parameter is required to take into account the characteristics of the aggregates and the paste. In the following, the normalised solid content and the relative layer thickness are considered as the same characteristic since they are linearly correlated (Figs. 6.1-2). The best correlation was derived with the product of the mini-slump flow [in mm] and the normalised aggregate content, which is denoted as the 'slump flow factor (SFF)'. This factor was almost constant for the yield value and the slump flow of the reference mixtures of series PS/OS (Figs. 6.8-9). The average factor of series OS was 171 and increased slightly at increasing slump flow (Fig. 6.9).

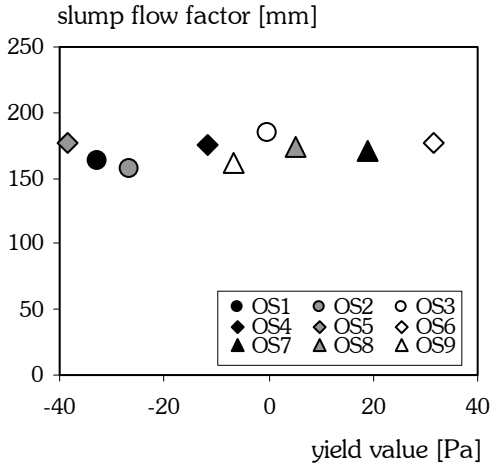


Fig. 6.8 Prediction of the yield value by the slump flow factor

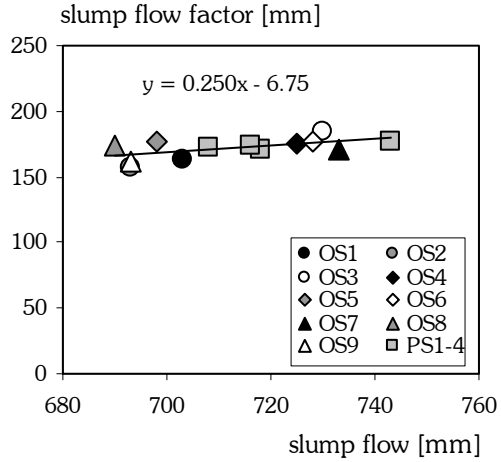


Fig. 6.9 Prediction of the slump flow by the slump flow factor

A linear regression line relates the slump flow factor and the slump flow (Fig. 6.9 and Equation 6.5). Rheological measurements were carried out with mixtures of series OS only; mixtures of series PS are also included in Equation 6.5. The mean error of the slump flow predictions of mixtures with a maximum aggregate size of 8 or 16 mm is 27 mm (STD: 15 mm).

$$\text{slump flow [mm]} = (6.75 + SFF) \cdot \frac{1}{0.250} \tag{6.5}$$

with: $$\text{slump flow factor (SFF)} = MS \cdot \left(\frac{\phi}{\phi^*} \right)_g^{-1} \tag{6.6}$$

where: MS = mini-slump flow [mm]
$(\phi/\phi^*)_g$ = normalised solid content (fibres and aggregates) [-]

Fig. 6.10 compares the slump flows of mixtures of series PS/OS with the predictions of Equation 6.5. The reference mixtures of series MS are also included in Fig. 6.10. The predictions for mixtures MS2-3 were acceptable; the slump flow of mixture MS1 (highest paste content of series MS) was significantly overestimated. Krell [1985] found that the

accuracy of his predictions was less accurate for mortar. Once the excess of paste is out of proportion (SCC is not optimised) the previous assumptions are not valid anymore; a minimum relative water layer thickness is required to obtain a flowable paste. Equation 6.5 can be applied to predict the slump flow of SCC (target range: 710±20 mm) with a maximum aggregate size of 8 or 16 mm.

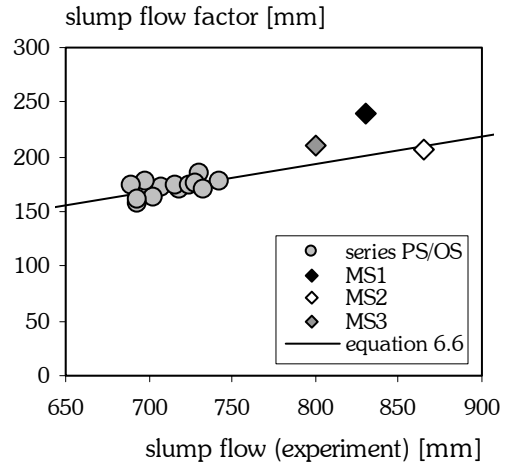


Fig. 6.10 Reference mixtures of series PS/OS/MS compared with predictions of Equation 6.6

Plastic viscosity of SCC

Fig. 6.11 shows the relation between the relative paste layer thickness (RPL) and the plastic viscosity. Nine reference mixtures of series OS were tested with the BML-Viscometer. The plastic viscosity is defined as the slope of the Bingham model. The best correlation of both components of SCC was obtained for the plastic viscosity and the relative paste layer thickness divided by the normalised paste content (Fig. 6.12). The contribution of the paste on the plastic viscosity is less affecting compared with the RPL.

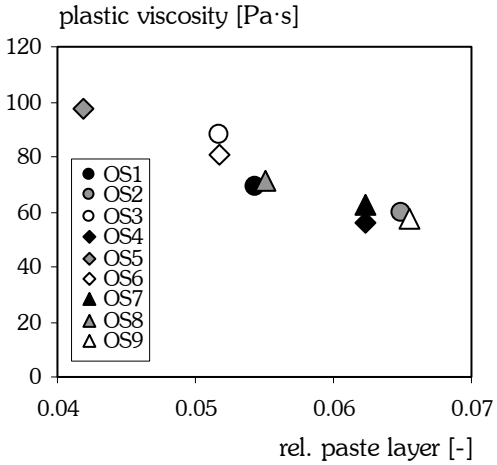


Fig. 6.11 Relation between the relative paste layer thickness and the plastic viscosity of SCC (series OS)

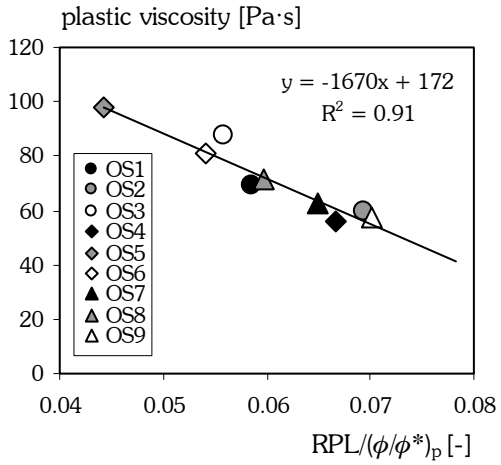


Fig. 6.12 The relative paste layer thickness divided by the normalised paste content compared with the plastic viscosity (series OS)

Equation 6.7 predicts the plastic viscosity of plain SCC. The mean error of the predictions of mixtures of series OS was 3.1 Pa·s (STD: 2.8 Pa·s).

$$\text{plastic viscosity [Pa·s]} = 172 - 1670 \cdot PVF \tag{6.7}$$

with:

$$\text{plastic viscosity factor (PVF)} = RPL \cdot \left(\frac{\phi}{\phi^*} \right)_p^{-1} \tag{6.8}$$

where: RPL = relative paste layer thickness [-]
$(\phi/\phi^*)_p$ = normalised paste content [-]

6.3 Effect of the steel fibres on the characteristics of SCC

The steel fibres decrease the packing density of the granular skeleton at increasing fibre factor. Fig. 6.13 shows the predictions obtained with the CPM for series PS/OS. To include the fibres into the concept of the relative layer thickness, the surface area of the fibres was multiplied by their diameter (Equation 6.1). The main effect of the fibres is the decrease of the paste surplus, which is about 2.0 Vol.-% at a fibre factor of 0.5. The paste surplus of mixtures of series PS/OS was in the range of 17.4-27.8 Vol.-%.

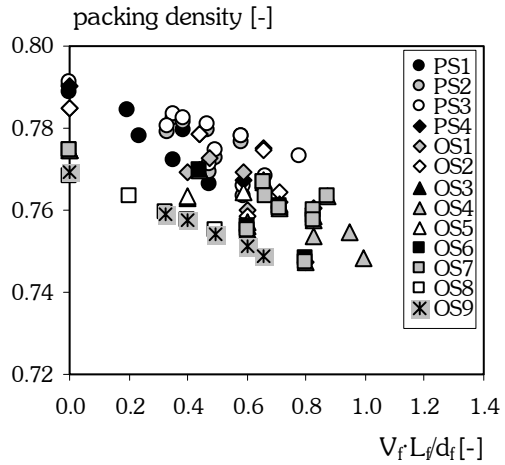


Fig. 6.13 Decrease of the packing density of the aggregates and steel fibres at increasing fibre factor (series PS/OS)

6.3.1 Effect of the fibres on the slump flow

The fibre factor ($V_f \cdot L_f/d_f$) describes the effect of the type and the content of the steel fibres on the slump flow of SCC (Chapter 5.4.2). The composition and the characteristics of SCC in the fresh state determine to what degree the slump flow decreases at increasing fibre factor. To determine the effect of the mixture composition the approach was as follows: First, the slump flow results of SCFRC were normalised relative to the result of the reference SCC without fibres (reference SCC=1.0). The slump flow of mixtures of series PS/OS was about 710 mm (series MS: about 800 mm). Second, the slope of a linear regression line having an intersection at 1 was calculated. Fig. 6.14 shows the regression line for series OS8. The slope of the relative slump flow is

not an indication of the appearance and the homogeneity of SCFRC. The purpose of the applied approach was to predict the slump flow of SCFRC, not to optimise the mixture composition.

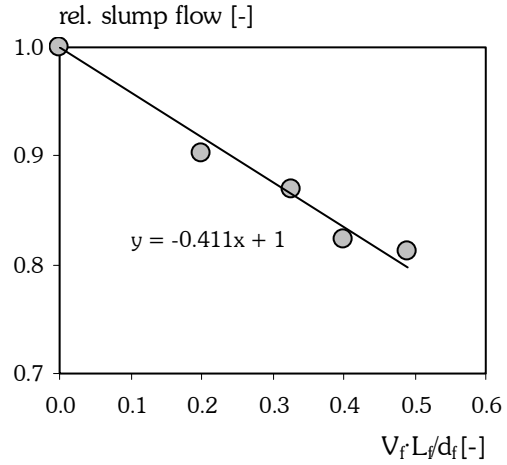


Fig. 6.14 Effect of the fibre factor on the decrease of the relative slump flow (series OS8)

Third, an analysis of the slopes of the reference mixtures of series PS/OS/MS was carried out (Fig. 6.15); a factor related to the granular skeleton and the paste ought to be found that affected the slope. The best correlation was obtained with the normalised aggregate content divided by the paste flow-time. This result implies that a lower slope might be achieved by increasing the flow-time. The combination of both parameters characterises a stable SCFRC; keeping the normalised paste content constant and decreasing the flow-time probably increases the filling ability but decreases the segregation resistance of SCFRC. Appendix F shows the slope of each reference mixture.

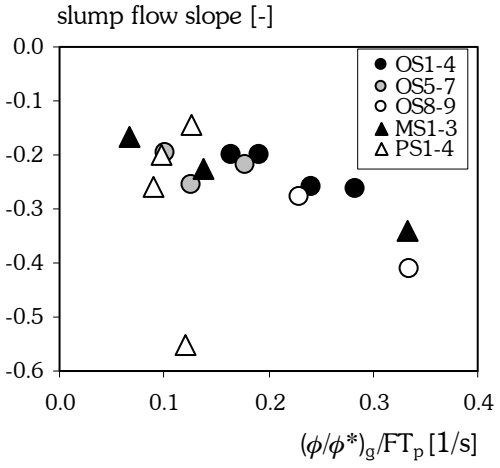


Fig. 6.15 The slope of the relative slump flow versus the normalised aggregate content divided by the paste flow-time (series PS/OS/MS)

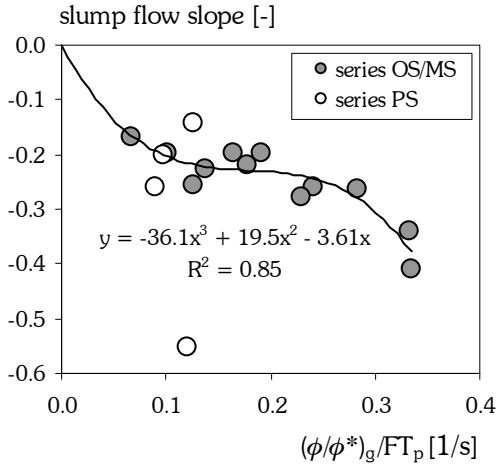


Fig. 6.16 Prediction of the slope of the relative slump flow (series OS/MS)

Equation 6.9 fits the data points best (Fig. 6.16). Under consideration of the slump flow of the reference mixture (measured or predicted by Equation 6.5) and the slope of Equation 6.9 the slump flow of SCFRC can be predicted.

$$\text{slump flow slope (SFS)} = -36.1 \cdot IF^3 + 19.5 \cdot IF^2 - 3.61 \cdot IF \qquad (6.9)$$

$$\textit{with:} \quad \text{influencing factor (IF)} = \left(\frac{\phi}{\phi^*}\right)_g \cdot \frac{1}{FT_p} \qquad (6.10)$$

where: $(\phi/\phi^*)_g$ = normalised solid content (fibres and aggregates) [-]
FT_p = flow-time mortar funnel [s]

Mixtures of series PS are excluded from Equation 6.9. The slump flows of series PS scattered more (R^2 was lower) due to the increased variation of the moisture content of the coarse aggregates. In case of higher scatter the effect of the fibre factor on the slope was less pronounced. The slope of series PS1 is much steeper (-0.55); the content of the coarse aggregates is the highest of all reference mixtures. Groth & Nemegeer [1999] concluded that fibres cannot be added to all types of SCC. The relation between the fibre factor and relative slump flow is assumed to be linear. This is true for series PS/OS but not for series MS (Fig. 5.12).

Accuracy of the slump flow predictions

Equations 6.5 and 6.9 are combined to predict the slump flow of SCFRC. The accuracy check distinguishes between predictions, which are based on measurements from reference mixtures (method 1) or on predicted slump flows (method 2; Equation 6.5). Fig. 6.17 shows the slump flow predictions of series PS/OS/MS in case the measured slump flow of the reference mixture was applied (method 1).

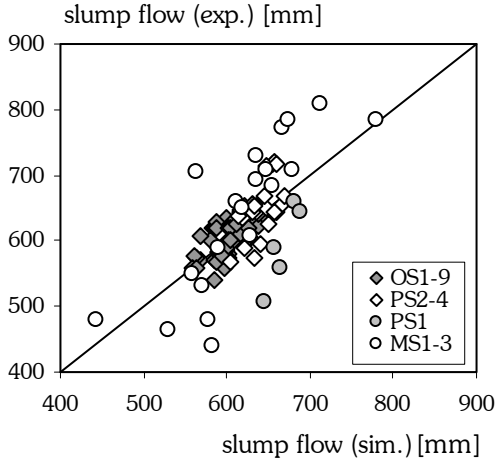


Fig. 6.17 Slump flow predictions of SCFRC based on the measured slump flow of plain SCC and Equation 6.9

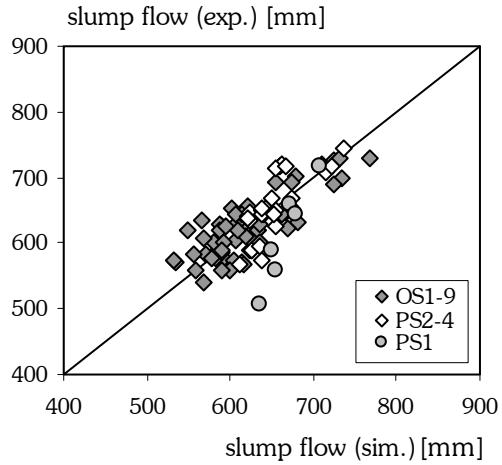


Fig. 6.18 Slump flow predictions of SCFRC (based on Equations 6.5 and 6.9)

The results of the reference mixtures are excluded from Fig. 6.17. Fig. 6.18 summarises the predictions in case the slump flow of the reference mixtures is predicted by Equation 6.5. Table 6.1 shows the averages and the standard deviations of different test series and two different methods of analysis. The best accuracy is obtained with series OS and method 1; it is in the range of the accuracy of the slump flow test itself. No accuracy check was carried out for series MS with method 2. Fig. 6.10 shows that the predictions of the slump flow of the reference mortars are not accurate.

Table 6.1 Mean error and standard deviation of slump flow predictions for SCFRC

Series	*Method 1 (excl. ref. SCC, only fibre mixtures) [mm]*	*Method 2 (incl. ref. SCC, all mixtures) [mm]*
OS 1-9	17 (11)	25 (17)
PS 2-4	29 (21)	25 (21)
PS 1	76 (47)	57 (48)
MS 1-3	66 (45)	-

The error of series PS is larger than that of series OS, which is caused by the variation of the moisture content of the aggregates and the high slope of series PS1. The error of the predictions for series MS is rather high. The relation between the slump flow and the fibre factor is a curve rather than a straight line, which results in an underestimation of the slump flow at a low fibre factor; at a high fibre factor the slump flow is overestimated (Fig. 6.17).

6.3.2 Effect of the fibres on the yield value

The slump flow of mixtures with a moderate surplus of paste (series PS/OS) decreases almost linearly due to the addition of the fibres. Deviating flow patterns of different fibre types (long fibres or fibres with a high surface area) cause a higher variation once the maximum fibre content is surpassed. Figs. 5.12 and 6.19 show the increase of the yield value at decreasing slump flow; the degree to which depends on the composition and the characteristics of the reference SCC. No general relation is obtained between the slump flow and the yield value. In this section, the differences between both measurements are quantified.

Fig. 6.19 presents the slump flow and the yield value of self-compacting mixtures of series OS; mixtures that were not self-compacting are excluded from the data set. Once the maximum fibre content is surpassed, the interaction between the fibres governs the yield value; the yield value increases more than proportional. The aim of this analysis was to predict the effect of the mixture composition on the yield value. Fig. 6.20 relates the difference of the normalised slump flow (see also Fig. 6.14) to the normalised yield value (references mixtures: both parameters become zero). At a given normalised difference of the slump flow, the yield value can be rather different (Fig. 6.20).

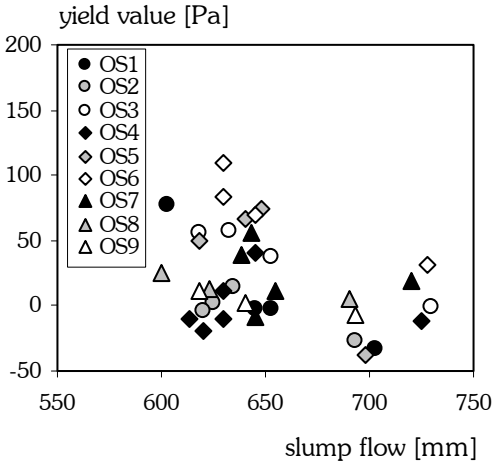


Fig. 6.19 Slump flow versus yield value measurements of mixtures of series OS that were self-compacting

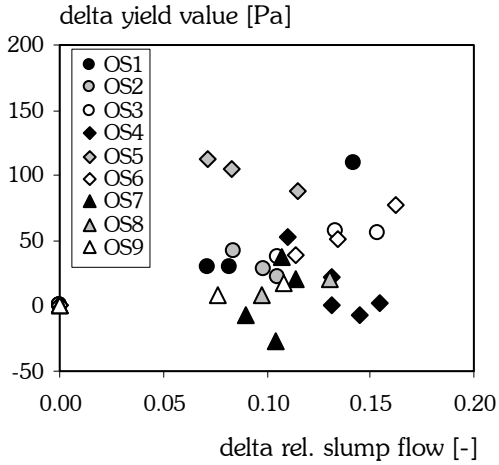


Fig. 6.20 Normalised differences of the slump flow and the yield value (self-compacting mixtures of series OS)

A linear regression line with an intersection of zero was calculated to best fit the results of Fig. 6.20. The slopes of series OS1-9 were determined (Appendix F) and an analysis was carried out to link the slope with the mixture composition of plain SCC. Fig. 6.21 relates the normalised paste content, which is the paste volume divided by the packing density of the granular skeleton, to the slopes of series OS. The higher the normalised paste content, the less the yield value increased at decreasing slump flow.

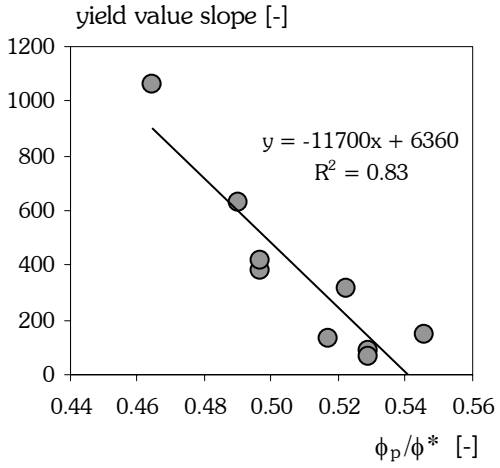


Fig. 6.21 Relation between the ratio of the paste content to packing density of the aggregates compared with the slope of linear regression lines of Fig. 6.20

The yield value of SCFRC can be estimated with Equation 6.11 and was calculated as the sum of the yield value of plain SCC and a second part, which describes the effect of the fibres. The slope of mixture OS9 is chosen to be zero; a negative slope was predicted. The regression line (Fig. 6.21) passes zero at a normalised paste content of about 0.54. The mean error of the predictions of self-compacting mixtures of series OS is 19.1 Pa (STD: 11.0 Pa). Fig. 6.22 compares experimental results and predictions on

the yield value. The number of experiments and the range of yield values are limited; the yield values of the reference mixtures were close to zero.

$$\tau_{0,SCFRC}[Pa] = \tau_{0,SCC} + \Delta_{SF} \cdot (-11.7 \cdot 10^3 \cdot \frac{\phi_p}{\phi^*} + 6.36 \cdot 10^3) \quad (6.11)$$

where: $\tau_{0,SCFRC}$ = yield stress SCC with fibres [Pa]
$\tau_{0,SCC}$ = yield stress SCC without fibres [Pa]
Δ_{SF} = difference of the relative slump flow due to the fibres' addition [-]
ϕ_p/ϕ^* = ratio of paste content (incl. air) to packing density of the aggregates [-]

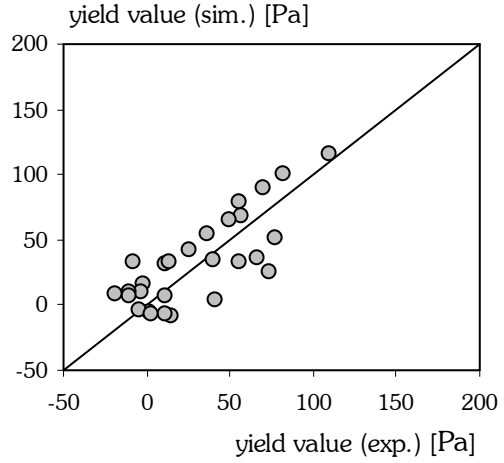


Fig. 6.22 Comparison between experimental and predicted yield values of series OS

6.3.3 Effect of the fibres on the plastic viscosity

The plastic viscosity of plain SCC is predicted with Equation 6.7. In the following, the effect of the steel fibres on the plastic viscosity is discussed. The plastic viscosity increases at decreasing thickness of the relative paste layer (Fig. 6.23). It is noted that not all mixtures of Fig. 6.23 were self-compacting. The steel fibres significantly increase the friction of the granular skeleton due to their irregular shape; the degree of it depends on the reference mixture. In contrast to the slump flow, the increase of the plastic viscosity at increasing fibre factor was not linear but increased more than proportional. Wallevik [2003] found 160 Pa·s as a maximum plastic viscosity of plain SCC. The highest plastic viscosity of SCFRC, which fulfilled all criteria, was 267 Pa·s (mixture 71); the plastic viscosity of the corresponding reference mixture was 81 Pa·s (OS6).

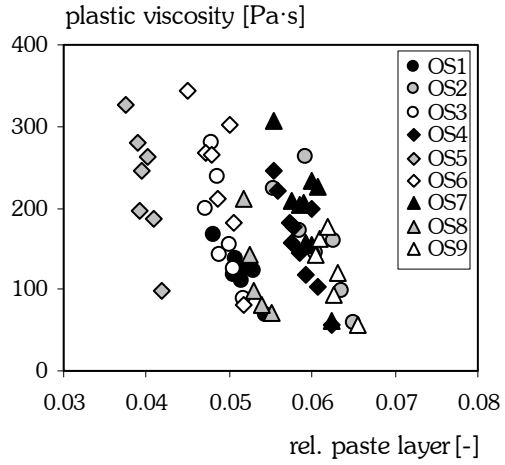


Fig. 6.23 Increase of the plastic viscosity at decreasing thickness of the relative paste layer (series OS)

Two effects of the fibres are accounted for: First, the relative paste layer thickness decreases due to the decreasing packing density at increasing fibre factor (Fig. 6.13). The conclusion of preliminary calculations was that the experimental plastic viscosity increases more than proportional at increasing fibre factor when compared with predictions using Equation 6.7. Second, an additional contribution (a frictional part) is incorporated, which depends on the fibre factor. The best accuracy is obtained with Equation 6.12.

$$PV_{SCFRC}\,[Pa \cdot s] = PV_{WF} + V_f \cdot \frac{L_f}{d_f} \cdot PV_{WF}^{\,1.19} \qquad (6.12)$$

where: PV_{SCFRC} = plastic viscosity of SCFRC [Pa·s]
PV_{WF} = plastic viscosity with fibres, RPL thinner compared with SCC [Pa·s]
V_f = fibre content (volume) [Vol.-%]
L_f/d_f = aspect ratio [-]

The first part (PV_{WF}) is obtained with Equation 6.7 considering the effect of the fibres on the packing density and the relative paste layer thickness. The second part includes the fibre factor. Fig. 6.24 shows the comparison between predicted and experimental results on the plastic viscosity of series OS. The mean error of the model (mixtures with steel fibres only) is 31 Pa·s (STD: 23 Pa·s).

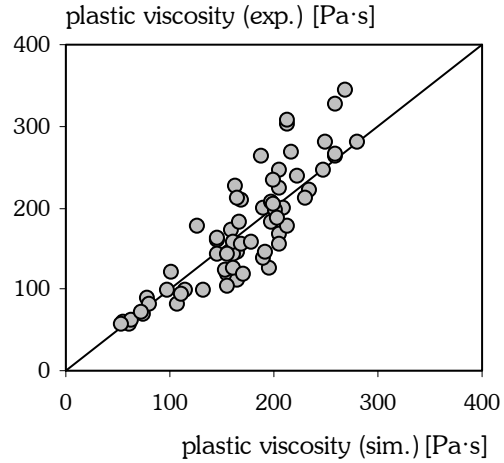


Fig. 6.24 Predictions versus experimental results of the plastic viscosity of SCC with and without steel fibres

Flow-time T_{50}

The flow-time T_{50} is the time required to pass a prescribed circle of 500 mm after lifting the cone. T_{50} is correlated with the plastic viscosity [Níelsson & Wallevik, 2003] and depends on the final slump flow [Sedran, 1999]. The closer the final slump flow is to 500 mm the higher the variation of T_{50} becomes [Emborg et al., 2003]. Fig. 6.25 shows the relation between the experimentally found plastic viscosity and T_{50}.

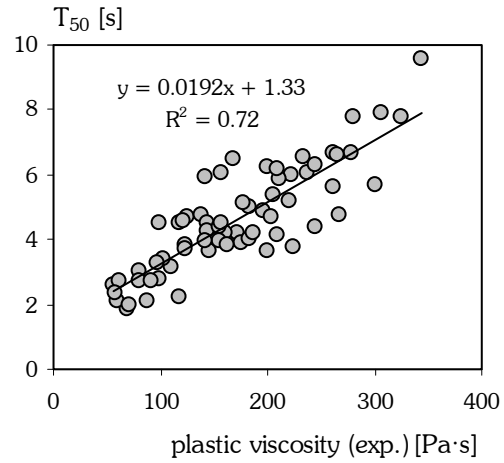


Fig. 6.25 Experimental results: plastic viscosity versus flow-time T_{50} (series OS)

T_{50} can be predicted with Equation 6.13; the mean error is 0.65 s (STD: 0.54 s) and 0.80 s (STD: 0.64 s) in case of the predicted plastic viscosity (Equation 6.12).

$$T_{50}\,[s] = 1.33 + 19.2 \cdot 10^{-3} \cdot PV_{SCFRC}\,[Pa \cdot s] \qquad (6.13)$$

Fibre funnel flow-time

A mixture with long steel fibres (L_f=60 mm) was tested in the early stage of this research project in a conventional V-funnel; the fibres caused blocking. To test SCFRC, a larger funnel (fibre funnel) was applied, which has an opening gap of at least two times the maximum fibre length (125 mm in square). All mixtures of series PS/OS were tested with this fibre funnel. Fig. 6.26 shows the relation between the experimental plastic viscosity and the fibre funnel flow-time. The increase in flow-time at increasing plastic viscosity due to the fibres was smaller compared with T_{50}. Equation 6.14 predicts the fibre funnel flow-time; the mean error is 0.37 s (STD: 0.25 s) with the experimentally found plastic viscosity and 0.37 s (0.29 s) with the predicted plastic viscosity (Equation 6.12).

$$Fibre\ funnel\ flow-time\ [s] = 2.33 + 8.41 \cdot 10^{-3} \cdot PV_{SCFRC}\ [Pa \cdot s] \qquad (6.14)$$

Fig. 6.27 compares the experimental and predicted flow-times of the fibre funnel and T_{50} of series PS. The predicted flow-times were calculated from the predicted plastic viscosity (Equation 6.12), since no rheological measurements were carried out on series PS. Fig. 6.27 shows that the experimental flow-times of the fibre funnel of series PS are relatively higher compared with T_{50}, which might be due to the fact that the fibre funnel flow-times of series PS1-4 are more affected by passing ability.

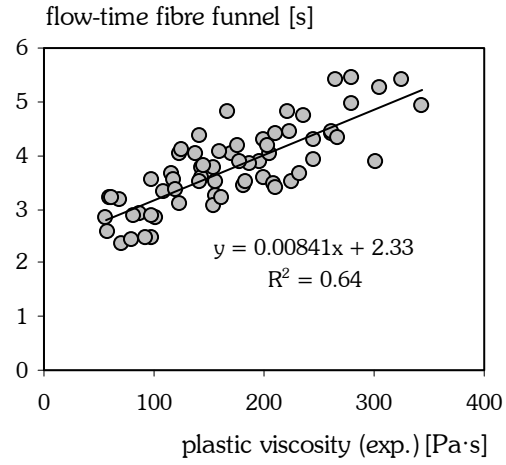


Fig. 6.26 Relation between the experimental plastic viscosity and the fibre funnel flow-time (series OS)

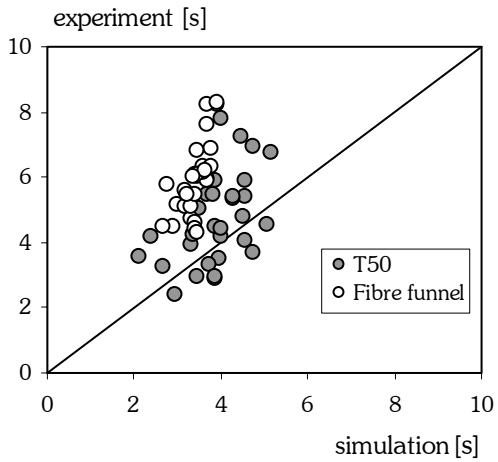


Fig. 6.27 Predictions of T_{50} and fibre funnel flow-times of series PS versus experimental results

6.3.4 Passing ability of SCFRC

The prediction of the minimum bar spacing required for SCFRC to avoid blocking is an essential tool to optimise the mixture composition. Experiments indicate that the bar spacing of SCFRC has to be increased compared with SCC; the fibres are usually the largest components. Self-compacting mortars with short steel fibres (6 and/or 13 mm)

were able to pass the J-ring test at a bar spacing of 36 mm without blocking [Grünewald & Walraven, 2001b]. In contrast, the bar spacing required to avoid blocking of mixtures with long steel fibres might be 99 mm or larger (Table 5.6). Table 3.2 provides a guideline for the minimum bar spacing required for SCFRC. The fibre contents, to which this guideline applies, are lower than most of the fibre contents tested in this study. According to Groth [2000b], the affecting parameters on the bar spacing are the aspect ratio, the fibre content and the length of the steel fibres. The following parameters were considered as affecting parameters on the bar spacing of SCFRC:

- Fibre content
- Fibre length and type
- Content and composition of the aggregates.

Effect of the aggregates

The CBI-approach 'risk of blocking (ROB)' (Fig. 2.3) takes into account the effect of the aggregates (crushed or natural) on the passing ability of SCC. The inclusion of the steel fibres extends this approach. The applied aggregates of this study are assumed to be 'natural' aggregates. Fig. 6.28 presents the ROB of SCC with and without fibres at the 'non-blocking' bar spacing for series PS/OS. The volume of the fibres slightly decreased the aggregate content of the reference mixture. The non-blocking bar spacing of mixtures with steel fibres was at least 62 mm; only mixtures that fulfilled the design criteria for SCFRC were considered in the following analysis.

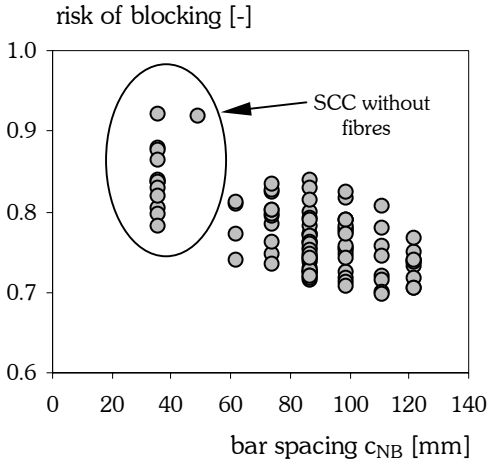


Fig. 6.28 The risk of blocking of aggregates for mixtures of series PS/OS at the 'non-blocking' bar spacing (c_{NB})

The ROB of the reference mixtures was lower than the theoretical optimum of 1; the paste content and/or the ratio sand to total aggregate in most cases were higher compared with optimised SCC. In a second step, the ROB is calculated for bar spacings at which blocking occurred; the ROB increases at decreasing bar spacing (~13 mm).

Fig. 6.29 shows the differences of the ROB for blocking and non-blocking bar spacings. The difference is negligible for SCFRC, whereas it is significant for plain SCC.

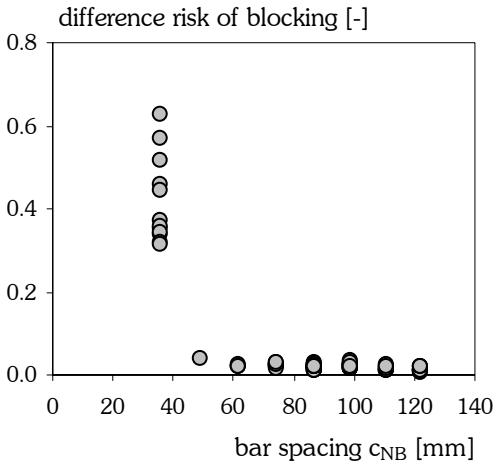


Fig. 6.29 Difference in the risk of blocking for bar spacings at which 'blocking' (c_B) and 'non-blocking' (c_{NB}) was obtained

Predicting the required bar spacing for 'non-blocking' for SCFRC

The 'non-blocking' bar spacing of SCFRC, which was determined from tests with the J-ring, is normalised to the fibre length to generalise the model. In order to exclude the effect of fibre clustering, which might affect the heights of concrete around the bars of the J-ring, only self-compacting mixtures are analysed (below or equal to the maximum fibre content). Three parameters affect the passing ability of SCFRC; the blocking factor (Equation 6.15) is defined as follows:

$$Blocking\ factor\,(BF) = ROB_{(BS)} \cdot V_f \cdot BD \qquad (6.15)$$

where: $ROB_{(BS)}$ = risk of blocking (depends on the chosen bar spacing) [-]
V_f = fibre content (volume) [Vol.-%]
BD = blocking diameter (depends on fibres' diameter) [-]

The blocking factor includes the effect of the aggregates and the type and the content of the steel fibres and is the product of three components:

- the risk of blocking (contribution aggregates), which depends on the bar spacing
- the content of the steel fibres (Vol.-%)
- the blocking diameter BD (depends on the diameter of the steel fibre)

The fibre diameter was applied to characterise different fibre types. The effect of the diameter on the passing ability increased at decreasing diameter; a dimensionless factor BD was included in Equation 6.15 to take this fact into account. Fig. 6.30 shows the relation between the diameter of the fibre and the factor BD.

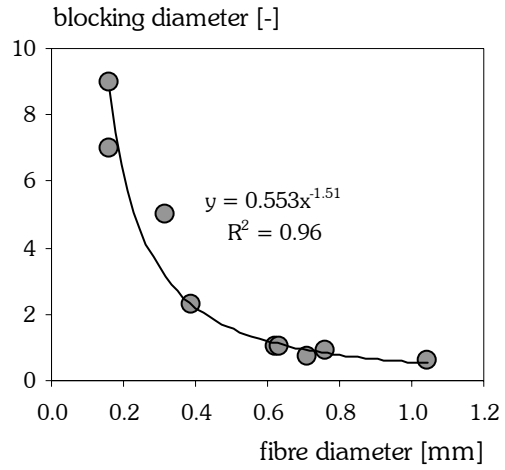


Fig. 6.30 Relation between the diameter of the steel fibres and the blocking diameter (BD)

The data points of Fig. 6.30 were obtained by a successive addition of different fibre types, while controlling the coefficient of regression (linear relation) between the normalised ratio of bar spacing to fibre length and the blocking factor (for 'non-blocking'). The factor BD of the fibre type Dramix 45/30 BN was set to 1 to start the analysis. Equation 6.16 can be applied to estimate the blocking diameter BD (R^2=0.96):

$$\text{Blocking diameter (BD)} = 0.553 \cdot d_f^{\,-1.51} \qquad (6.16)$$

where: d_f = fibre diameter [mm]

Fig. 6.31 relates the normalised ratio of bar spacing to fibre length for 'blocking' and 'non-blocking' with the related blocking factor.

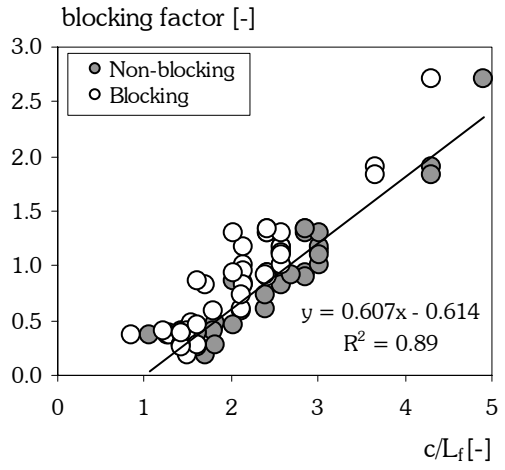


Fig. 6.31 Comparison between the average model (model 1) and test results at 'non-blocking' and 'blocking' bar spacings for SCFRC

The straight line is the linear regression line of the data points for non-blocking for which the highest coefficient of regression was obtained. Few white dots ('blocking' bar spacings, c_B) surpass the prediction of model 1 (Equation 6.17).

$$BF = 0.607 \cdot \frac{c}{L_f} - 0.614 \text{ (model 1)} \tag{6.17}$$

where: BF = blocking factor of SCFRC [-]
c = clear spacing between reinforcement [mm]
L_f = fibre length [mm]

The actual bar spacing for 'blocking' is not exactly known since the bar spacing of the J-ring had to be increased in predefined steps (Chapter 5.2.4). It is somewhere between the bar spacing for 'blocking' and 'non-blocking'. The predictions are on the safe side in case none of the data points surpass the model. The models' line was shifted parallel to model 1; the intersection with the data point at the largest distance from model 1 resulted in the second model (Equation 6.18).

$$BF = 0.607 \cdot \frac{c}{L_f} - 0.857 \text{ (model 2)} \tag{6.18}$$

where: BF = blocking factor of SCFRC [-]
c = clear spacing between reinforcement [mm]
L_f = fibre length [mm]

Fig. 6.32 shows model 2 compared with the test results; the predictions indicate 'non-blocking' in each case.

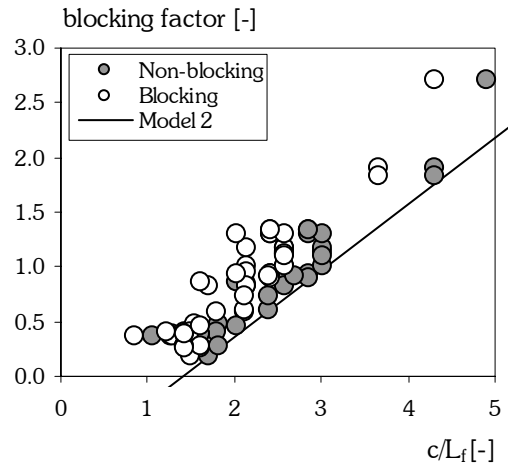


Fig. 6.32 Predictions of the bar spacing for non-blocking (model 2) compared with the test results of SCFRC

The effect of short steel fibres on the passing ability of self-compacting mortar was studied, too. Most mixtures passed the J-ring at a bar spacing of 36 mm without blocking [Grünewald & Walraven, 2001b]. Since the smallest bar spacing was 36 mm,

the actual bar spacing required for 'non-blocking' could be determined for a few mixtures only. Equation 6.15 was applied to analyse the results of series MS. A correction (0.25 times the blocking factor) was applied to obtain results, which can be compared with the results of mixtures containing long steel fibres (Fig. 6.33). Fig. 6.33 summarises experimental results and predictions of series PS/OS/MS. Predictions with long steel fibres (20 mm or larger) are more reliable.

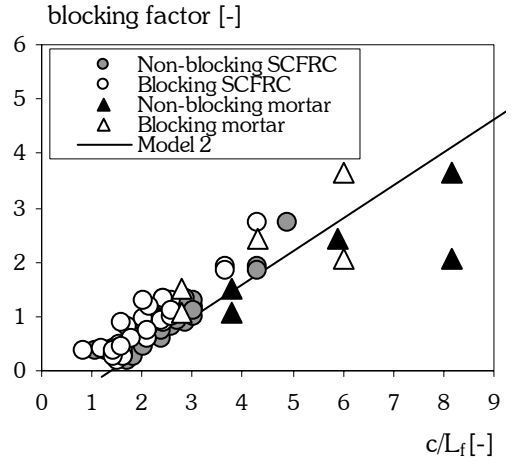


Fig. 6.33 Predictions and experimental results on the passing ability of SCFRC (series PS/OS/MS)

Predicting the bar spacing for SCFRC

The ROB has to be determined with the actual bar spacing; the prediction of the bar spacing becomes an iteration. Model 2 can be applied in two ways: First, in case the design bar spacing is known, the blocking factor can be calculated with model 2 under consideration of the chosen fibre length. The diameter of the fibre can be calculated from the aspect ratio. The remaining parameters, the fibre volume and the ROB, might be chosen. The fibre content has to remain below the maximum fibre content (Chapter 6.3.5). The content and the grading of the aggregates determine the ROB at this bar spacing. The actual blocking factor has to be smaller than the predicted blocking factor. Second, model 2 might be applied to calculate the bar spacing required for non-blocking. The blocking factor is determined from the mixture composition. To calculate the ROB, the actual bar spacing needs to be estimated. A comparison between the estimated and calculated bar spacings is required to control the assumed bar spacing.

6.3.5 Maximum fibre content of SCFRC

The maximum fibre content is by definition the highest possible amount of steel fibres, which can be added to SCC; SCFRC is self-compacting below this fibre content. The criteria on SCFRC are discussed in Chapter 5.3. The affecting parameters are the type of steel fibre and the composition and the characteristics of plain SCC. In the following, a model is discussed, which predicts the maximum fibre factor ($V_f \cdot L_f/d_f$) for fibre lengths

in the range of 6-60 mm. The model refers to SCC, which has characteristics in the fresh state (slump flow and stability) similar with that of the reference mixtures of this study.

Predicting the maximum fibre content

The CBI-concept 'risk of blocking' takes into account the effect of the aggregates on the bar spacing. This concept is applied to predict the maximum fibre factor. The approach was as follows: The bar spacing to aggregate fraction diameter ratio of the CBI-concept was replaced by the ratio of the fibre length to aggregate fraction diameter. The content and the distribution of the aggregates determine the maximum fibre content. The characteristic points of the 'nature' line (Fig. 2.3) were altered to achieve the best correlation with the maximum fibre factor. Fig. 6.34 shows the relation between the ratio fibre length to aggregate diameter and $n_{a,mfi}$ (relative effect on maximum fibre content, MFC-ratio). The analysis indicates that relatively large aggregates ($L_f/D_{af} < 1.8$) result in a lower MFC-ratio; $n_{a,mfi}$ is about constant at higher ratios of $L_f/D_{af.}$.

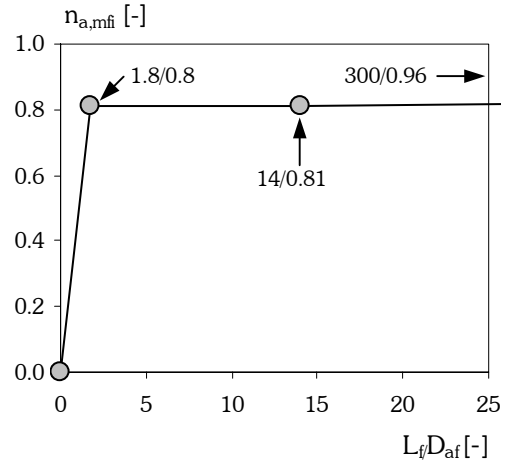


Fig. 6.34 Relation between the ratio fibre length to aggregate diameter and the MFC-ratio ($n_{a,mfi}$)

Fig. 6.35 relates the maximum fibre factor of mixtures of series PS/OS/MS to the maximum fibre content volume (MFC) of the aggregates. The maximum fibre content ($V_f \cdot L_f/d_f$) can be calculated as the intersection with the regression line (Equation 6.19).

$$\text{Maximum fibre factor} = \frac{0.781 - MFC}{0.211} \qquad (6.19)$$

where: MFC = maximum fibre content volume [-]

SCC is self-compacting at a given fibre factor in case the MFC-volume is equal or lower compared with the regression line of Fig. 6.35. The mixture, which was optimised for sheet piles (Chapter 10.2), is also included in Fig. 6.35 (mix sheet piles); its maximum aggregate size was 1 mm.

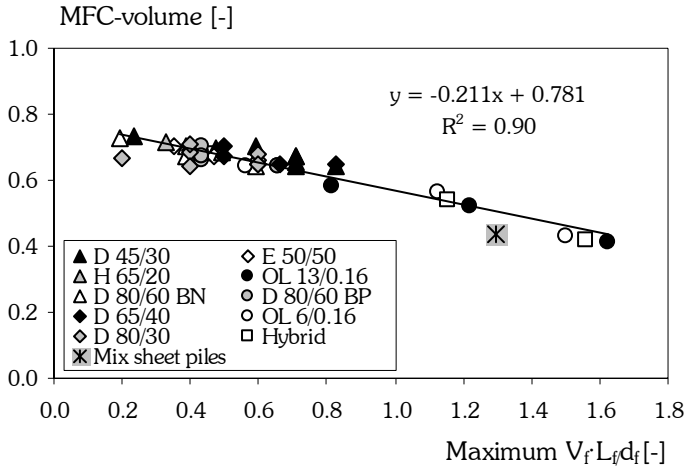


Fig. 6.35 Relation between the maximum fibre factor and the MFC-volume

The fibre length was the weighed average in case a hybrid mixture of short fibres (6 and 13 mm) was applied. The model is calibrated with mixtures, which contained exclusively round aggregates. A single mixture contained crushed aggregates (B105, Dramix 80/60 BP, 60 kg/m^3). The composition was the same (in Vol.-%) as for mixture OS4; crushed instead of round coarse aggregates were applied. In spite of the crushed coarse aggregates the mixture was self-compacting. Fig. 6.36 shows the comparison of the experimental results for self-compacting or non-self-compacting mixtures and the proposed model. Few results were found to be at the 'wrong side' (white dots below and grey dots above) of the proposed threshold line (Fig. 6.36). The fibre contents of series PS/OS were increased in steps of 20 kg/m^3 (MS: 0.5 Vol.-%); the actual maximum fibre content is between the 'self-compacting' and 'non-self-compacting' result. The mixtures had a maximum aggregate size of 4/8/16 mm and long, short or a combination of short fibres was tested. To increase the maximum fibre content the following parameters might be altered: fibres of a lower aspect ratio, increasing the content of cement paste, replacing coarse with finer aggregates. Once aggregate fractions with a ratio $L_f/D_{af} < 1.8$ are excluded, the paste content becomes the governing parameter.

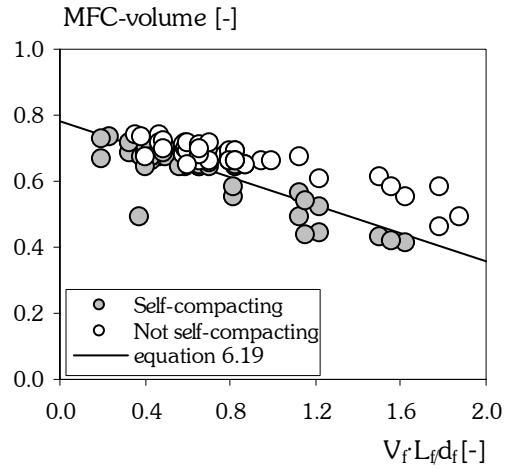


Fig. 6.36 Predictions on the maximum fibre content versus experimental results of SCFRC

The author remarks the following about the principle of the maximum fibre content and the criteria chosen to determine it: Observations on the homogeneity of fibres in SCFRC were obtained from the slump flow test, which might not be an adequate prediction of the flow behaviour in case a larger volume of SCFRC is cast (e.g. vertically from a skip). Mixtures of higher fibre factors (fibre length ≤ 20 mm) have been successfully applied in Ultra-High-Strength Concrete. Fibre clustering occurs according to the design criteria of Chapter 5.3. It seems that fibre clustering is more serious the longer the fibres are. Bending tests [Grünewald & Walraven, 2002b] showed that clustering of long (60 mm) fibres affected the performance in the hardened state and more fibres remained at the position at which the concrete was cast. A cluster-free and homogeneous distribution of the fibres along the flow assures a complete embedment in paste and probably a higher efficiency of a single fibre.

6.4 Examples of predictions of characteristics in the fresh state

In the following, calculations with the models for SCFRC in the fresh state are presented; a mixture from series OS4 with Dramix 80/60 BP steel fibres (Appendix G, mixture 56, V_f = 60 kg/m^3) was chosen as an example. The discussed characteristics are the maximum fibre content, the required bar spacing for non-blocking, the slump flow and further characteristics of SCFRC in the fresh state.

Maximum fibre factor (Equation 6.19) = 0.668
Actual fibre factor $V_f \cdot L_f/d_f$: 60 kg/m^3·85.7/(7850 kg/m^3) = 0.66 < 0.668

Grading of the aggregates (round sand and coarse aggregates): Table 4.4
Sand-to-total aggregate 68 %, paste content 41.0 Vol.-% (incl. 2.0 Vol.-% Air)
MFC-volume: 0.64 (Appendix G, mixture 56)

Required bar spacing:
Model 1 (Equation 6.17): c/L_f = 1.85 (113 mm for L_f = 61.1 mm)
Model 2 (Equation 6.18): c/L_f = 2.25 (137 mm for L_f = 61.1 mm)
measured bar spacing for non-blocking: 87 mm; c/L_f=1.42

$ROB_{(BS)}$ = 0.72 for 137 mm - requires Iteration: 100 mm (0.73); 150 mm (0.71)
BD (d_f = 0.713 mm, Equation 6.16) = 0.922
V_f = 60 kg/m^3/7850 kg/m^3 = 0.764 Vol.-%

Slump flow reference mixture (Equation 6.5): 725 mm
measured slump flow reference mixture: 725 mm (Appendix G, mixture 53)

Mini-slump: 133 mm (Appendix F, mixture OS4)
$(\phi/\phi^*)_g$ = 0.762 (Appendix G, mixture 53)

Predicted slump flow SCFRC: 616 mm (Equations 6.5 and 6.9)
measured slump flow 645 mm (Appendix G, mixture 56)

Paste flow-time: 4.0 s (Appendix F, Mixture OS4)
$(\phi/\phi^*)_g$ = 0.762 (Appendix G, mixture 53)
Slump flow slope (Equation 6.9: -0.230)
Actual fibre factor $V_f \cdot L_f/d_f$: 85.7·60 kg/m^3/7850 kg/m^3 = 0.66
Relative slump flow: 1-0.66·0.23 = 0.85 (0.85·725 mm = 616 mm)

Yield value $\tau_{0,SCFRC}$ (Equation 6.11): 6.8 Pa *measured yield value: 41.2 Pa (Appendix G, mixture 56)*
$\tau_{0,SCC}$ (Appendix G, mixture 56): -11.9 Pa Δ_{SF} = 1- (645 mm/725 mm) = 1-0.89 = 0.11 (slump flow with/without fibres) ϕ_p = 0.41 (paste content) ϕ^* = 0.775 (Appendix G, mixture 53)
Plastic viscosity PV_{SCFRC} (Equation 6.12): 153.8 Pa·s *measured plastic viscosity: 102.3 Pa·s (Appendix G, mixture 56)*
RPL (Appendix G, mixture 56): 0.061 $(\phi/\phi^*)_p$ (Appendix F, mixture OS4): 0.935 PV_{WF} (Equation 6.7) = 63.0 Pa·s Actual fibre factor $V_f \cdot L_f/d_f$: 85.7·60 kg/m^3/(7850 kg/m^3) = 0.66
Flow-time T_{50} (Equation 6.13): 4.3 s; with measured plastic viscosity: 3.3 s *Test result T_{50}: 3.4 s* *Flow-time fibre funnel (Equation 6.14): 3.6 s, with measured plastic viscosity: 3.2 s* *Test result fibre funnel: 2.8 s*

6.5 Optimisation of SCFRC

The addition of the steel fibres requires an adjustment of the mixture composition and defined characteristics of plain SCC in the fresh state. The range of SCCs, which is applicable for high fibre contents, is smaller compared with plain SCC. Segregation resistance is the most important characteristic of SCFRC; the addition of a viscosity agent to a 'powder-type SCC' enhances the stability of the fibres. In order to compensate for the effect of the fibres, the demands for an optimised SCC for high fibre contents can be summarised as follows:

1. Yield value of about zero: The fibres decrease the filling ability (flowability) of SCC. The plastic viscosity was a less affecting parameter.

2. Provide 'space' for the fibres: The packing density should be optimised to increase the surplus of paste and the relative paste layer thickness. Due to the decrease of the packing density, the paste content has to be adjusted.

3. High viscosity of cement paste: In spite of the increased relative paste layer thickness compared with optimised SCC, the plastic viscosity of mixtures of series OS was high (56-98 Pa·s). A high plastic viscosity of cement paste counteracts the segregation of the fibres.

4. Moderate coarse aggregate content: Coarse aggregates (relative to the fibre length) decrease the maximum fibre content and increase the bar spacing required to avoid blocking. The range of aggregates has to be as wide as possible to increase the packing density of the granular skeleton.

High fibre contents can be added to powder- and viscosity agent-type SCCs; the 'lattice-type SCC' [Wallevik, 2003; Chapter 2.3.2] is not applicable for high fibre contents because it does not fulfil the demands 1-3 of the ideal SCFRC. The design principles for SCFRC can be summarised as follows: First, keep the fibre content below the maximum fibre content, which implies that the required space for fibres is provided by optimising the granular skeleton and the paste content. Second, choose the type and the content of the steel fibres to meet the demands on passing ability or the performance in the hardened state. Third, compose the paste to fulfil the demands on filling ability and segregation resistance; the optimisation of SCC for fibres is easier to perform without adding the fibres in the stage of the mix design.

6.6 Concluding remarks

Chapter 6 discussed the effect of the type and the content of the steel fibres on filling ability and passing ability of SCC; the powder-type SCC was an applicable concept to counteract the segregation of the steel fibres. Models are proposed, which allow predicting the key characteristics of SCFRC and provide tools to optimise the mixture composition. Based on reference SCC mixtures with defined characteristics in the fresh state, the effect of adding steel fibres on the slump flow, the yield value, the plastic viscosity, T_{50} and the fibre funnel flow-time is quantified. The addition of the fibres increases the number of variables available in mix design compared with SCC; the proposed models reduce the number of experiments. The maximum fibre content is the fibre content below which SCC remains self-compacting. The content and the distribution of the aggregates determine the maximum fibre content; the effect of the type and the content of the steel fibres is best described by the fibre factor. The mixture composition can be optimised for lower fibre contents, which results in more economical and performance-based mixtures.

The contribution of the paste to the slump flow can be best described by the mini-slump flow; no general relation with layer or packing concepts was found. The fibres decrease the slump flow and increase the yield value and the plastic viscosity, the degree to which is discussed. Due to the elongated shape of the steel fibres, they have a significant effect on the passing ability of SCC. The CBI-approach 'risk of blocking' was extended for the effect of the steel fibres. To calculate the bar spacing for non-blocking, the content and the distribution of the aggregates as well as the type and the content of the steel fibres has to be considered.

Chapter 6 concludes part I of the thesis, which discussed the performance of SCFRC in the fresh state. Part II describes the effect of the steel fibres on SCC in the hardened state.

Chapter 7:

Cement-based fibre reinforced matrices in the hardened state

7.1 Introduction

This chapter provides an overview of the literature on the behaviour of fibre reinforced cement-based matrices in the hardened state: from the level of the single fibre pull-out up to the performance of structural elements. Chapter 7 is divided into three parts, which introduce the theoretical background for Chapters 8-10. The three parts are: fibre reinforced cement-based matrices in the hardened state, test methods for FRC and the orientation and the distribution of the fibres.

Fibres are produced from a wide variety of materials, and in various sizes and shapes. They improve the characteristics of cement-based matrices in the hardening and the hardened state, e.g. are able to bridge cracks, to transmit stress across a crack and to counteract crack growth. FRC becomes an option whenever durability (limited crack widths) or safety considerations are design criteria. The fibres improve the fatigue behaviour and increase the wear resistance. Since a crack often starts at the weakest point of a composite material, the fibres have to be as homogeneously distributed as possible. The direction in which the fibres are oriented and whether a fibre ruptures or is pulled out determine their effectiveness. Fibres have been added to concrete in combination with bar reinforcement, prestressing strands or as the only reinforcement. The application of FRC often has not been considered because of a lack of standardisation or for economical reasons. SCFRC already has been successfully applied in floors, walls and in Ultra-High-Strength Concrete. With further understanding of what causes the variation of test responses (the effect of the orientation and the distribution of the fibres) and insight into how to optimise the mixture composition it is possible to increase the number and the fields of applications.

7.2 Characteristics in the hardened state

7.2.1 Single fibre pull-out test

The composite behaviour of fibre reinforced concrete depends on the pull-out behaviour of a single fibre from the matrix, as well as on their orientation and distribution over the crack surface. The production process and the characteristics of concrete in the fresh state also determine the quality of the matrix around a fibre. The single fibre pull-out test is a test on the anchorage capacity of a single fibre at specified conditions. Several researchers modelled the pull-out behaviour of straight steel fibres [Naaman, 1999; Stang & Li, 2001] and of hooked-end fibres [Alwan et al., 1999; Van Gysel, 2000; Weiler et al., 1999]. Groth [1996] performed single fibre pull-out tests with hooked-end steel fibres embedded in SCC. Fig. 7.1 compares the stages during pull-out of straight and hooked-end steel fibres: it shows the adhesive, the mechanical and the frictional bond areas.

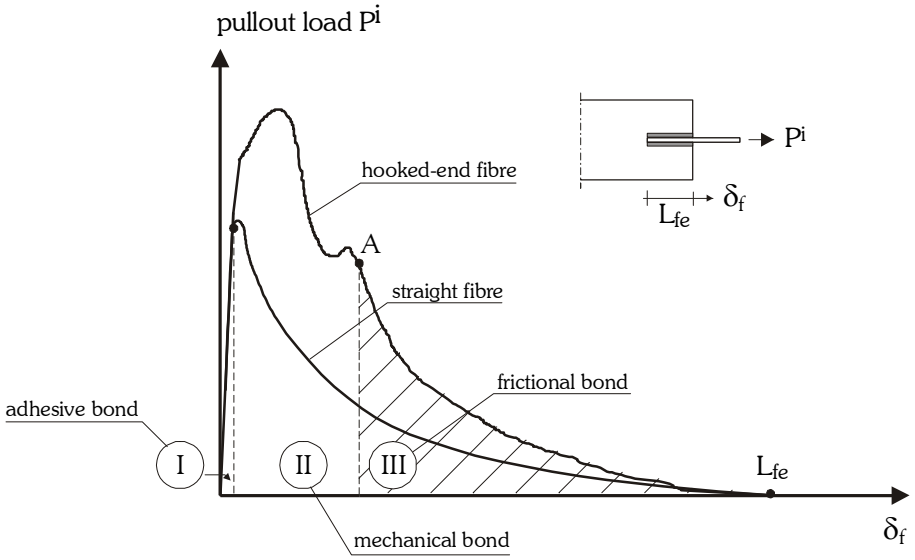


Fig. 7.1 Pull-out performance of straight and hooked-end steel fibres [after: Alwan et al., 1999]

According to Van Gysel [2000], the pull-out process of a hooked-end fibre is a combination of five distinguished processes. A hooked-end fibre enters the straight channel at point A (Fig. 7.1).

- Elastic deformation: bond due to adhesion
- Debonding between matrix and fibre
- Plastic deformation of the hook
- Coulomb friction due to normal forces and curvature of the hook
- Frictional force between matrix and fibre in the channel

Van Gysel [2000] concluded from single fibre pull-out tests with hooked-end and straight steel fibres and conventional concrete the following:

The hook significantly increases the maximum pull-out force compared with the same fibre type without a hook due to the plastic deformation and Coulomb friction of the hooked end. The hook also increases the frictional resistance once the fibres completely entered the straight channel (the fibre hook is not perfectly straight). Fibres having a higher tensile strength result in a higher pull-out force; a higher load is required to deform them. The embedded fibre length improves both the maximum pull-out force (contribution of adhesion of the straight part) as well as the dissipation of energy during pull-out. The angle with which a straight fibre is oriented into the direction of the force affects the maximum pull-out force. It increases the maximum load up to 50%. The maximum pull-out force and the dissipated energy of hooked-end fibres are about the same when embedded in different angles. According to Van Gysel, the explanation is that the axial force already is high enough to deform the fibre at the place where the fibre leaves the channel. The embedded length of the fibre and the strength of the matrix determine whether pull-out occurs or spalling of a matrix cone decreases the effectiveness of the fibre. The chance that concrete spalling or fibre rupture take place increase at increasing angle to the direction of the load.

'Mechanical' fibre factor (MFF)

According to Glavind [1992], the (mechanical) fibre factor (MFF) is the governing factor that describes the effect of the fibre addition on the linear part of the compressive strain curve. The parameters required to determine the MFF were derived from experiments and from the mixture composition. The mechanical fibre factor (MFF) can be calculated with Equation 7.1 [Glavind, 1992]:

$$MFF = V_f \cdot \frac{L_f}{d_f} \cdot \alpha_f \qquad (7.1)$$

with: $$\alpha_f = PD_p \cdot \frac{\beta_f}{w/c} \qquad (7.2)$$

where:
- MFF = mechanical fibre factor [MPa]
- V_f = fibre content (volume) [Vol.-%]
- L_f/d_f = aspect ratio [-]
- α_f = bond factor [MPa]
- PD_p = packing density of paste [-]
- β_f = factor incorporating the difference in shear stress of different fibre types [MPa]
- w/c = water-cement ratio [-]

The bond factor α_f includes the packing density of the dry paste material (PD), the water-cement ratio (w/c) and a factor β_f (MPa) that incorporates the difference between different fibre types. The w/c-ratio of Equation 7.2 was replaced by the water-binder ratio in the further analysis, which was calculated according to CUR-Recommendation 70 [1999]. Glavind considered α_f to be equal to the frictional shear strength (determined

from Aarre, 1992); β_f was 1.9 MPa for straight and 2.1 MPa for hooked-end steel fibres. The bond factor was 2.3 MPa for normal-strength concrete and 4.9 MPa for high-strength concrete. Kützing [2000] summarised results from literature on the average shear stress from single fibre pull-out tests (Table 7.1), which fit with the results of Glavind very well. It should be noted that the average shear stress always is an intermediate stress between the maximum pull-out stress until the fibre hook completely reaches its straight channel and the frictional shear resistance.

Table 7.1 Dependency of the average shear stress on the matrix quality for conventional concrete [summary from literature; after Kützing, 2000]

Matrix compressive strength class	$f_{ccm,cyl}$ *[MPa]*	*Frictional shear stress* τ_{fric} *[MPa]*
Normal strength	≤ 50 MPa	2.0-3.0 MPa
Medium strength	≥ 50; ≤ 70 MPa	3.5-4.5 MPa
High strength	> 70 MPa	5.0-6.0 MPa

7.2.2 Tensile behaviour of SFRC

The post-cracking response of SFRC can be directly determined with the uni-axial tensile test [Gettu & Barragán, 2003; Stroband, 1998a/b]. This test has been executed with or without notch. Relatively few studies on the uni-axial tensile behaviour of SFRC are reported in literature. The production of the specimens and the wall-effect affect the test response and often the scatter is rather high, since only a few (long) fibres cross the crack [Stroband, 1998a]. Compared with plain concrete larger specimens have to be prepared in order to limit the effect of the walls on the test response as much as possible. Alternatively, cylinders can be drilled from larger specimens; the fibres located close to the outer surface are not fully embedded in concrete. The preparation and the execution of the test is complex and experienced personnel is required. No direct tensile tests have been carried out in the study on SCFRC. Fig. 7.2 shows the effect of the content of 30 mm steel fibres on the post-cracking behaviour; the maximum tensile strength is hardly affected.

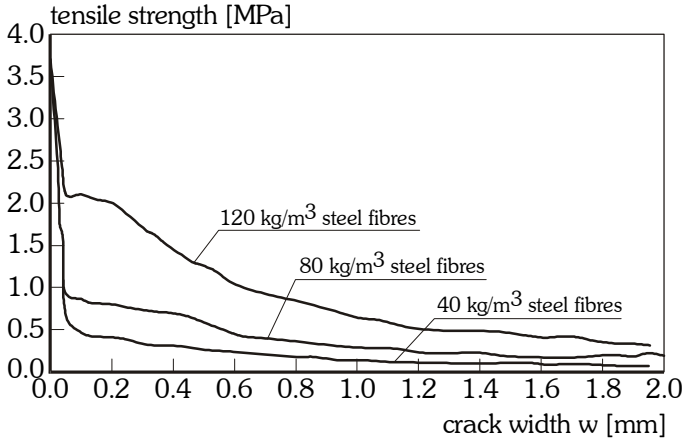


Fig. 7.2 Results of direct tensile tests on SFRC ($f_{fccm,cyl}$=40 MPa; 30 mm steel fibres) [after: Kützing, 2000]

Rossi et al. [1987] described the tensile behaviour of the fibre reinforced matrices by two distinguished levels: the micro- and the macro-level. The micro-level is initiated after the linear elastic stage is surpassed: Small cracks arise within the matrix, which start from initial flaws (air pores, interfaces, material weaknesses), while they are macroscopically not yet visible. At increasing load, the length of the cracks increases and micro-cracks localise. Due to the high number of short fibres (at a given fibre content), they are more likely to cross micro-cracks. In the macro-level stage, a crack gradually opens in the direction of the principal tensile stress. Long fibres improve the performance once a macro-crack appears. The geometry and the shape of the fibres determine at what stage they are active. Combining short and long fibres (hybrid fibre concrete) improves the initial tensile strength as well as the performance in the post-cracking regime.

7.2.3 Compressive behaviour of SFRC

Several researchers [Maidl, 1995; König & Kützing, 1999; Sato et al., 2000] found that the addition of the steel fibres has hardly any effect on the compressive strength just as on the tensile strength. The ductility increases due to the addition of the fibres. Fig. 7.3 compares the responses of plain concrete and SFRC in compression.

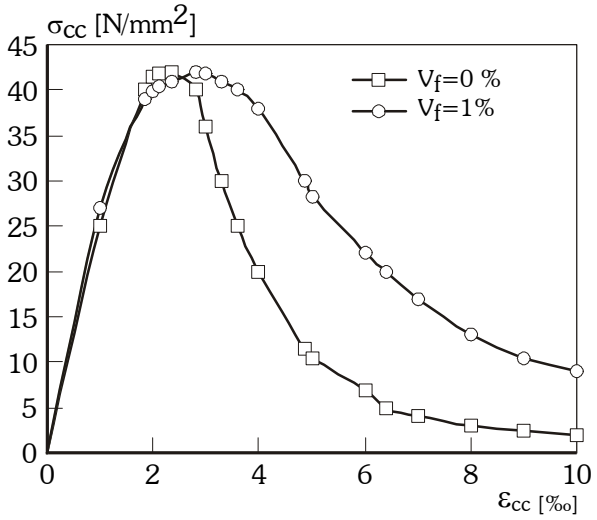


Fig. 7.3 Plain concrete and SFRC in compression ($f_{ccm,\,cyl}$=42 MPa) [after: König & Kützing, 1999]

Markeset [1993] modelled the compressive behaviour of plain concrete (Compressive Damage Zone Model). She distinguishes between two failure modes: First, longitudinal cracks appear within a specified range of the specimen (damage zone) after the linear elastic stage is passed. Second, after the maximum load is surpassed, those longitudinal tensile cracks coalesce together, form a shear band and finally, the specimen fails. Just as for direct tension fibres might counteract the occurrence of cracks of both types of failure modes and improve the performance of concrete.

No reference was found on the compressive behaviour of SCFRC. Recently, deformation-controlled compression tests with SCFRC have been carried out at the Delft University of Technology [Schumacher, 2001/2003a]. Compressive strength classes of B45 and B105 were considered and mixtures with different types and contents of the steel fibres were tested.

7.2.4 Bending behaviour of SFRC

The bending test is the most common test method to determine the post-cracking behaviour of SFRC. Kooiman [2000] discussed the advantages and the disadvantages of test methods for SFRC. Two types of deformation-controlled bending tests have been applied: the four-point and the three-point bending tests. The three-point bending test might be executed with or without notch. Design recommendations are usually based on experimental results of bending tests [JCI, 1984; DBV, 2001; ASTM, 1998; Vandewalle et al., 2002]. In order to keep the weight of the test specimen as low as possible, the dimensions of the specimen are limited, which has the drawback that the variation of different test responses is rather high. Kooiman [2000] showed that the scatter decreased at increasing width of the specimen.

The four-point bending test promotes the crack to occur at the weakest point within the region of the constant moment between the external loading points. Usually, this test is controlled on the deflection at mid-span.

The three-point bending test, which was chosen in the study on SCFRC, might be controlled either by the deflection at mid-span or by the crack opening at the tip of the notch. In order to force the crack to occur where the actual displacement is recorded, the beam has been notched in the middle. The maximum bending strength was higher for unnotched beams (>10 %) [Vandewalle & Dupont, 2001], which might be explained by the fact that the notch eliminates to some degree the effect of oriented fibres within the area close to the boundaries. A notch also introduces a stress concentration at its top.

The Swiss Standard on SFRC [SIA 162/6, 1999] recommends testing a round plate and applying a single load in the middle. The height of the plate has to be adjusted depending on the fibre length. The advantage of this test is a low variation of the test results (redistribution of forces in a statically indetermined structure). The disadvantage is that 'specimen behaviour' rather than 'material behaviour' is measured. Due to the higher weight of the specimens, they are more difficult to handle.
It was decided to follow Kooiman's approach and deformation-controlled three-point bending tests (with notch) were performed for SCFRC. Fig. 7.4 shows a comparison of the bending behaviour of plain concrete and SFRC. The maximum bending strength and the ductility might significantly increase due to the addition of the fibres; the increase depends on the matrix and the applied type and content of the fibres.

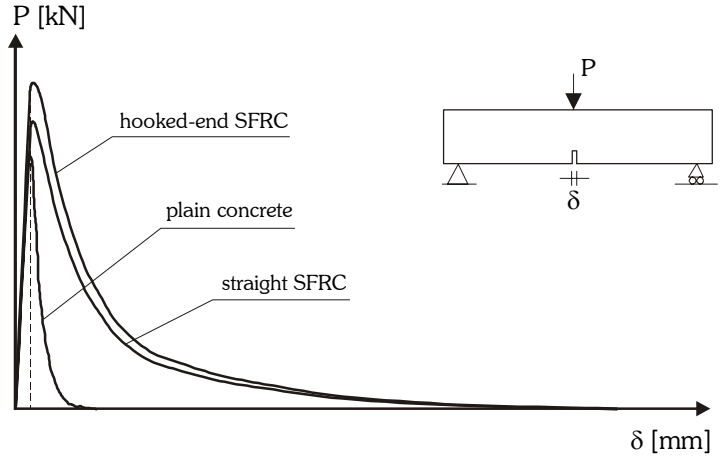


Fig. 7.4 Bending performance of plain concrete and SFRC [after: Kooiman, 2000]

7.2.5 Effect of the fibres on other mechanical characteristics

The replacement of bar reinforcement facilitates the production process. According to Rosenbusch & Teutsch [2003], the contribution of steel fibres on the shear strength can be taken into account.

Corrosion of the fibres positioned under the surface skin of concrete usually does not affect the durability, as the composite is uncracked. They corrode quickly, which is in most cases an esthetical problem only. Once concrete is cracked, the progress of corrosion of a fibre depends on the crack width. Crack widths smaller than 0.5 mm have no adverse effect on the corrosion of the fibres [Nemegeer et al., 2003]. Spalling of concrete due to the corrosion of a single fibre is not to be expected even with low-strength concrete.

The fatigue behaviour and the impact resistance of cement-based materials can be significantly enhanced by the addition of steel fibres. Buitelaar [2002] reports on High-Strength Concrete overlays to rehabilitate a steel bridge in the Netherlands, which increases the life-span of both the bridge and the overlay. The overlay consists of a composite of High-Strength Concrete, steel bar reinforcement and steel fibres. The matrix had a high early-age strength, which limited the traffic hinder due to the rehabilitation. Other examples of successful applications of SFRC are column-beam joints in earthquake areas and heavily-loaded industrial floors.

Fibres can improve the fire resistance of cement-bonded materials by counteracting spalling [Clayton & Lennon, 2000]. Polypropylene fibres are known to melt when heated. They create additional space and reduce the water pressure. Steel fibres (0.4 Vol.-%) improved the fire resistance of SCC (~80 MPa). Polypropylene fibres (0.2 Vol.-%) had no effect [Hertel et al., 2002]. To be self-compacting the volume of polypropylene fibres was chosen to be 0.2 Vol.-%, which was not sufficiently high to improve the fire resistance. Ultra-High-Performance Concrete was tested in the same

study; a mixture of steel and polypropylene fibres (0.2 Vol.-% each) decreased the damage compared with the reference mixture.

Volume changes due to shrinkage at an early age cause cracks in cement-bonded materials in case the deformation is restrained and the tensile strength is not sufficient to transmit the stress. Bars and fibres do not avoid cracking but they reduce the crack width compared with plain concrete.

7.3 Orientation and distribution of the fibres

7.3.1 Orientation numbers: 1D, 2D and 3D

In the following, theoretical considerations on the orientation of the fibres are presented to compare them with measurements on orientation numbers of SCFRC (Chapters 8 and 10). The orientation number is 1 for a fibre parallel to the direction of the tensile stress and 0 for a fibre that is oriented perpendicular to the tensile stress. The more the fibres are aligned into the direction of the tensile stress the more effective they are. Van Gysel [2000] showed that the performance of hooked-end fibres was not significantly affected by the angle with which they are embedded. The chance that a concrete cone breaks at the crack surface is lower the more aligned the fibre is. The number of fibres bridging a crack is obtained by Equation 7.3, which contains the orientation number (η_φ) as a factor [Krenchel, 1975].

$$N_f = \frac{V_f}{A_f} \cdot \eta_\varphi \qquad (7.3)$$

where: N_f = number of steel fibres per unit area [1/mm^2]
V_f = fibre content (volume) [Vol.-%]
A_f = area of the cross-section of a single fibre [mm^2]
η_φ = orientation number [-]

- *1D-situation*

The highest orientation number is obtained in case all fibres are aligned into the direction of the load. The orientation number equals 1; the fibre's cross-section appears as a point on the crack surface. The maximum effective embedded length of the fibre is equal to half the fibre length.

- *2D-situation*

Kameswara Rao [1979] determined the 2D-orientation number from projecting the mean fibre length on the axis that represents the direction of the tensile stress. Equation 7.4 was derived to determine the orientation number of randomly oriented fibres in a plane. Fig. 7.5 shows the fibre in a two-dimensional system. The projection of the mean fibre embedded length in the 2D-situation is L_f / π.

$$\eta_{\theta 2D} = \int_0^{\pi} \frac{\sin\theta \cdot d\theta}{\pi} = \frac{2}{\pi} = 0.637 \qquad (7.4)$$

where: $\eta_{\Theta 2D}$ = theoretical number of random oriented fibres in a plane [-]

Schönlin [1988] derived a 2D-orientation number of 0.785, which is higher compared with the orientation number of Equation 7.4.

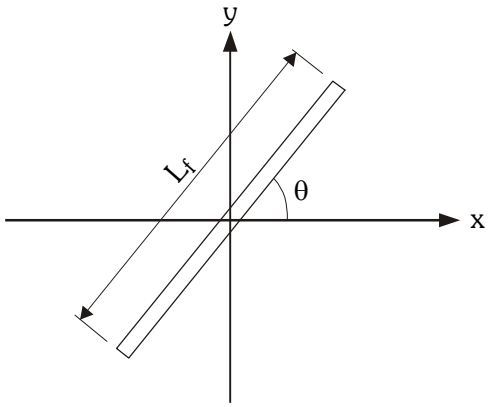


Fig. 7.5 Two-dimensional schematisation of the fibre orientation

- *3D-situation*

Schönlin [1988] summarised results of theoretical orientation numbers derived by several authors and reported on rather deviating numbers. Theoretical orientation numbers in literature vary between 0.20 and 0.825 (for 3D) and depended on the boundary conditions and assumptions of the authors. Stroeven [1978] calculated the spatial-random effectiveness based on the geometric probability theory. Projecting the fibre into two directions leads to a larger number of ends at the outer layer of the projection circle. According to Stroeven [1978], the mean projected fibre length was $L_f \cdot \pi/4$. After obtaining the mean projected fibre length the orientation number was calculated with the approach of Kameswara Rao [1979]; Equation 7.5 was obtained. The average projected embedded length in the 3D-situation is $L_f/4$. Like for the 2D-situation, Schönlin [1988] obtained a higher orientation number (0.66) for the 3D-situation compared with other authors.

$$\eta_{\theta 3D} = \int_0^{\pi} \frac{\frac{\pi}{4} \cdot \sin\theta \cdot d\theta}{\pi} = \frac{1}{2} \qquad (7.5)$$

where: $\eta_{\Theta 3D}$ = theoretical number of random oriented fibres in 3D-space [-]

Geometrical boundaries

The 2D- and 3D-orientation numbers obtained from Equations 7.4-5 are valid only in an infinite space. In reality, geometrical boundaries affect the orientation to various degrees. With the approach of Soroushian & Lee [1990] this influence can be accounted for. Kooiman [2000] applied their approach and calculated the average orientation number of beams of different dimensions under consideration of the geometrical boundaries of the mould. Fig. 7.6 shows the relation between the orientation number and the ratio beam depth (h) to fibre length (L_f). With 60 mm fibres and $h/L_f = 2.5$ the orientation number becomes 0.70 and for 30 mm fibres with $h/L_f = 5.0$ this is 0.66 (a = notch depth).

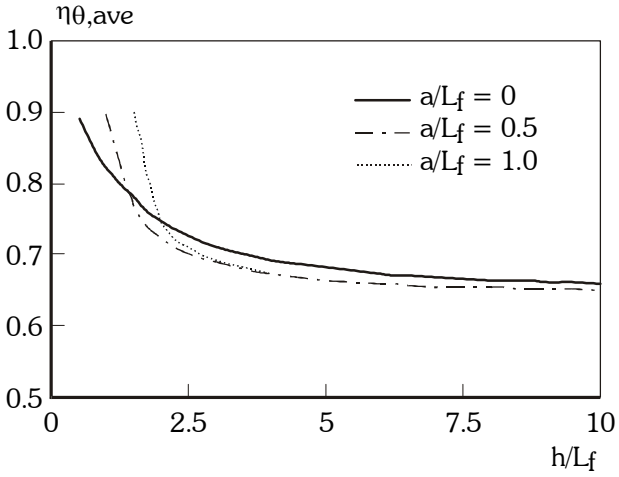


Fig. 7.6 The average orientation number as a function of the ratio of the beam depth h [after: Kooiman, 2000]

7.3.2 Distribution of the fibres

The post-cracking performance of SFRC is correlated with the number of fibres crossing the crack [Schönlin, 1988]. Kooiman [2000] and Vandewalle & Dupont [2003] reported on counting fibres in the cracked cross-sections of beams tested in bending. The number of fibres was correlated with the toughness. The variation on the bending performance of SFRC depended on the fibre content and was 15-25% (fibre content: 25 kg/m^3) and 10-20% for 75 kg/m^3 [Vandewalle & Dupont, 2003]. The variation decreased at increasing width of the beam [Kooiman, 2000]. Segregation of fibres in SCC increases the variation and affects the performance. Gettu & Barragán [2003] performed uni-axial tensile tests on cylindrical specimens with a diameter of 150 mm, different heights and a notch depth of 15 mm. The maximum load was not correlated with the amount of fibres but the toughness was. The high variation (up to 30%) in the peak load and toughness parameters was assigned to the variation of the amount of fibres in the cracked cross-section. Toutanji & Bayasi [1998] tested SFRC beams having a low to high flowability in bending and in two different directions (parallel and perpendicular to the direction of casting). The toughness was about the same in case the

flowability was low, whereas the differences increased at increasing flowability due to the segregation of the fibres.

7.3.3 Influence of the production method

Soroushian & Lee [1990] found that vibrating the mould causes the fibres to orient into horizontal planes. In contrast, SCFRC flows due to its own weight only and requires no compaction. The influence of the flow, the production method and the walls on the orientation of the fibres is not clear. Nemegeer [1999] reported on a study on the orientation of steel fibres in SCFRC. The L-Box, a test method to investigate the passing ability of SCC, was applied without any bar reinforcement. The height of the lower part of the L-Box is 150 mm; its width is 200 mm. SCFRC was put into the L-Box and flowed after the opening gap was opened. Once hardened, slices were sawn into three different directions. X-ray photographs showed that the fibres were preferably aligned into the direction of the flow. 60 mm steel fibres were applied in this study; just as for small beams a significant wall-effect can be expected.

7.4 Orientation and distribution of the fibres: case studies

Kooiman [2000] reports on two case studies on the orientation and the distribution of the steel fibres:

- *Underwater slab*

A trial slab of a length of 10 m was cast (the distance of the pump from the wall was 0.5 m) to study the effect of the flow on the orientation and the distribution of the steel fibres. X-ray photographs indicated that the orientation was spatial-random close to the place where the pump was positioned. At increasing distance a preferred planar-random orientation was obtained. The fibres tended to orient into the direction of the flow and parallel to the bottom of the slab. Cylinders were drilled and crushed and the number of fibres was counted. A good distribution was obtained (added: 30 kg/m^3, average in cylinders: 33.5 kg/m^3, standard deviation: 6.6 kg/m^3). Kooiman simulated the bending behaviour and showed that a difference in the orientation number affects the post-cracking performance of SCFRC rather than the maximum load. The fibres were more aligned in beams due to the presence of the walls, whereas the flow might have oriented the fibres more in the slab. The translation from the result of the bending test into the performance of the slab is difficult to perform.

- *Tunnel segments*

SFRC in tunnel segments was applied in a pilot project in the Netherlands (2nd Heinenoord tunnel in Rotterdam); 112 segments and 16 keystones were produced. Concrete was cast in the middle of the segment. Deformation-controlled splitting tensile tests on drilled cylinders from different positions of a tunnel segment were performed.

The results indicated that the fibres were not spatial-random oriented. Bleeding was observed during vibrating the segments. This caused differences in the concrete quality over the height of a cylinder. The steel fibres tended to segregate due to compaction; the same occurred when compacting the specimens for bending tests. The walls oriented the fibres. Fig. 7.7 shows the preferred orientation of the fibres in a tunnel segment due to compaction and the flow.

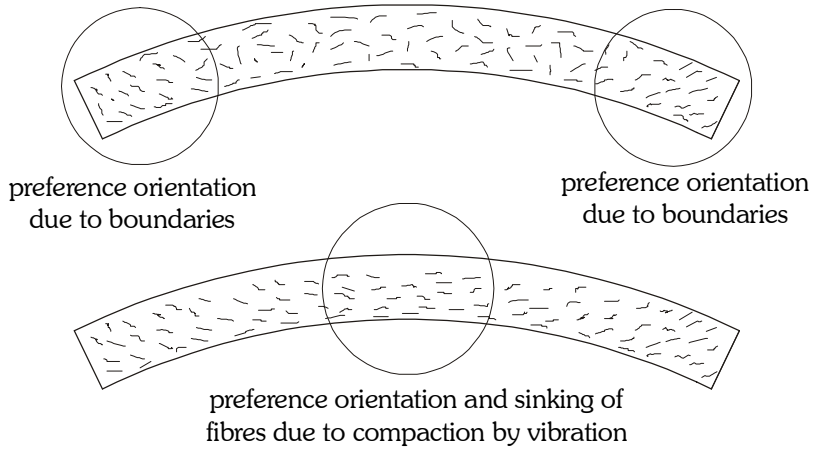


Fig. 7.7 Effect of casting and vibrating the mould on the orientation and the distribution of steel fibres in tunnel segments [after: Kooiman, 2000]

7.5 Concluding remarks

This chapter discussed literature dealing with three aspects of fibre reinforced concrete in the hardened state: mechanical characteristics, testing as well as the orientation and the distribution of fibres.

Fibres improve the mechanical characteristics of FRC once the matrix starts cracking. In the initial phase of testing micro-cracks open and localise in macro-cracks later on; the phase at which a fibre starts to transmit a force depends on the fibre type. The performance and the variation of characteristics of FRC after cracking are directly related to the characteristics, the orientation and the number of fibres in the cracked cross-section. Segregation resistance is the most important characteristic of SCFRC and affects the distribution of the fibres. The orientation of the fibres due to the flow, the walls and the production method determines their effectiveness, which might be an advantage or a disadvantage dependent on the application and whether it can be controlled. The assumption that fibres are randomly 3D-oriented is difficult to keep, even for very stiff concrete, since it has to be vibrated. In order to describe the effect of various parameters that affect the alignment of fibres, the orientation number has to be determined. Without this essential information, test results are difficult to translate into the structural performance.

Chapter 8:

The effect of steel fibres on characteristics of SCC in the hardened state

8.1 Introduction

This chapter presents results of three experimental studies: bending tests, image analysis on the orientation of steel fibres in beams and single fibre pull-out tests. The experimental set-up allows identifying differences in the behaviour between SCC and conventional concrete and provides the basis for modelling the bending behaviour of SCFRC, which is reported in Chapter 9.

Steel fibres improve several characteristics of SCC in the hardened state. To quantify their effect on the post-cracking behaviour of SCFRC, deformation-controlled three-point bending tests with a notch were carried out. Seventeen different mixtures were tested; two different casting methods were applied and compared. Differences between SCFRC and SFRC were found and are discussed. The orientation of the fibres in beams was determined by means of an image analysis. For this purpose, beams were cut and photographs were taken from the cross-sections. Computer software was applied to extract the areas that reflected light (fibres) and to calculate the orientation numbers. Single fibre pull-out tests were conducted to find whether the anchorage capacity of steel fibres in SCC differs from that in conventional concrete.

8.2 Three-point bending tests

The bending tests were performed to develop a tensile model for SCFRC. Chapter 8.2 describes the experimental set-up of the study and summarises the results of the tests. The parameters of the proposed tensile model are derived from an inverse analysis (Chapter 9) and are related to characteristics of SCFRC or its components. Kooiman [1998a, 2000] reported on three-point bending tests with SFRC. It was decided to carry out the same three-point bending tests with a notch on SCFRC to directly compare the results with those of SFRC. The test set-up allows measuring the opening of a discrete crack at the tip of the notch. The crack is forced to open at the location were the notch is placed, which allows developing a stress-crack width relation. The fibres preferably

align into the direction of the main tensile stress close to the wall of the mould; the notch eliminates this effect within a height of 25 mm.

8.2.1 Specimens for bending tests

Table 8.1 provides an overview over seventeen mixtures. Most of the mixtures contained the maximum fibre amount and were selected from studies on the fresh state of SCFRC. Mixture 14 was composed to meet the requirements of the sheet piles (Chapter 10.2). Mixtures 15-17 were tested later on [Schumacher et al., 2003b] and were part of the analysis presented in Chapter 9. Appendix D (Table D2) presents the composition of mixtures 1-17. The compressive strength, the type and the content of the steel fibres, the filling method and the maximum aggregate size were varied. Mixtures 6 and 14 contained straight steel fibres; hooked-end steel fibres were added to all other mixtures.

Table 8.1 Experimental program of the bending tests

No.	*Mixture*	$d_{g,max}$ *[mm]*	*Strength class*	f_{fccm}	$f_{fctm,spl}$	*Filling method*	*Fibre type*	V_f *[kg/m³]*
1	L-R-60-60	16	B45	54.0	6.3	RILEM	80/60	60
2	L-R-30-60	16	B45	57.6	6.6	RILEM	80/30	60
3	L-R-40-100	16	B45	51.9	6.6	RILEM	65/40	100
4	L-R-30-140	16	B45	55.8	7.6	RILEM	45/30	140
5	M-R-30-40	8	B65	70.3	7.6	RILEM	80/30	40
6	M-R-20-60	8	B65	75.6	7.4	RILEM	65/20	60
7	M-R-60-60	16	B65	75.1	8.7	RILEM	80/60	60
8	M-R-30-60	16	B65	72.3	8.1	RILEM	80/30	60
9	M-R-40-100	16	B65	73.5	8.9	RILEM	65/40	100
10	M-R-30-140	16	B65	78.1	9.8	RILEM	45/30	140
11	M-F-60-60	16	B65	75.3	8.1	Flow	80/60	60
12	M-F-30-140	16	B65	71.7	9.6	Flow	45/30	140
13	H-R-60-60	16	B105	116.7	12.4	RILEM	80/60	60
14	H-R-13-125	1	B105	120.3	14.1	RILEM	OL13/0.16	125
15	P1	16	B45	52.2	5.6	RILEM 2	45/30	60
16	P2	16	B45	55.5	7.3	RILEM 2	45/30	120
17	P2	16	B105	114.4	11.6	RILEM 2	80/30	60

The notation of the mixtures is as follows:

- Compressive strength (B 45=L(ow), B 65=M(iddle) and B 105=H(igh))
- Filling method (RILEM=R, Flow=F)
- Fibre length [mm]
- Fibre content [kg/m^3]

Example: M-R-60-60, SCFRC of strength class B 65, cast according to the RILEM-method, with a fibre length of 60 mm and a steel fibre content of 60 kg/m^3.

Five different matrices were applied. Each of the applied fibre contents of mixtures 1-13 was the maximum amount of the specific fibre type for the chosen mixture composition. This test set-up allowed comparing the performance of different fibre types at the maximum fibre content.

Production and storage of the specimens

The production process has a significant influence on the performance of conventional SFRC. The method and the intensity of compaction affect the orientation and the distribution of the steel fibres and the variation in test responses [Kooiman, 2000]. To study the effect of different casting methods on mechanical characteristics of SCFRC two variants were chosen: the 'RILEM' and the 'Flow' method. SCFRC specimens cast with both methods already undergo different degrees of orientation due to the walls of the bucket or the shovel. The angle with which the shovel is directed towards the mould also affects the fibre orientation. The prisms for the E-modulus tests were cast in the same way as the beams for the bending tests.

The 'RILEM-method' (Fig. 8.1) for casting SFRC was proposed by RILEM TC162-TDF [2000]. The volume of the concrete put in the middle of the mould has to be twice the volume of that put at both ends. In the study on SCFRC, the shovel was rotated over 45 degrees compared with both the bottom and the walls of the mould. Before, concrete was sampled from the mixer from the entire height of the batch and filled into a 10 litres-bucket. Then, the bucket was transported to the moulds and remixed with a stick before shovelling. The same person filled the moulds.

The 'Flow-method' (Fig. 8.2) consisted of filling the concrete from one side into the mould and allowed the concrete to level itself. Concrete was taken directly from the mixer from the entire height of the batch in the mixer.

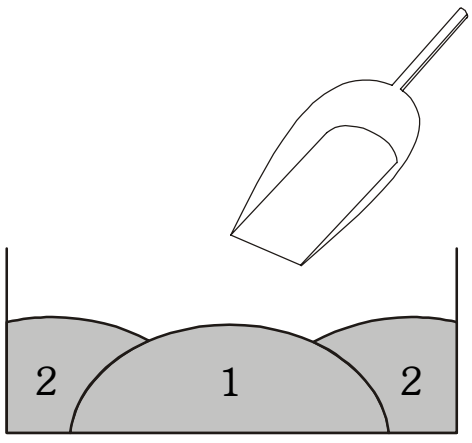


Fig. 8.1 Filling method 'RILEM'

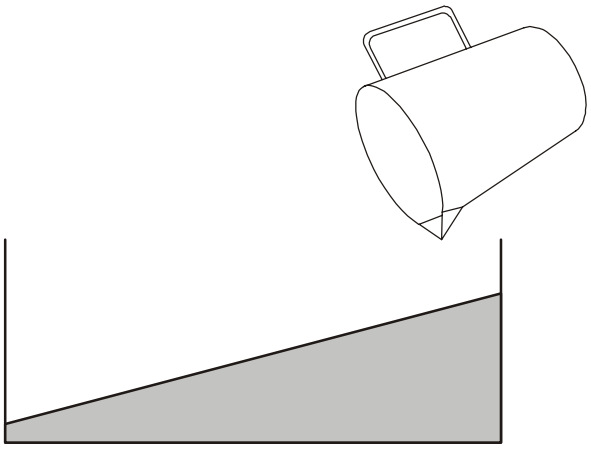


Fig. 8.2 Filling method 'Flow'

The specimens were stored in the laboratory for 1-2 days (Temperature 21 ± 3°C), depending on the expected strength development. After demoulding, the specimens were placed in a climate-conditioned room at 20°C and at a relative humidity over 95%. The bending tests were carried out at an age of 28 ± 1 days.

The E-modulus test and the compressive [NEN 5968, 1988] and splitting tensile strength tests [NEN 5969, 1988] were done at an age of 28 days. The standard experimental program consisted of four bending tests and three tests to determine the E-modulus, the compressive and splitting tensile strengths respectively. Five bending tests were carried out for mixture No. 13 and three for mixtures 15-17. The dimensions of the specimens were: beams of 600·150·150 mm (bending test), prisms of 400·100·100 mm (E-modulus) and cubes of 150 mm (splitting tensile and compressive strengths). The load-controlled standard tests were carried out according to the Dutch regulations. Mixtures 15-17 (P1-P3) were tested in the scope of the research project 'Rotation Capacity of SCFRC'. The production method of these beams also was the RILEM-method (Fig. 8.1). The moulds were filled by different persons, which affected both the scatter and the performance of the beams.

Experimental test set-up

A deformation-controlled three-point bending test (Fig. 8.3) with notch according to RILEM TC 162-TDF [2000] was conducted to determine the load-displacement relation of the beams in bending.

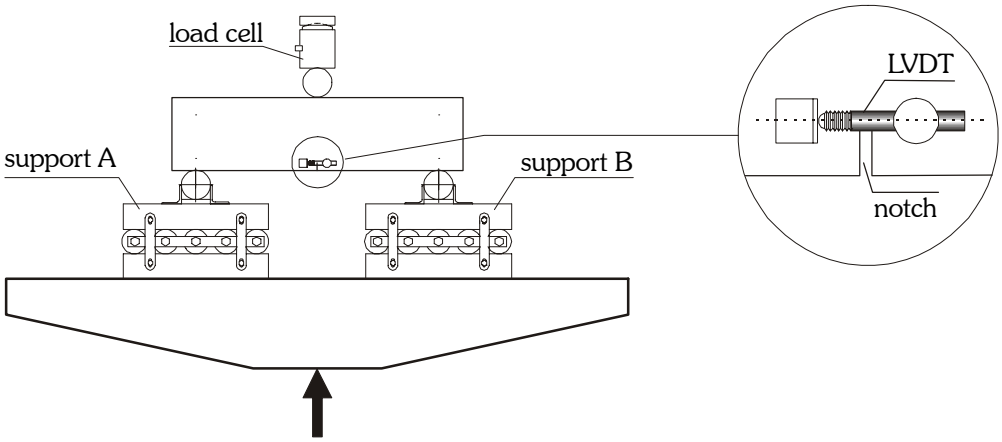
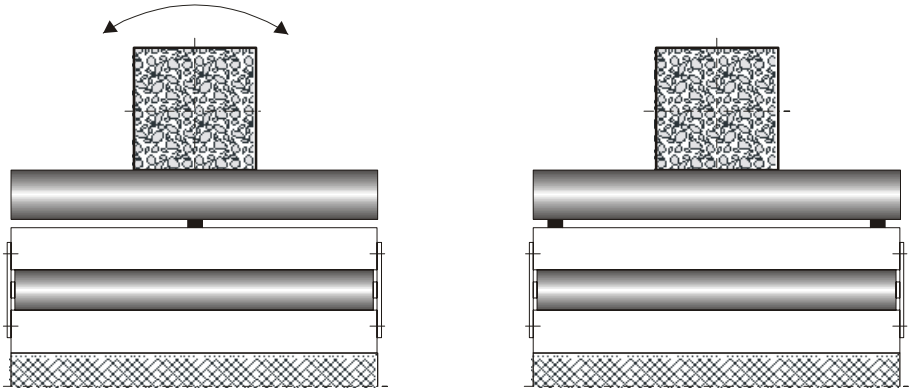


Fig. 8.3 Test set-up of the three-point bending test with notch [after: Kooiman, 2000]

The span between the two supports was 500 mm. The notch in the middle of the beam had a depth of 25±1 mm and intended to force the crack to occur where the actual deformation was measured. The effective height of the beams was 125 mm; their width was 150 mm. Since concrete deforms elastically without visible cracks in the initial phase, the notation load-CMOD relation would be misleading; in the following, reference is made to the deformation of the LVDT as 'displacement (δ)'. The measured deformation (δ_m) was adjusted with a geometrical correction to obtain the horizontal component; the geometrical derivation is shown in Appendix H. In the following, test results are presented as load-displacement relations. Two LVDTs (Linear Variable Displacement Transducers) were arranged at the tip of the notch in order to determine the horizontal displacement. One LVDT was placed at the front side and another at the back side of the beam (Fig. 8.3). The experiments were carried out deformation-controlled at a constant rate of deformation of 50 μm/s. The rate was chosen to

measure the complete load-displacement curve of a mixture with long fibres (60 mm) within 30 min; the test was stopped when the load was below 0.2 kN. Both LVDTs had a measuring length of 100 mm. The control signal was the average of both LVDT measurements.

The bending tests were carried out in a stiff steel frame. The central support was connected to a load cell that was fixed to the test frame. The beams were supported on two steel rolls (diameter: 60 mm), which were fixed on a system of steel roller supports to avoid frictional resistance as much as possible. A rubber block was arranged below one supporting roll to allow free rotation (Fig. 8.4). According to Kooiman, torsion occurs due to non-symmetrical size differences and a non-homogeneous fibre distribution in the cross-section, which is quantified by the difference of the displacement registered by both LVDTs. The testing frame and machine were the same as in the study of Kooiman [2000].



Side view support A Side view support B

Fig. 8.4 Roll support systems [after: Kooiman, 2000]

8.2.2 Results of the bending tests

In the following, the results of the bending tests are summarised. Grünewald & Walraven [2002b; for mixtures 1-14] and Schumacher et al. [2003b; for mixtures 15-17] provide a detailed discussion about the bending tests on SCFRC. Appendix K presents all the measurements up to a displacement of 10 mm. Table 8.2 summarises average characteristics of the bending tests. In each case, the load significantly increased after the first crack appeared. The related displacements at the maximum load are listed in Table 8.2 (δ_{max}). After the maximum load was reached, softening took place. The fracture energy was calculated as the area below the load-displacement curve according to Equation 8.1 [RILEM 50-FMC, 1985].

$$G_F = (W_0 + m \cdot g \cdot \delta_0) / A_{lig} \quad (8.1)$$

where: G_F = fracture energy bending test [kN/mm]
W_0 = area under the load-displacement curve [kN/mm]
m = $m_1 + m_2$ [kg]
m_1 = weight of the beam between the supports [kg]
m_2 = weight of the part of machine that is not attached to machine [kg]
g = acceleration due to gravity (9.81 kg/s^2) [kg/s^2]
δ_0 = deformation at the final failure of the beam [mm]
A_{lig} = effective cross-section of beam [(h-a)·b] [mm^2]

The fracture energies of each mixture at 2 and 10 mm are listed in Table 8.2; the variation of each result is also given. The equivalent flexural tensile strength was calculated with the assumption of an uncracked cross-section ($f_{fctm,fl}$=M/W; M=0.25·P_{max}·l).

Table 8.2 Bending tests: average and variation of results of seventeen SCFRC mixtures

No.	*Mixture*	P_{max}	P_{max} *variation*	$f_{fctm,fl}$	δ_{max} *(at* P_{max}*)*	$G_{F,2mm}$	$G_{F,2mm}$ *variation*	$G_{F,10mm}$	$G_{F,10mm}$ *variation*
		[kN]	*[%]*	*[MPa]*	*[mm]*	*[N/mm]*	*[%]*	*[N/mm]*	*[%]*
1	L-R-60-60	32.5	10.2	10.4	1.1	3.3	11.1	12.1	7.3
2	L-R-30-60	28.2	4.1	9.0	0.8	2.8	5.0	8.0	8.3
3	L-R-40-100	32.2	10.8	10.3	0.6	3.2	10.5	9.3	12.2
4	L-R-30-140	34.0	10.0	10.9	0.4	3.2	9.9	8.5	12.6
5	M-R-30-40	27.9	11.8	8.9	0.9	2.8	10.5	7.4	17.9
6	M-R-20-60	28.9	8.5	9.2	0.2	2.4	9.5	7.2	9.8
7	M-R-60-60	42.1	2.4	13.5	0.8	4.2	6.9	14.9	7.9
8	M-R-30-60	36.8	5.1	11.8	0.8	3.7	5.0	10.2	10.2
9	M-R-40-100	37.8	11.3	12.1	0.5	3.6	11.5	9.9	12.0
10	M-R-30-140	42.6	6.6	13.6	0.4	3.9	7.8	9.9	10.5
11	M-F-60-60	36.9	7.7	11.8	0.8	3.7	6.2	12.9	7.5
12	M-F-30-140	42.5	7.3	13.6	0.4	4.0	7.2	10.4	13.5
13	H-R-60-60	56.9	5.8	18.2	1.2	5.6	8.3	21.7	12.9
14	H-R-13-125	73.0	7.5	23.4	0.6	7.2	9.1	16.7	10.9
15	P1	21.5	5.6	6.9	0.6	2.1	3.9	5.0	6.7
16	P2	27.6	6.6	8.8	0.3	2.6	7.9	6.3	9.4
17	P3	42.8	11.8	13.7	0.5	4.1	13.3	10.9	19.0

Discussion of the bending tests on SCFRC

In the following, examples of average bending responses are presented and compared. Fig. 8.5 shows the effect of the compressive strength class (B45/B65/B105, which corresponds to mixtures 1/7/13) for SCFRC with 60 kg/m^3 of Dramix 80/60 BP steel fibres. The maximum flexural load was obtained at displacements of 0.8-1.2 mm (Table 8.2).

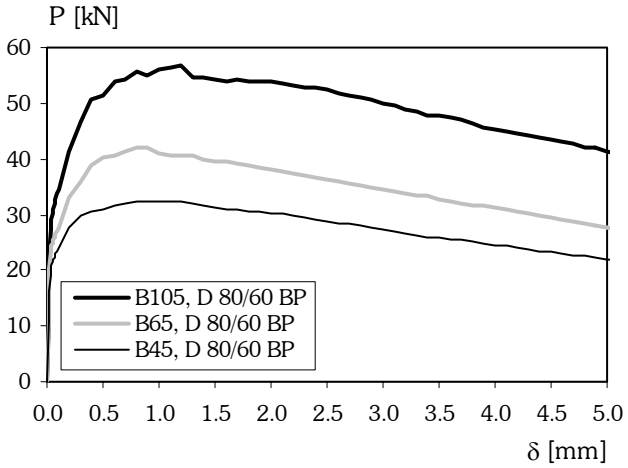


Fig. 8.5 Effect of the strength class on the bending performance of SCFRC (for fibre type: Dramix 80/60 BP; V_f = 60 kg/m^3)

Fig. 8.6 compares four SCFRC mixtures in strength class B65, which contained four different types of steel fibres at the maximum fibre content. The applied fibre content depends on the fibre type and was 60 kg/m^3 (Dramix 80/60 BP - mixture 7; Dramix 80/30 BP - mixture 8), 100 kg/m^3 (Dramix 65/40 BN - mixture 9) and 140 kg/m^3 (Dramix 45/30 BN - mixture 10) respectively. The lowest maximum load of the four hooked-end types at the maximum fibre content was found for type 80/30 (strength classes: B45 and B65); the highest was found for type 45/30. The related displacement was the smallest for Dramix 45/30 BN (0.4 mm) and the highest for Dramix 80/60 BP (0.8 mm).

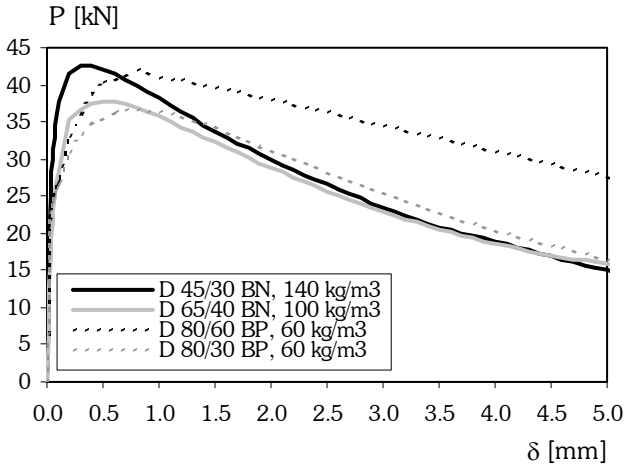


Fig. 8.6 Effect of the maximum fibre content for four types of steel fibres on the bending performance of SCFRC (strength class: B65)

The following observations were made on bending tests of seventeen SCFRC mixtures:

- The maximum flexural load ($f_{fctm,fl}$) and the fracture energy ($G_{F,2mm}$) of mixture 14 was the highest of mixtures 1-17, whereas the fracture energy ($G_{F,10mm}$) of

mixture 13 was the highest. Longer fibres were found to be more effective at the same fibre content.

- Mixture 6 (straight fibres, L_f=20 mm) reached the peak load at the smallest displacement of all mixtures (0.2 mm).
- The variation in the maximum load of mixtures 1-17 was in the range of 2.4-11.8%. Mixture 5 contained only 40 kg/m^3 fibres and resulted in the highest variation of the first test series (mixtures 1-14). A significant difference of the maximum load of mixture 17 (P3) and mixture 13 was found for the strength class B105, whereas it was much smaller for B45 and B65. Since the fibres did not break, this fact was assigned to the reproducibility of the production method of the specimens. The highest variation of all results of Table 8.2 was found for mixture 17 (variation of $G_{F,10mm}$: 19%).
- The performance of two identical mixtures cast with two different casting methods differed for long fibres only (60 mm; mixtures 7 and 11). The performance of mixtures 10 and 12 was about the same. The average number of fibres in the cross-section of the beams of mixtures 7 and 11 was determined [Grünewald & Walraven, 2002a/b] and was lower in the case of the Flow-method (1.15 fibres/cm^2) compared with the RILEM-method (1.31 fibres/cm^2). Clustering of the fibres at the end of the mould during casting counteracted a homogenous distribution. The number of short fibres in the middle of the beam was about the same (RILEM-method: 3.39 fibres/cm^2; Flow-method: 3.41 fibres/cm^2).

8.2.3 Comparing SCFRC and SFRC

Kooiman [1998a] tested a SFRC, which was comparable with mixture 7 (M-R-60-60), but was not self-compacting. He applied the same fibre type and content (Dramix 80/60 BP; 60 kg/m^3). The compressive and splitting tensile strengths were 81.1 MPa and 4.6 MPa respectively, whereas those of mixture 7 were 75.1 MPa and 8.6 MPa respectively. The rate of deformation in the study of Kooiman was 1 μm/s up to a displacement of 5 mm and 50 μm/s beyond 5 mm (SCFRC: constant 50 μm/s). Referring to a study of Gopalaratnam & Shah [1986], a minor influence of this difference on the maximum flexural load can be expected. Fig. 8.7 compares SCFRC (mixture 7) and the equivalent SFRC [Kooiman, 1998a]. An increase of the load after first cracking of SFRC was observed for one specimen only; the scatter in the results was rather high. The performance of SCFRC and SFRC was rather different: the performance of SCFRC was much better and the variation of the results was lower. The average maximum flexural load of mixture 7 was 42.1 kN. The difference between the splitting tensile strengths of SFRC (4.6 MPa) and SCFRC (8.6 MPa) was significant; the splitting tensile strength of the SFRC cubes is what is expected for a B65 without fibres. In contrast, the fibres increased the splitting tensile strength of SCFRC compared with that of the plain SCC mixture ($f_{ctm,spl}$ = 5.3 MPa, Appendix I).

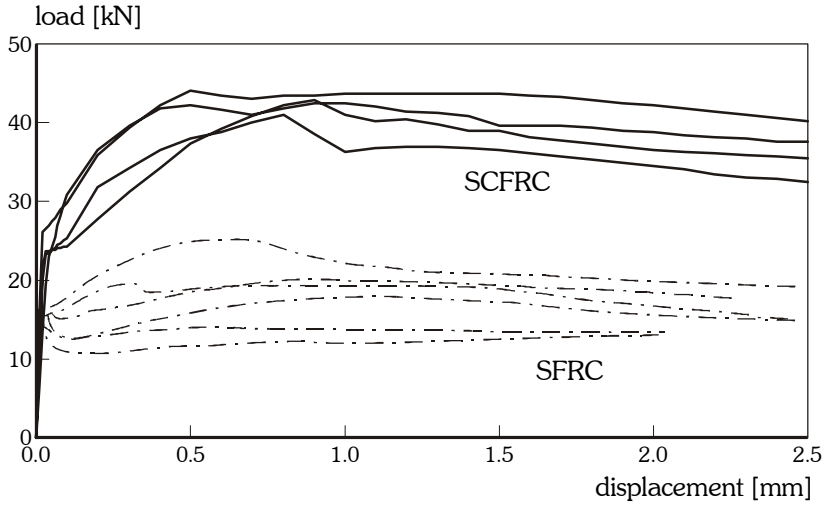


Fig. 8.7 Test results of three-point bending tests: SCFRC (mixture 7) versus SFRC [Kooiman, 1998a] (strength class: B65, Dramix 80/60 BP, V_f=60 kg/m^3)

Table 8.3 presents results from two corresponding mixtures (strength class: B65, Dramix 80/60 BP, V_f=60 kg/m^3), the fracture energies $G_{F,2\ mm}$ and its variation. One is an SFRC [Kooiman, 2000], the other an equivalent SCFRC (mixture 7).

Table 8.3 Fracture energy and its variation (B65, Dramix 80/60 BP, V_f=60 kg/m^3)

Specimen width	*Mix 'Kooiman'*		*Mixture 7, M-R-60-60*	
	$G_{F,2\ mm}$ [kN/mm]	*Variation [%]*	*$G_{F,2\ mm}$ [kN/mm]*	*Variation [%]*
b=150 mm	1.83	21.3%	4.16	6.9%
b=300 mm	2.79	9.0%	-	-
b=450 mm	2.87	4.2%	-	-

The production process and the specimen size affected the variation. The fracture energy of the SCFRC specimens was significantly higher; its variation was lower (standard width: 150 mm). Kooiman increased the width of the beams (from 150 to 300 and 450 mm) and demonstrated that the variation decreased. The fracture energy of SFRC still was lower. To answer the question why SCFRC and SFRC differed that much, two additional studies on the orientation of the steel fibres in beams and the single fibre pull-out behaviour were conducted.

8.3 Fibre orientation in small beams

8.3.1 Analysis of a cross-section by image analysis

Steel fibres reflect the light of the flash of a camera, whereas concrete absorbs it. Bright light on the surface of a steel fibre results in a white spot on the photograph. Schönlin [1988] applied this principle to analyse fibre reinforced cross-sections. In the study on SCFRC, one beam of each mixture, which was most close to the average fracture energy ($G_{F,2mm}$), was used to determine the orientation number [Grünewald &

Walraven, 2002a]. According to Schönlin [1988], the orientation number can be determined with an image analysis by applying Equation 8.2, which represents an average of all fibres of a cross-section; the angle φ indicates the inclination (cos φ = $d_f/L_{f,act}$) of a fibre to the plane under consideration. An orientation number of 1 indicates that only a circle is visible; the minimum and maximum lengths of a reflected area are the same. The higher the orientation number the more the 'average fibre' is oriented perpendicular to the plane under consideration.

$$\eta_\varphi = \frac{1}{N_{sf}} \cdot \sum_{1}^{N_{sf}} \cos\varphi \qquad (8.2)$$

where: N_{sf} = number of steel fibres [-]
φ = inclination of a fibre relative to the plane of consideration [-]; cos $\varphi = d_f/L_{f,act}$
d_f = fibre diameter [mm]
$L_{f,act}$ = actual fibre length in a plane [mm]

Fig. 8.8 shows extracted areas, which are reflections of the light of the camera and were obtained from the 'Photoshop' analysis.



Fig. 8.8 Steel fibres in a plane (output of 'Photoshop': extracted areas)

A photograph requires a planar surface. Especially the cracked area of beams with 60 mm steel fibres was very rough. For this reason, starting at the mid-span 70 mm of half a beam were removed to assure that no fibres were pulled out from the cross-section. The photos were analysed by applying the computer software 'Photoshop, 5.0' and 'Optimas, 6.2'. The minimum (d_f) and actual length ($L_{f,act}$) of each area were determined with 'Optimas'-software.

8.3.2 Results of the image analysis

When the number of fibres increases, the chance increases that fibres neighbour (mixture 14: 19.0 fibres/cm^2). A cluster of fibres appears as an apparently longer fibre on the image and causes an apparent underestimation of the orientation number. Only a few fibres of mixtures with hooked ends were found to be in contact. Fig. 8.9 shows

the relation between the fibre length and the orientation number of the cross-sections of mixtures 1-14 (Appendix I, Table I1). No image analysis was carried out for the mixtures 15-17. Chapter 7.3 discusses how experimental orientation numbers and theoretical derivations relate.

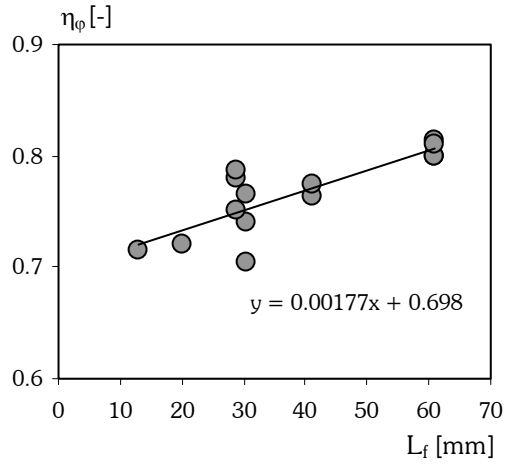


Fig. 8.9 Relation between the fibre length and the orientation number

The longer the fibre was, the higher was the orientation number (Equation 8.3); so the performance of beams with longer fibres is more favourably affected by the orientation of the fibres.

$$\eta_\varphi = 0.698 + 1.77 \cdot 10^{-3} \cdot L_f \qquad (8.3)$$

The highest number is obtained with 60 mm fibres (mixture 7: 0.813), whereas mixture 14 (13 mm fibres) resulted in an orientation number of 0.715. The orientation numbers of 30 mm steel fibres are in the range of 0.7-0.8; only the result of mixture 2 (0.704) significantly differs from the other results. The effect of the flow and the walls on the orientation depends also on the production method and the dimensions of the applied mould; these influences could not be separately quantified. Almost no fibres were found to be oriented perpendicular to the concrete surface during casting. Kooiman [2000] calculated theoretical orientation numbers of 0.70 for SFRC and 60 mm steel fibres and 0.66 for 30 mm fibres respectively (dimensions of the beam: 600·150·150 mm). These numbers were obtained using a model that takes into account the wall-effect of the fibres [Soroushian & Lee, 1990]. The fibre is assumed to orient within an area of one times the fibre length. The orientation numbers of SCFRC were higher than the theoretical numbers of SFRC.

8.4 Single fibre pull-out tests

8.4.1 Experimental set-up

The previous sections discussed the differences between SCFRC and SFRC concerning the bending performance and the orientation of the fibres. In the following, a study is

described that aimed at comparing the anchorage capacity of single fibres. Markovic et al. [2002] report on additional details of this study. The same tests were performed for SCC and conventional concrete (CC) to quantify differences at the single fibre level. The parameters of this study were:

- Concrete type: SCC and CC
- Compressive strength class: B45, B65 and B105
- Type of steel fibre: Dramix 80/60 BP and Dramix 80/30 BP
- Embedded length: 10 mm and 30 mm (Dramix 80/60 BP only)

The SCC mixtures were the same as applied for the bending tests: B45 (mixtures 1-4, 15 and 16), B65 (mixtures 7-12) and B105 (mixtures 13 and 17). The mixture composition of B65 (CC) was the same as reported by Kooiman [1998a]; only the content of superplasticiser was adjusted to achieve the required slump. The mixture composition of B45 and B105 (CC) required further adjustments. The maximum aggregate size of all mixtures was 16 mm. The slump flow of SCC was in the range of 650-710 mm, whereas the slump of CC was in the range of 170-210 mm. CC was compacted on a vibration table, while surface finishing only was applied for SCC. Appendix D (Table D3) presents the composition of six self-compacting and conventional concrete mixtures. Table 8.4 provides an overview over 47 single fibre pull-out tests (SCC: 23, CC: 24).

Table 8.4 Experimental program of single fibre pull-out tests (SCC/CC)

Fibre type	*80/60*	*80/60*	*80/30*
L_{fe} [mm]	*10*	*30*	*10*
	Number of tests (SCC/CC)		
B45	2/2	3/3	3/3
B65	2/2	3/3	3/3
B105	2/2	3/3	2/3

Eight cylinders (diameter: 65 mm, height: 50 mm) were drilled from a larger specimen and were glued on a steel plate. Fig. 8.10 shows the test set-up of the single fibre pull-out test.

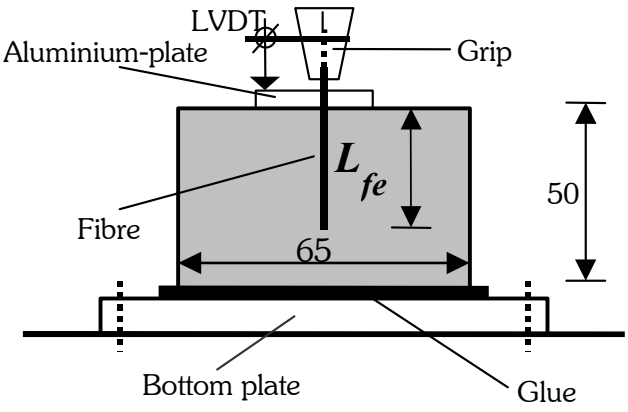


Fig. 8.10 Test set-up of the single fibre pull-out test [after: Markovic et al., 2002]

The pull-out force was recorded, while the test was controlled on the slip of the fibre relative to the matrix. The rate of displacement was 5 μm/s. The fibres had to be clamped into the grip; the maximum possible embedded length of Dramix 80/30 BP was 10 mm. Table 8.5 shows the compressive and splitting tensile strengths (without fibres) as an average of three measurements. SCC and CC resulted in about the same compressive strength; the splitting tensile strengths of SCC were 17-29% higher.

Table 8.5 Mechanical characteristics at an age of 28 days (150 mm cubes)

Strength class	$f_{ccm}/f_{ctm,spl}$ *SCC [MPa]*	$f_{ccm}/f_{ctm,spl}$ *CC [MPa]*	*Ratio* $f_{fctm,spl}$ *SCC/CC*
B45	50.4 / 4.39	50.6 / 3.75	1.17
B65	70.0 / 5.30	65.7 / 4.12	1.29
B105	117.6 / 7.42	112.4 / 6.71	1.21

8.4.2 Results of single fibre pull-out tests

- *Pull-out forces: SCC versus CC*

Table 8.6 summarises the average single fibre pull-out forces for the following three cases: the maximum, the average force (the length of the hook is equal to the displacement the fibre requires to completely enter the straight channel) and the average frictional force (up to the slip at which the load rapidly dropped to zero). L_{EL} is the total fibre length minus the measured straight part. Fig. 8.11 shows the parameters $P_{f,max}$, $P_{f,hook}$ and $P_{f,fric}$ for steel fibre type Dramix 80/60 BP (in SCC, strength class B65, L_{fe}=10 mm).

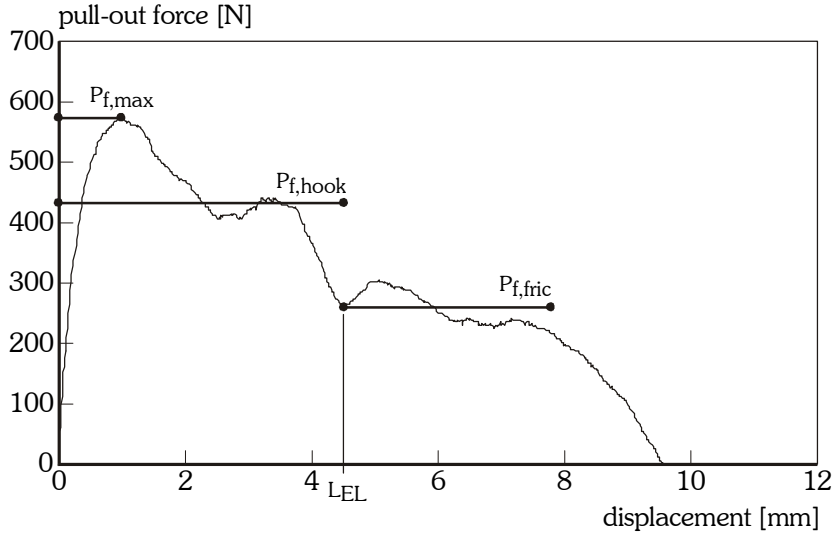


Fig. 8.11 Three parameters ($P_{f,max}$, $P_{f,hook}$ and $P_{f,fric}$) to characterise results of single fibre pull-out tests

Fibre rupture was not observed. The total length of the hook (L_{EL}) of both fibre types was 4.54 mm and was determined by the following procedure: the straight part of ten fibres was measured; under consideration of the diameter and the weight of the fibres the total length was calculated.

Table 8.6 Mean values of the pull-out forces of hooked-end steel fibres

Fibre type	*80/60*	*80/60*	*80/30*	*80/60*	*80/60*	*80/30*	*80/60*	*80/60*	*80/30*
L_{fe} [mm]	*10*	*30*	*10*	*10*	*30*	*10*	*10*	*30*	*10*
	[N]	*[N]*	*[N]*	*[N]*	*[N]*	*[N]*	*[N]*	*[N]*	*[N]*
Mixture	*Maximum force ($P_{f,max}$)*			*Average hook ($P_{f,hook}$)*			*Frictional resistance ($P_{f,fric}$)*		
SCC, B45	557.4	496.0	177.6	378.2	386.8	109.3	157.0	175.6	32.3
SCC, B65	590.4	614.9	193.2	427.5	462.2	110.9	227.7	215.8	23.6
SCC, B105	661.6	624.8	181.4	446.4	464.7	103.8	136.5	206.4	24.4
CC, B45	498.9	510.4	131.9	353.9	383.7	73.5	186.2	181.6	17.0
CC, B65	488.9	529.3	164.4	360.4	403.5	87.2	155.9	186.5	16.4
CC, B105	611.9	626.5	176.6	424.0	446.3	106.6	137.3	143.8	29.5

In most cases, SCC resulted in higher pull-out forces (Fig. 8.12). Fig. 8.13 presents the results for different strength classes: no clear tendency was found. The maximum pull-out force and the average force within the length of the hook (L_{EL}) of SCC were in most cases at least those of CC and were in some cases significantly higher (Fig. 8.13). The frictional resistance was also larger in most cases but a few results were found to be lower. The largest differences were found for the strength class B65, which was the strength class in which the bending tests on SCFRC and SFRC are compared (Chapter 8.2.3).

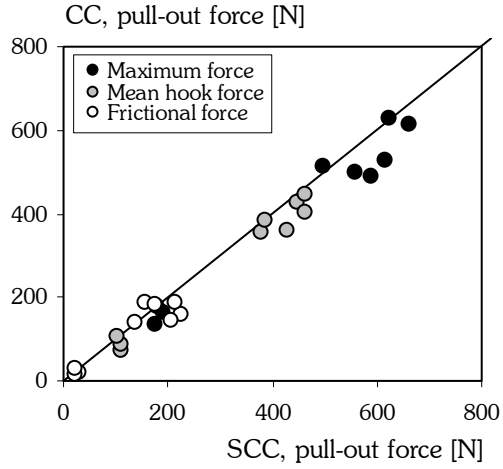


Fig. 8.12 Comparison of pull-out forces of steel fibres from SCC and CC matrices

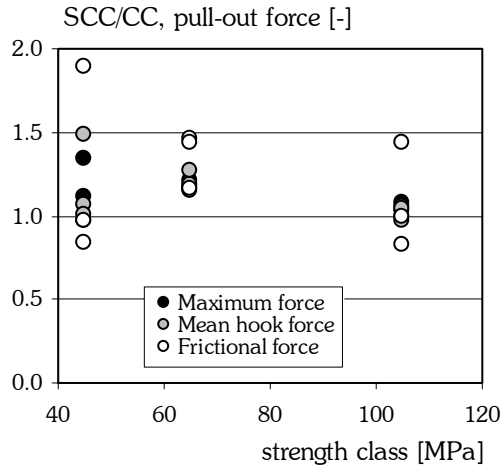


Fig. 8.13 Effect of the strength class on the ratio of pull-out forces of SCC and conventional concrete

The pull-out forces of SCC in the strength class B65 were 15-50% higher compared with CC. The scatter of the ratio of forces between SCC and CC was highest for B45, and lowest for B65. B105 results of SCC and CC were about the same, with some

exceptions on the frictional resistance. The average frictional resistance of Dramix 80/30 BP was relatively low; the ratio of forces between SCC and CC becomes in some cases rather high (Fig. 8.13), whereas the actual difference was small. The fibres contribute most to the bending performance at small displacements; the maximum force and the force up to the length of the hook (L_{EL}) are therefore most important. The improvement of the anchorage capacity contributes to the fact that the performance of fibres in SCC improves. The frictional resistance (i.e. the resistance of the fibre once it completely enters its straight channel) was in some cases lower for a High-Strength Concrete (B105) compared with B45 concrete. The degree to which the fibre is straightened before it reaches the channel affects the pull-out force. $P_{f,fric}$ is not correlated with the matrix strength; less straightened fibres result in higher pull-out forces. The average bond strength is calculated from the following equation:

$$\tau_{avg} = \frac{P_{f,\max}}{\pi \cdot d_f \cdot L_f} \tag{8.4}$$

where: τ_{avg} = average bond strength [MPa]
$P_{f,max}$ = maximum pull-out force [N]
d_f = fibre diameter [mm]
L_f = fibre length [mm]

Table 8.7 presents the average shear stress. The results indicate that a longer embedded length not necessarily leads to a higher average shear stress. The difference between different strength classes is relatively small, which indicates that the main contribution to the pull-out force is the result of the plastic deformation of the fibre. The difference between different compressive strength classes was smaller than suggested by Table 7.1.

Table 8.7 Average shear stress (Equation 8.4)

Fibre type	*80/60*	*80/60*	*80/30*
L_{fe} [mm]	*10*	*30*	*10*
	[MPa]	*[MPa]*	*[MPa]*
Mixture	*Average shear stress*		
SCC, B45	4.1	3.6	4.8
SCC, B65	4.3	4.5	5.2
SCC, B105	4.8	4.6	4.9
CC, B45	3.6	3.7	3.5
CC, B65	3.6	3.9	4.4
CC, B105	4.5	4.6	4.7

- *Efficiency of the fibres*

A high maximum load is not the only criterion to be met by a fibre; the energy dissipated until the fibre completely enters the channel contributes to the fracture energy in the post-cracking regime of a bending response. Fig. 8.14 compares (relative to the maximum pull-out force) responses for different types of concrete, fibre types and embedded lengths for three different strength classes.

In most cases, the longer the embedded length of Dramix 80/60 BP was the higher was the pull-out force. Relative to the maximum pull-out force, Dramix 80/30 BP resulted in a lower frictional force ($\eta_{f,fric}$) (SCC: 0.10-0.18, CC: 0.10-0.17) compared with Dramix 80/60 BP (SCC: 0.21-0.37, CC: 0.22-0.37). The latter fibre type is relatively more effective, which adds to the energy dissipated during pull-out. The same was found for the average pull-out force ($\eta_{f,hook}$, displacement < L_{EL}): Dramix 80/30 BP resulted in lower pull-out forces (SCC: 0.57-0.62, CC: 0.53-0.60) compared with Dramix 80/60 BP (SCC: 0.67-0.78, CC: 0.69-0.76). The effect of the type of concrete (SCC or CC) on the efficiency of both fibre types was small.

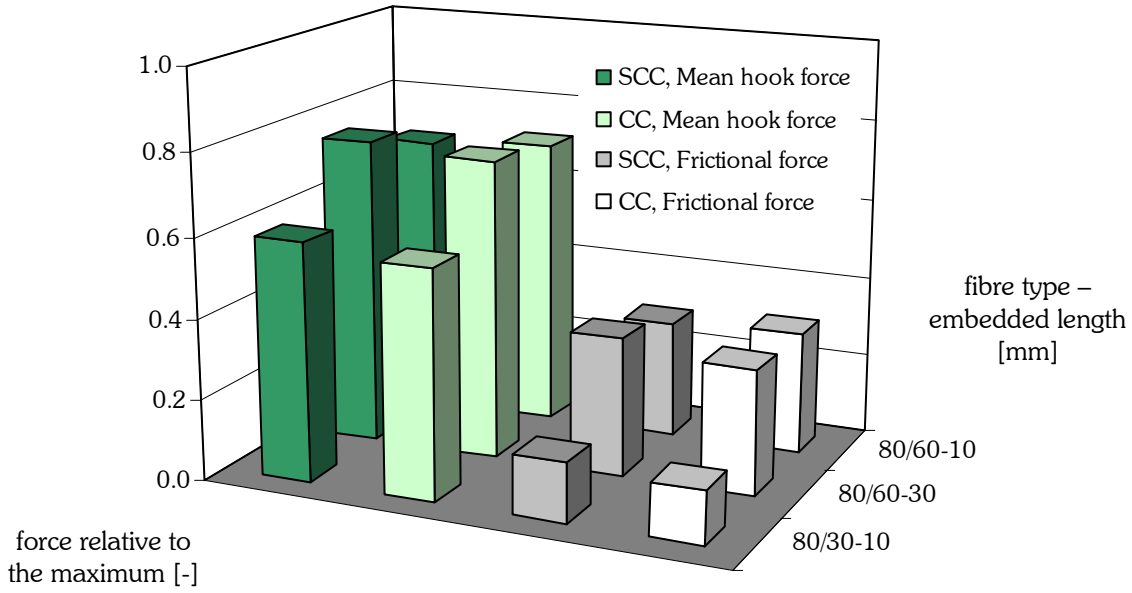


Fig. 8.14 Fibre effectiveness $\eta_{f,hook}$ and $\eta_{f,fric}$ as a percentage of the maximum pull-out force (average of different strength classes)

- *Variation of pull-out forces: SCC versus CC*

A maximum of three pull-out tests was carried out; Table 8.8 compares the variation of maximum pull-out forces (for three tests). The differences in this test series between SCC and CC are small, with the tests on B105 (Dramix 80/60 BP) as an exception; the variation of CC (B105) was the highest of all series.

Table 8.8 Variation of the maximum pull-out forces

	Variation [%]	*Variation [%]*
Fibre type	*80/60*	*80/30*
Concrete type	*L_{fe}=30 mm*	*L_{fe}=10 mm*
SCC / CC, B45	8.9 / 5.4	4.3 / 6.5
SCC / CC, B65	2.0 / 2.5	8.0 / 9.0
SCC / CC, B105	4.2 / 12.3	- / 5.3

8.5 Concluding remarks

In this chapter results of three different experimental studies on SCFRC are presented and discussed, which are bending tests, an image analysis of cross-sections of beams and single fibre pull-out tests.

The comparison of the bending behaviour of SCFRC and SFRC indicated significant differences concerning the performance and the variation in the test response: SCFRC performed much better. To determine the origin of the differences two additional studies were performed: First, orientation numbers for cross-sections of beams were obtained by image analysis. The fibres in SCFRC were more favourably aligned into the direction of the flow; the longer the fibre the higher was the orientation number. Second, a comparison between the pull-out behaviour of single fibres from SCC and conventional concrete showed that in most cases higher pull-out forces were obtained with SCC. In strength class B105 almost no differences were found.

The microstructure around the matrix, the distribution and the orientation of the fibres are different in SCC and conventional concrete. To achieve self-compacting concrete, the fibre content has to remain below the maximum fibre content. Due to this fact each fibre is fully embedded in the matrix. The photographs of cross-sections of beams showed that only a few fibres were connected. The single fibre pull-out test might give a better indication of the actual performance of a fibre in SCC than in conventional concrete. The slump of conventional concrete without fibres in this study was 170-210 mm, which is difficult to obtain with SFRC. Entrapped air and neighbouring fibres affect the performance of a fibre in SFRC more than in SCFRC. The variation in bending responses is not a material characteristic but depends on the segregation resistance of SCFRC and the reproducibility of the production process. The variation of the single fibre pull-out forces was not different for SCC and conventional concrete.

Chapter 9:

Modelling the bending behaviour of SCFRC

9.1 Introduction

Chapter 9 describes the development of a combined stress-strain/stress-crack width model for SCFRC in tension. Its parameters are derived from an inverse analysis of deformation-controlled three-point bending tests. Fifteen different mixtures with hooked-end fibres are analysed to calibrate the model; the varied parameters are the type and the content of the steel fibres, the compressive strength class and the casting method.

Chapter 9 also introduces the theoretical background of the inverse analysis to modelling. In contrast to the stress-strain model the stress-crack width model refers to the formation of a discrete crack. Both approaches are applied in a combination. The latter is applied, since a discrete crack appeared in all cases, which is due to the notch in the middle of the beams. An inverse analysis with the multi-layer procedure [Hordijk, 1991] is conducted to simulate the bending responses. Kooiman [2000] developed a stress-crack width relation for SFRC by applying the multi-layer procedure. The parameters of Kooiman's model are determined for SCFRC and compared with his recommendations for SFRC. Some adjustments were required to simulate the bending tests for SCFRC. Most input parameters of the model are derived from experimental data and are related with the composition and the characteristics of SCFRC. A combined stress-strain/stress-crack width relation in tension is proposed, which applies for SCFRC with hooked-end steel fibres. The error of the predictions in average is below 8%.

9.2 Development of a tensile model for SCFRC

In general, two approaches can be distinguished to take into account the tensile behaviour of concrete: the stress-strain and the stress-crack width approach. Both approaches are compatible in case the crack width is converted into a strain with the help of an influence length. The stress-strain method is used in most standards for concrete structures.

9.2.1 Stress-crack width approach

Hillerborg et al. [1976] subdivided the response of concrete in tension into two parts: a linear elastic part (the tensile strength is not yet exceeded) and a softening branch, which was described by a stress-crack width relation. Fig. 9.1 shows the softening branch of the tensile response of plain concrete related to the so-called 'cohesive zone' in which stress still is transmitted. Within this zone the stress increases from zero up to the tensile strength at the fictitious crack tip. Hillerborg [1986] also applied the principle of the fictitious crack on SFRC.

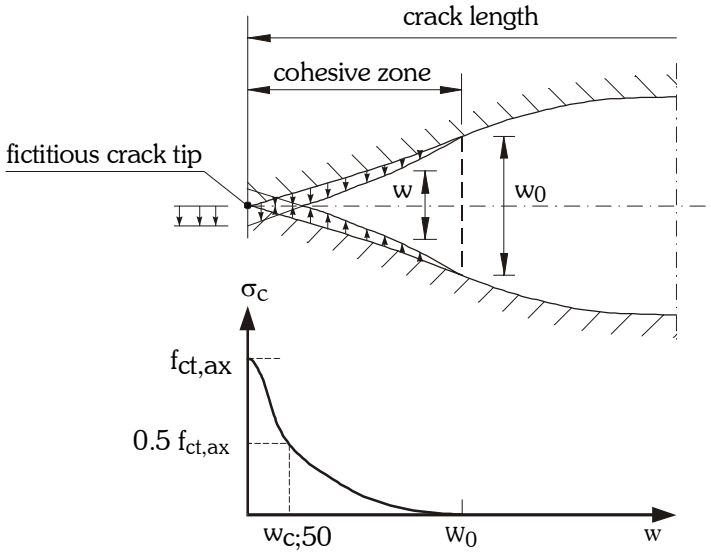


Fig. 9.1 Fictitious crack model [after: Hillerborg et al., 1976]

To make strains and crack widths compatible, Bažant & Oh [1983] introduced the 'crack band width', which limited the influence of a crack to a zone having a width of three times the maximum aggregate size. With their approach, the stress-crack width relation of concrete could be implemented into Finite Element programs used for structural analysis. Fig. 9.2 shows the assumptions of the smeared crack approach. The crack opening is transmitted into a strain, with the help of the crack band width (l_{cb}) as a factor ($\delta=\varepsilon_c \cdot l_{cb}$). The output from the simulation depends, among others, on l_{cb} and the structure of the element mesh.

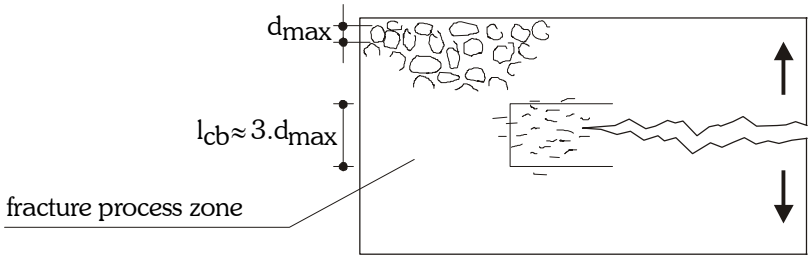


Fig. 9.2 Definition of the crack band width [after: Bažant & Oh, 1983]

9.2.2 Inverse modelling

Different tests can be performed to obtain material parameters and to determine the post-cracking behaviour of SFRC: the bending test can be considered as the standard test method for FRC. From this test various stress-strain relationships have been developed; design recommendations on SFRC are usually based on the stress-strain method. The stress-crack width relation can be recalculated from the bending test by an inverse analysis; the crack opening of a notched beam (three-point bending) has to be measured. The inverse analysis also can be executed based on results from the wedge splitting test. The stress-crack width relation can be directly determined with the uni-axial tensile test. Kooiman [2000] performed three-point bending tests on notched beams and applied the inverse analysis to model the tensile behaviour of SFRC. Computer software for inverse modelling is available; its procedure consists of four parts [Roelfstra & Wittman, 1986]: the input level, the numerical level, the accuracy check, and the output level. Fig. 9.3 presents the four levels of the inverse modelling technique.

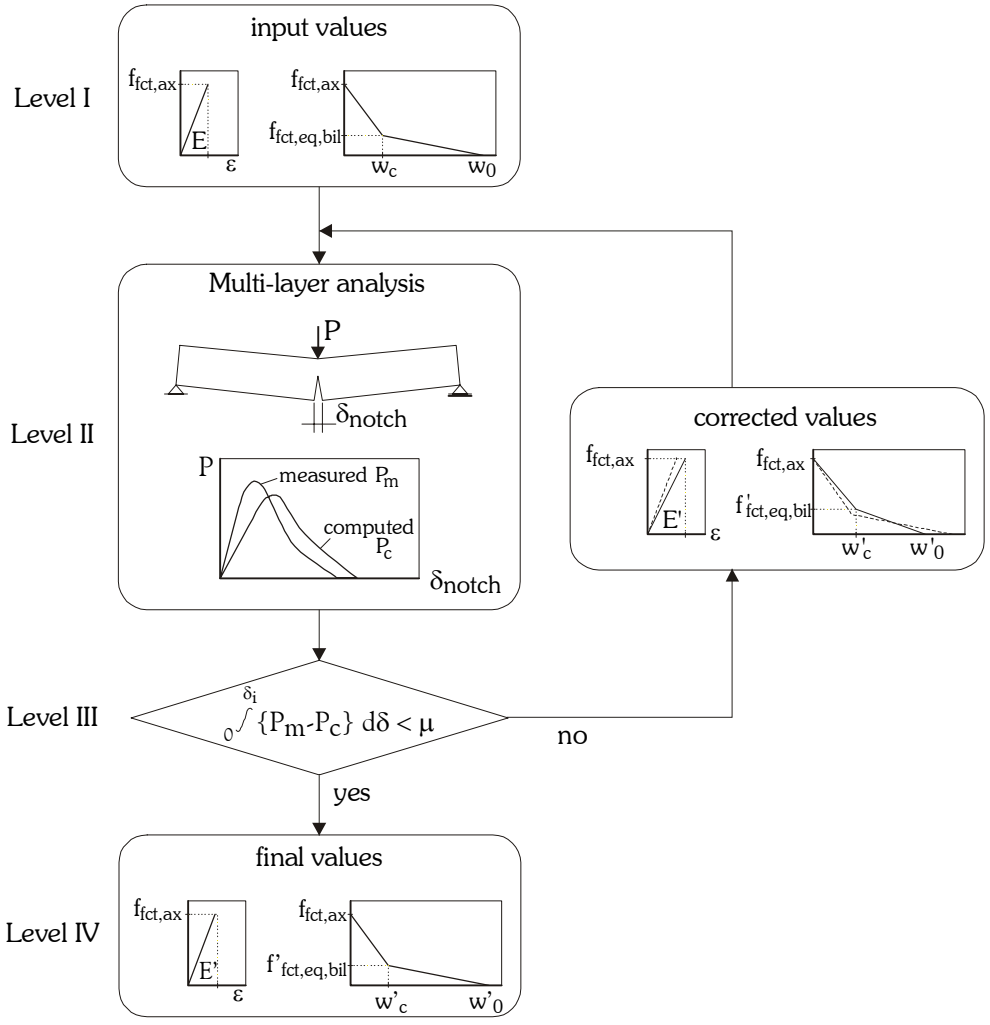


Fig. 9.3 Inverse modelling procedure [after: Roelfstra & Wittman, 1986]

The four steps for the inverse modelling procedure are the following:

- *Input level:* The starting point of the inverse analysis is the assumption of the uni-axial behaviour of a composite material in tension and compression. Furthermore, geometrical boundaries have to be set in order to start the calculation.
- *Numerical level:* The analysis is performed under consideration of the geometry of the specimen, the influence length and the material characteristics.
- *Accuracy check:* Given criteria have to be checked on this level whether the obtained solution solves the problem with sufficient accuracy. For this purpose the deviation between numerical and experimental results has to be calculated.
- *Output level:* When the accuracy criteria have been met, the chosen solution can be used as the post-cracking tensile behaviour of concrete for structural analysis.

9.2.3 Multi-layer procedure

Hordijk [1991] developed the 'multi-layer procedure' to study and to model the behaviour of plain concrete in bending. In the following, the three basic principles of the 'multi-layer procedure' are described, which are: a 'finite number of layers', 'balance of forces to calculate the bending moment' and the 'variation of strains'.

- *Finite number of layers*

Two halves of a beam are connected within a finite area. This region consists of a defined number of layers, which are connected by springs. The response of the beam is the sum of the behaviour of all springs. Fig. 9.4 shows a beam as a combination of a finite number of layers.

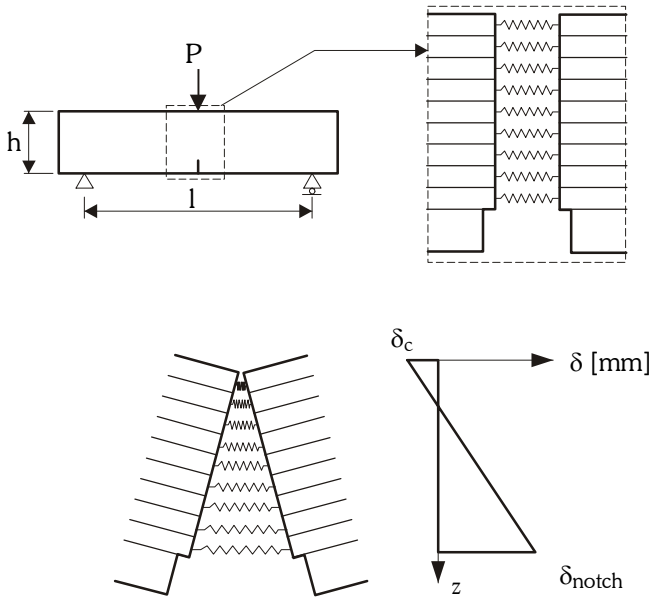


Fig. 9.4 Multi-layer procedure: finite number of layers [after: Hordijk, 1991]

A linear distribution of displacements across the height is assumed. While the beam outside this region is considered to be infinitely stiff, a fracture zone of a finite length ('influence length') has to be accounted for in order to convert discrete displacements into strains.

- *Balance of forces to calculate the bending moment*

Knowing the distribution of displacements over the height of the beam at one iteration step allows calculating the average stress of each layer. If the stress-crack width relation is defined (in Fig. 9.5 a bilinear descending branch for the softening curve) equilibrium is found in case the sum of horizontal internal forces is equal to zero; the external load (bending moment) can be calculated from the internal bending moment. Since this procedure is iterative, a spreadsheet with solver might be applied to determine the equilibrium for any iteration step. Fig. 9.5 shows the balance of forces within the cross-section and how to calculate the external load.

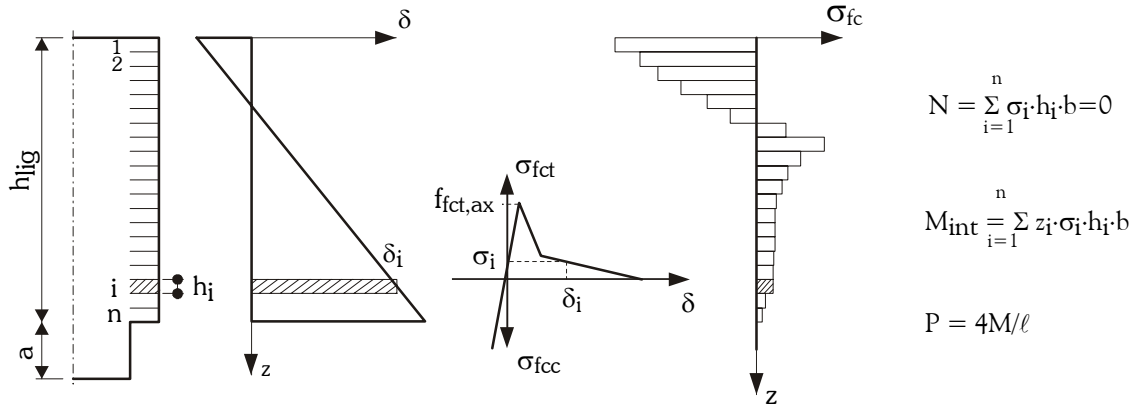


Fig. 9.5 Multi-layer procedure: calculation of the forces of each layer and of the bending moment [after: Hordijk, 1991]

- *Variation of strains*

The displacement at the notch has to be incrementally increased at each iteration step (Fig. 9.6). The target of fixing the strain at the notch and varying the strain at the upper side of the beam is the equilibrium of normal forces; a point of the load-displacement curve is obtained by calculating the bending moment. To obtain compatibility of strain and crack width, the crack width has to be divided by an influence length, which is a factor that determines the stiffness and the response of the whole system. The choice of the influence length determines the stiffness for small displacements and the maximum load [Hordijk, 1991; Kooiman, 2000].

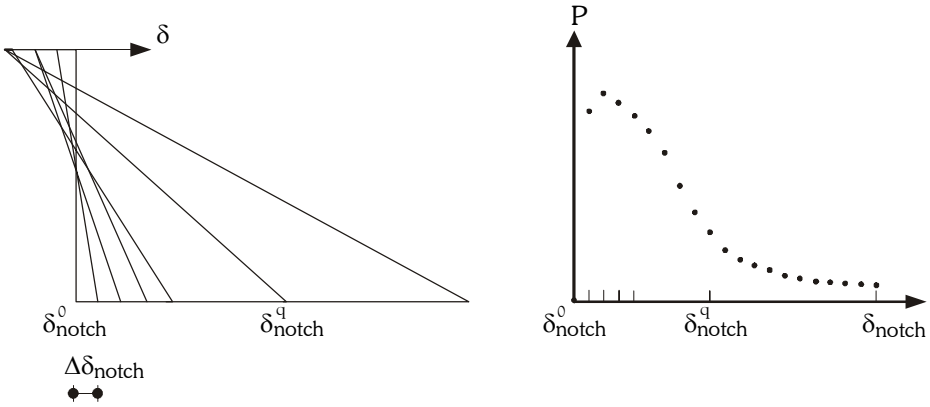


Fig. 9.6 Multi-layer procedure: variation of strains [after: Hordijk, 1991]

9.3 Model 'Kooiman' - a bilinear stress-crack width relation for SFRC

Kooiman [2000] applied the multi-layer procedure of Hordijk to determine the post-cracking behaviour of SFRC. In the following, his assumptions about the compressive and tensile regimes are summarised; the model of the post-cracking tensile behaviour is described. He carried out three-point bending tests with notch from which he developed a bilinear stress-crack width relation for SFRC. Parameters like the influence length, the number of layers were varied as well as different material parameters to study their influence on the result of simulations. The assumptions and proposed input parameters are the following [Kooiman, 2000]:

Multi-layer procedure

- *Number of layers:* 500
- *Influence length:* half the effective height of the beam (62.5 mm; notch depth: 25 mm)

Compressive behaviour of SFRC

Fig. 9.7 shows the idealised compressive behaviour, which Kooiman assumed for his simulations. The same idealised shape was applied for calculations on SCFRC.

- *Elastic compressive strain:* linear up to 1.75‰ (compressive strengths: 59/81 MPa)
- *Compressive strength:* experimentally determined from 150 mm cubes
- *Maximum compressive strain limit:* 8-10‰, linearly decreasing from 1.75‰ (8‰ - 30 mm fibres, 10‰ - 60 mm fibres). According to Kooiman, the shape and the maximum strain limit of the post-cracking compressive regime (strain > 1.75‰) did not affect the results of the simulations. The simulation suddenly dropped to zero in case the maximum compressive strain was chosen too small (<8-10‰); higher strain limits did not affect the result.

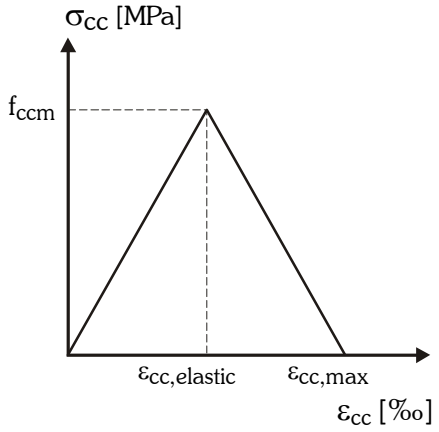


Fig. 9.7 Idealised compressive behaviour of SFRC and SCFRC

Tensile behaviour of SFRC

- *Elastic strain limit:* 0.8‰ (best fitting of the simulation and the bending response)
- *Uni-axial tensile strength:* derived from the inverse analysis
- *Post-cracking tensile behaviour (stress-crack width relation):* Fig. 9.8 shows four characteristic points of a bilinear relation.

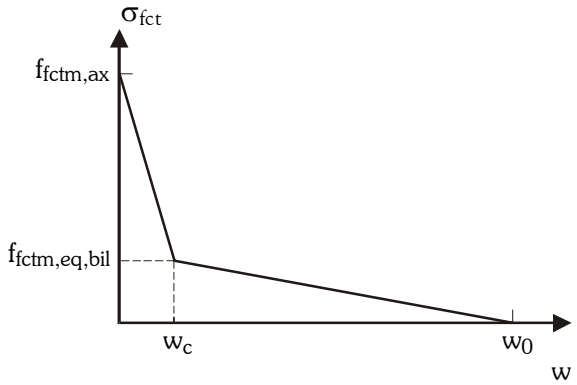


Fig. 9.8 Bilinear stress-crack width relation for SFRC in tension [after: Kooiman, 2000]

The four points of the bilinear stress-crack width relation were obtained from the inverse analysis [Kooiman, 2000]:

- The uni-axial tensile strength ($f_{fctm,ax}$) was between 0.7-0.8 times the splitting tensile strength (0.8: 60 mm fibres; 0.7: 30 mm fibres). The latter was determined on cubes of 150 mm.
- The critical crack width (w_0) depended on the fibre length, the orientation number and the fibre type. After optimisation, w_0 was 0.33 (30 mm fibres) and 0.425 (60 mm fibres) times the fibre length.

- The equivalent post-cracking strength ($f_{fctm,eq,bil}$) was calculated as the product of the mechanical fibre factor [Glavind, 1992; Equation 7.1] and a fitting parameter ($c_f \sim 0.4$). $f_{fctm,eq,bil}$ was about 30% of the uni-axial tensile strength for 30 mm fibres (60 mm fibres: 20%).
- The characteristic crack width (w_c/w_0) at which the slope of the bilinear relation changed was 1/5-1/6 of the critical crack width w_0.

9.4 Modelling the bending behaviour of SCFRC

Deformation-controlled three-point bending tests were conducted with seventeen different SCFRC mixtures. The multi-layer procedure of Hordijk [1991] was applied to recalculate the bending response; the bilinear stress-crack width relation of Kooiman [2000] was used for preliminary simulations. Kooiman's model was adjusted to obtain better predictions of the tensile behaviour of SCFRC. The applied modelling steps were as follows:

- Simulation: preliminary calculations with the assumptions of Chapter 9.3
- Description of an adjusted model for SCFRC in tension
- Simulation: iterative optimisation of the parameters for best fitting
- Formulation of a model for each parameter
- Simulations with the proposed models
- Accuracy check

9.4.1 A combined stress-strain/stress-crack width model

The simulations with the multi-layer procedure were started with the same assumptions Kooiman [2000] outlined in his thesis. Significant differences were found between experimental results and simulations, which mainly concern the response up to the displacement at which the maximum flexural load was reached. The differences concern the maximum flexural load and the initial stiffness; an adjustment of Kooiman's model was required. Appendix J presents the results of the analysis of the combined stress-strain/stress-crack width model (Table J1) and the bilinear model of Kooiman (Table J2).

Uni-axial tensile strength ($f_{fctm,ax}$)

The chosen uni-axial tensile strength significantly affects the maximum flexural load. The ratio of the uni-axial to splitting tensile strengths of SCFRC mixtures was found to be significantly lower than 0.7-0.8, as was proposed by Kooiman for SFRC. Fig. 9.9 shows the effect of the variation of the uni-axial tensile strength on the maximum flexural load, which was 0.59 for mixture 7 after an optimisation (Table 9.1).

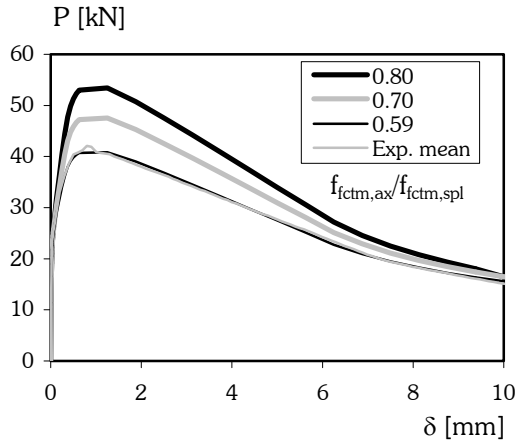


Fig. 9.9 Variation of $f_{fctm,ax}$ (simulations with mixture 7)

Initial bending stiffness

Kooiman varied the elastic tensile strain in order to fit the experimental bending results with his simulations; 0.8‰ fitted the experimental results best. In contrast, the initial bending response of SCFRC can be best split into two distinguished parts: first, an increase of the load until the initial stiffness significantly changes (elastic strain) and second, a phase, which is characterised by a reduced stiffness (reduced elastic strain). To perform the simulations with one initial stiffness either over- or underestimates the response. According to Kooiman, the effect of varying elastic tensile strains on the maximum flexural load was negligible.

Kooiman demonstrated that the complete bending response (until the bending load becomes zero) could be simulated with the bilinear stress-crack width approach for SFRC in tension; some adjustments are required for SCFRC. Fig. 9.10 shows the combined stress-strain/stress-crack width relation, which was applied to simulate the bending behaviour of SCFRC.

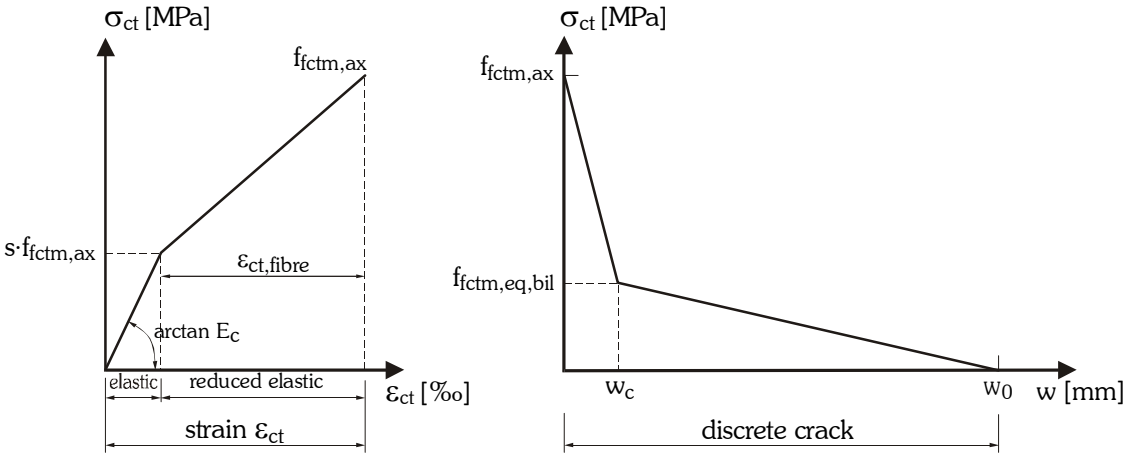


Fig. 9.10 A combined stress-strain/stress-crack width approach for SCFRC in tension (left: stress-strain for the elastic and the reduced elastic phases; right: stress-crack width relation for the softening phase)

The tensile model consists of three parts: one that accounts for the elastic behaviour of the beam, the second allows to model the reduced elastic regime and a third, which is identical with the stress-crack width relation of Kooiman. Seven input parameters are required to perform the simulation: besides the four of the model of Kooiman, these are:

- The initial stiffness (E_{fc}) of the tensile regime, which was determined from E-modulus tests on prisms (in compression)
- The tensile strength, at which the initial stiffness decreases, relates to the linear elastic limit of SCFRC in tension (expressed as a percentage of the splitting tensile strength ($s \cdot f_{fctm,ax}$)
- The reduced elastic tensile strain ($\varepsilon_{ct,fibre}$)

9.4.2 Simulations with the combined tensile model

The average bending response was used for the analysis. The remaining six parameters (Fig. 9.10; E_{fc} was experimentally determined) are related in the following with the composition and the characteristics of SCFRC, which allows predicting the bending response without performing a bending test. Models are proposed to predict each of the parameters. The approach to determine the input parameters was divided into three steps: First, the uni-axial tensile strength was varied to fit the experimental maximum flexural load. Second, the post-cracking tail was approximated by varying the equivalent post-cracking strength ($f_{fctm,eq,bil}$), the characteristic (w_c) and critical crack widths (w_0). Finally, two parameters ($s \cdot f_{fctm,ax}$ and $\varepsilon_{ct,fibre}$) were varied, to adequately fit the bending response until the maximum load was reached. An optimised fit of the average bending response and the simulation with the multi-layer procedure was obtained by varying the model parameters. The bending response was fitted up to the displacement at which the bending load was lower than 0.2 kN. Four accuracy checks were carried out; the deviation of each check (simulation/experiment) was lower than 4%. The following accuracy checks were performed:

- Bending load (at the maximum and 75% of the experimental maximum load)
- Fracture energy (up to 75% of the experimental maximum load and up to 10 mm)

The simulations were carried out with the following assumptions and experimental results; Appendix I summarises the input parameters of seventeen mixtures and the model parameters of the optimised simulations.

Multi-layer procedure

- *Number of layers:* 500
- *Influence length:* half the height of the beam (62.5 mm)

Compressive behaviour

- *Elastic compressive strain ($\varepsilon_{cc,elastic}$):* was experimentally obtained from the E-modulus test (prisms of 400·100·100 mm) and was the strain at which the maximum compressive load was obtained.

- *Uni-axial compressive strength (f_{fccm}):* experimentally obtained from the E-modulus test (prisms of 400·100·100 mm) as the maximum compressive stress of the prism.

- *Maximum compressive strain ($\varepsilon_{cc,max}$):* The multi-layer simulation dropped to zero in case the maximum compressive strain was not sufficiently large (Fig. 9.11). The assumed compressive strain limits (fibre lengths: 30 mm or shorter: 8‰, 40 mm: 12‰, 60 mm: 15‰) were not experimentally determined but are chosen to simulate the complete bending response. Schumacher et al. [2003a] reports on deformation-controlled compressive tests on SCFRC; from which it turns out that a maximum compressive strain of 8-10‰ is a realistic range.

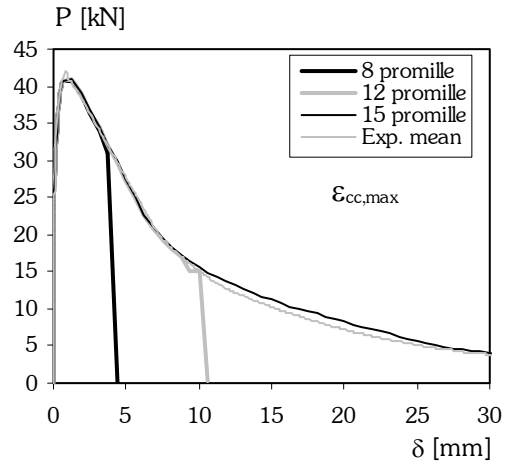


Fig. 9.11 Variation of the maximum compressive strain ($\varepsilon_{cc,max}$) (simulations for mixture 7)

9.4.3 Kooiman's model: Input parameters for SCFRC

Table 9.1 presents the four parameters of Kooiman's model (Fig. 9.8) for seventeen SCFRC mixtures. Kooiman calibrated his tensile model for SFRC with hooked-end steel fibres. The following discussion includes results of two mixtures with straight fibres (mixtures 6 and 14). These results are excluded from most of the models because they significantly differed from the parameters for hooked-end steel fibres.

Table 9.1 Summary of the four parameters of Kooiman's post-cracking tensile model obtained from simulations with SCFRC

Mix No.	*Mixture description*	*Fibre type*	V_f [kg/m^3]	$f_{fctm,ax}$ [% of $f_{fctm,spl}$]	$f_{fctm,eq,bil}/f_{fctm,ax}$ [-]	w_c/w_0 [-]	w_0/L_f [-]
1	L-R-6060	80/60	60	62	0.34	0.25	0.38
2	L-R-3060	80/30	60	53	0.28	0.36	0.34
3	L-R-40100	65/40	100	61	0.26	0.28	0.32
4	L-R-30140	45/30	140	57	0.35	0.35	0.26
5	M-R-3040	80/30	40	46	0.21	0.34	0.35
6	M-R-2060	65/20	60	55	0.57	0.07	0.36
7	M-R-6060	80/60	60	59	0.26	0.25	0.39
8	M-R-3060	80/30	60	57	0.22	0.36	0.35
9	M-R-40100	65/40	100	55	0.26	0.23	0.31
10	M-R-30140	45/30	140	57	0.33	0.28	0.27
11	M-F-6060	80/60	60	56	0.31	0.22	0.37
12	M-F-30140	45/30	140	58	0.33	0.34	0.26
13	H-R-6060	80/60	60	56	0.24	0.28	0.42
14	H-R-13125	OL13/0.16	125	68	0.42	0.48	0.37
15	P1	45/30	60	48	0.30	0.31	0.28
16	P2	45/30	120	49	0.31	0.29	0.26
17	P3	80/30	60	45	0.20	0.34	0.34

Uni-axial tensile strength ($f_{fctm,ax}$): Kooiman [2000] found factors between 0.7-0.8 with which the splitting tensile strength had to be multiplied to obtain the uni-axial tensile strength. Comparative studies showed that the ratio of uni-axial tensile strength to splitting tensile strength was 70-80% [Körmeling, 1986] and 61-86% [Hartwich, 1986]. This factor was much lower for SCFRC (45-68%). Fig. 9.12 shows the ratio of the uni-axial tensile strength to the splitting tensile strength for SCFRC. The ratio was not correlated with the fibre length, which was assumed by Kooiman. Since the uni-axial tensile strength determines to a large extend the maximum flexural load, the model and parameters proposed by Kooiman significantly overestimated the bending response of SCFRC.

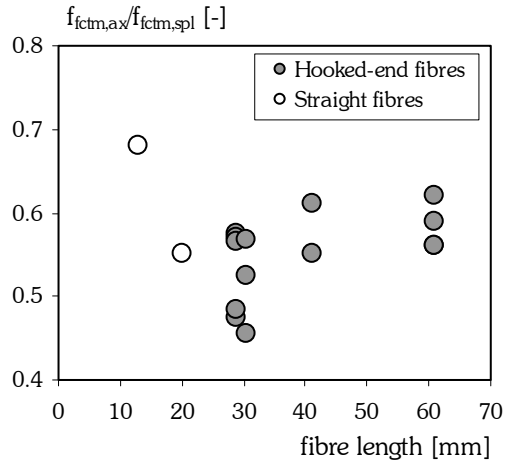


Fig. 9.12 Fibre length compared with the ratio of $f_{fctm,ax}$ to $f_{fctm,spl}$

Equivalent post-cracking strength ($f_{fctm,eq,bil}$): The percentage of the uni-axial tensile strength in case of SFRC was 20-30% (dependent on the fibre type); for SCFRC and hooked-end steel fibres this was 20-35%, which is about the same range. The division of the equivalent post-cracking strength by the mechanical fibre factor results in a factor that was in all cases significantly higher than 0.4, which Kooiman found for SFRC (SCFRC: 0.60-1.08). The increased equivalent post-cracking strength of SCFRC contributes to G_F. Fig. 9.13 shows the effect of the variation of the equivalent post-cracking strength.

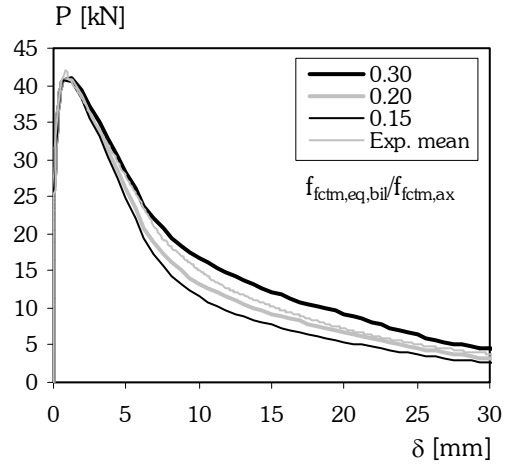


Fig. 9.13 Variation of the equivalent post-cracking strength $f_{fctm,eq,bil}$ (simulations for mixture 7)

Characteristic crack width (w_c): Kooiman found this parameter to be about 20% of the fibre length; this was 22-36% for SCFRC, which is larger in each case and could be even twice as high. Fig. 9.14 shows the effect of a varying characteristic crack width for mixture 7.

Critical crack width (w_0): Fig. 9.15 indicates that the choice of the critical crack width becomes affecting at crack widths, which are not relevant for most practical applications (>5-10 mm).

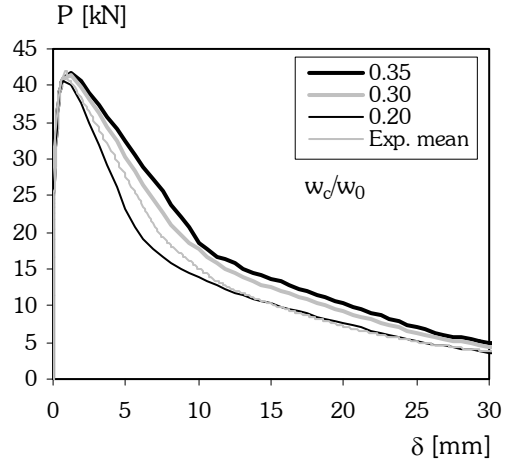


Fig. 9.14 Variation of the characteristic crack width w_C (simulations for mixture 7)

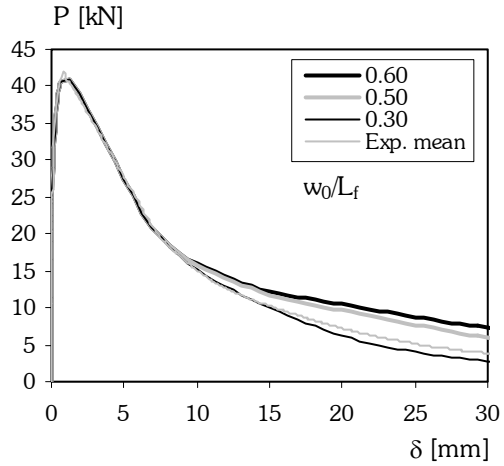


Fig. 9.15 Variation of the critical crack width w_0 (simulations for mixture 7)

The maximum crack width of SFRC is between 0.33-0.425 times the fibre length; the factor was 0.26-0.42 for SCFRC, which is about the same.

9.4.4 Input parameters of the combined tensile model

In the following, the six parameters of the combined stress-strain/crack width model of Fig. 9.10 are related to the mixture composition of SCFRC.

Step 1: Maximum flexural load

Uni-axial tensile strength ($f_{fctm,ax}$)

The increase of the splitting tensile strength and the bending performance due to the fibres depends on their orientation and distribution. The casting method and the flow of SCFRC affect the performance (Chapter 8.2.2). The loading conditions of both tests are not the same; the splitting tensile test is performed load-controlled (bending test: deformation-controlled). It is questionable, whether it is adequate to compare results of both tests. At least, the orientation of the fibres plays an important role, which has to be taken into account. Still, it was the aim to establish a relation between the splitting tensile test and the calculated uni-axial tensile strength ($f_{fctm,ax}$). The prediction of this parameter significantly affects the accuracy of the simulation.

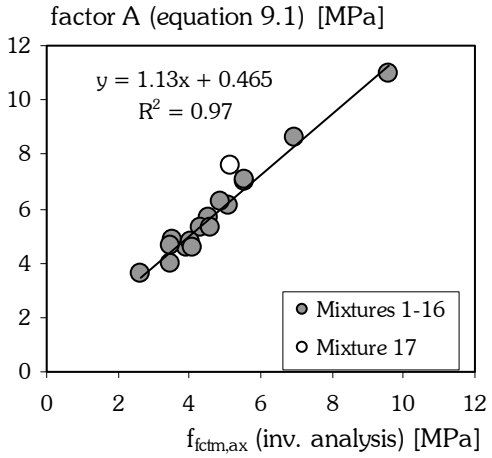


Fig. 9.16 Relation between the uni-axial tensile strength (form the inverse analysis) and factor A (Equation 9.1)

A correction has to be applied (Fig. 9.16, Equation 9.1) to better predict the uni-axial tensile strength from the splitting tensile strength (R^2=0.97). Factor A is the correction factor of the splitting tensile strength, which is correlated with the uni-axial tensile strength.

$$f_{fctm,ax} = \frac{A - 0.465}{1.13} \quad \text{with:} \quad A = \eta_{\varphi} \cdot \left((f_{ctm,spl} + (f_{fctm,spl} - f_{ctm,spl}) \cdot (V_f \cdot \frac{L_f}{d_f}) \right) \tag{9.1}$$

where: $f_{fctm,ax}$ = mean axial tensile strength of SFRC or SCFRC [MPa]
$f_{fctm,spl}$ = mean splitting tensile strength of SFRC of SCFRC [MPa]
$f_{ctm,spl}$ = mean splitting tensile strength of plain concrete [MPa]
$V_f \cdot L_f / d_f$ = fibre factor [-]
η_{φ} = orientation number [-]

The splitting tensile strengths were determined with and without fibres to estimate the effect of the type and the content of the steel fibres. The orientation numbers of the beams are applied to take the effect of the flow into account. Mixture 17 (white circle) was excluded from Equation 9.1, since it differed too much from the other test results; its flexural load was too low compared with the splitting tensile strength. This difference might be caused either by a lower number of fibres in the cross-section of the beams or by a higher number of fibres in the cubes.

Step 2: Post-cracking regime

Critical crack width (w_0)

Kooiman proposed to relate the critical crack width with the orientation number and the fibre length. Related to both parameters, the higher the aspect ratio the larger was the critical crack width (Fig. 9.17). The discussion in Chapter 9.4.3 already indicated that this parameter was in the same range as was proposed by Kooiman for SFRC.

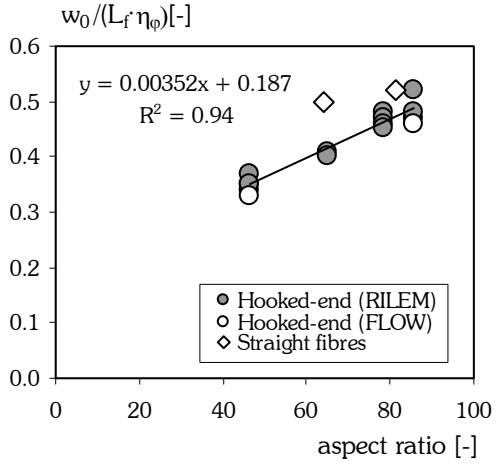


Fig. 9.17 Prediction of the critical crack width (w_0)

The critical crack width can be predicted by applying Equation 9.2 (R^2=0.94). This equation was derived from the results of mixtures with hooked-end fibres, which were cast according to the RILEM method; mixture 6 (straight steel fibres, length: 20 mm) had a larger critical crack width compared with its aspect ratio.

$$w_0 = (0.187 + 3.52 \cdot 10^{-3} \cdot \frac{L_f}{d_f}) \cdot L_f \cdot \eta_\varphi \qquad (9.2)$$

where: w_0 = critical crack width [mm]
L_f/d_f = aspect ratio [-]
L_f = fibre length [mm]
η_φ = orientation number [-]

Characteristic crack width (w_c)

The characteristic crack width (w_c/w_0) of SFRC is in the range of 1/5-1/6 of w_0 [Kooiman, 2000]. The characteristic crack width was separated from the maximum crack width to determine whether other parameters also affect it. Fig. 9.18 shows that the characteristic crack width depends on the type of steel fibre (length and diameter).

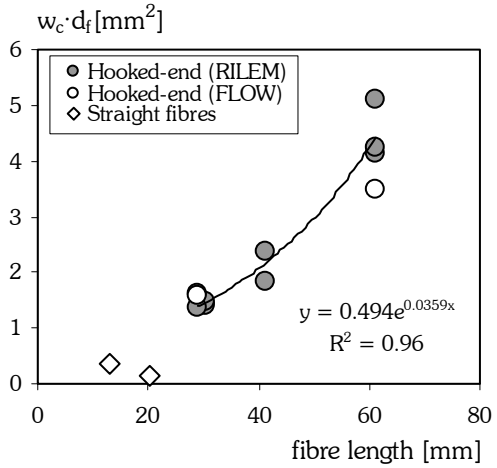


Fig. 9.18 Relation between the fibre length and the product of the characteristic crack width and the diameter of the steel fibres

Equation 9.3 predicts the characteristic crack width of mixtures with hooked-end fibres and produced according to the RILEM casting method (R^2=0.96). Mixture 11 (casting method: Flow) was different compared with other mixtures with hooked-end fibres. Straight steel fibres are excluded from Equation 9.18 to obtain a better accuracy for hooked-end fibres.

$$w_C = \frac{0.494}{d_f} \cdot e^{0.0359 \cdot L_f} \qquad (9.3)$$

where: w_c = characteristic crack width [mm]
d_f = fibre diameter [mm]
L_f = fibre length [mm]

Equivalent post-cracking strength ($f_{fctm,eq,bil}$)

The critical and characteristic crack widths are parameters in Kooiman's model that are affected by the orientation number. He calculated the equivalent post-cracking strength as the product of the mechanical fibre factor (Chapter 7.2.1) and a correction factor c_f (~0.4). Kützing [2000] included the orientation number in his model on the uni-axial tensile behaviour of SFRC. He found that the higher the orientation number was the higher the tensile strength at the characteristic crack width becomes.

The fibre efficiency factor (FEF) is defined and obtained by dividing the equivalent post-cracking strength by the mechanical fibre factor and the orientation number (Fig. 9.19). Two conclusions are drawn: first, the fibre efficiency factor is not constant but depends on the fibre type and second, the response of straight steel fibres differed from that of hooked-end steel fibres. The results from mixtures 15 and 16 with Dramix 45/30 BN steel fibres scattered around an average fibre efficiency factor.

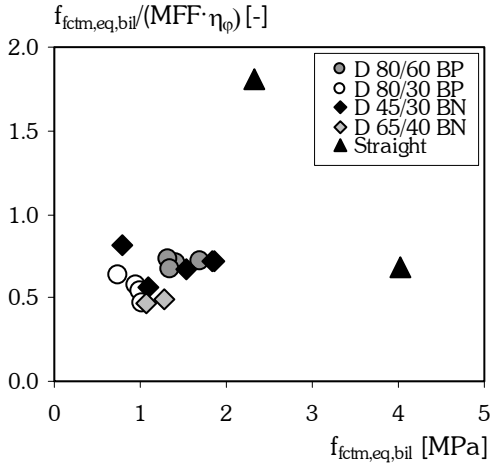


Fig. 9.19 Relation between the equivalent post-cracking strength ($f_{fctm,eq,bil}$) and the fibre efficiency factor

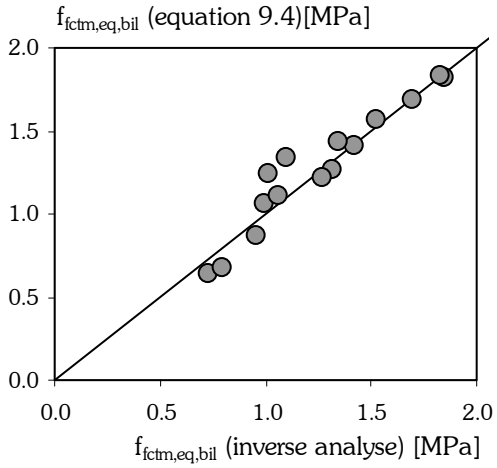


Fig. 9.20 Comparison of the analytical and the predicted equivalent post-cracking strengths (Equation 9.4)

Table 9.2 presents the average fibre efficiency factors of different hooked-end fibres, which are independent of the compressive strength class. The ratio of fibre efficiency factors of Dramix 80/60 BP to Dramix 80/30 BP was 1.17. In Chapter 8.4, the efficiency of a fibre in single fibre pull-out tests was discussed; the ratios of the percentages of forces (displacement < L_{EL}) relative to the maximum pull-out force of both fibre types are in about the same range (Dramix 80/60 BP (L_{fe}=10 mm) to Dramix 80/30 (L_{fe}=10 mm): 1.18; Dramix 80/60 (L_{fe}=30 mm) to Dramix 80/30 BP (L_{fe}=10 mm): 1.29). This similarity cannot be checked for other fibre types since no results are available. An increase of the average fibre load until it completely reaches the straight channel contributes to the fracture energy in bending.

Table 9.2 Fibre efficiency factors (FEF) of hooked-end steel fibres

Fibre type	*Fibre efficiency factor*
Dramix 80/60 BP	0.873
Dramix 80/30 BP	0.745
Dramix 45/30 BN	0.912
Dramix 65/40 BN	0.625

Equation 9.4 predicts the equivalent post-cracking strength of SCFRC for mixtures with hooked-end fibres as a product of the mechanical fibre factor (MFF, Equation 7.1), the orientation number and the fibre efficiency factor (FEF).

$$f_{fctm,eq,bil} = MFF \cdot \eta_{\varphi} \cdot FEF \tag{9.4}$$

where: $f_{fctm,eq,bil}$ = mean equivalent post-cracking strength [MPa]
MFF = mechanical fibre factor (Equation 7.1] [MPa]
η_{φ} = orientation number [-]
FEF = fibre efficiency factor (Table 9.2)[-]

Fig. 9.20 compares the predicted and the analytical equivalent post-cracking strengths of mixtures with hooked-end fibres. It was discussed in Chapter 8.4.2 that the performance of a fibre relative to the maximum pull-out force during the pull-out process depends on the fibre type. Dramix 80/60 BP dissipates relatively more energy compared with Dramix 80/30 BP after the maximum pull-out force is surpassed. The mechanical fibre factor of both fibre types is the same; the fibre efficiency factor takes into account this difference.

Step 3: Elastic and reduced elastic tensile strain ranges

The third step was to adjust the simulations to the experimental bending response up to a displacement at which the maximum flexural load is obtained. Two parameters are determined by inverse analysis; these are the first cracking strength ($s \cdot f_{fctm,ax}$), the strength at which the initial stiffness decreases and the reduced elastic tensile strain ($\varepsilon_{ct,fibre}$).

First cracking strength ($s \cdot f_{fctm,ax}$)

The E-modulus in compression was chosen as the initial stiffness of the elastic tensile regime. All beams of mixtures 1-17 resulted in a load increase after the first crack appeared; the maximum flexural load was reached at displacements of 0.2-1.2 mm. In order to accurately model the bending behaviour up to the maximum flexural load, the decrease of the initial stiffness is accounted for; this point is defined as the 'first cracking strength'. Fig. 9.21 shows that the first cracking strength was about 40% of the splitting tensile strength (with fibres) independent of the compressive strength or the type or the content of the fibres. Mixture 14 (B105 with short, straight steel fibres) resulted in a higher first cracking strength (about 60%). In order to demonstrate the effect of various first cracking strengths, Fig. 9.22 compares simulations and the mean experimental result (mixture 7, first cracking strength: 40%). A higher first cracking strength slightly

increases the maximum flexural load and decreases the related displacement. A first cracking strength of 40% was used in further simulations.

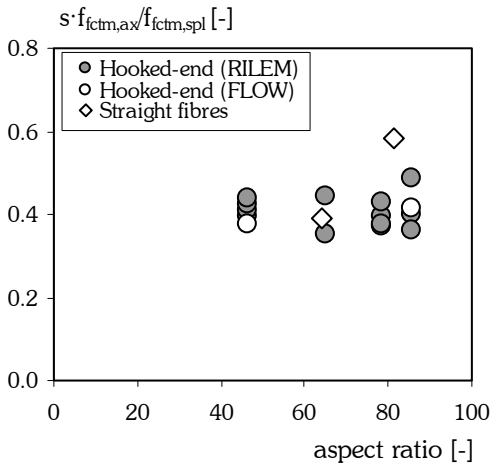


Fig. 9.21 First cracking strength ($s \cdot f_{fctm,ax}$) of SCFRC as a percentage of the splitting tensile strength

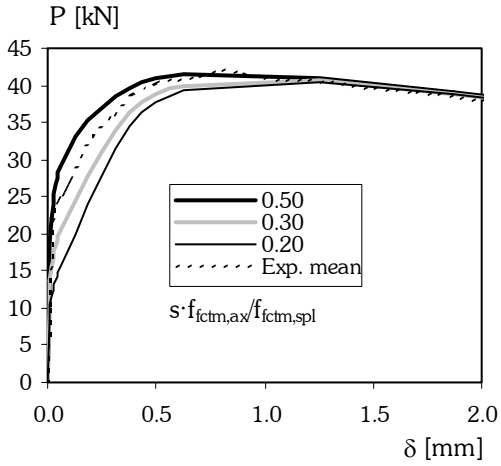


Fig. 9.22 Variation of the first cracking strength ($s \cdot f_{fctm,ax}$) (simulations for mixture 7)

Reduced elastic tensile strain ($\varepsilon_{ct,fibre}$)

Kooiman [2000] varied the elastic tensile strain limit in order to fit experimental and analytical results; 0.8‰ fitted his experimental data best. The additional (to the elastic) reduced elastic tensile strain was varied to obtain the actual stiffness of SCFRC. $\varepsilon_{ct,fibre}$ correlates with the aspect ratio (Fig. 9.23).

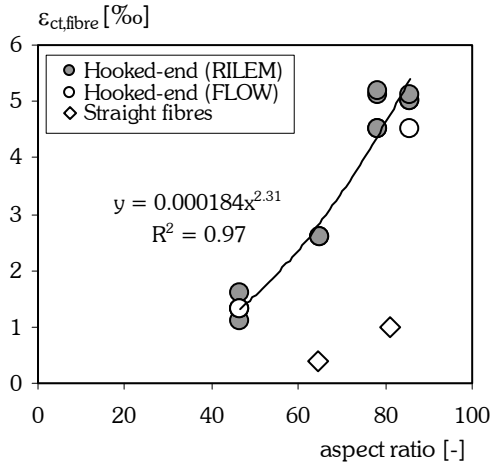


Fig. 9.23 The aspect ratio of the steel fibres versus the reduced elastic tensile strain ($\varepsilon_{ct,fibre}$)

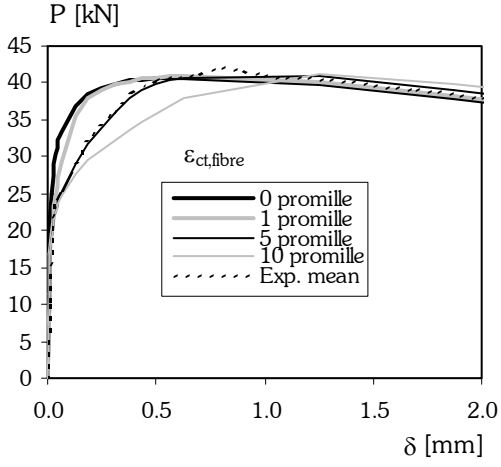


Fig. 9.24 Effect of various reduced elastic tensile strains (simulations for mixture 7)

Before the maximum load was reached, in some cases more than one crack opened; once the maximum flexural load was surpassed the softening coincided with the opening of a discrete crack. Longer fibres promoted the occurrence of multiple cracking. The assumption of a (reduced elastic) strain range was chosen to describe the

experimental observations in the pre-peak regime. The additional tensile strain of mixtures with straight fibres was smaller compared with hooked-end fibres; the maximum flexural load was reached at a smaller displacement. The reduced elastic tensile strain of hooked-end fibres depends on the fibre type and can be calculated by Equation 9.5 (R^2=0.97). Fig. 9.24 shows the comparison of different levels of reduced elastic tensile strains for mixture 7. The best fit was obtained at a reduced elastic tensile strain of 5‰. The effect of the tensile strain on the maximum flexural load was negligible [Kooiman, 2000].

$$\varepsilon_{ct,fibre} = 0.184 \cdot 10^{-3} \cdot \left(\frac{L_f}{d_f}\right)^{2.31} \qquad (9.5)$$

where: $\varepsilon_{ct,fibre}$ = reduced elastic strain of SCFRC in tension [‰]
L_f/d_f = aspect ratio [-]

9.4.5 Accuracy check

Two accuracy checks (for the maximum flexural load and the fracture energy up to 75% of the experimental maximum flexural load) were carried out. Fig. 9.25 compares the results of fifteen mixtures.

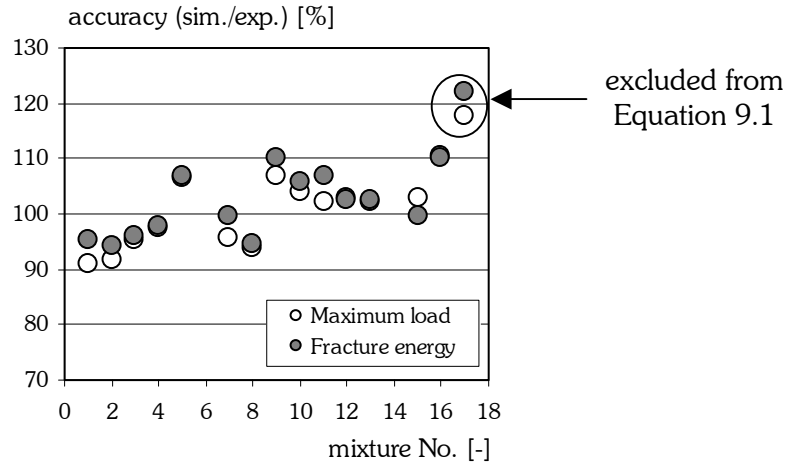


Fig. 9.25 Accuracy of the multi-layer predictions: simulations versus experimental results

The accuracy check includes mixtures with hooked-end steel fibres and both casting methods ('RILEM' and 'Flow' method). Straight steel fibres differed from hooked-end fibres in various respects. Therefore, the results of mixtures 6 and 14 are excluded from the accuracy check. The higher variation of mixture 17 (about 20%) originates from the fact that this mixture was excluded from Equation 9.1, which improved the accuracy of the predictions of the other mixtures with hooked-end fibres. The results of simulations (Appendix K) are obtained with input parameters from Equations 9.1-5. The accuracy of the fracture energies was close to that of the maximum flexural loads, which supports the importance of an accurate prediction of the uni-axial tensile strength. The average

error of the maximum flexural load (mixtures 6/14/17 are excluded) is 7.2% (fracture energy: 7.4%). The error is 5.7 and 5.5%, respectively, in case mixtures P1-P3 (different casting procedure) and mixtures with straight fibres (mixtures 6 and 14) are excluded. Appendix K presents the experimental results of three-point bending tests (individual and average results up to a displacement of 10 mm) as well as the results of simulations with the multi-layer procedure. Figs. 9.26 and 9.27 present experimental results and simulations for Dramix 80/60 BP (Fig. 9.26; V_f=60 kg/m^3) and Dramix 45/30 BN (Fig. 9.27; V_f=140 kg/m^3). The mixtures with long steel fibres are mixtures 1/7/13 for strength classes B45/B65/B105. Fig. 9.27 compares the predictions and experimental results for mixtures with 30 mm steel fibres (mixtures 4 and 10).

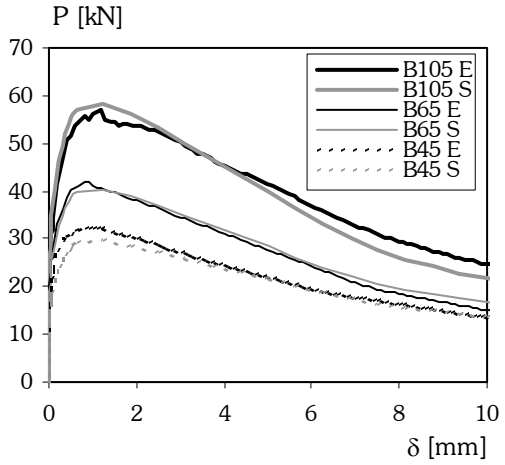


Fig. 9.26 Simulations (S) versus experimental (E) results: effect of the strength class (Dramix 80/60 BP, V_f=60 kg/m^3)

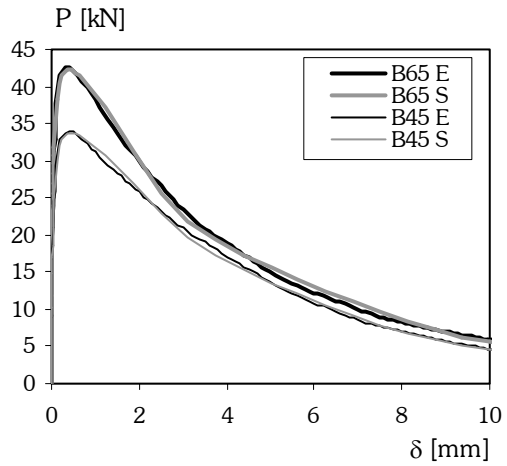


Fig. 9.27 Simulations (S) versus experimental (E) results: effect of the strength class (Dramix 45/30 BN, V_f=140 kg/m^3)

9.5 Discussion of the proposed tensile model

In the following, the tensile model of Kooiman and the combined stress-strain/stress-crack width model are discussed. The bending responses of SCFRC and SFRC were rather different concerning the initial stiffness, the post-cracking behaviour as well as the variation of the test results. The different bending responses required some adaptations of Kooiman's model to be applicable for SCFRC.

Two different types of concretes

In Chapter 8, a SCFRC mixture was compared with an equivalent SFRC. The differences in performance and variation are discussed. A second example is the case study of Kooiman [2000, p. 129], a tunnel segment containing steel fibres as the only reinforcement was designed. By applying his tensile model he proved that the tunnel segments of the 2nd Heinenoord-tunnel are properly designed. The input parameters were derived from an inverse analysis of three-point bending tests. His case study is used to further discuss the test responses of SFRC and SCFRC as well as the tensile

model of Kooiman and the combined tensile model (Chapter 9.4.1). Fig. 9.28 compares the average bending response of two mixtures (SFRC and SCFRC: mixture 1; L-R-60-60) of the same strength class (B45, V_f=60 kg/m^3).

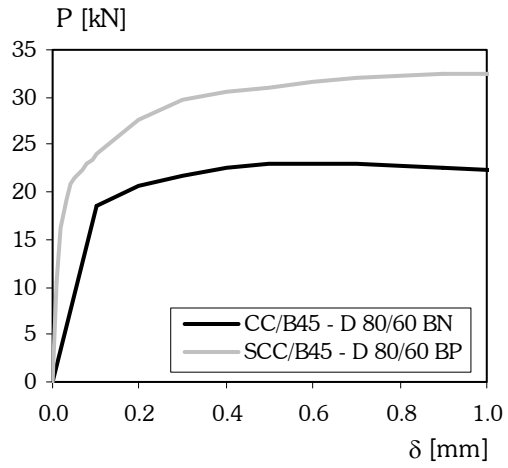


Fig. 9.28 Comparison of the initial stiffness of conventional and self-compacting fibre reinforced concrete

The self-compacting mixture contained high strength steel fibres (Dramix 80/60 BP), whereas normal strength steel fibres (Dramix 80/60 BN) were added to conventional SFRC. The initial bending response of SCFRC was much stiffer. The E-modulus, which was determined in a compressive test, was applied to model the bending response of SCFRC for small displacements. The rate of deformation up to a displacement of 2 mm was different for SFRC and SCFRC (1 μm/s compared to 50 μm/s), which might have contributed to the fact that the initial response of SCFRC was stiffer. Kooiman [2000] increased the elastic tensile strain limit to take the weaker initial response of SFRC into account.

The splitting tensile strength (with steel fibres) of mixture 1 (L-R-60-60) was 6.3 MPa, whereas that of the SFRC mixture of Kooiman's study was 3.5 MPa; rather different maximum flexural loads also reflect this difference (Fig. 9.28). The type of concrete (SCFRC or SFRC), the fibre type (normal or high strength), the orientation of the fibres and the rate of deformation might have contributed to the fact that significant differences were obtained. The variation of the results of the SFRC mixtures was higher.

Comparison of two tensile models

To indicate the differences between the tensile model of Kooiman and the combined model (Chapter 9.4.1), simulations with the multi-layer procedure were carried out. Figs. 9.29-30 show individual results of the bending tests up to displacements of 0.5 and 5 mm [Kooiman, 2000, p. 129] and the average bending responses. The simulations with the input parameters of the model 'Kooiman' as well as the simulation with parameters of the combined tensile model fitted the results of this SFRC mixture.

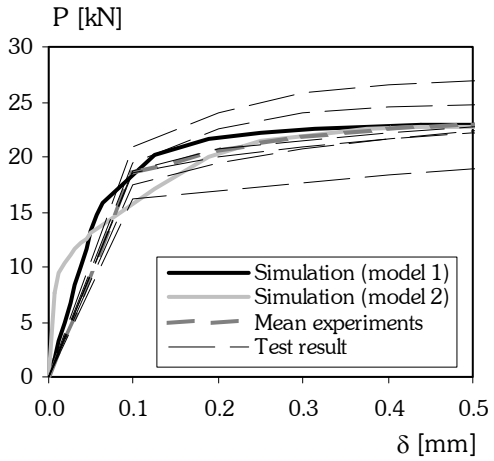


Fig. 9.29 Experimental results and simulations with the multi-layer procedure (displacement<0.5 mm)

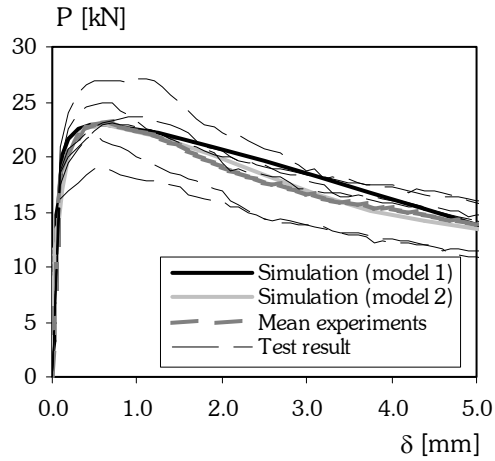


Fig. 9.30 Experimental results and simulations with the multi-layer procedure (displacement<5 mm)

Table 9.3 shows the input parameters for simulations with the multi-layer procedure according to the model of Kooiman [2000] and the combined tensile model.

Table 9.3 Input parameters for predictions with the multi-layer procedure

Parameter	*Model 1* *Model Kooiman* *[Kooiman, 2000, p. 132]*	*Model 2* *Optimisation study with* *the combined tensile model*
Elastic tensile strain limit [‰]	0.8	-
E_{fc} [MPa]	-	39100
$s \cdot f_{fctm,ax}$ [% of $f_{fctm,spl}$]	-	54
$\varepsilon_{ct,fibre}$ [‰]	-	2.5
$f_{fctm,ax}$ [MPa]	2.8	2.8
$f_{fctm,ax}$ [% of $f_{fctm,spl}$]	80	80
$f_{fctm,eq,bil}$ [MPa]	0.8	1.3
w_c [mm]	5.1	3.1
w_0 [mm]	25.5	19.0

and $\varepsilon_{cc,max}$=10‰, $\varepsilon_{cc,elastic}$=1.75‰, f_{fccm}=56 MPa
$f_{fctm,spl}$=3.5 MPa, E_{fc}=36250 MPa (for model 1 only) - [NEN 6720, 1995]

After optimisation, both models resulted in the same uni-axial tensile strength, which is correlated with the maximum flexural load. The effect of the remaining parameters is relatively small (Fig. 9.30). In spite of different input parameters, the accuracy of both predictions was comparable. The experimental splitting tensile strength of 3.5 MPa of SFRC (with fibres) is not higher than what is expected for plain concrete at a compressive strength of 56 MPa. The CEB-fib Model Code [1990] predicts a splitting tensile strength (mean value) of 4.4 MPa; the effect of the fibres on the splitting tensile strength was negligible. The initial stiffness affects the bending response at small displacements only (<0.2 mm). The combined tensile model (model 2) requires the E-modulus as an input parameter. Fig. 9.29 shows that the initial stiffness for SFRC is overpredicted. To compensate for the higher initial stiffness of SCFRC obtained with the combined tensile model, the reduced elastic tensile strain $\varepsilon_{ct,fibre}$ was chosen to obtain

about the same fracture energy compared with the average experimental result. The model of Kooiman (model 1) was calibrated with experimental results and predicts the initial stiffness very well. Based on the comparison of two different tensile models the following conclusions are drawn:

- The number of results of comparable SCFRC and SFRC mixtures is not sufficient to draw well-supported conclusions. The bending responses of both types of concrete were rather different; as a consequence the models' parameters differ, too.

- The parameter $f_{fctm,ax}$ (the uni-axial tensile strength of the proposed tensile model) is the most important parameter for the accuracy of the predictions of the bending response. To predict this parameter, the splitting tensile tests with and without fibres and the orientation number have to be determined. Equation 9.1 was derived from bending results of SCFRC; the bending load increased for all tested mixtures once the limit of proportionality was surpassed.

- In case the post-cracking bending load is lower or equal to the load at the limit of proportionality, the approach of Kooiman to include one elastic tensile region ($s \cdot f_{fctm,a} = f_{fctm,ax}$ and E_{fc} different from the E-modulus in compression) should be followed. The elastic tensile strain limit can be derived from the inverse analysis. To accurately model the bending behaviour of SCFRC mixtures of the present study the change of the initial stiffness had to be taken into account. Straight fibres cause higher first cracking strengths and lower reduced elastic strains compared with hooked-end fibres. Further tests should be performed with SCFRC to obtain more information concerning the initial phase of the bending response in case the maximum bending load is equal or lower compared with the load at the limit of proportionality.

- The equivalent post-cracking strength of SCFRC mixtures was higher and the characteristic crack width larger compared with SFRC. The models' parameters for straight steel fibres in most cases were different from that of hooked-end fibres.

9.6 Concluding remarks

Seventeen different SCFRC mixtures were tested on their bending performance. Based on the experimental results a combined stress-strain/stress-crack width model for SCFRC in tension was developed. The model was calibrated with results of fifteen mixtures, which contained hooked-end steel fibres. By applying the multi-layer procedure of Hordijk an inverse analysis was performed. First simulations showed that Kooiman's bilinear stress-crack width model for SFRC resulted in an overestimation of the maximum flexural load. The uni-axial tensile strength is the most important parameter for the accuracy of the predictions. In order to determine the accuracy of the model of Kooiman, which was developed for SFRC, the parameters of his tensile model were also determined for SCFRC. Significant differences were found for some of the models' parameters. To improve the accuracy of the predictions, the model of Kooiman was

extended. The proposed stress-strain/stress-crack width model distinguishes three tensile regions: the elastic and the educed elastic strain ranges and a softening branch. The difference between results of simulations with the combined tensile model and experimental results in average is below 8%.

Chapter 10:

Case studies on SCFRC

10.1 Introduction

Chapter 10 discusses three full-scale structural applications in which SCFRC is applied: sheet piles, tunnel segments and large beams. The effects of the flow and the production process on the orientation and the distribution of the fibres are studied.

Conventional SFRC is often assumed to have the same characteristics in three principal directions (3D-orientation) and is therefore considered as a bulk material on a higher level without having integrated the effect of the orientation of the fibres. In case the concrete is rather stiff, vibrating the concrete affects the orientation of the fibres. Along the flow of SCFRC, the fibres are thought to rotate into the flow direction [Nemegeer, 1999]. Several studies indicated that the assumption of randomly oriented fibres has to be handled with care [Schönlin, 1988; Kooiman, 1998b/2000]. As the results of the bending tests indicated (Chapter 8.2), the production process has a significant influence on the characteristics of SCFRC in the hardened state. The actual orientation of the steel fibres as well as their distribution is important to design structural elements with SCFRC. The degree to which segregation of fibres is counteracted determines their distribution; blocking or clustering also lead to an inhomogeneous fibre distribution. Methods to determine the orientation number are: image analysis, X-ray photographs, counting the fibres and recalculation from mechanical characteristics. Recently, computer tomography has been applied to study the effect of the flow on the orientation of the steel fibres in SCFRC [Linsel & Dehn, 2002].

10.2 Case study 1: Sheet piles

10.2.1 Experimental set-up

Sheet piles are ground and water-retaining structures, which are usually made of steel. 'SPANBETON', a Dutch producer of prefabricated concrete elements fabricates sheet piles made out of concrete. These elements are prestressed and reinforced with steel bars. Compared with a steel sheet pile, concrete elements are more durable and can be used as a load-carrying part of a structure.

Prestressed sheet piles produced with SCFRC have several advantages compared with a standard concrete sheet pile: the placement of the concrete is easier (no bar

reinforcement has to be arranged), the storage of the segments requires less space, more sheet piles can be transported with one truck (they are lighter and occupy less space) and the placement in the ground is easier (less resistance). SPANBETON performed a study, which aimed at developing a prestressed sheet pile without any bar reinforcement. Without an increase of the total production costs, the load bearing capacity should be at least that of a comparable concrete sheet pile of the same static height. Preliminary studies were performed at the Delft University of Technology. The case study on the sheet piles consisted of four parts:

- Sato et al. [2000] carried out a preliminary study on the characteristics of a high strength mortar with steel fibres in the hardened state. In this study, the type and the content of short steel fibres (length: 6 and/or 13 mm) were varied.
- Van der Kolk [2001] optimised the geometry of the sheet pile under consideration of e.g. structural and economical aspects. An optimised sheet pile was the result; the calculation indicated that the sheet pile with SCFRC would be economical in case the price of the mixture would be below 450 Euro/m^3.
- Based on the study of Sato et al., an optimised mixture was developed, which fulfilled all design criteria [Grünewald et al., 2002]. Several tests were carried out on the characteristics of the optimised mixture in the hardened state.
- Full-scale trials were performed at SPANBETON in order to determine the feasibility of the new sheet pile. Six sheet piles (Fig. 10.1, left) were cast and tested on several characteristics; three were placed in the ground. Tol [2002] and Jansze et al. [2002] reported on detailing, the casting process and testing of the sheet piles.



Fig. 10.1 Prestressed sheet piles cast with self-compacting fibre reinforced mortar (left) and conventional concrete (right: B65 with bar reinforcement)

10.2.2 Mixture optimisation

In the following, the optimisation of the applied mixture is discussed and important conclusions of this case study are summarised. The choice of the type and the content of the steel fibres was based on economical as well as on performance considerations [Sato et al., 2000]. The list of requirements for the innovative element was the following:

- Load bearing capacity (shear force and bending moment) equal to or better when compared with the conventional element of the same static height
- Material price < 450 Euro/m^3
- An early-age cube strength of at least 60 MPa one day after casting
- Self-compacting with steel fibres (Dramix OL 13/0.16, V_f=125 kg/m^3)
- Passing ability: spacing 16 mm

The thickness of the optimised sheet pile was 45 mm in the web and 50 mm in the flanges. Eighteen strands were arranged, which had a diameter of 12.5 mm. The free spacing between the mould and the strands in the web was about 16 mm. Short steel fibres (length: 13 mm) were used to avoid blocking. Based on results of earlier studies a first approximation of the granular skeleton was derived. Fig. 10.2 shows the content of aggregates and steel fibres of the mixture applied for sheet piles compared with results on the maximum fibre content of self-compacting concrete and mortar [Grünewald & Walraven, 2001a/b]. In order to limit the effect of the aggregates on the passing ability as much as possible, the maximum aggregate size was 1 mm. The paste content was slightly increased compared with what is suggested by the results of Fig. 10.2 to compensate for the reduced number of grain fractions. Grünewald et al. [2002] present a detailed description of the optimisation of the mixture for sheet piles.

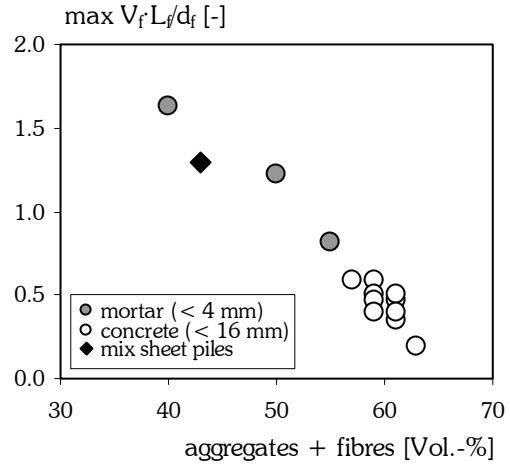


Fig. 10.2 Effect of the content of aggregates and steel fibres and the maximum aggregate size on the maximum fibre content;
(series PS: concrete $d_{g,max}$ < 16 mm, series OS: mortar $d_{g,max}$ < 4 mm)

Table 10.1 shows the composition of the optimised mixture and the price of the components. Bending tests were performed with this mixture; the results are reported in Chapter 8 (mixture 14 / H-R-13-125).

Table 10.1 Mixture composition and costs of the self-compacting mortar for sheet piles (price level: 2001)

Component	*Content [kg/m³]*	*Costs [Euro/m³]*
CEM I 52.5 R	358	32
CEM III/A 52.5	555	47
Silica fume	61	30
Sand (0.125-0.5)	549	6
Sand (0.5-1.0)	549	6
Steel fibres (OL13/0.16)	125	282
Superplasticiser	(21)	39
Total water	226	0
w/c-ratio	0.25	*Sum: 442*

The costs of the steel fibres were 64% of the total material costs. However, the price depends on the volume of the delivery and the quality requirements. The superplasticiser was accounted for by its volume to the water content. The average cube strengths (100 mm cubes) were 74.3 MPa (24 hours) and 134.3 MPa (28 days). A slump flow of 718 mm was measured after mixing, while the flow-time T_{50} was 3.2 s. Corresponding tests at the plant of SPANBETON showed that the mixture was reproducible with their own materials, which were from the same producers but from different batches.

10.2.3 Performance of the sheet piles

Six sheet piles were cast; three of them were placed in the ground. Each sheet pile had a length of 12.5 m and about 1 m^3 of concrete was required to fill the mould. The strands were released 24 hours after casting. Tests on the segregation resistance of the mixture were carried out at SPANBETON. It was found that the fibres were homogeneously distributed, even after adjusting the water content in order to minimise air entrapments [Tol, 2002]. Several tests on the performance of the sheet piles in the hardened state were conducted. The following conclusions were drawn:

- The fibres mainly oriented along the flow [Tol, 2002]. This conclusion was drawn from calculations of the shear capacity, which showed that the tensile strength of the mortar (with fibres) in the direction perpendicular to the longest side of the sheet pile was equal to the tensile strength without fibres. Further testing of the segments confirmed the previous conclusion. Especially in the lower flanges the flow distance was rather long (length of sheet pile: 12.5 m). The fibres oriented along the flow in the lower flanges, while their orientation was more random in the upper flange. Tol recommended assuming a tensile strength

equal to that of mortar without fibres in case the principal tensile stress was perpendicular to the direction of the flow.

- The placement of the segments in sand soil took place by vibration. It took 7-15 minutes to place the segments. The process of placement was not adjusted for the decreased thickness of the segments; the connections were hardly damaged [Jansze et al., 2002]
- The performance of the segments in the hardened state was according to the expectations, taking into account the orientation of the steel fibres and their effect on the tensile strength [Tol, 2002].
- In order to gather more experience, the Dutch Ministry of Transport, Public Works and Water Management decided to place a front of 100 m of innovative sheet piles.

10.3 Case study 2: Tunnel segments

10.3.1 Introduction

Tunnel segments often undergo damage in the construction stage. Fibres can avoid spalling of concrete that is caused by tolerance differences and inaccurate placement of the segments. During their service life, tunnel linings might be subjected to a temperature increase caused by a fire load. Fibres are able to prevent the deterioration and spalling of the concrete, which depends on the type and the content of the fibres. Steel fibre reinforced tunnel segments have been successfully applied in several infrastructural projects. In most cases the bar reinforcement could be completely left out, which simplified the production process.

Kooiman [1998b] investigated the effect of the production process on the orientation and the distribution of steel fibres in a tunnel segment. Cylinders were drilled from various positions and in different directions and were tested to determine the splitting tensile strength (deformation-controlled). He found that the upper side of the cylinders in most cases had a lower strength compared with the bottom side, which was a result of bleeding and segregation of the fibres. The position from which a cylinder was drilled and the direction in which it was tested affected the test results. According to Kooiman, vibrating the moulds, the flow and the walls affect the orientation and the distribution of the steel fibres.

10.3.2 Experimental set-up

The case study on SCFRC in tunnel segments [Grünewald et al., 2003] focused on two targets: First, to determine how the flow affects the orientation of the fibres, and second, how the orientation relates to mechanical characteristics of the concrete. This project was carried out in cooperation with partners from the industry, namely: Strukton Group

(a Dutch contractor), Cementbouw (a producer of ready-mix concrete) and Bekaert (a producer of steel fibres). The cylinders were tested at the Delft University of Technology. Two segments were cast with SCFRC and two different types of steel fibres were used (Dramix 80/60 BN; L_f/d_f=80, L_f=60 mm or Dramix 45/30 BN; L_f/d_f=45, L_f=30 mm). Each segment contained 60 kg/m^3 steel fibres. The segments were not vibrated. An optimised, stable mixture from the laboratory study was chosen, Table 10.2 presents the composition of the applied basic mixture.

Table 10.2 Mixture composition of SCFRC for tunnel segments

Mixture composition	*[kg/m^3]*
CEM III 42.5 N	382
Fly ash	179
Sand (0.125-4 mm)	1044
Coarse aggregates (4-16 mm)	489
Water (incl. superplasticiser)	183
Superplasticiser LR	(2.43)
Superplasticiser HR	(1.17)
Steel fibres	60

Production and appearance of the tunnel segments

SCC without fibres was prepared at the ready-mix plant of Cementbouw; the fibres were added manually from paper bags into the inlet gap of the truck mixer. The slump flow of the mixture with Dramix 80/60 BN fibres was 620 mm (Dramix 45/30 BN: 590 mm). Fig. 10.3 shows the casting of a tunnel segment. The moulds were filled within 2 minutes (Dramix 80/60 BN) and 9 minutes (Dramix 45/30 BN) respectively.



Fig. 10.3 Orientation of the pipe during casting and distribution pattern of SCFRC

The segments were demoulded two days after casting, whereas the shields of the moulds were opened at the same day, a few hours after the casting was finished. The details and the lines at the sides of the segments were sharp and the surfaces were smooth (Fig. 10.4).



Fig. 10.4 A tunnel segment fabricated with SCFRC

Especially the bottom sides of both elements were very smooth and had an even colour. The higher casting rate caused an increase of entrapped air, which could be observed on the surface of the hardened cylinders. A circular pattern of air pockets on the upper side of the segment (below the shields) was observed, which was less pronounced for mixture No. 2 (Dramix 80/60 BN). Separation of fly ash of mixture No. 1 (Dramix 45/30 BN) was observed and deviations in colour appeared on the upper side and the sides of this segment, which might be caused by an interaction with formwork oil.

Testing of the cylinders

The thickness of the tunnel segment was 400 mm. The inner length (L) of the tunnel mould at the bottom was 4.23 m; its width (B) was 1.47 m. In total, sixty cylinders were drilled from the segments. This test set-up allowed studying the effect of the flow on the orientation of the fibres. Deformation-controlled splitting tensile tests were carried out and slices were sawn from cylinders in order to take X-ray photographs. The orientation of the fibres was determined and related to the performance of the cylinders (splitting tensile test). Fifteen cylinders (Fig. 10.5) from one half of a tunnel segment were drilled (to determine the splitting tensile strength). Fifteen additional cylinders were drilled point-symmetric to the point of casting to take X-ray photographs of slices. A distance of 150 mm between the wall of the mould and the outer circle of the cylinders was kept in order to minimise the influence of the walls on the fibre orientation.

The effective length of the vertical cylinders (diameter: 144 mm) was about 300 mm; 50 mm at both the top and the bottom of the cylinders were removed to eliminate a possible wall-effect (fibre orientation due to the presence of a wall).

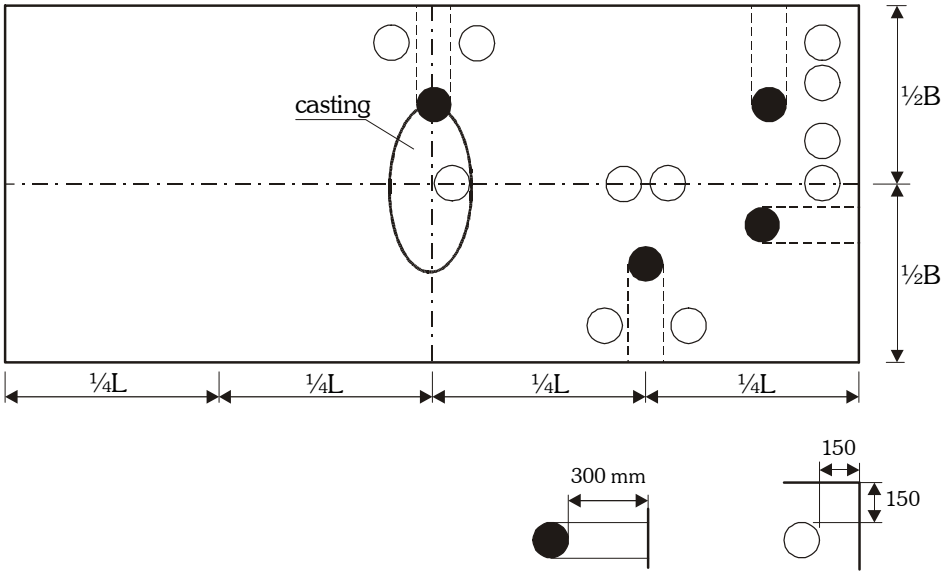


Fig. 10.5 Top view of the segment and location of the first series of cylinders

Two tests were performed: First, deformation-controlled splitting tensile tests were conducted at a deformation rate of 1.0 µm/s (Fig. 10.6). The control signal of the displacement was the average of both LVDTs that were arranged in the centre of the cylinders and at the front- and the back-side. The highest of two defined loads, namely the load when first cracking occurred (a load drop was recorded) and the maximum in the post-cracking region, was used for further analysis and is called the 'splitting tensile strength'.

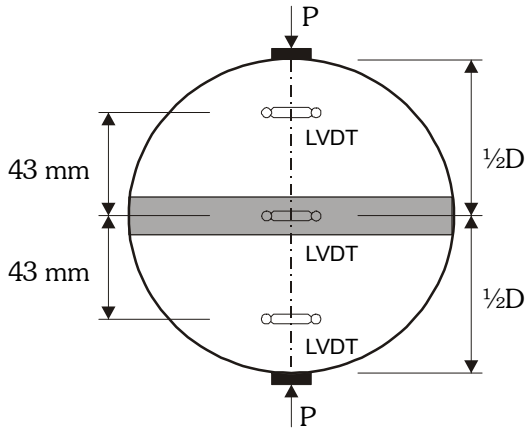


Fig. 10.6 Test set-up of the splitting tensile test and the cutting direction of a slice from a cylinder taken from the opposite half of the segment

Second, fifteen cylinders from the opposite side of the tunnel segment were sawn in slices (thickness: 18 mm), from which X-ray photographs were taken. Since the fibres act especially perpendicular to the plane in which cracking occurs, the slices were taken in this direction (Fig. 10.6). De Keukelaere [1993] described the routine to analyse X-ray photographs. A line of a defined length had to be drawn into the direction under consideration. The number of fibres, which crossed the line of an X-ray photograph,

represents the amount of fibres in the cross-section in a 3D-space. Assuming a constant distribution of the steel fibres throughout the tunnel segment, the orientation number was determined by Equation 7.3.

10.3.3 Characteristics of the cylinders in the hardened state

Table 10.3 shows the mechanical characteristics E-modulus, compressive and splitting tensile strengths of SCFRC at an age of 28 days. These tests were carried out according to the Dutch Standards.

Table 10.3 Mechanical characteristics of SCFRC for tunnel segments (at an age of 28 days)

Mechanical characteristic	E_{fC}	f_{fccm}	$f_{fctm,spl}$
Mixture	*[MPa]*	*[MPa]*	*[MPa]*
No. 1, Dramix 45/30 BN, segment A	39000	66.4	5.7
No. 2, Dramix 80/60 BN, segment B	39200	67.5	5.6

The position of the cylinders and the direction in which they were tested affected the test response. Fig. 10.7 shows the maximum splitting tensile strengths in the middle of the segments (B/2) of both segments and at different distances from the point of casting. The two directions of testing were 'along the flow' and 'perpendicular to the flow', which indicates the orientation of the concrete slices compared with the direction of the flow; the slices were sawn perpendicular to the direction of testing (Fig. 10.6).

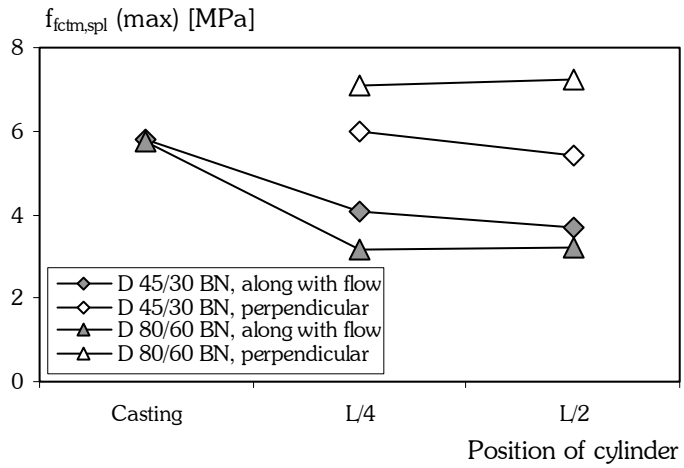


Fig. 10.7 Effect of the flow distance and the test direction on the maximum splitting tensile strength

The cylinders, which contained long fibres (Dramix 80/60 BN), had a lower maximum splitting tensile strength in the direction 'along the flow' compared with those with shorter fibres; the opposite result was obtained in the direction 'perpendicular to the flow'. Table 10.4 summarises the orientation numbers (Equation 7.3) of the cylinders of Fig. 10.7. The orientation numbers significantly differed in both directions; higher orientation numbers were found in the direction 'perpendicular to the flow' compared with 'along the flow', which coincided with higher fibre numbers. The highest

orientation number of 30 mm fibres was found at the point of casting; more fibres might remain in the region around the casting point, which causes the orientation number to increase.

Table 10.4 Orientation numbers of the slices of cylinders (middle of the segment, B/2)

	Dramix 45/30 BN		*Dramix 80/60 BN*	
Position of the cylinders	*Along the flow*	*Perpendicular to the flow*	*Along the flow*	*Perpendicular to the flow*
Casting point	0.84	-	0.71	-
L/4	0.21	0.66	0.28	0.77
L/2	0.28	0.74	0.24	0.91

The fibres were homogeneously distributed over the height of the cylinders; counting the fibres indicated that segregation did not occur (Fig. 10.8 a/b). The X-ray photographs show the difference between two perpendicular directions (at B/2 and L/2: at the end of the mould) of the segment with 60 mm fibres; the cylinders were drilled perpendicular to the upper side of the segments. More than three times more fibres crossed the plane (vertical line) within which the crack appears (Fig. 10.8 b compared with Fig. 10.8 a); consequently the splitting tensile strengths were rather different. The test response depended on the position of the cylinders and on the direction in which they were tested. The range was wider for 60 mm fibres since they are more susceptible to the orientation. The correlation between the maximum splitting tensile strengths and orientation numbers was better for 60 mm fibres; the post-cracking strength was higher at an increasing orientation number.

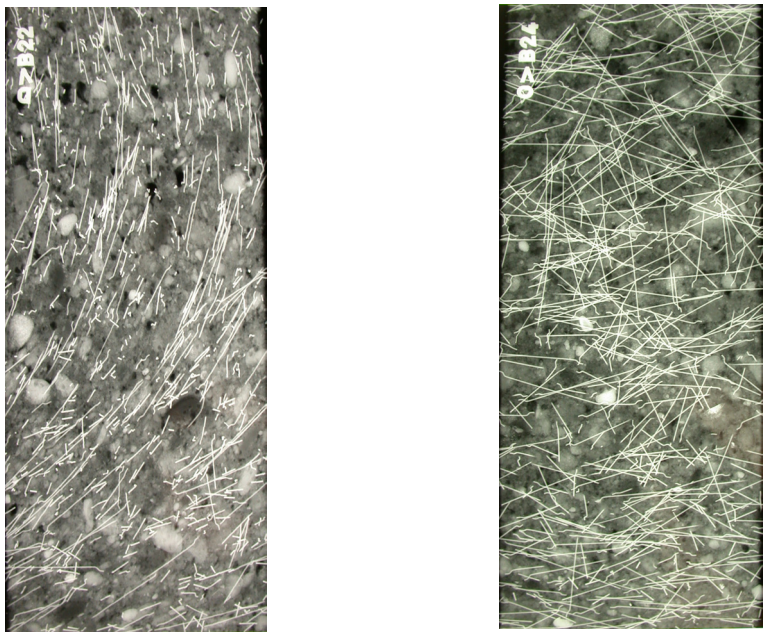


Fig. 10.8 a/b X-ray photographs in the middle of the tunnel segment at L/2 (left: along the flow (η_φ=0.24), right: perpendicular to the flow (η_φ=0.91))

The fibres are most effective in case they are oriented perpendicular to the direction of the splitting test loading. Taking this fact into account, the actual orientation of the steel fibres can be assumed from the direction the load was applied (Fig. 10.6). Fig. 10.7 shows that the orientation of the fibres was rather perpendicular than along the flow. Fig. 10.9 schematically shows the assumed orientation of the steel fibres.

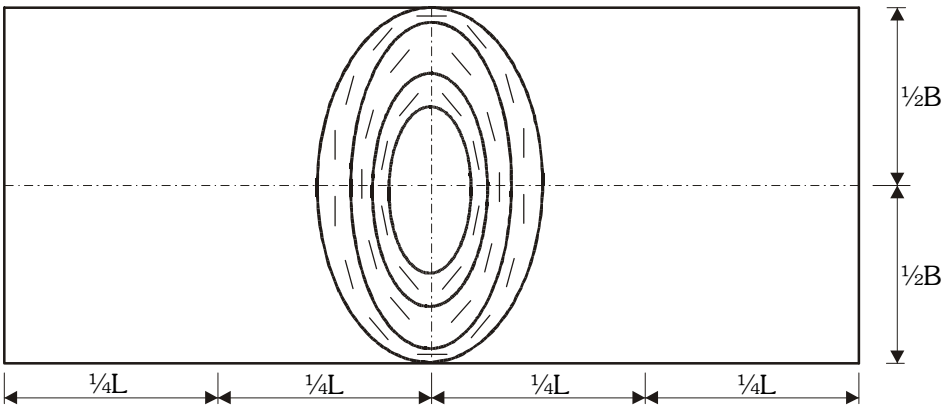


Fig. 10.9 Assumed orientation of the steel fibres after casting

Nemegeer [1999] concluded that steel fibres orient along the flow; a contrary result was found in the study on tunnel segments. The splitting tensile strengths also were about constant at L/4 and L/2, which means that the fibres did not reorient into the direction of the flow.

The reason that the fibres were oriented perpendicular to rather than along the flow was assigned to the production process of the tunnel segments. SCFRC flowed through the pipe of the truck mixer into the mould; the pipe was directed perpendicular to the longer side of the mould (Fig. 10.3). During the flow through the pipe, its walls oriented the fibres. This effect was more pronounced for 60 mm fibres compared with 30 mm fibres. Concrete dropped vertically into the mould and distributed in a circular stream pattern. At the casting point, the maximum splitting tensile strength was slightly higher than the average (Fig. 10.7); the fibres were relatively randomly oriented. The fibres distributed parallel to the flow front. The orientation of the fibres was the same at the end of the mould (L/2) as it was at the end of the pipe. The splitting tensile strengths and orientation numbers were about constant at the flow distances of L/4 and L/2; the fibres did not reorient due to the flow. Walls did not affect the flow in the middle of the segment. The results of tests on cylinders, which were taken close to the walls, indicated that the fibres were rather randomly oriented; the walls reoriented the fibres again. From the previous discussion the following conclusions are drawn: The flow along the walls orients the fibres more than the flow itself; the walls are more effective in orienting the fibres the longer the fibres are. The production process (the application and direction of a pipe) affects the orientation of the fibres, which determines their effectiveness.

The splitting tensile strengths and orientation numbers of SCFRC in tunnel segments varied within a wide range (Figs. 10.10-11), which indicates that the fibres were not randomly oriented in the tunnel segment.

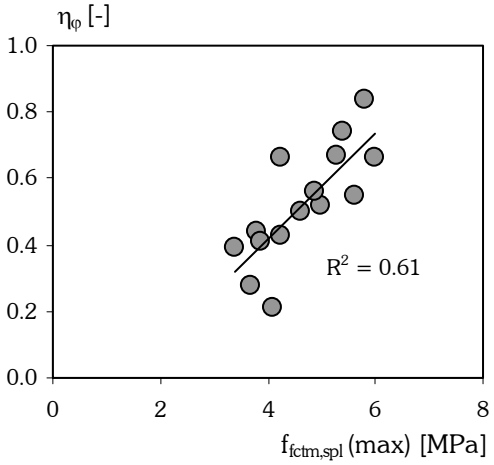


Fig. 10.10 Segment A: Splitting tensile strengths versus orientation numbers (Dramix 45/30 BN)

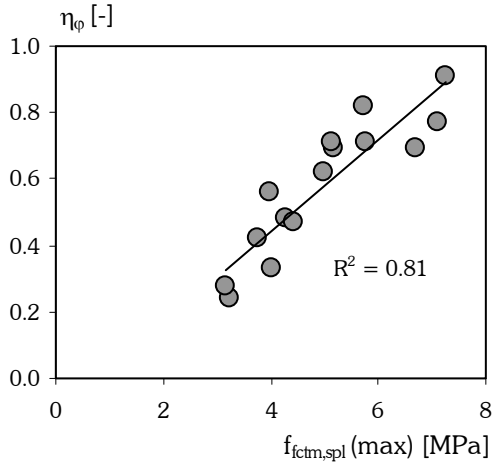


Fig. 10.11 Segment B: Splitting tensile strengths versus orientation numbers (Dramix 80/60 BN)

10.4 Case study 3: Large beams

10.4.1 Experimental set-up

An image analysis of cross-sections of small beams (Chapter 8.3) indicated that fibres orient the more the longer they are. The walls of the mould might cause this difference. The study on large beams aimed at investigating the effect of the flow and the fibre length on the orientation of the fibres. Two beams having a length of 3.7 m, a height of 0.5 m and a width of 0.2 m were cast. Two different types of steel fibres were applied: a 30 mm fibre (Dramix 45/30 BN) and a 50 mm fibre (Dramix 45/50 BN), which had the same aspect ratio (L_f/d_f); the fibre content of each beam was 50 kg/m^3. Both fibre types are expected to have a comparable effect on the behaviour of SCC in the fresh state. Fig. 10.12 shows the position of various cross-sections of the beam; the test set-up of both beams was the same. No bar reinforcement was arranged in the mould.

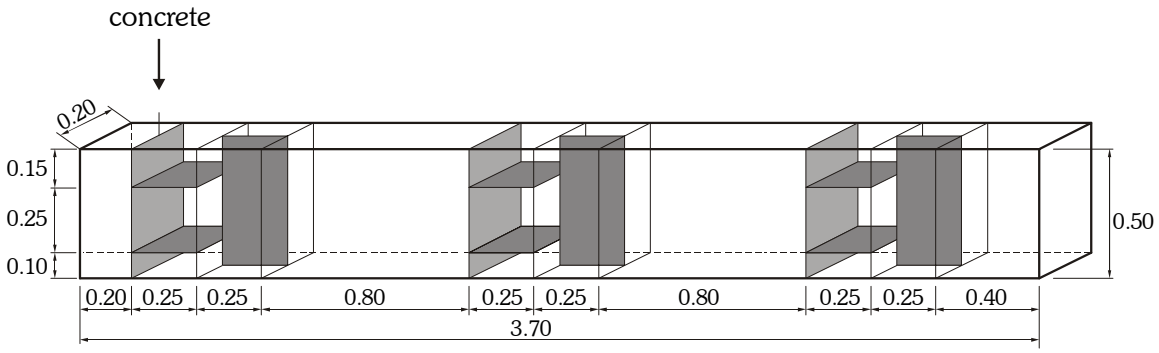


Fig. 10.12 Test set-up: different directions and positions of the cross-sections

Several cross-sections in different directions and at various distances from the point of casting were sawn in order to determine the average fibre orientation. SCC was delivered from a ready-mix plant; the fibres were added from paper bags into the inlet gap of the truck mixer. The concrete was poured at one end of the beam by a skip and was allowed to flow through the entire formwork.

Digital photographs were taken from the cross-sections using a flashlight camera. The procedure to analyse the pictures and to determine the orientation number by an image analysis is described in Chapter 8.3. Some cross-sections had a height of 500 mm and not all fibres reflected the light of the camera. Still, the number of fibres within the analysed area was sufficiently high to be representative for the complete cross-section. The higher the orientation number (the average length of the fibres cross-sections in a plane decreases) the more the fibres are oriented perpendicular to the plane under consideration. An overall low but constant orientation number in different directions indicates a random fibre orientation.

10.4.2 Orientation of the fibres due to the flow

Figs. 10.13-15 present the orientation numbers of twenty-four cross-sections in three different directions. These three directions are 'parallel to the wall' (along with the flow), 'parallel to the bottom of the mould' and 'perpendicular to the flow'.

Planes parallel to the wall (along the flow)

The orientation numbers of planes parallel to the wall decreased at increasing distance from the point of casting; the fibres rotate into the plane parallel to the wall of the mould (Fig. 10.13).

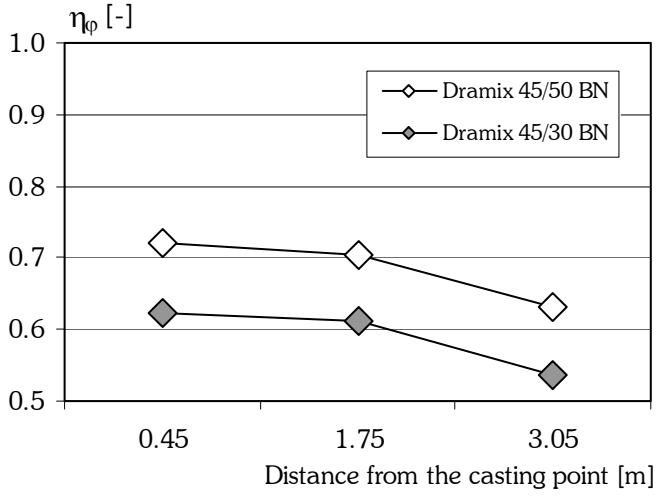


Fig. 10.13 Orientation number of cross-sections parallel to the walls

The orientation number of cross-sections with 30 mm fibres (Dramix 45/30 BN) was lower at the casting point compared with 50 mm fibres, which is not the result of the

flow. The orientation numbers of both fibre types undergo exactly the same decrease at increasing flow distance. The effect of the walls seems to be independent of the fibre length. The distance of the slices from the wall was 100 mm (at least two times the fibre length). The continuing orientation of the fibres indicates that the influence area of a wall extends over more than one times the fibre length. At a flow distance of 3.05 m the lowest orientation numbers of all cross-sections for both fibre types were found.

Planes parallel to the bottom of the mould

Due to the wall-effect of the bottom of the mould, the fibres in the lower planes were less oriented perpendicular to the bottom of the mould. Each orientation number of these planes was lower compared with the upper plane. Different tendencies for both fibre types were found for planes parallel to the bottom of the mould at increasing flow distance (Fig. 10.14). 50 mm fibres oriented parallel to the bottom of the mould, whereas the orientation number of the 30 mm fibres was almost constant along the flow; even a slight increase can be observed.

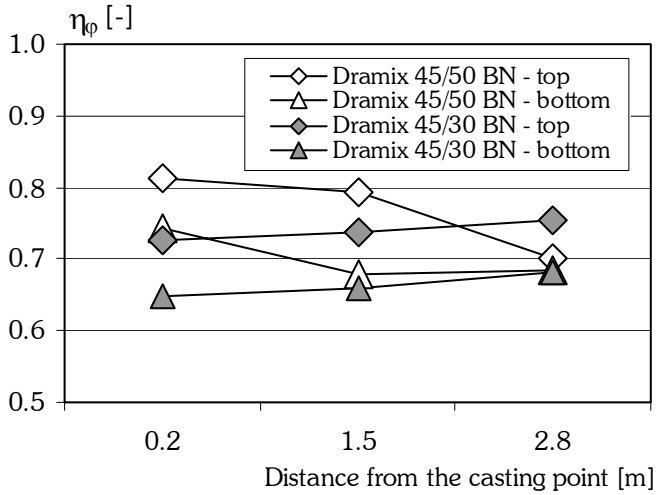


Fig. 10.14 Orientation number of cross-sections parallel to the bottom of the mould

Planes perpendicular to the flow

Long steel fibres (50 mm) did orient parallel to the wall and from the vertical direction into the horizontal plane. Consequently, they align into the direction of the flow, which is the remaining dimension. Short fibres (30 mm) only oriented into the plane along the wall; the alignment into the direction of the flow is therefore less pronounced. Fig. 10.15 reflects the results of Figs. 10.13-14. At increasing flow distance both fibre types aligned into the direction of the flow; the effect was more pronounced for 50 mm fibres. Short steel fibres were more randomly oriented even at an increasing flow distance.

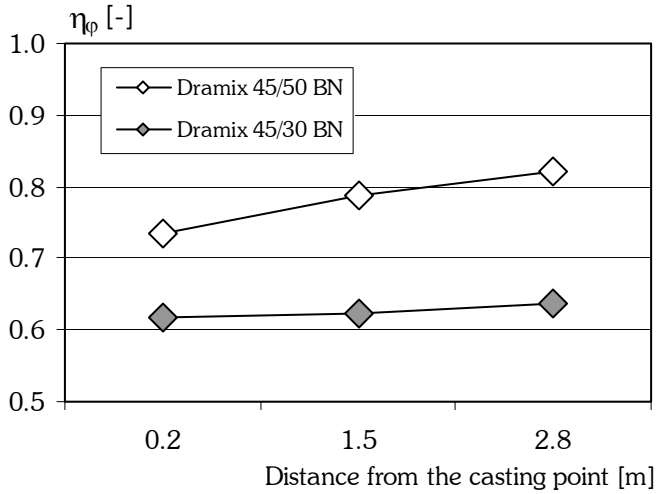


Fig. 10.15 Orientation number of cross-sections perpendicular to the flow

10.5 How the flow orients the fibres

Several case studies were carried out to determine the effect of the flow on the orientation of fibres: sheet piles, tunnel segments and small (Chapter 8.3) and large beams. The efficiency of a single fibre, the performance of SCFRC and the variation of characteristics in the hardened state depend on the orientation and the distribution of the fibres.

Composing SCFRC with segregation resistance and passing ability assures an initial homogeneous distribution of the fibres. Stability rather than passing ability was the design criterion on SCFRC for these case studies; the exception was the mixture for sheet piles, which had to fulfil both criteria. Once SCFRC is stable, the effect of the flow on the orientation can be studied. Walls have a significant effect over a distance larger than the fibre length. Walls always have to be considered, since concrete needs to be cast in a mould. This is especially important in case of small specimens (e.g. beams for bending tests).

However, the shovel, the flow through the mould, clustering of fibres and the direction with which a pipe, a shovel or a bucket is oriented, already influences the fibres' orientation in the mould. It is difficult to cast SCFRC without a preorientation of the fibres. From the case studies on SCFRC the following conclusions are drawn:

- In order to obtain reproducible results exactly the same production method has to be followed. To interpret a test result it should be linked with an orientation number and the number of fibres. The knowledge about how fibres orient allows adequate dimensioning of structural elements at positions where the fibres are not preferably oriented.

- The flow along the walls causes fibres to orient more than the flow itself does. Due to the casting the fibres already might be preoriented.
- The casting method can be a tool to preorient fibres or to obtain an orientation as random as possible. Due to the wall-effect, the geometry of a mould also determines the efficiency of the fibres; this effect can be increased by arranging additional walls or decreased by cutting a specimen from a larger element.

10.6 Concluding remarks

Three case studies on SCFRC were presented in this chapter: sheet piles, tunnel segments and large beams. The focus was on the orientation of the steel fibres; the effect of various parameters was discussed. Different techniques were applied to quantify 'orientation'. SCFRC was found to be an inhomogeneous material; the fibres are rarely randomly oriented. The preferred orientation of the fibres can be considered as a benefit or, the opposite as an intrinsic weakness of SCFRC. However, the orientation of fibres in stiff SFRC also might differ from the random orientation, since it has to be vibrated. Applying stable SCFRC counteracts the segregation of the fibres. The studies on sheet piles and tunnel segments demonstrated that applications with SCFRC can be economical, offer products with interesting characteristics and present innovative solutions. The production process is an important factor, which affects the performance of SCFRC.

Chapter 11:

Conclusions and future perspectives

11.1 Conclusions

SCFRC is an innovative type of concrete, which combines the advantages and extends the possibilities of both SCC and FRC. This thesis summarises various studies on the characteristics of SCFRC in the fresh and the hardened state. It contains models that predict the performance of a wide range of mixture compositions and offer design tools that decrease the number of laboratory experiments required to obtain an optimised SCFRC. The thesis consists of three distinguished parts:

First (Chapters 2-6), three experimental parameter studies were carried out to determine the effect of the addition of the steel fibres on the characteristics of SCC in the fresh state. Optimised SCFRC mixtures were tested, which were based on SCC mixtures without fibres. The applied contents of the steel fibres were chosen close to the maximum fibre content, which was determined by varying the fibre content in defined steps. Additionally, studies were performed on the characteristics of the components of SCFRC e.g. the granular skeleton and the paste. The 'Compressible Packing Model' was applied to calculate the packing density of the granular skeleton; the required input parameters were experimentally determined. Models, which are based on experimental results, were developed to predict the performance of SCFRC in the fresh state. The models consider two key characteristics of SCFRC: filling ability and passing ability.

Second (Chapters 7-9), attention was given to the behaviour of SCFRC in the hardened state. Three-point bending tests with optimised SCFRC, single fibre pull-out tests and an image analysis were carried out to characterise SCFRC in the hardened state and to demonstrate how SCFRC differs from conventional SFRC. A combined stress-strain/stress-crack width relation for SCFRC in tension was developed from an inverse analysis on the bending tests. It takes into account the characteristics and the mixture composition of SCFRC. The accuracy of the predictions is in average 5-8%, depending on the applied casting procedure.

Finally (Chapter 10), three case studies on sheet piles, tunnel segments and large beams indicated how the production process and the flow affect the performance of SCFRC.

From the experimental parameter studies and the analyses of the results the following conclusions are drawn:

SCFRC in the fresh state

- The addition of the steel fibres to a SCC affects the structure of the granular skeleton. The packing density decreases so a higher content of finer grains is required to compensate for it. The effect of the steel fibres is incorporated in the 'Compressible Packing Model' that predicts the packing density.

- The concepts of the relative layer thickness and the normalised solid content to characterise a SCC mixture describe the same characteristic of the granular skeleton. No general relation, which allows predicting the slump flow, was found between these parameters for paste and aggregates. The mini-slump flow test should be applied to characterise the cement paste.

- The applicable range of mixture compositions and characteristics in the fresh state of SCC containing a high fibre content (close to the maximum fibre content) is relatively small when compared with SCC. The principles to design SCFRC are discussed in this thesis.

- Steel fibres affect the key characteristics of SCC. Design principles and methods to determine whether a SCFRC mixture is self-compacting or not are proposed. The content and the distribution of the aggregates as well as the fibre type determine the bar spacing required for non-blocking; to predict the maximum fibre content the fibre content also has to be considered.

SCFRC in the hardened state

- The performance of SCFRC depends on the direction in which a specimen is tested. A comparison of the bending behaviour of SCFRC and SFRC indicated that SCFRC has a better performance and a lower variation. The variation depends on the production process and the segregation resistance of SCFRC. The fibres are more oriented due to the walls of the mould and the flow when compared with SFRC.

- Case studies on SCFRC showed that the production process significantly affects the orientation of the fibres. The flow of SCFRC, once understood, is an effective tool to improve the efficiency of the fibres. The flow along walls orients the fibres more than the flow without any obstruction. Often, the fibres in SCFRC are not randomly oriented.

- The anchorage capacity of single fibres in SCC improved compared with conventional concrete; the degree of it depended on the strength class.

- An inverse analysis with the multi-layer procedure was conducted to model the tensile behaviour of SCFRC. Linear-elastic pre-peak behaviour combined with a post-peak stress-crack width relation was not sufficiently accurate to recalculate the bending tests. The predictions are improved by adding a non-linear pre-peak behaviour to the tensile model, thus introducing the effect of micro-cracking and fibre-bridging in the pre-peak stage.

11.2 Future perspectives

The application of SCC facilitates the production process and its conditions, since vibration is eliminated. The benefits of SCC also apply for SCFRC in case the effect of the fibres on the key characteristics filling ability, passing ability and segregation resistance is taken into account.

The segregation of the fibres has to be counteracted; a stable SCC without fibres does not guarantee a homogeneous fibre distribution in all cases. To stabilise SCFRC, viscosity agents might be applied either to enhance the segregation resistance of the 'powder-type SCFRC' or to design a 'viscosity-agent type SCFRC'. Few tests have been performed with these types of SCFRC. This study mainly focused on steel fibres; other types like plastic, glass or carbon fibres might be added to SCC.

The flow of SCFRC affects the orientation of the fibres, which is an advantage and a disadvantage at the same time. The production method becomes a design tool for SCFRC to improve the efficiency of the fibres and to control their orientation. To exploit the full potential of SCFRC, the orientation has to be quantified. It is important for standardisation and modelling of SCFRC and flowable SFRC to take this fact into account. Few studies have been performed on how the flow and the production method affect the orientation and on how the results relates to the performance of a structural element. The orientation of the fibres also might affect rheological measurements of e.g. the BML-viscometer. The repeatability with which specimens for standard tests are produced affects the variation of the results. Detailed descriptions of the casting procedures are required in order to obtain comparable results. A better understanding of how the fibres distribute and orient provides the basis for more economical fibre reinforced concretes. The method to determine the orientation and the distribution of the fibres needs to be quicker and less cost intensive to become an additional tool for the design of fibre reinforced concrete.

The price of SCFRC can be much higher compared with conventional concrete. Self-compactability improves the performance of Ultra-High-Strength FCR, since the plastic viscosity significantly increases due to the addition of the fibres and a very low water-to-cement ratio, which makes it difficult to compact. In various cases, the bar reinforcement can be partially or completely replaced by the fibres. Economically competitive solutions with SCFRC require the optimisation of aspects like the shape of structural elements, the production process, the storage and the transport. The production of structural elements often requires testing on full-scale, which increases the costs. Higher demands on working conditions, intensified research and an increasing number of applications will promote SCFRC.

References

Aarre, T. (1992): Tensile characteristics of FRC with special emphasis on its applicability in a continuous pavement, PhD-thesis, Department of Structural Engineering, Technical University of Denmark, Lyngby.

ACI 544 (1993): Guide for Specifying, Proportioning, Mixing, Placing, and Finishing Steel Fiber Reinforced Concrete, ACI Committee 544, ACI Materials Journal, Vol. 90, No. 1, Jan.-Feb. 1993, pp. 94-101.

Alwan, J.M., Naaman, A.E., Guerrero, P. (1999): Effect of mechanical damping on the pullout response of hooked steel fibres embedded in cementitious matrices, Concrete Science and Engineering, Vol. 1, March 1999, pp. 15-25.

Ambroise, J., Rols, S. Pera, J. (1999): Properties of self-levelling concrete reinforced by steel fibres, High Performance Fiber Reinforced Cement Composites (HPFRCC 3), Mainz, RILEM publications PRO 6, Cachan, pp. 9-17.

Ando, T., Sakai, H., Takahashi, K., Hoshjima, T., Awata, M., Oka, S. (1990): Fabrication and properties for a new carbon fibre reinforced cement product, Thin-Section Fiber Reinforced Concrete and Ferrocement, American Concrete Institute Special, Publication SP-124, pp. 39-60.

ASTM (1998): The American Society for Testing and Materials - ASTM C1018-97, Standard Test Method for Flexural Toughness and First Crack Strength of Fibre Reinforced Concrete (Using Beam with Third-Point Loading), ASTM Annual Book of Standards, Vol. 01.02, 1998, pp. 506-513.

Bartos, P.J.M., Hoy, C.W. (1996): Interaction of particles in fibre reinforced concrete, Production Methods and Workability of Concrete, Edited by Bartos, Marrs and Cleland, E&FN Spon, London, pp. 451-461.

Bartos, P.J.M., Sonebi, M., Tamimi, A. K. (2000): Workability and Rheology of Fresh Concrete: Compendium of Tests, Report of Technical Committee TC 145 WSM, Workability of Special Concrete Mixes, RILEM publications, Report 24, Cachan.

Bažant, Z.P., Oh, B.H. (1983): Crack band theory or fracture of concrete, Materials and Structures, Vol. 16, pp. 155-177.

Beaupré, D. (1994): Rheology of High Performance Shotcrete, PhD-thesis, The University of British Columbia.

Ben-Aïm, R. (1970): Etude de la texture des empilements de grains. Application à la detérmination de la perméabilité des mélanges binaries en régime moléculaire, intermédiaire, laminaire, Thèse d'Etat de L'Université de Nancy (in French).

Bennenk, H.W. (2000): Zelfverdichtend beton in de prefab-betonindustrie, Cement, No. 3, pp. 78-81 (in Dutch).

Bennenk, H.W. (2001): SCC as applied in the Dutch precast concrete industry, Second Int. Symposium on SCC, 2001, Edited by Ozawa and Ouchi, University of Tokyo, COMS Engineering Publication, pp. 625-632.

Billberg, P. (1999): Fine mortar rheology in mix design of SCC, First Int. Symposium on SCC, Stockholm, Edited by Skarendahl and Petersson, RILEM publications PRO 7, Cachan, pp. 47-58

Billberg, P. (2003): Form pressure generated by self-compacting concrete, Third Int. Symposium of SCC, Reykjavik, Edited by Wallevik and Níelsson, RILEM publications PRO 33, Bagneux, pp. 271-280.

BS 812: Part 2 (1975): Methods for testing aggregate, British Standards Institute, London.

Bui, V.K. (1994): A Method for the Optimum Proportioning of the Aggregate Phase of Highly Durable Vibration-Free Concrete, Master thesis, Asian Institute of Technology, Bangkok.

Buitelaar, P. (2002): Ultra Thin Heavy Reinforced High Performance Concrete Overlays, Sixth Int. Symposium on High Strength/High Performance Concrete, Edited by König, Dehn and Faust, Leipzig, pp. 1577-1590.

CEB-fib Model Code (1990): Thomas Telford Services Ltd., London.

Clayton, N., Lennon, T. (2000): High-grade concrete columns in fires, Concrete, March, p. 51.

Cumberland, D.J., Crawford, R.J. (1987): The Packing of Particles, Elsevier Science Publishers, Amsterdam.

CUR-Recommendation 35 (1994): Bepaling van de buigtreksterkte, de buigtaaiheid en de equivalente buigtreksterkte van staalvezelbeton, CUR Gouda (in Dutch).

CUR-Recommendation 70 (1999): Toepassing van vliegas in mortel en beton, CUR Gouda (in Dutch).

CUR-Recommendation 93 (2002): Zelfverdichtend beton, CUR Gouda (in Dutch).

DBV (2001): Deutscher Beton- und Bautechnik-Verein E.V., DBV-Merkblatt Stahlfaserbeton, Fassung Oktober 2001(in German).

De Jong, A. (1998): Hoogvloeibaar beton, Cement, No. 5, pp. 16-20 (in Dutch).

De Keukelaere, G. (1993): Studie van de vezelverdeling en de invloed ervan op de mechanische eigenschappen van staalvezelbeton, Master thesis, Laboratory Magnel of Reinforced Concrete, University of Ghent (in Dutch).

De Larrard, F. (1999): Concrete Mixture Proportioning - a scientific approach, E&FN Spon, London, ISBN: 0419235000.

De Larrard, F., Ferraris, C.F., Sedran, T. (1998): Fresh concrete: A Herschel-Bulkley material, Materials and Structures, Vol. 31, 8/9, pp. 494-498.

De Larrard, F., Sedran, T. (1994): Optimization of Ultra-High-Performance Concrete by the use of a packing model, Cement and Concrete Research, Vol. 24, No. 6, pp. 997-1009.

Edgington, J., Hannant, D.J., Williams, R.I.T. (1978): Steel fibre reinforced concrete, Fibre reinforced materials, The Construction Press, Lancaster, England, pp. 112-128.

EFNARC (2001): Specification and Guidelines for Self-Compacting Concrete, November 2001, Hampshire, www.efnarc.org.

Emborg, M., Grünewald, S., Hedin, C., Carlswärd, J. (2003): Test methods for filling ability of SCC, Third Int. Symposium of SCC, Reykjavik, Edited by Wallevik and Níelsson, RILEM publications PRO 33, Bagneux, pp. 323-334.

German, R.M. (1989): Particle Packing Characteristics, Metal Powder Industries Federation, ISBN: 0918404835.

Gettu, R., Barragán, B.E. (2003): Direct Tension Test and Interpretation, Test and Design Methods for Steel Fibre Reinforced Concrete - Background and Experiences, Edited by Schnütgen and Vandewalle, RILEM publication PRO 31, Bagneux, pp. 15-30.

Glavind, M. (1992): Evaluation of the Compressive Behaviour of Fibre Reinforced High Strength Concrete, PhD-thesis, Department of Structural Engineering, Technical University of Denmark, Lyngby.

Gopalaratnam, V.S., Shah, S.P. (1986): Strength, deformation and fracture toughness of fiber cement composites at different rates of flexural loading, Steel Fiber Concrete, US-Sweden Joint Seminar, Stockholm, Edited by Shah and Skarendahl, Elsevier Applied Science Publishers, New York, pp. 299-332.

Gray, W.A. (1968): The Packing of Solid Particles, Chapman and Hall, London.

Groth, P. (1996): Cracking in concrete - crack prevention with air-cooling and crack distribution with steel fibre reinforcement, Licentiate thesis, Luleå University of Technology.

Groth, P. (2000a): Fibre reinforced concrete - Fracture mechanics methods applied on self-compacting concrete and energetically modified binders, PhD-thesis, Department of Civil and Mining Engineering, Luleå University of Technology.

Groth, P. (2000b): Steel Fibre Reinforced SCC, Final report of task 6, Brite Euram project (BE 96-3801) - Rational production and improved working environment through using SCC, Doc. No.: RT6-v1.doc.

Groth, P., Nemegeer, D. (1999): The use of steel fibres in self-compacting concrete, First Int. Symposium on SCC, Stockholm, Edited by Skarendahl and Petersson, RILEM publications PRO 7, Cachan, pp. 497-508.

Grünewald, S., Bolo, T., Van der Veen, C., Walraven, J.C. (2002): Performance-based design of a high strength self-compacting fibre reinforced mortar, Stevin-report 25.5-01-30, Department of Structural and Building Engineering, Delft University of Technology.

Grünewald, S., Walraven, J.C (2002a): Self-compacting fibre reinforced concrete - orientation and distribution of steel fibres in beams, Stevin-report No. 25.5-02-33, Department of Structural and Building Engineering, Delft University of Technology.

Grünewald, S., Walraven, J.C (2002b): Tailoring self-compacting fibre reinforced concrete - Mechanical characteristics, Stevin-report 25.5-02-03, Department of Structural and Building Engineering, Delft University of Technology.

Grünewald, S., Walraven, J.C. (2000): Self-compacting fiber reinforced concrete - Test methods and properties of the fresh state, Ibausil, 14. Int. Baustofftagung, Weimar, pp. 51-66.

Grünewald, S., Walraven, J.C. (2001a): Maximum content of steel fibres in self-compacting concrete, Second Int. Symposium on SCC, 2001, Edited by Ozawa and Ouchi, University of Tokyo, COMS Engineering Publication, pp. 137-146.

Grünewald, S., Walraven, J.C. (2001b): Rheological study on the workability of fibre-reinforced mortar, Second Int. Symposium on SCC, Edited by Ozawa and Ouchi, University of Tokyo, COMS Engineering Publication, pp. 127-136.

Grünewald, S., Walraven, J.C. (2001c): Stahlfaserbeton mit selbstverdichtenden Eigenschaften, Innovationen im Bauwesen, Tagung Leipzig (Selbstverdichtender Beton), Edited by König, Holschemacher and Dehn, Bauwerk Verlag, pp. 95-108 (in German).

Grünewald, S., Walraven, J.C. (2003): Rheological measurements on self-compacting fibre reinforced concrete, Third Int. Symposium of SCC, Reykjavik, Edited by Wallevik and Níelsson, RILEM publications, PRO 33, Bagneux, pp. 49-58.

Grünewald, S., Walraven, J.C. (2004): Characterisation of cement paste for self-compacting concrete, 5th International PhD conference Delft, A.A. Balkema Publishers, Rotterdam (to be published).

Grünewald, S., Walraven, J.C., Obladen, B., Zegwaard, J.W., Langbroek, M., Nemegeer, D. (2003): Tunnel segments of self-compacting steel fibre reinforced concrete, Third Int. Symposium on SCC, Reykjavik, Edited by Wallevik and Níelsson, RILEM publications, PRO 33, Bagneux, pp. 715-724.

Hartwich, K. (1986): Zum Riss- und Verformungsverhalten von stahlfaserverstärkten Stahlbetonstäben unter Längszug, PhD-thesis, TU Braunschweig (in German).

Hertel, C., Orgass, M., Dehn, F. (2002): Brandschutztechnische Aspekte bei Faserbetonen, Faserbeton, Innovation im Bauwesen, Bauwerk-Verlag, Berlin, pp. 63-76 (in German).

Hillerborg, A. (1986): Determination and significance of the fracture toughness of steel fibre concrete, Steel Fiber Concrete, US-Sweden Joint Seminar, Stockholm, Edited by Shah and Skarendahl, Elsevier Applied Science Publishers, New York, pp. 257-272.

Hillerborg, A., Modéer, M., Petersson, P.E. (1976): Analysis of crack formation and crack growth in concrete by means of fracture mechanics and finite elements, Cement and Concrete Research, 6, pp. 773-782.

Hordijk, D. (1991): Local approach to fatigue of concrete, PhD-thesis, Department of Structural and Building Engineering, Delft University of Technology.

Hoy, C.W. (1998): Mixing and Mix Proportioning of Fibre Reinforced Concrete, PhD-thesis, Advanced Concrete and Masonry Centre, University of Paisley.

Jansze, W., Peters, M., Van der Veen, C. (2002): Application of High Strength Fibre Reinforced Self Compacting Concrete in Prefabricated Prestressed Concrete Sheet Piles, Proceedings of the First fib Congress, Osaka Japan, Vol. 2, pp. 5-6.

JCI (1984): Japanese Concrete Institute - JCI Standards for Test Methods of Fibre Reinforced Concrete, pp. 57-59 and 65-68.

Johnston, C.D. (1996): Proportioning, mixing and placement of fibre-reinforced cements and concretes, Production Methods and Workability of Concrete, Edited by Bartos, Marrs and Cleland, E&FN Spon, London, pp. 155-179.

Johnston, C.D. (2001): Fiber-Reinforced Cements and Concretes, Gordon and Breach Science Publishers, Amsterdam, ISBN: 9056996940.

Kameswara Rao, C.V.S. (1979): Effectiveness of random fibres in composites, Cement and Concrete Research, 9, 1979, pp. 685-693.

Kennedy, C.T. (1940): The Design of Concrete Mixtures, Proceeding ACI, 36, pp. 373-400.

Khayat, K.H., Roussel, Y. (1999): Testing and performance of fiber-reinforced self-consolidating concrete, First Int. Symposium on SCC, Stockholm, Edited by Skarendahl and Petersson, RILEM publications PRO 7, Cachan, pp. 509-521.

König, G., Kützing, L. (1999): Modelling the increase of ductility of HPC under compressive forces - a fracture mechanical approach, Proceedings of the Third International RILEM Workshop 'High Performance Fibre Reinforced Cementitious Composites' (HPFRCC 3), Mainz, 1999, pp. 251-260.

Kooiman, A.G. (1996): Staalvezelbeton in de linings van boortunnels, een state-of-the-art, Stevin-report 25.5-96-10, Department of Structural and Building Engineering, Delft University of Technology (in Dutch).

Kooiman, A.G. (1998a): Schaaleffecten in het nascheurgedrag van staalvezelbeton, Stevin-report 25.5-98-9, Department of Structural and Building Engineering, Delft University of Technology (in Dutch).

Kooiman, A.G. (1998b): Staalvezelbeton in de Tweede Heinenoord Tunnel - voorkeursoriëntatie t.g.v. productieproces, Stevin-report 25.5-98-03, Department of Structural and Building Engineering, Delft University of Technology (in Dutch).

Kooiman, A.G. (2000): Modelling Steel Fibre Reinforced Concrete for Structural Design, PhD-thesis, Department of Structural and Building Engineering, Delft University of Technology.

Körmeling, H.A. (1986): Strain rate and temperature behaviour of steel fibre concrete in tension, PhD-thesis, Department of Structural and Building Engineering, Delft University of Technology.

Krell, J. (1985): Die Konsistenz von Zementleim, Mörtel, und Beton und ihre zeitliche Veränderung, PhD-thesis, Faculty of Civil Engineering, Rheinisch-Westfälische Technische Hochschule Aachen (in German).

Krenchel, H. (1975): Fibre Spacing and Specific Fibre Surface, Fibre Reinforced Cement and Concrete, Edited by Neville, The Construction Press, UK, pp. 69-79.

Kützing, L. (2000): Tragfähigkeitsermittlung stahlfaserverstärkter Betone, PhD-thesis, University of Leipzig, Teubner Verlag, Stuttgart (in German), ISBN: 3519052679.

Linsel, S., Dehn, F. (2002): Determination of fibre distribution in self-compacting steel fibre concrete (SCSFC) by computer tomography (CT), Sixth Int. Symposium on High Strength/High Performance Concrete, Edited by König, Dehn and Faust, University of Leipzig, pp. 1129-1137.

Maeyama, A., Maruyama, K., Midorikawa, T., Sakata, N. (1998): Characterization of Powder for Self-Compacting Concrete, Second Int. Workshop on SCC, Kochi, Edited by Ozawa and Ouchi, Concrete Engineering Series, No. 30, Japan Society of Civil Engineers, pp. 191-200.

Maidl, B.R. (1995): Steel Fibre Reinforced Concrete, Ernst & Sohn, Berlin, ISBN: 3433012881.

Markeset, G. (1993): Failure of concrete under compressive strain gradients, PhD-thesis, Norwegian Institute of Technology, Trondheim.

Markovic, I., Grünewald, S., Walraven, J.C., Van Mier, J.G.M. (2002): Characterization of bond between steel fibres and concrete - conventional fibre reinforced versus self-compacting fibre reinforced concrete, Bond in Concrete - from research to standards, Third Int. Symposium, Budapest, Publishing Company of Budapest University of Technology, pp. 520-528.

Markovic, I., Walraven, J.C., Van Mier, J.G.M. (2003): Development of High Performance Hybrid Fibre Concrete, High Performance Fiber Reinforced Cement Composites (HPFRCC 4), Ann Arbor, RILEM publications PRO 30, Bagneux, pp. 277-300.

Midorikawa, T., Pelova, G.I., Walraven, J.C. (2001): Application of "The Water-layer Model" to self-compacting mortar with different size distribution of fine aggregate, Second Int. Symposium on SCC, 2001, Edited by Ozawa and Ouchi, University of Tokyo, COMS Engineering Publication, pp. 237-246.

Milewski, J.V. (1973): A study of the packing of fibres and spheres, PhD-thesis, Rutgers University, New Jersey.

Naaman, A.E. (1999): Fibres with slip hardening bond, Proceedings of the Third Int. RILEM Workshop 'High Performance Fibre Reinforced Cementitious Composites' (HPFRCC 3), Mainz, RILEM proceedings PRO 6, Cachan, pp. 371-386.

Narayanan, R., Kareem-Palanjian, A.S. (1982): Factors influencing the workability of steel-fibre reinforced concrete, Concrete, Part 1: Vol.16, No. 10, pp.45-48, Part 2: Vol. 17, No. 2, pp. 43-44.

Nemegeer, D. (1999): Zelfverdichtend Staalvezelbeton, Proceedings Constructeursmiddag Betonvereniging, Ede, The Netherlands (in Dutch).

Nemegeer, D. (2001): J-ring als testmethode voor staalvezels in zelfverdichtend beton, Cement 2001, No. 1, pp. 92-93 (in Dutch).

Nemegeer, D., Vanbrabant, J., Stang, H. (2003): Brite Euram Program on Steel Fibre Concrete, Subtask Durability: Corrosion Resistance of Cracked Fibre Reinforced Concrete, Test and Design Methods for Steel Fibre reinforced Concrete - Background and Experiences, Edited by Schnütgen and Vandewalle, RILEM publication PRO 31, Bagneux, pp. 47-66.

NEN 5961 (1988): Determination of the air content of fresh concrete (displacement method), Concrete, Nederlands Normalisatie Instituut (in Dutch).

NEN 5968 (1988): Determination of the compressive strength of test specimens, concrete and mortar, Nederlands Normalisatie Instituut (in Dutch).

NEN 5969 (1988): Determination of the tensile splitting strength of test specimens, concrete and mortar, Nederlands Normalisatie Instituut (in Dutch).

NEN 6720 (1995): Voorschriften Beton, Constructieve eisen en rekenmethoden, VBC 1995, Nederlands Normalisatie Instituut (in Dutch).

Níelsson, I., Wallevik, O.H. (2003): Rheological evaluation of some empirical test methods, preliminary results, Third Int. Symposium of SCC, Reykjavik, Edited by Wallevik and Níelsson, RILEM publications PRO 33, Bagneux, pp. 59-68.

Obladen, B. (2002): Ervaringen met zelfverdichtend beton, Infrastructuur voor het kerntraject van de Zuidtangent (4), Cement, No. 8, pp. 70-75 (in Dutch).

Oh, S.G., Noguchi, T., Tomosawa, F. (1999): Towards mix design for rheology of self-compacting concrete, First Int. Symposium on SCC, Stockholm, Edited by Skarendahl and Petersson, RILEM publications PRO 7, Cachan, pp. 361-372.

Okamura, H., Maekawa, K., Ozawa, K. (1993): High Performance Concrete, Gihodo Publishing (in Japanese).

Okamura, H., Ouchi, M. (1999): Self-Compacting Concrete. Development, Present Use and Future, First Int. Symposium on SCC, Stockholm, Edited by Skarendahl and Petersson, RILEM publications PRO 7, Cachan, pp. 3-14.

Oude Kempers, J.H.M. (1999): Schoon beton in Haagse Schouwburg, Cement, No. 3, pp. 30-34 (in Dutch).

Petersson, Ö. (1998): Preliminary Mix Design - Final Report of Task 1, Brite Euram project (BE 96-3801) - Rational production and improved working environment through using SCC, Document RT1_v2.doc.

Petersson, Ö. (2003): Private communication.

Petersson, Ö., Billberg, P., Österberg, T. (1998): Applications of self compacting concrete for bridge castings, Second Int. Workshop on SCC, Kochi, Edited by Ozawa and Ouchi, Concrete Engineering Series, No. 30, Japan Society of Civil Engineers, pp. 318-327.

RILEM (2000): Self-compacting concrete, State-of-the-art report of RILEM Technical Committee 174-SCC, Edited by Skarendahl and Petersson, Report 23, RILEM publications, Cachan.

RILEM 50-FMC (1985): Determination of the fracture energy of mortar and concrete by means of three-point bend test on notched beams, Draft Recommendation, Materials and Structures, Vol. 18, No. 106, pp. 285-290.

RILEM TC 162-TDF (2000): Test and design methods for steel fibre reinforced concrete, Draft recommendation, Materials and Structures, Vol. 33, January-February 2000, pp. 3-5.

Roelfstra, P.E., Wittmann, F.H. (1986): Numerical method to link strain softening with failure of concrete, Fracture Toughness and Fracture Energy, Edited by Wittmann, Elsevier, London.

Rosenbusch, J., Teutsch, M. (2003): Shear Design with σ-ε Method, Test and Design Methods for Steel Fibre reinforced Concrete - Background and Experiences, Edited by Schnütgen and Vandewalle, RILEM publication PRO 31, Bagneux, pp. 105-118.

Rossi P., Acker, P., Malier, P. (1987): Effect of steel fibres at two different stages: the material and the structure, Materials and Structures, Vol. 20, pp. 436-439.

Rossi, P., Harrouche, N. (1990): Mix design and mechanical behaviour of some steel-fibre-reinforced concretes used in reinforced concrete structures, Materials and Structures, 1990, Vol. 23, pp. 256-266.

Saak, A.W. (2000): Characterization and Modeling of the Rheology of Cement Paste: With Applications Toward Self-Flowing Materials, PhD-thesis, Northwestern University of Evanston, Illinois.

Sato, Y., Van Mier, J.G.M., Walraven, J.C. (2000): Mechanical characteristics of multi-modal fiber-reinforced cement based composites, BEFIB 2000, Edited by Rossi and Chanvillard, Fifth Int. RILEM Symposium, RILEM Publications PRO 15, pp. 791-800.

Schönlin, K. (1988): Ermittlung der Orientierung, Menge und Verteilung der Fasern in faserbewehrtem Beton, Beton- und Stahlbetonbau 83, No. 6, pp. 168-171 (in German).

Schumacher, P., Braam, C.R., Walraven, J.C. (2001): Cylinders under uniaxial compressive loading - preliminary tests, Stevin-report 25.5-01-06, Department of Structural and Building Engineering, Delft University of Technology.

Schumacher, P., Den Uijl, J.A., Braam, C.R., Walraven, J.C. (2003a): Self-compacting steel fiber reinforced concrete prisms under compressive loading, Stevin-report 25.5-03-11, Department of Structural and Building Engineering, Delft University of Technology.

Schumacher, P., Den Ujil, J.A., Walraven, J.C. (2003b): Fracture energy determined from three-point bending tests on self-compacting steel fiber reinforced concrete, Stevin-report 25.5-03-18, Department of Structural and Building Engineering, Delft University of Technology.

Sedran, T. (1999): Rheologie et Rheometrie des Betons. Applications aux Betons Autonivelants, PhD-thesis, LCPC, Nantes (in French).

SIA 162/6 (1999): Schweizerischer Ingenieur- und Architektenverein, Empfehlung SIA 162/6, Stahlfaserbeton, Zürich.

Smeplass, S., Mørtsell, E. (2001): The particle matrix model applied on SCC, Second Int. Symposium on SCC, Edited by Ozawa and Ouchi, University of Tokyo, COMS Engineering Publication, pp. 267-276.

Soroushian, P., Lee, C.-D. (1990): Distribution and orientation of fibres in steel fiber reinforced concrete, ACI Materials Journal, Sept.-Oct. 1990, pp. 433-439.

Stang, H., Li, V.C. (2001): Mechanics of Fibre Reinforced Cement Based Composites, Course at Technical University of Denmark, Lyngby, Int. Graduate Research School in Applied Mechanics.

Stroband, J. (1998a): Onderzoek naar de treksterkte van staalvezelbeton, Stevin-report 25.5-97-15, Department of Structural and Building Engineering, Delft University of Technology (in Dutch).

Stroband, J. (1998b): Onderzoek naar standaardisering van een beproevingsmethode voor staalvezelbeton, Stevin-report 25.5-98-14, Department of Structural and Building Engineering, Delft University of Technology (in Dutch).

Stroeven, P. (1978): Morphometry of fibre reinforced cementitious materials – Part 1: Efficiency and spacing in idealized structures, Materials and Structures, Vol. 11, No. 61, pp. 31-37.

Swamy R.N. (1975): Fibre reinforcement of cement and concrete, Materials and Structures, Vol. 8, No. 45, pp. 235-254.

Swamy, R.N., Mangat, P.S. (1974): Influence of fibre-aggregate interaction on some properties of steel fibre reinforced concrete, Materials and Structures, Vol. 7, No. 41, pp. 307-314.

Takada, K. (2004): Influence of Admixtures and Mixing Efficiency on the Properties of Self Compacting Concrete - The Birth of SCC in the Netherlands, PhD-thesis, Department of Structural and Building Engineering, Delft University of Technology.

Takada, K., Pelova, G.I., Walraven, J.C. (1997): Development of self-compacting concrete in the Netherlands, First report, Department of Structural and Building Engineering, Delft University of Technology.

Tattersall, G.H. (1991): Workability and Quality Control of Concrete, E&FN Spon, London, ISBN: 0419148604.

Tattersall, G.H., Banfill, P.F.G. (1983): The Rheology of Fresh Concrete, Pitman Books Limited, London, ISBN: 0273085581.

Tol, R. (2002): Spanwand van HSVVZVB (hogesterkte vezelversterkt zelfverdichtend beton) - een ontwerp beproefd, Master thesis, Department of Structural and Building Engineering, Delft University of Technology (in Dutch).

Toutanji, H., Bayasi, Z. (1998): Effects of manufacturing techniques on the flexural behavior of steel fiber-reinforced concrete, Cement and Concrete Research, Vol. 28, No. 1, pp. 115-124.

Van Aalst, G.J., Vonk, N., De Koning, S.J.F. (1996): Toepassing verdichtingarme betonspecie bij de Waalbrug, Cement, No. 2, pp. 19-20 (in Dutch).

Van der Kolk, M.J. (2001): Haalbaarheid van hoge sterkte vezelversterkt vloeibeton voor spanwandprofielen (Eindrapport), Master thesis, Department of Structural and Building Engineering, Delft University of Technology (in Dutch).

Van Gysel, A. (2000): Studie van het uittrekgedrag van staalvezels ingebed in een cementgebonden matrix met toepassing op staalvezelbeton onderworpen aan buiging, PhD-thesis, Laboratory Magnel of Reinforced Concrete, University of Ghent (in Dutch).

Van Halderen, M.W.A.M. (1995): Ervaringen met zelfverdichtend beton, Cement, No. 6, pp. 15-19 (in Dutch).

Vandewalle et al. (2002): Recommendation of RILEM TC 162-TDF: Test and design methods for steel fibre reinforced concrete, final recommendation for bending test, Materials and Structures, Vol. 35, pp. 579-582.

Vandewalle, L. (1993): Vezelversterkt Beton, Studiedag 'Speciale Betonsoorten en Toepassingen, Katholieke Universiteit Leuven, Departement Burgerlijke Bouwkunde, pp. 77-98.

Vandewalle, L., Dupont, D. (2001): Comparison between the bending tests according to RILEM, NBN, JCI, ASTM and the uniaxial tension test, Brite Euram project 'Test and Design Methods for Steel Fibre reinforced Concrete' (BRPR-CT98-0813), Final report task 2.3.

Vandewalle, L., Dupont, D. (2003): Bending Test and Interpretation, Test and Design Methods for Steel Fibre reinforced Concrete - Background and Experiences, RILEM publication PRO 31, Bagneux, 2003, pp. 1-14.

Wadell, H. (1935): ibid, 43, pp. 250-280.

Wallevik, O.H. (2000): Rheology of Coarse Particle Suspensions, such as Cement Paste, Mortar and Concrete, Course on Rheology, The Icelandic Research Institute.

Wallevik, O.H. (2003): Rheology - A scientific approach to develop self-compacting concrete, Third Int. Symposium of SCC, Reykjavik, Edited by Wallevik and Níelsson, RILEM publications PRO 33, Bagneux, pp. 23-34.

Walraven, J.C. (1998): The Development of Self-Compacting Concrete in the Netherlands, Second Int. Workshop on SCC, Kochi, Edited by Ozawa and Ouchi, Concrete Engineering Series, No. 30, Japan Society of Civil Engineers, pp. 87-96.

Walraven, J.C., Takada, K., Pelova, G.I. (1999): Zelfverdichtend beton, hoe maak je dat?, Cement No. 3, pp. 68-72 (in Dutch).

Weiler, B., Grosse, C., Reinhardt, H.W. (1999): Debonding behaviour of steel fibres with hooked ends, Proceedings of the Third International RILEM Workshop 'High Performance Fibre Reinforced Cementitious Composites' (HPFRCC 3), Mainz, pp. 423-436.

Yu, A.B., Standish, N., McLean, A. (1993): Porosity calculation of binary mixtures of non-spherical particles, Journal of the American Ceramic Society, Vol. 76, No. 11, pp. 2813-2816.

Yu, A.B., Zou, R.P. (1998): Prediction of the porosity of particle mixtures, Kona, No.16, pp. 68-81.

Zou, R.P., Yu, A.B. (1996): Evaluation of the packing characteristics of mono-sized non-spherical particles, Powder Technology, Vol. 88, pp. 71-79.

Appendices: overview

Appendix A: Test methods for SCC and SCFRC in the fresh state

Appendix B: Packing density: K-index of the applied compaction method

Appendix C: Experimental packing density of aggregates and steel fibres

Appendix D: Mixture compositions

Appendix E: Characteristics of the components of SCC and SCFRC

Appendix F: Paste characteristics in the fresh state

Appendix G: SCC and SCFRC in the fresh state

Appendix H: Geometrical correction of the displacement (bending tests)

Appendix I: Input parameters for the inverse analyse (bending tests)

Appendix J: Results; parameters of the inverse analyse (bending tests)

Appendix K: Simulations and experimental results (bending tests)

Appendix A: Test methods for SCC and SCFRC in the fresh state (1)

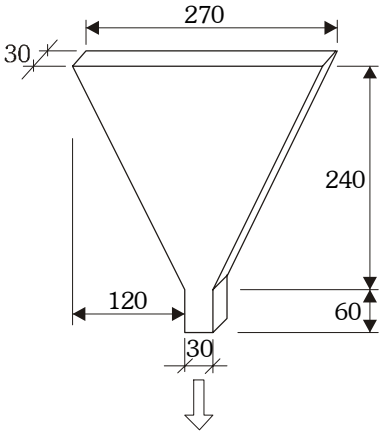


Fig. A1 Mortar funnel [in mm]
[Takada et al., 1997]

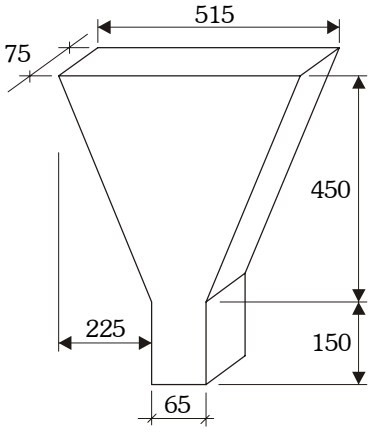


Fig. A2 V-funnel [in mm]
[CUR-recommendation 93, 2002]

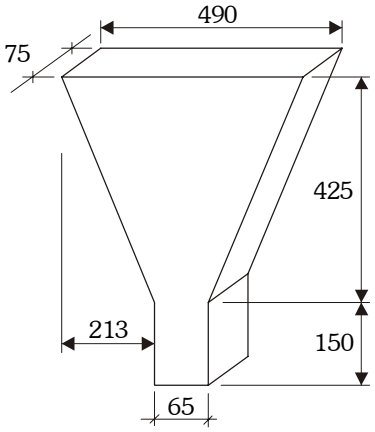


Fig. A3 V-funnel [in mm]
[EFNARC, 2001]

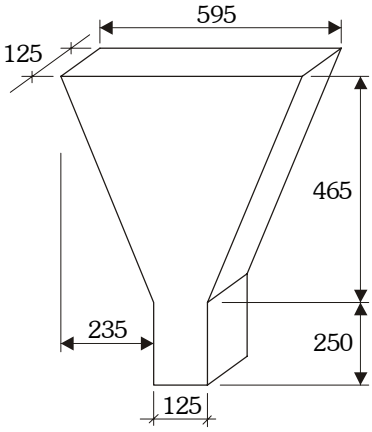


Fig. A4 Fibre funnel [in mm]

h_1: height concrete at casting side
h_2: height concrete behind bars

Filling degree (%) = $(h_1+h_2)\cdot 100/(2\cdot h_1)$

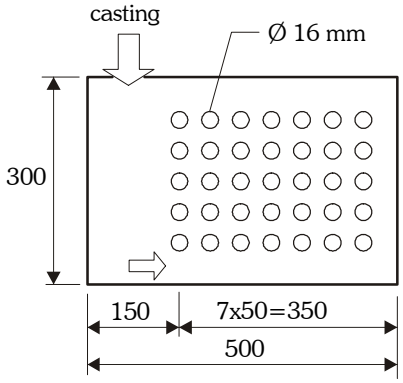


Fig. A5 Cross-section of the filling vessel test [in mm]
[Takada et al., 1997]

Appendix A: Test methods for SCC and SCFRC in the fresh state (2)

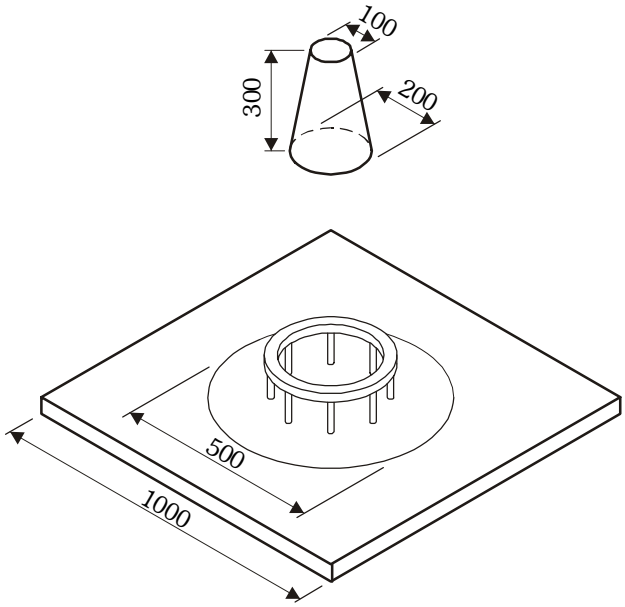


Fig. A6 Slump flow test with J-ring [in mm]

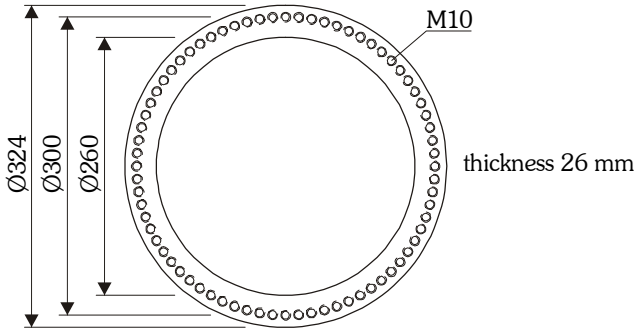


Fig. A7 Top view of the J-ring [in mm], fabricated at University of Paisley

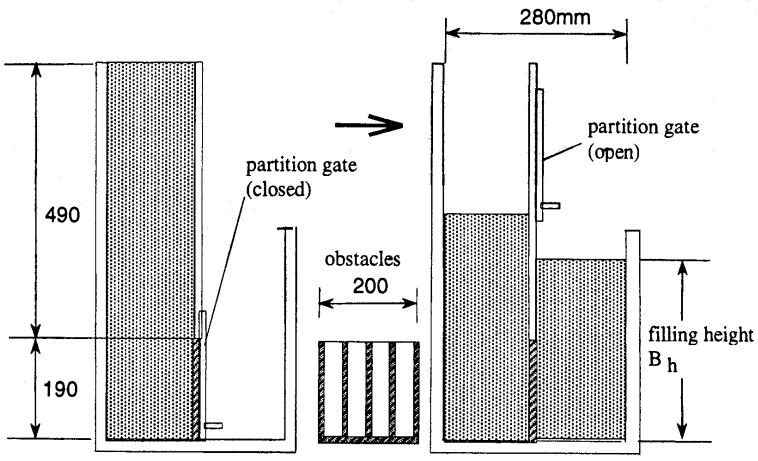


Fig. A8 Box test; left and right the cross-section before and after testing, respectively.
In the middle the front view of the obstacles in the partition gate [in mm] [Takada et al., 1997]

Appendix A: Test methods for SCC and SCFRC in the fresh state (3)

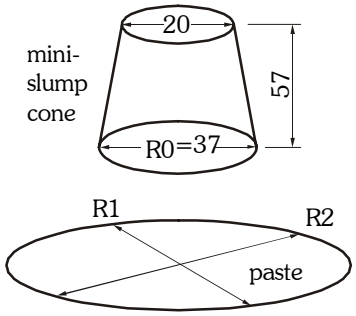


Fig. A9 Mini-slump flow cone [in mm]

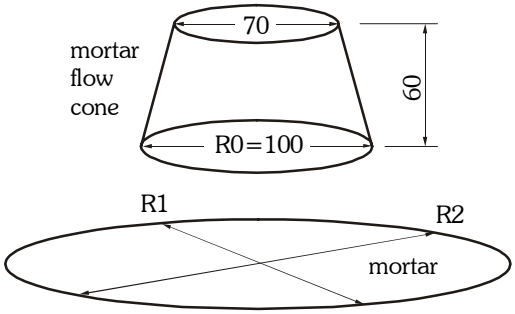


Fig. A10 Mortar flow cone [in mm]
[Takada et al., 1997]

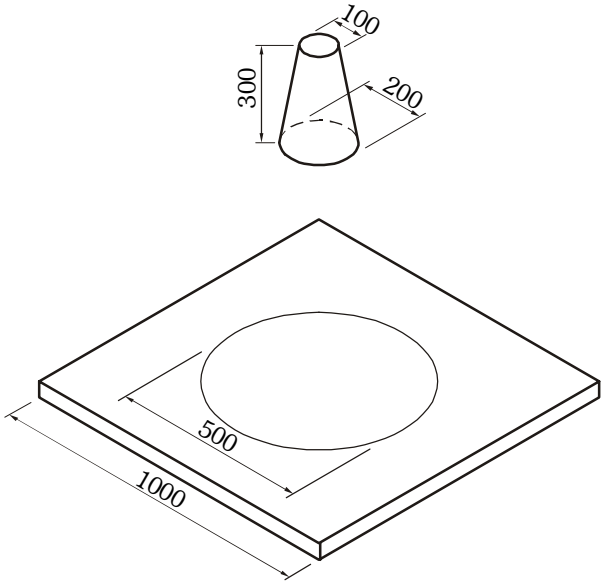
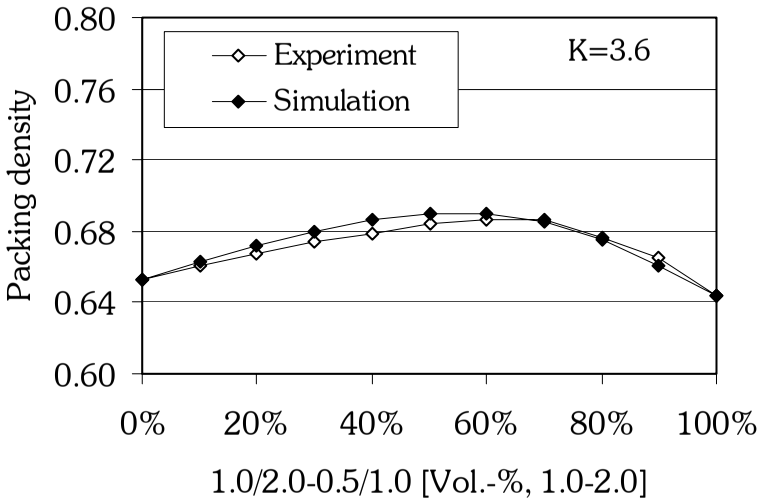


Fig. A11 Slump flow test [in mm]

Appendix B: Packing density: K-index of the applied compaction method (1)

Table and Fig. B1: Comparison of experiments and simulations; K = 3.6 (fractions: 1.0/2.0 and 0.5/1.0)

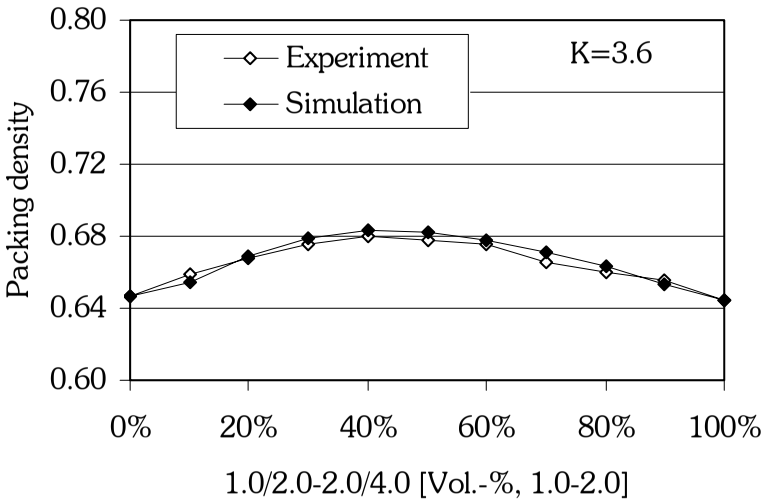
1.0-2.0 [Vol.-%]	*Experiment*	*CPM*	*Error*
100%	0.644	0.644	-
90%	0.665	0.661	0.62%
80%	0.676	0.675	0.12%
70%	0.686	0.685	0.12%
60%	0.686	0.690	0.58%
50%	0.684	0.690	0.86%
40%	0.679	0.686	1.03%
30%	0.674	0.680	0.82%
20%	0.667	0.672	0.67%
10%	0.661	0.663	0.23%
0%	0.653	0.653	-
		Mean error	*0.56%*
		Maximum error	*1.03%*



Appendix B: Packing density: K-index of the applied compaction method (2)

Table and Fig. B2: Comparison of experiments and simulations; K = 3.6 (fractions: 1.0/2.0 and 2.0/4.0)

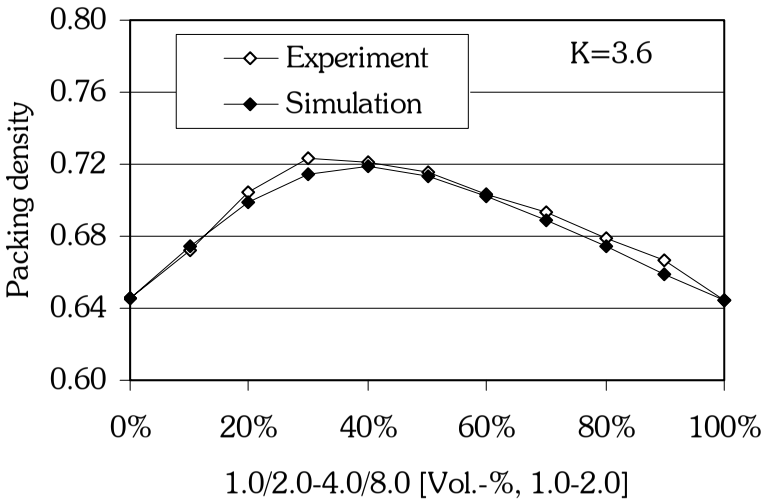
1.0-2.0 [Vol.-%]	*Experiment*	*CPM*	*Error*
100%	0.644	0.644	-
90%	0.655	0.654	0.18%
80%	0.660	0.663	0.47%
70%	0.666	0.671	0.81%
60%	0.675	0.678	0.47%
50%	0.678	0.683	0.66%
40%	0.680	0.683	0.43%
30%	0.676	0.678	0.36%
20%	0.668	0.669	0.09%
10%	0.659	0.655	0.67%
0%	0.647	0.647	-
		Mean error	*0.46%*
		Maximum error	*0.81%*



Appendix B: Packing density: K-index of the applied compaction method (3)

Table and Fig. B3: Comparison of experiments and simulations; K = 3.6 (fractions: 1.0/2.0 and 4.0/8.0)

1.0-2.0 [Vol.-%]	*Experiment*	*CPM*	*Error*
100%	0.644	0.644	-
90%	0.667	0.659	1.18%
80%	0.679	0.674	0.74%
70%	0.693	0.689	0.61%
60%	0.703	0.702	0.09%
50%	0.716	0.713	0.36%
40%	0.721	0.719	0.29%
30%	0.723	0.715	1.13%
20%	0.705	0.699	0.85%
10%	0.672	0.674	0.36%
0%	0.646	0.646	-
		Mean error	*0.62%*
		Maximum error	*1.18%*



Appendix C: Experimental packing density of aggregates and steel fibres (1)

Table C1: Packing density of steel fibres: studies with K=3.6 and on the wall-effect

Fibre type	*Fibre length [mm] (Aspect ratio [-])*	*Standard packing method, K=3.6*	*Vibration only, small container*	*Vibration only, big container*	*Wall-effect* k_{SF}	*Maximum packing density (solver)*
Harex SF32/0.1	32.4 (32.8)	0.109	0.098	0.102	0.582	0.177
Eurosteel 50/50	47.8 (45.8)	0.111	0.087	0.908	0.520	0.190
Dramix 45/30	28.8 (46.3)	0.121	0.115	0.118	0.634	0.191
Dramix 65/40	41.2 (64.9)	0.068	0.058	0.060	0.503	0.123
Dramix 80/60 BN	57.9 (76.1)	0.054	0.043	0.045	0.456	0.112
Dramix OL 13/016	13.0 (81.3)	0.076	0.077	0.078	0.663	0.111
Dramix OL 6/0.16	6.0 (37.5)	0.158	0.173	0.175	0.649	0.234
Dramix 80/60 BP	61.1 (85.7)	0.046	0.038	0.039	0.475	0.095
Dramix 80/30 BP	30.5 (78.5)	0.048	0.044	0.045	0.560	0.079
Harex 65/20	20.2 (64.3)	0.082	0.075	0.077	0.635	0.117

Appendix C: Experimental packing density of aggregates and steel fibres (2)

Table C2: Packing density of coarse aggregates and steel fibres

Fibre content	*Dramix 80/60 BP MAS: 16 mm*		*Dramix 80/60 BN MAS: 16 mm*		*Dramix 80/30 BP MAS: 16 mm*		*Dramix 65/40 BN MAS: 16 mm*		*Dramix 45/30 BN MAS: 16 mm*	
[Vol.-%]	*average*	*variation*	*average*	*variation*	*average*	*variation*	*average*	*variation*	*average*	*variation*
0.0%	0.660	0.29%	0.660	0.29%	0.660	0.29%	0.660	0.29%	0.660	0.29%
0.5%	0.637	0.15%	0.643	0.05%	0.638	0.40%	0.644	0.15%	0.649	0.15%
1.0%	0.623	0.15%	0.625	0.05%	0.617	0.36%	0.628	0.35%	0.640	0.25%
1.5%	0.602	0.46%	0.607	0.10%	0.592	0.16%	0.615	0.05%	0.629	0.59%
2.0%	0.582	0.37%	0.583	0.16%	0.566	0.60%	0.594	0.36%	0.619	0.10%
3.0%	0.524	1.73%	0.536	0.11%	0.523	0.52%	0.557	0.11%	0.599	0.00%
4.0%	-	-	0.488	0.12%	-	-	0.517	0.19%	0.578	0.15%
5.0%	-	-	-	-	-	-	0.475	0.06%	0.558	0.62%

Table C3: Packing density of coarse aggregates and steel fibres, continued

Fibre content	*Eurosteel 50/50 MAS: 16 mm*		*Harex 32/0.1 MAS: 16 mm*		*Harex 65/20 MAS: 8 mm*		*Dramix 80/30 BN MAS: 8 mm*	
[Vol.-%]	*average*	*variation*	*average*	*variation*	*average*	*variation*	*average*	*variation*
0.0%	0.660	0.29%	0.660	0.29%	0.633	0.79%	0.633	0.79%
0.5%	0.651	0.05%	0.649	0.15%	0.617	0.77%	0.616	0.36%
1.0%	0.641	0.24%	0.630	0.10%	0.596	0.59%	0.591	0.43%
1.5%	0.631	0.34%	0.617	0.30%	0.575	0.05%	0.561	0.11%
2.0%	0.623	0.10%	0.602	0.15%	0.561	0.38%	0.540	0.74%
3.0%	0.601	0.35%	0.581	0.10%	0.521	0.41%	0.502	0.48%
4.0%	0.587	0.20%	0.558	0.21%	0.489	0.67%	-	-
5.0%	0.561	0.10%	0.531	0.55%	-	-	-	-

Appendix C: Experimental packing density of aggregates and steel fibres (3)

Tables C4: Packing density of sand (0.125-4 mm) and coarse aggregates (4-16 mm)

Sand content	*No fibres*	
[0.125-4 mm]	*average*	*variation*
100%	0.717	0.20%
80%	0.755	0.16%
60%	0.797	0.14%
50%	0.803	0.17%
40%	0.809	0.77%
20%	0.745	0.19%
0%	0.656	0.16%

Table C5: Packing density of sand (0.125-4 mm), coarse aggregates (4-16 mm) and steel fibres (fibre content: 1.5 Vol.-%)

(CPM: predictions; AV: average of experiments, VA: variation of experiments)

Sand content	*Harex SF32/0.1*			*Dramix 45/30*			*Eurosteel 50/50*			*Dramix 65/40*			*Dramix 80/60 BN*		
[0.125-4 mm]	*1.5 Vol.-%*			*1.5 Vol.-%*			*1.5 Vol.-%*			*1.5 Vol.-%*			*1.5 Vol.-%*		
	CPM	*Av*	*Va*	*CPM*	*Av*	*Va*	*CPM*	*Av*	*Va*	*CPM*	*Av*	*Va*	*CPM*	*Av*	*Va*
100%	0.730	0.711	0.09%	0.732	0.715	0.21%	0.734	0.714	0.21%	0.731	0.715	0.18%	0.731	0.714	0.30%
75%	0.756	0.758	0.06%	0.759	0.762	0.12%	0.763	0.765	0.24%	0.758	0.764	0.06%	0.759	0.763	0.22%
50%	0.765	0.786	0.12%	0.776	0.796	0.19%	0.780	0.793	0.15%	0.770	0.776	0.09%	0.774	0.767	0.49%
25%	0.722	0.716	0.34%	0.735	0.735	0.35%	0.749	0.742	0.18%	0.732	0.705	0.23%	0.739	0.703	0.14%
0%	0.637	0.617	0.21%	0.649	0.629	0.42%	0.662	0.631	0.24%	0.646	0.615	0.04%	0.654	0.607	0.07%

Appendix C: Experimental packing density of aggregates and steel fibres (4)

Table C6: Packing density of sand (0.125-4 mm), coarse aggregates (4-16 mm) and steel fibres (fibre content: 3.0 Vol.-%)
(CPM: predictions; AV: average of experiments, VA: variation of experiments)

Sand content [0.125-4 mm]	*Harex SF32/0.1 3.0 Vol.-%*			*Dramix 45/30 3.0 Vol.-%*			*Eurosteel 50/50 3.0 Vol.-%*		
	CPM	*Av*	*Va*	*CPM*	*Av*	*Va*	*CPM*	*Av*	*Va*
100%	0.723	0.711	0.17%	0.729	0.718	0.14%	0.733	0.719	0.23%
75%	0.742	0.758	0.20%	0.752	0.764	0.21%	0.759	0.766	0.17%
50%	0.737	0.786	0.23%	0.755	0.784	0.38%	0.771	0.782	0.38%
25%	0.680	0.716	0.15%	0.706	0.702	0.31%	0.732	0.700	0.11%
0%	0.599	0.617	0.07%	0.623	0.599	0.14%	0.648	0.601	0.25%

Appendix D: Mixture compositions (1)

Table D1: Mixture compositions of the reference mixtures of series PS/OS/MS

Reference mixture of series:	*PS1*	*PS2*	*PS3*	*PS4*	*OS1*	*OS2*	*OS3*	*OS4*	*OS5*	*OS6*	*OS7*	*OS8*	*OS9*	*MS1*	*MS2*	*MS3*
	[kg/m³]	*[kg/m³]*	*[kg/m³]*	*[kg/m³]*	*[kg/m³]*	*[kg/m³]*	*[kg/m³]*	*[kg/m³]*	*[kg/m³]*	*[kg/m³]*	*[kg/m³]*	*[kg/m³]*	*[kg/m³]*	*[kg/m³]*	*[kg/m³]*	*[kg/m³]*
CEM III 42.5 N	342	362	386	408	155	149	149	143	335	352	367	151	164	983	787	683
CEM I 52.5 R	-	-	-	-	249	263	249	269	-	-	-	228	246	-	-	-
Fly ash	179	191	204	216	142	173	146	173	168	192	217	166	180	-	-	-
Free water	159	164	171	178	172	181	171	181	155	164	173	181	188	269	235	220
Coarse aggregate (4-16 mm) - round	1019	942	855	767	682	655	508	487	528	508	487	-	-	-	-	-
Coarse aggregate (4-8 mm) - round	-	-	-	-	-	-	-	-	-	-	-	467	449	-	-	-
Sand (0.125-4 mm) - round	610	640	676	712	913	876	1089	1045	1134	1089	1045	1100	1058	1042	1303	1433
Superplasticiser CUGLA LR	(1.76)	(2.09)	(2.19)	(2.27)	(2.58)	(2.88)	(2.59)	(2.78)	(2.10)	(2.10)	(2.17)	(2.68)	(2.73)	(2.80)	(2.34)	(2.39)
Superplasticiser CUGLA HR	(0.70)	(0.84)	(0.87)	(0.91)	(1.58)	(1.44)	(2.12)	(1.85)	(1.26)	(1.18)	(1.09)	(1.49)	(1.31)	(1.87)	(1.56)	(1.59)
Water/cement ratio	0.46	0.45	0.44	0.44	0.42	0.44	0.43	0.44	0.46	0.47	0.47	0.48	0.46	0.27	0.30	0.32
Water/binder ratio[1]	0.44	0.42	0.42	0.41	0.38	0.39	0.39	0.39	0.43	0.44	0.44	0.43	0.41	-	-	-
Comp. strength (150 mm cubes)																
at 7 days	-	-	-	-	58.6	53.5	58.3	54.1	39.4	37.7	35.8	49.6	49.9	61.0[2]	58.4[2]	52.3[2]
at 28 days	-	55.9	56.9	-	77.9	73.1	78.0	75.3	58.6	53.8	53.0	70.8	69.5	81.6[2]	76.9[2]	71.7[2]

[1]CUR-Recommendation 70, 1999 [2]measured on prisms of 160·40·40 mm

Appendix D: Mixture compositions (2)

Table D2: Mixture composition of seventeen SCFRCs for bending tests

Mixture No. (Table 8.1)	1/2/15	3	4	16	5	6	7/8/11	9	10/12	13/17	14
	D 80/60 BP D 80/30 BP D 45/30 BN	D 65/40 BN	D 45/30 BN	D 45/30 BN	D 80/30 BP	H 65/20	D 80/60 BP D 80/30 BP	D 65/40 BN	D 45/30 BN	D 80/60 BP D 80/30 BP	OL13/0.16
$d_{g,max}$ [mm]	16	16	16	16	8	8	16	16	16	16	16
Strength class	B45	B45	B45	B45	B65	B65	B65	B65	B65	B105	B105
	[kg/m^3]	[kg/m^3]	[kg/m^3]	[kg/m^3]	[kg/m^3]	[kg/m^3]	[kg/m^3]	[kg/m^3]	[kg/m^3]	[kg/m^3]	[kg/m^3]
Fibre content	60	100	140	120	40	60	60	100	140	60	125
CEM III 42.5 N	367	367	367	367	164	164	143	143	143	-	-
CEM III 52.5 A	-	-	-	-	-	-	-	-	-	-	555
CEM I 52.5 R	-	-	-	-	246	246	269	269	269	443	358
Fly ash	217	217	217	217	180	180	173	173	173	133	-
Microsilica (powder)	-	-	-	-	-	-	-	-	-	-	61
Microsilica (slurry (50% solids))	-	-	-	-	-	-	-	-	-	32	-
Free water	173	173	173	173	188	188	181	181	181	169	226
Coarse aggregate (4-16 mm) - round	481	477	472	474	-	-	481	477	472	-	-
Coarse aggregate (4-16 mm) - crushed	-	-	-	-	-	-	-	-	-	488	-
Coarse aggregate (4-8 mm) - round	-	-	-	-	445	443	-	-	-	-	-
Sand (0.125-4 mm)	1032	1023	1014	1018	1048	1044	1032	1023	1014	1048	-
Fine aggregate (0.125-1 mm)	-	-	-	-	-	-	-	-	-	-	1097
Superplasticiser CUGLA HR	(1.09)	(1.09)	(1.09)	(1.09)	(1.31)	(1.31)	(1.85)	(1.85)	(1.85)	(7.33)	(20.45)
Superplasticiser CUGLA LR	(2.17)	(2.17)	(2.17)	(2.17)	(2.73)	(2.73)	(2.78)	(2.78)	(2.78)	(11.00)	-
Water/cement ratio	0.47	0.47	0.47	0.47	0.46	0.46	0.44	0.44	0.44	0.38	0.25
Water/binder ratio[1]	0.44	0.44	0.44	0.44	0.41	0.41	0.39	0.39	0.39	0.34	-

[1]CUR-Recommendation 70, 1999

Appendix D: Mixture compositions (3)

Table D3: Mixture compositions for single fibre pull-out tests, (conventional and self-compacting concrete)

Type of concrete	*Conventional*			*Self-compacting*		
Strength class	*B45*	*B65*	*B105*	*B45*	*B65*	*B105*
Mixture component	*[kg/m^3]*	*[kg/m^3]*	*[kg/m^3]*	*[kg/m^3]*	*[kg/m^3]*	*[kg/m^3]*
CEM III 42.5 N	236	263	-	365	141	-
CEM I 52.5 R	79	88	475	-	265	440
Fly ash	-	-	-	216	171	132
Microsilica (solid slurry - 50%)	-	-	26	-	-	32
Free water	142	156	165	172	178	168
Coarse aggregate (4-16 mm) - round	824	973	-	485	480	-
Coarse aggregate (4-16 mm) - crushed	-	-	959	-	-	492
Sand (0.125-4 mm) - round	858	898	785	1040	1030	1054
Plasticiser Addiment FM 951	3.1	3.5	4.2	-	-	-
Superplasticiser CUGLA HR	-	-	-	1.08	1.82	7.28
Superplasticiser CUGLA LR	-	-	-	2.16	2.74	10.92
Water/cement ratio	0.47	0.45	0.35	0.47	0.44	0.38
Water/binder ratio[1]	-	-	-	0.44	0.39	0.34

[1]CUR-Recommendation 70, 1999

Appendix E: Characteristics of the components of SCC and SCFRC (1)

Table E1: Characteristics of the powders

Powder classification	*Producer / type*	*Abbreviation*	*Applied for*	*Specific gravity [kg/dm^3]*
CEM III 42.5 N	ENCI IJmuiden	HO 1	PS 1-3	2.95
CEM III 42.5 N	ENCI IJmuiden	HO 2	PS 4, MS 1-3	2.98
CEM III 42.5 N	ENCI IJmuiden	HO 3	OS 1-9	2.98
CEM I 52,5 R	ENCI Maastricht	PO	OS 1-4, 8-9, B105 (mix 13,17)	3.15
Fly ash	SMZ	FA 1	PS 1-4, OS 5-7, B105 (mix 13, 17)	2.34
Fly ash	SMZ	FA 2	OS 1-4, 8-9	2.30
CEM III 52.5 A	ENCI Rotterdam	HHO	B105-1 (mix 14)	3.00
Microsilica (powder)	CUGLA, Fesil	M 1	B105-1 (mix 14)	2.36
Microsilica (slurry)	Silicol (50% solid)	M 2	B105-2 (mix 13/17)	1.68

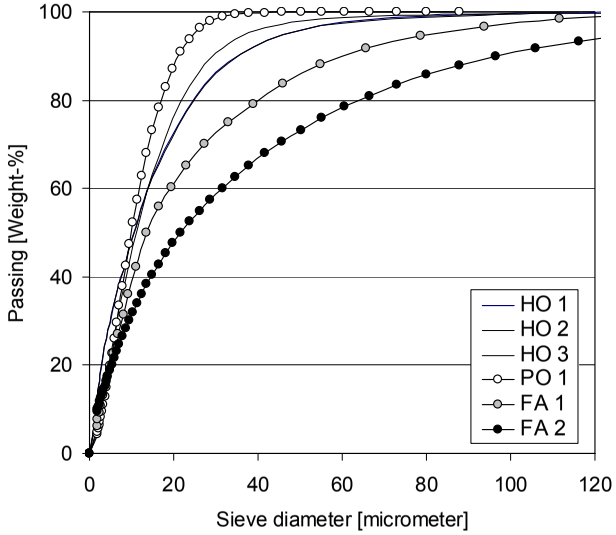


Fig. E1: Size distribution of the powders

Appendix E: Characteristics of the components of SCC and SCFRC (2)

Table E2: Characteristics of the superplasticisers

Superplasticiser	*Cugla (20%)-LR*	*Cugla (35%)-HR*
Chemical description	Polycarboxylic ether complex	Polycarboxylic ether complex
Specific gravity (kg/dm^3)	1.05 *	1.10 *
Solid concentration	20%	35%

* on solution-base

Table E3: Characteristics of the aggregates

Aggregate		*Coarse aggregate*	*Coarse aggregate*	*Coarse aggregate*	*Sand*	*Fine aggregate*
Size	[mm]	4 - 16 mm	4 - 16 mm	4 - 8 mm	0.125 - 4 mm	0.125 -1 mm
Shape	[-]	round - river	crushed	round - river	round - river	round - river
Specific gravity *	[kg/dm^3]	2.58	2.58	2.58	2.60	2.65
Absorption	[%]	1.12	0.89	1.08	0.52	-
Fineness modulus	[-]	6.65	-	6.00	2.94	2.30
Fines (< 0.125 mm)	[%]	-	-	-	0.2	-

* saturated-surface-dry-based

Appendix F: Paste characteristics in the fresh state

Table F1: Characteristics of SCC and the paste of SCC

Reference mixture No.	*PD paste [-]*	*Mini-slump [mm]*	*FT_p [s]*	*RWL [$\cdot 10^{-5}$]*	*Solid content paste [Vol.-%]*	*$(\phi/\phi^*)_p$ [-]*	*Relative slope slump flow [-]*	*Relative slope yield value [-]*
PS 1	0.572	136	6.6	10.73	54.7	0.955	-0.552	-
PS 2	0.583	133	6.1	10.79	55.6	0.954	-0.143	-
PS 3	0.583	130	7.7	8.89	56.1	0.962	-0.200	-
PS 4	0.587	128	8.0	8.64	56.5	0.963	-0.260	-
OS 1	0.570	128	3.2	17.15	53.0	0.930	-0.261	633
OS 2	0.573	118	4.6	15.12	53.7	0.938	-0.199	312
OS 3	0.572	147	2.8	17.84	53.0	0.927	-0.264	383
OS 4	0.574	133	4.0	15.75	53.7	0.935	-0.198	90
OS 5	0.576	146	4.6	12.88	54.5	0.947	-0.218	1064
OS 6	0.576	140	6.3	10.42	55.1	0.956	-0.257	417
OS 7	0.579	130	7.4	9.22	55.7	0.961	-0.196	65
OS 8	0.566	137	2.4	20.03	52.1	0.920	-0.411	131
OS 9	0.569	122	3.3	16.71	53.0	0.932	-0.278	150
MS 1	0.577	128	7.9	10.19	55.1	0.955	-0.167	-
MS 2	0.565	138	4.8	14.51	53.0	0.934	-0.226	-
MS 3	0.563	154	2.2	21.98	51.2	0.910	-0.341	-

Appendix G: SCC and SCFRC in the fresh state (1)

Table G1: Measurements and characteristics of the granular skeleton

Mix No.		V_f	*Slump flow*	*Yield value*	T_{50}	*Fibre funnel*	*Plastic viscosity*	*Aggregate SI-index*	*Fibre SI-index*	c_{NB}	c_B	*Air content*	*PD (CPM)*	*RPL*	$(\phi/\phi^*)_g$	*MFC-volume*
		[kg/m³]	*[mm]*	*[Pa]*	*[s]*	*[s]*	*[Pa·s]*	*[-]*	*[-]*	*[mm]*	*[mm]*	*[Vol.-%]*	*[-]*	*[-]*	*[-]*	*[-]*
1	**PS 1**	**0**	**718**	**-**	**2.4**	**5.1**	**-**	**-**	**-**	**49**	**36**	**1.9%**	**0.789**	**0.050**	**0.797**	**-**
2	45/30	40	660	-	3.5	6.0	-	-	-	87	74	2.2%	0.778	0.047	0.809	0.73
3	45/30	60	559	-	5.9	7.6	-	-	-	99	87	2.5%	0.772	0.046	0.815	0.74
4	45/30	80	506	-	6.8	8.2	-	-	-	87	74	2.7%	0.766	0.044	0.821	0.74
5	80/60 BN	20	645	-	3.3	4.7	-	-	-	99	87	2.3%	0.784	0.049	0.802	0.73
6	80/60 BN	40	588	-	5.4	8.2	-	-	-	111	99	2.3%	0.779	0.047	0.807	0.73
7	**PS 2**	**0**	**708**	**-**	**3.3**	**4.5**	**-**	**-**	**-**	**36**	**-**	**2.0%**	**0.790**	**0.057**	**0.773**	**-**
8	45/30	80	643	-	4.8	6.0	-	-	-	74	62	2.2%	0.769	0.052	0.795	0.70
9	45/30	100	648	-	4.6	8.3	-	-	-	87	74	2.2%	0.763	0.051	0.801	0.71
10	50/50	60	718	-	2.9	4.6	-	-	-	74	62	2.2%	0.782	0.056	0.781	0.70
11	50/50	80	652	-	5.3	6.3	-	-	-	99	87	1.8%	0.779	0.055	0.784	0.71
12	65/40	40	720	-	3.0	4.4	-	-	-	74	62	1.9%	0.779	0.055	0.785	0.71
13	65/40	60	650	-	4.0	5.9	-	-	-	99	87	2.5%	0.773	0.053	0.791	0.70
14	80/60 BN	40	650	-	4.2	4.3	-	-	-	87	74	1.9%	0.781	0.055	0.782	0.70
15	80/60 BN	60	636	-	3.7	6.3	-	-	-	111	99	2.0%	0.777	0.054	0.787	0.71
16	**PS 3**	**0**	**716**	**-**	**4.2**	**5.7**	**-**	**-**	**-**	**36**	**-**	**2.0%**	**0.791**	**0.066**	**0.747**	**-**
17	45/30	80	713	-	4.5	6.1	-	-	-	62	49	1.8%	0.771	0.062	0.766	0.69
18	45/30	100	643	-	5.4	6.1	-	-	-	74	62	2.4%	0.766	0.060	0.771	0.67
19	45/30	120	638	-	6.9	6.9	-	-	-	87	74	2.5%	0.760	0.059	0.777	0.69
20	50/50	60	655	-	3.9	5.1	-	-	-	74	62	2.4%	0.784	0.065	0.754	0.69
21	50/50	80	625	-	5.5	5.1	-	-	-	87	74	2.1%	0.781	0.064	0.757	0.67
22	50/50	100	654	-	4.4	6.1	-	-	-	99	87	2.0%	0.778	0.063	0.759	0.69
23	65/40	40	669	-	4.2	5.6	-	-	-	74	62	2.3%	0.780	0.064	0.757	0.69
24	65/40	60	668	-	5.9	5.5	-	-	-	87	74	2.5%	0.775	0.062	0.763	0.68
25	65/40	80	589	-	7.3	6.2	-	-	-	99	87	2.3%	0.768	0.061	0.769	0.69
26	80/60 BN	40	718	-	2.9	4.1	-	-	-	62	49	2.4%	0.783	0.064	0.755	0.67
27	80/60 BN	60	573	-	7.8	6.8	-	-	-	122	111	2.3%	0.778	0.063	0.759	0.68
28	80/60 BN	80	568	-	10.9	12.8	-	-	-	122	111	2.2%	0.773	0.062	0.764	0.68

Appendix G: SCC and SCFRC in the fresh state (2)

Table G2: Measurements and characteristics of the granular skeleton, continued

Mix No.		V_f	*Slump flow*	*Yield value*	T_{50}	*Fibre funnel*	*Plastic viscosity*	*Aggregate SI-index*	*Fibre SI-index*	c_{NB}	c_B	*Air content*	*PD (CPM)*	*RPL*	$(\phi/\phi^*)_g$	*MFC-volume*
		[kg/m³]	*[mm]*	*[Pa]*	*[s]*	*[s]*	*[Pa·s]*	*[-]*	*[-]*	*[mm]*	*[mm]*	*[Vol.-%]*	*[-]*	*[-]*	*[-]*	*[-]*
29	**PS 4**	**0**	**743**	**-**	**3.5**	**4.5**	**-**	**-**	**-**	**36**	**-**	**2.1%**	**0.790**	**0.075**	**0.722**	**-**
30	45/30	100	644	-	5.1	5.5	-	-	-	74	62	2.7%	0.767	0.070	0.743	0.64
31	45/30	120	594	-	5.4	6.0	-	-	-	87	74	2.5%	0.762	0.069	0.748	0.66
32	**OS 1**	**0**	**703**	**-32.7**	**1.9**	**3.2**	**69.2**	**0.48**	**-**	**36**	**-**	**1.9%**	**0.785**	**0.054**	**0.783**	**-**
33	80/30	40	645	-2.2	2.3	3.6	116.8	0.53	0.39	87	74	2.2%	0.769	0.051	0.799	0.69
34	80/30	60	583	42.2	6.5	4.8	167.8	0.53	0.52	99	87	2.5%	0.760	0.048	0.809	0.70
35	80/60 BP	40	603	77.4	3.9	4.0	122.9	0.49	0.49	99	87	2.0%	0.779	0.053	0.790	0.69
36	80/60 BP	60	583	20.5	4.7	4.1	125.0	0.54	0.51	99	87	2.0%	0.775	0.052	0.794	0.69
37	45/30	80	653	-2.7	3.1	3.3	109.9	0.51	0.47	74	62	1.8%	0.773	0.052	0.796	0.69
38	45/30	100	580	444.4	4.8	4.0	137.5	0.54	0.48	87	74	2.2%	0.769	0.051	0.799	0.70
39	**OS 2**	**0**	**693**	**-26.5**	**2.1**	**3.2**	**59.4**	**0.52**	**-**	**36**	**-**	**2.2%**	**0.785**	**0.065**	**0.751**	**-**
40	80/30	60	635	15.0	4.2	4.0	171.1	0.51	0.48	87	74	2.2%	0.759	0.058	0.778	0.66
41	80/30	80	570	633.1	6.0	4.4	223.2	0.48	0.51	99	87	2.7%	0.747	0.055	0.789	0.67
42	80/60 BP	40	625	2.0	2.8	3.5	98.6	0.52	0.41	99	87	2.1%	0.778	0.063	0.758	0.66
43	80/60 BP	60	583	103.8	4.2	4.1	159.9	0.51	0.38	122	111	1.8%	0.775	0.063	0.762	0.66
44	45/30	120	620	-3.8	4.5	3.8	144.3	0.52	0.48	87	74	2.5%	0.765	0.060	0.772	0.65
45	45/30	140	573	310.2	6.7	4.4	262.0	0.49	0.53	122	111	2.1%	0.761	0.059	0.776	0.67
46	**OS 3**	**0**	**730**	**-0.2**	**2.1**	**2.9**	**87.9**	**0.51**	**-**	**36**	**-**	**2.6%**	**0.775**	**0.052**	**0.794**	**-**
47	80/30	40	633	56.8	4.3	3.6	143.1	0.52	0.52	87	74	2.9%	0.763	0.049	0.806	0.68
48	80/30	60	598	107.6	6.3	4.3	199.3	0.49	0.52	99	87	2.9%	0.756	0.047	0.813	0.69
49	80/60 BP	40	653	36.9	3.7	3.1	124.3	0.51	0.53	111	99	2.5%	0.770	0.051	0.799	0.67
50	80/60 BP	60	590	240.2	4.4	3.8	154.8	0.50	0.52	122	111	2.5%	0.767	0.050	0.802	0.68
51	45/30	120	618	55.7	6.0	4.7	237.0	0.49	0.50	87	74	2.5%	0.761	0.049	0.808	0.67
52	45/30	140	578	278.0	6.7	5.4	279.3	0.49	0.49	122	111	2.4%	0.758	0.048	0.811	0.69

Appendix G: SCC and SCFRC in the fresh state (3)

Table G3: Measurements and characteristics of the granular skeleton, continued

Mix No.		V_f	*Slump flow*	*Yield value*	T_{50}	*Fibre funnel*	*Plastic viscosity*	*Aggregate SI-index*	*Fibre SI-index*	c_{NB}	c_B	*Air content*	*PD (CPM)*	*RPL*	$(\phi/\phi^*)_g$	*MFC-volume*
		[kg/m³]	*[mm]*	*[Pa]*	*[s]*	*[s]*	*[Pa·s]*	*[-]*	*[-]*	*[mm]*	*[mm]*	*[Vol.-%]*	*[-]*	*[-]*	*[-]*	*[-]*
53	**OS 4**	**0**	**725**	**-11.9**	**2.6**	**2.9**	**56.0**	**0.50**	**-**	**36**	**-**	**2.5%**	**0.775**	**0.062**	**0.762**	**-**
54	80/30	60	613	-10.4	6.1	3.2	156.5	0.50	0.53	87	74	2.5%	0.755	0.058	0.781	0.65
55	80/30	80	578	268.0	6.3	4.0	245.3	0.48	0.52	111	99	2.5%	0.747	0.055	0.790	0.66
56	80/60 BP	60	645	41.2	3.4	2.9	102.3	0.50	0.48	87	74	2.6%	0.767	0.061	0.770	0.64
57	80/60 BP	80	600	54.9	3.6	3.6	199.7	0.51	0.48	99	87	2.7%	0.764	0.060	0.773	0.65
58	45/30	120	630	-10.5	4.5	3.6	117.5	0.51	0.48	87	74	2.7%	0.760	0.059	0.776	0.66
59	45/30	140	630	10.8	3.7	3.8	145.7	0.53	0.47	87	74	2.4%	0.758	0.059	0.779	0.64
60	45/30	160	608	-7.2	3.9	4.2	176.1	0.53	0.49	87	74	1.9%	0.754	0.058	0.782	0.66
61	65/40	100	620	-18.7	4.0	3.4	182.4	0.49	0.53	111	99	2.6%	0.754	0.057	0.783	0.65
62	65/40	120	560	457.7	5.2	4.8	221.1	0.52	0.49	122	111	2.8%	0.748	0.056	0.788	0.66
63	**OS 5**	**0**	**698**	**-38.3**	**3.3**	**2.9**	**97.6**	**0.51**	**-**	**36**	**-**	**3.5%**	**0.775**	**0.042**	**0.826**	**-**
64	80/30	40	648	73.5	4.9	3.9	195.8	0.51	0.47	74	62	4.2%	0.764	0.039	0.838	0.71
65	80/30	60	618	120.0	7.8	5.4	326.2	0.50	0.48	99	87	3.8%	0.757	0.037	0.845	0.72
66	80/60 BP	40	640	66.6	4.2	3.8	187.2	0.49	0.50	99	87	3.7%	0.770	0.041	0.831	0.70
67	80/60 BP	60	588	153.1	5.6	4.4	261.8	0.51	0.46	122	111	4.0%	0.767	0.040	0.834	0.71
68	45/30	100	618	23.3	4.4	4.3	245.3	0.51	0.48	87	74	3.2%	0.764	0.039	0.837	0.70
69	45/30	120	570	49.4	7.8	5.0	280.3	0.51	0.48	99	87	3.8%	0.762	0.039	0.840	0.72
70	**OS 6**	**0**	**728**	**31.4**	**3.0**	**2.9**	**81.0**	**0.49**	**-**	**36**	**-**	**3.6%**	**0.775**	**0.052**	**0.794**	**-**
71	80/30	60	630	82.7	4.8	4.3	266.8	0.49	0.51	87	74	3.6%	0.756	0.047	0.813	0.68
72	80/30	80	575	179.8	9.6	4.9	344.2	0.50	0.50	111	99	3.1%	0.749	0.045	0.822	0.69
73	80/60 BP	40	645	69.9	5.0	3.5	182.8	0.51	0.45	99	87	5.1%	0.770	0.051	0.799	0.67
74	80/60 BP	60	600	125.4	5.7	3.9	301.8	0.49	0.52	122	111	3.8%	0.767	0.050	0.802	0.68
75	45/30	120	630	109.3	5.9	4.4	211.5	0.51	0.48	74	62	3.6%	0.761	0.049	0.808	0.67
76	45/30	140	560	111.0	6.6	5.4	265.0	0.51	0.49	87	74	3.0%	0.758	0.048	0.811	0.69

Appendix G: SCC and SCFRC in the fresh state (4)

Table G4: Measurements and characteristics of the granular skeleton, continued

Mix No.		V_f	*Slump flow*	*Yield value*	T_{50}	*Fibre funnel*	*Plastic viscosity*	*Aggregate SI-index*	*Fibre SI-index*	c_{NB}	c_B	*Air content*	*PD (CPM)*	*RPL*	$(\phi/\phi^*)_g$	*MFC-volume*
		[kg/m³]	*[mm]*	*[Pa]*	*[s]*	*[s]*	*[Pa·s]*	*[-]*	*[-]*	*[mm]*	*[mm]*	*[Vol.-%]*	*[-]*	*[-]*	*[-]*	*[-]*
77	**OS 7**	**0**	**720**	**18.9**	**2.7**	**3.2**	**62.2**	**0.50**	**-**	**36**	**-**	**3.4%**	**0.775**	**0.062**	**0.762**	**-**
78	80/30	60	655	11.7	4.1	3.5	209.1	0.52	0.48	74	62	4.2%	0.755	0.058	0.781	0.65
79	80/30	80	600	118.2	8.0	5.3	306.1	0.52	0.49	87	74	3.4%	0.747	0.055	0.790	0.66
80	80/60 BP	60	638	39.6	3.8	3.5	224.8	0.48	0.52	99	87	4.1%	0.767	0.061	0.770	0.64
81	80/60 BP	80	578	367.9	6.5	3.6	233.1	0.51	0.50	122	111	3.5%	0.764	0.060	0.773	0.65
82	65/40	80	645	-8.1	4.0	3.1	155.2	0.49	0.52	99	87	4.4%	0.764	0.060	0.773	0.65
83	65/40	100	560	90.4	5.4	4.0	206.1	0.51	0.48	111	99	4.6%	0.760	0.059	0.776	0.66
84	45/30	120	643	55.6	4.5	3.5	157.1	0.51	0.51	87	74	3.4%	0.760	0.059	0.776	0.64
85	45/30	140	590	35.5	4.7	4.2	204.4	0.50	0.51	87	74	3.8%	0.758	0.059	0.779	0.66
86	**OS 8**	**0**	**690**	**4.9**	**2.0**	**2.4**	**71.3**	**0.50**	**-**	**36**	**-**	**2.0%**	**0.768**	**0.055**	**0.785**	**-**
87	80/30	20	623	13.5	2.7	2.4	80.8	0.54	0.50	62	49	3.0%	0.763	0.054	0.790	0.67
88	80/30	40	568	32.2	4.0	3.5	141.4	0.52	0.50	87	74	3.8%	0.758	0.052	0.796	0.67
89	65/20	40	600	25.2	4.5	2.5	98.7	0.50	0.51	87	74	3.5%	0.760	0.053	0.794	0.72
90	65/20	60	560	50.5	6.2	3.4	210.1	0.51	0.52	87	74	3.5%	0.755	0.052	0.799	0.72
91	**OS 9**	**0**	**693**	**-6.4**	**2.4**	**2.6**	**57.5**	**0.50**	**-**	**36**	**-**	**2.8%**	**0.769**	**0.065**	**0.754**	**-**
92	80/30	40	618	11.5	2.7	2.5	92.2	0.50	0.52	62	49	3.2%	0.757	0.063	0.766	0.64
93	80/30	60	578	78.2	3.8	3.2	162.4	0.50	0.51	87	74	3.0%	0.751	0.061	0.772	0.65
94	65/20	40	640	2.6	4.6	3.4	120.7	0.49	0.52	87	74	3.3%	0.759	0.063	0.764	0.69
95	65/20	60	625	96.5	5.1	3.9	177.3	0.49	0.50	99	87	3.2%	0.754	0.062	0.769	0.70
96	65/20	80	540	194.2	5.9	4.4	142.6	0.51	0.51	111	99	3.6%	0.749	0.060	0.774	0.70

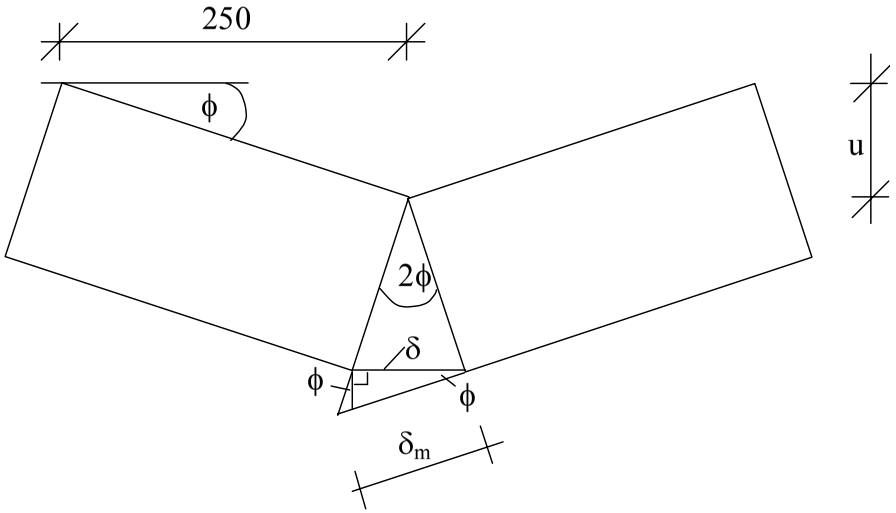
Appendix G: SCC and SCFRC in the fresh state (5)

Table G5: Measurements and characteristics of the granular skeleton, continued

Mix No.		*V_f*	*Slump flow*	*Yield value*	*T_{50}*	*V-funnel*[1]	*Plastic viscosity*	*Aggregate SI-index*	*Fibre SI-index*	*c_{NB}*	*c_B*	*Air content*	*PD (CPM)*	*RPL*	*$(\phi/\phi^*)_g$*	*MFC-volume*
		[kg/m³]	*[mm]*	*[Pa]*	*[s]*	*[s]*	*[Pa·s]*	*[-]*	*[-]*	*[mm]*	*[mm]*	*[Vol.-%]*	*[-]*	*[-]*	*[-]*	*[-]*
97	**MS 1**	**0**	**830**	**-**	**1.2**	**6.1**	**-**	**-**	**-**	**36**	**-**	**2.4%**	**0.736**	**0.176**	**0.533**	**-**
98	6	(1.0/0)	783	-	2.3	6.1	-	-	-	36	-	2.2%	0.716	0.174	0.548	0.49
99	6	(3.0/0)	708	-	2.4	6.9	-	-	-	36	-	2.5%	0.666	0.167	0.588	0.49
100	6	(4.0/0)	608	-	3.9	8.1	-	-	-	36	-	2.8%	0.637	0.159	0.615	0.43
101	6	(5.0/0)	480	-	11.9	10.9	-	-	-	-	-	3.1%	0.606	0.150	0.647	0.49
102	13	(0/1.5)	773	-	2.3	6.6	-	-	-	36	-	2.6%	0.694	0.170	0.565	0.44
103	13	(0/2.0)	658	-	2.5	7.4	-	-	-	49	36	2.5%	0.673	0.165	0.582	0.41
104	13	(0/3.0)	383	-	-	18.2	-	-	-	-	-	3.2%	0.619	0.148	0.633	0.44
105	6+13	(1.5/1.5)	590	-	3.3	8.9	-	-	-	49	36	2.6%	0.656	0.163	0.598	0.46
106	6+13	(2.0/0.5)	785	-	2.1	7.4	-	-	-	36	-	3.7%	0.678	0.169	0.578	0.43
107	6+13	(2.0/1.0)	650	-	3.3	7.8	-	-	-	49	36	2.5%	0.661	0.165	0.593	0.42
108	**MS 2**	**0**	**865**	**-**	**1.6**	**6.4**	**-**	**-**	**-**	**36**	**-**	**2.5%**	**0.736**	**0.099**	**0.666**	**-**
109	6	(3.0/0)	683	-	2.7	8.4	-	-	-	49	36	3.8%	0.682	0.088	0.718	0.56
110	6	(4.0/0)	440	-	16.4	28.8	-	-	-	-	-	4.8%	0.661	0.082	0.742	0.61
111	13	(0/1.0)	808	-	2.5	7.8	-	-	-	36	-	3.2%	0.716	0.095	0.684	0.55
112	13	(0/1.5)	730	-	2.1	7.4	-	-	-	36	-	4.1%	0.704	0.092	0.696	0.52
113	13	(0/2.0)	550	-	4.2	10.2	-	-	-	49	36	4.5%	0.690	0.088	0.710	0.55
114	6+13	(1.5/1.5)	465	-	10.0	20.4	-	-	-	-	-	5.0%	0.675	0.085	0.726	0.58
115	6+13	(2.0/0.5)	708	-	3.4	8.4	-	-	-	36	-	4.6%	0.691	0.090	0.709	0.54
116	6+13	(2.0/1.0)	530	-	7.8	16.3	-	-	-	-	-	5.1%	0.679	0.086	0.722	0.58
117	**MS 3**	**0**	**800**	**-**	**2.7**	**6.0**	**-**	**-**	**-**	**36**	**-**	**2.8%**	**0.736**	**0.071**	**0.732**	**-**
118	6	(1.5/0)	693	-	2.8	6.1	-	-	-	49	36	4.5%	0.714	0.066	0.755	0.64
119	6	(3.0/0)	365	-	-	-	-	-	-	-	-	8.0%	0.688	0.059	0.784	0.67
120	13	(0/1.0)	704	-	1.9	6.6	-	-	-	49	36	6.0%	0.718	0.067	0.750	0.58
121	13	(0/1.5)	480	-	3.2	8.9	-	-	-	74	62	5.6%	0.708	0.064	0.762	0.61

[1] V-funnel (Appendix A, Fig. A3)

Appendix H: Geometrical correction of the displacement (bending tests)



Applied correction: $\delta = \delta_m \cdot \dfrac{\sin\left(\dfrac{\pi}{2} - 2\phi\right)}{\sin\left(\dfrac{\pi}{2} + \phi\right)}$ with: $\dfrac{\delta}{\sin(90 - 2\cdot\phi)} = \dfrac{\delta_m}{\sin(90 + \phi)}$

and $\tan 2\phi = \dfrac{\delta_m}{125}$

Fig. H1: Geometrical correction of the measured displacement δ_m
[after: Schumacher, 2003b]

Appendix I: Input parameters for the inverse analysis (bending tests)

Table I1: Input parameters for SCFRC

Mix No.	*Mixture*	f_{fccm} *cube*	f_{fccm} *prism*	$\varepsilon_{fccm,elastic}$	E_{fc}	$f_{fctm,spl}$ *with fibres*	$f_{ctm,spl}$ *no fibres*	*w/b-ratio*[1]	*PD paste*	η_{φ}	*MFF*
		[MPa]	*[MPa]*	*[‰]*	*[MPa]*	*[MPa]*	*[MPa]*	*[-]*	*[-]*	*[-]*	*[MPa]*
1	L-R-60-60	53.98	49.33	1.84	35500	6.34	4.39	0.44	0.579	0.800	1.81
2	L-R-30-60	57.56	50.19	1.79	36700	6.57	4.39	0.44	0.579	0.704	1.66
3	L-R-40-100	51.85	47.00	1.71	36100	6.60	4.39	0.44	0.579	0.774	2.29
4	L-R-30-140	55.77	51.37	1.89	36300	7.60	4.39	0.44	0.579	0.751	2.28
5	M-R-30-40	70.31	62.49	2.36	37000	7.59	5.29	0.41	0.569	0.741	1.16
6	M-R-20-60	75.64	64.60	2.43	36600	7.42	5.29	0.41	0.569	0.721	1.29
7	M-R-60-60	75.05	63.23	2.08	39100	8.65	5.30	0.39	0.574	0.813	2.02
8	M-R-30-60	72.28	64.76	2.29	37600	8.07	5.30	0.39	0.574	0.765	1.85
9	M-R-40-100	73.51	63.35	2.16	37900	8.85	5.30	0.39	0.574	0.763	2.56
10	M-R-30-140	78.10	66.16	2.20	40000	9.82	5.30	0.39	0.574	0.779	2.55
11	M-F-60-60	75.33	62.16	2.28	37800	8.10	5.30	0.39	0.574	0.799	2.02
12	M-F-30-140	71.71	59.99	2.14	37700	9.64	5.30	0.39	0.574	0.787	2.55
13	H-R-60-60	116.65	103.36	2.80	43200	12.37	7.42	0.34	0.588	0.810	2.38
14	H-R-13-125	120.27	122.32	3.24	45700	14.12	9.80	0.25	0.601	0.715	5.91
15	P1	52.21	43.28	1.60	38000	5.59	4.39	0.44	0.579	0.751[2]	0.98
16	P2	55.52	47.55	1.64	36400	7.32	4.39	0.44	0.579	0.751[2]	1.96
17	P3	114.40	100.76	2.58	44100	11.61	7.42	0.34	0.588	0.765[2]	2.18

[1]CUR-Recommendation 70, 1999 [2] not measured, same as for mixtures 4 and 8 respectively.

Appendix J: Results; parameters of the inverse analysis (bending tests) (1)

Table J1: Six parameters of the tensile model for SCFRC (optimised simulations)

No.	*Mixture*	*MAS* *[mm]*	*Strength class*	*Casting method*	*Fibre type*	V_f *[kg/m^3]*	$s{\cdot}f_{fctm,ax}$ *[MPa]*	$\varepsilon_{ct,fibre}$ *[‰]*	$f_{fctm,ax}$ *[MPa]*	w_C *[mm]*	$f_{fctm,eq,bil}$ *[MPa]*	w_0 *[mm]*
1	L-R-60-60	16	B45	RILEM	80/60	60	3.07	5.0	3.93	5.8	1.32	23.0
2	L-R-30-60	16	B45	RILEM	80/30	60	2.59	5.1	3.45	3.7	0.96	10.3
3	L-R-40-100	16	B45	RILEM	65/40	100	2.94	2.6	4.03	3.7	1.06	13.1
4	L-R-30-140	16	B45	RILEM	45/30	140	2.99	1.3	4.33	2.6	1.53	7.4
5	M-R-30-40	8	B65	RILEM	80/30	40	2.80	5.2	3.45	3.6	0.73	10.6
6	M-R-20-60	8	B65	RILEM	65/20	60	2.91	0.4	4.08	0.5	2.33	7.3
7	M-R-60-60	16	B65	RILEM	80/60	60	3.45	5.0	5.10	5.9	1.35	23.8
8	M-R-30-60	16	B65	RILEM	80/30	60	3.45	4.5	4.58	3.8	0.99	10.7
9	M-R-40-100	16	B65	RILEM	65/40	100	3.13	2.6	4.87	2.9	1.27	12.6
10	M-R-30-140	16	B65	RILEM	45/30	140	4.03	1.1	5.55	2.2	1.85	7.9
11	M-F-60-60	16	B65	Flow	80/60	60	3.34	4.5	4.54	4.9	1.42	22.4
12	M-F-30-140	16	B65	Flow	45/30	140	3.60	1.3	5.54	2.5	1.83	7.5
13	H-R-60-60	16	B105	RILEM	80/60	60	4.45	5.1	6.93	7.1	1.69	25.7
14	H-R-13-125	1	B105	RILEM	OL13/0.16	125	8.23	1.0	9.60	2.3	4.02	4.8
15	P1	16	B45	RILEM2	45/30	60	2.37	1.6	2.66	2.4	0.79	8.0
16	P2	16	B45	RILEM2	45/30	120	3.20	1.3	3.55	2.2	1.10	7.6
17	P3	16	B105	RILEM2	80/30	60	4.38	4.5	5.17	3.6	1.02	10.5

Appendix J: Results; parameters of the inverse analysis (bending tests) (2)

Table J2: Results of the inverse analysis (parameters of Kooiman's model)

Mix No.	Mixture description	$d_{g,max}$ [mm]	Strength class	Casting method	Fibre type	V_f [kg/m^3]	$f_{fctm,ax}$ [% $f_{fctm,spl}$]	$f_{fctm,eq,bil}/f_{fctm,ax}$ [-]	w_c/w_0 [-]	w_0/L_f [-]	Fracture energy[1] [N/mm]
1	L-R-60-60	16	B45	RILEM	80/60	60	0.62	0.34	0.25	0.38	26.5
2	L-R-30-60	16	B45	RILEM	80/30	60	0.53	0.28	0.36	0.34	11.3
3	L-R-40-100	16	B45	RILEM	65/40	100	0.61	0.26	0.28	0.32	14.4
4	L-R-30-140	16	B45	RILEM	45/30	140	0.57	0.35	0.35	0.26	11.2
5	M-R-30-40	8	B65	RILEM	80/30	40	0.46	0.21	0.34	0.35	10.1
6	M-R-20-60	8	B65	RILEM	65/20	60	0.55	0.57	0.07	0.36	9.5
7	M-R-60-60	16	B65	RILEM	80/60	60	0.59	0.26	0.25	0.39	31.2
8	M-R-30-60	16	B65	RILEM	80/30	60	0.57	0.22	0.36	0.35	14.0
9	M-R-40-100	16	B65	RILEM	65/40	100	0.55	0.26	0.23	0.31	15.0
10	M-R-30-140	16	B65	RILEM	45/30	140	0.57	0.33	0.28	0.27	13.3
11	M-F-60-60	16	B65	Flow	80/60	60	0.56	0.31	0.22	0.37	27.0
12	M-F-30-140	16	B65	Flow	45/30	140	0.58	0.33	0.34	0.26	13.9
13	H-R-60-60	16	B105	RILEM	80/60	60	0.56	0.24	0.28	0.42	46.5
14	H-R-13-125	1	B105	RILEM	OL13/0.16	125	0.68	0.42	0.48	0.37	20.9
15	P1	16	B45	RILEM2	45/30	60	0.48	0.30	0.31	0.28	6.4
16	P2	16	B45	RILEM2	45/30	120	0.49	0.31	0.29	0.26	8.0
17	P3	16	B105	RILEM2	80/30	60	0.45	0.20	0.34	0.34	14.6

[1] calculated for the crack-width part of the combined model (softening branch)

Appendix K: Simulations and experimental results (bending tests) (1)

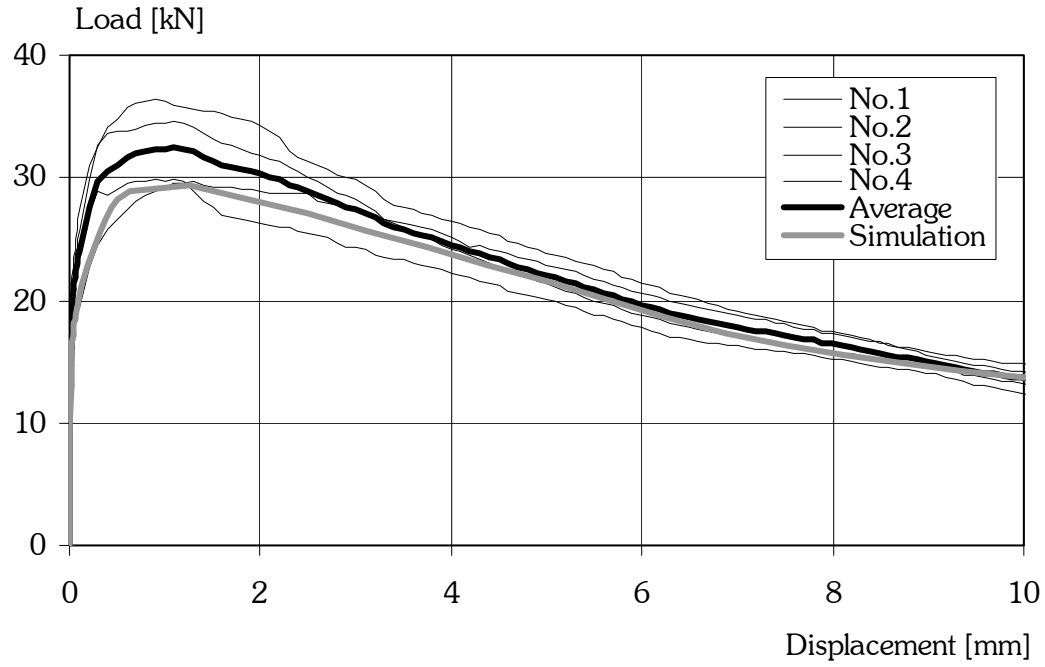


Fig. K1: Bending tests: results, average and simulation (mixture 1: L-R-60-60)

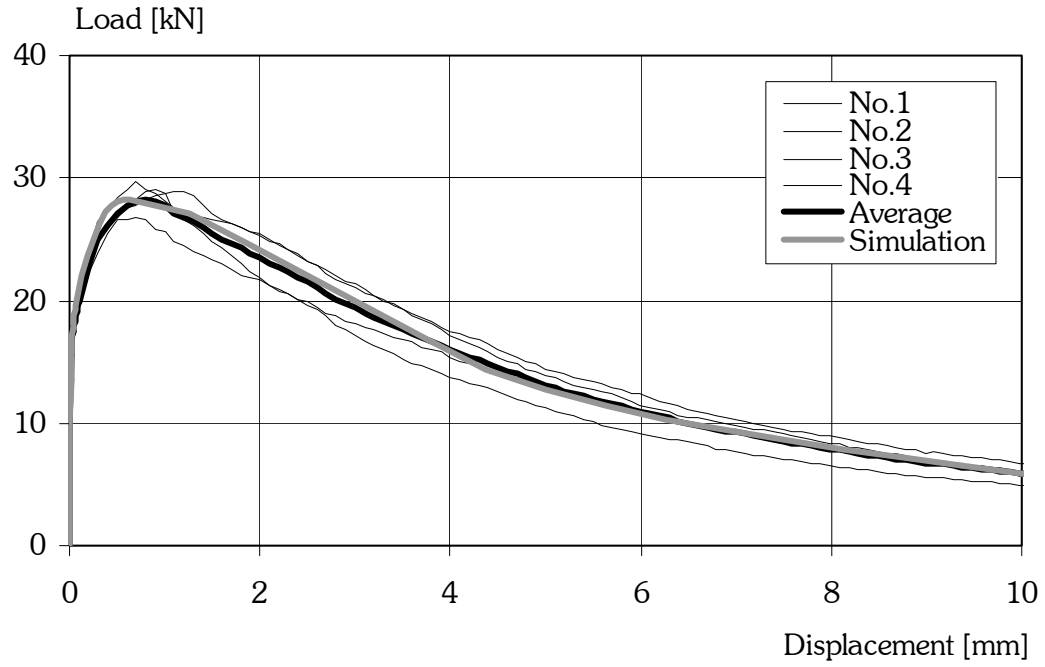


Fig. K2: Bending tests: results, average and simulation (mixture 2: L-R-30-60)

Appendix K: Simulations and experimental results (bending tests) (2)

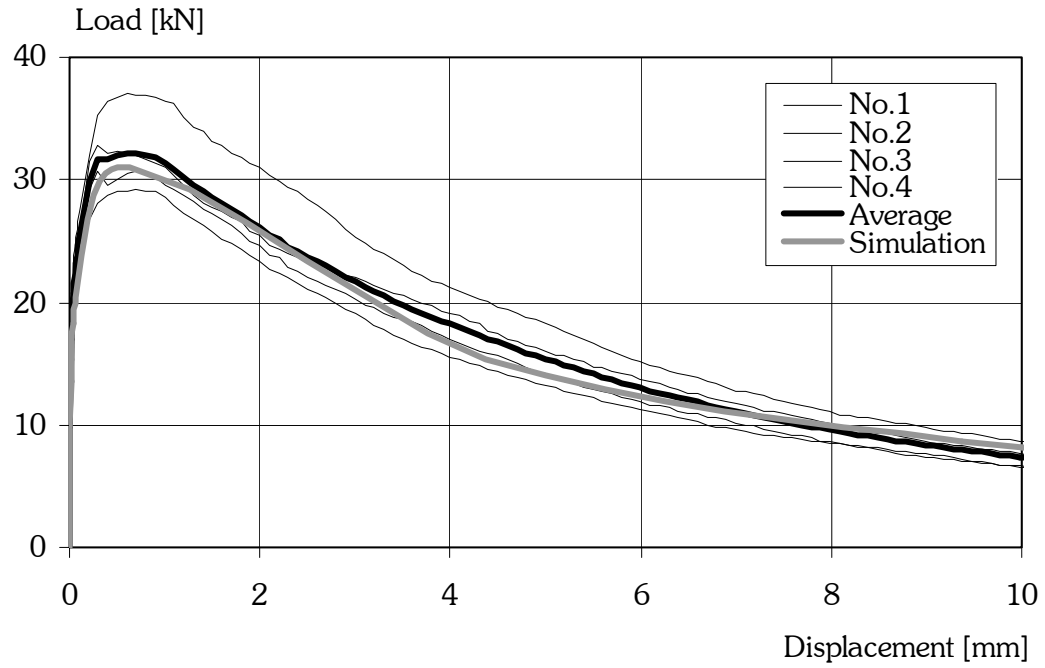


Fig. K3: Bending tests: results, average and simulation (mixture 3: L-R-40-100)

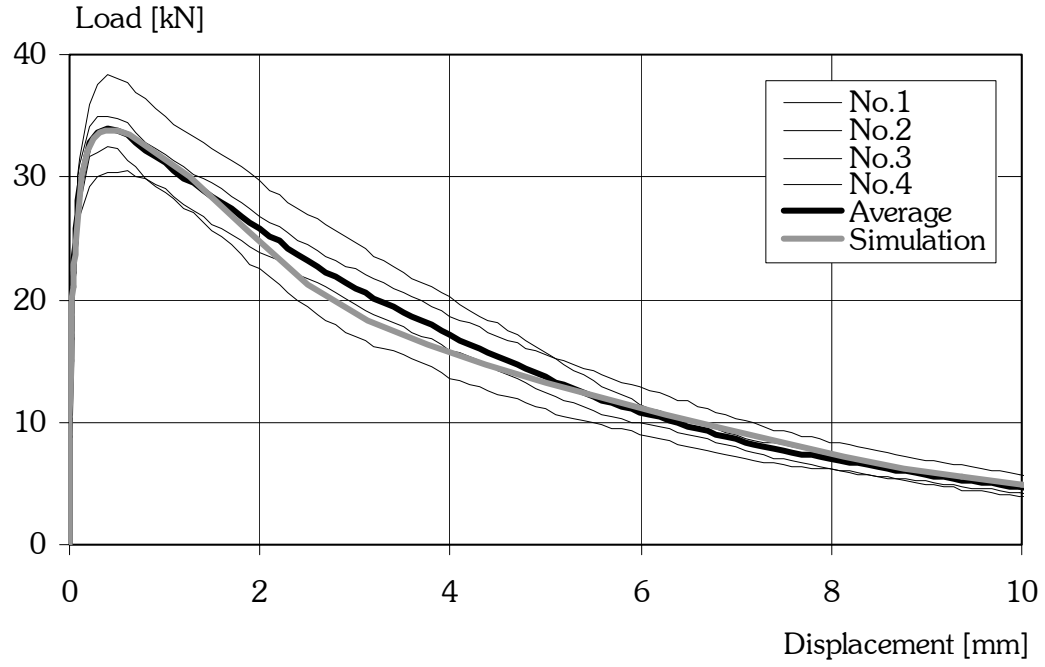


Fig. K4: Bending tests: results, average and simulation (mixture 4: L-R-30-140)

Appendix K: Simulations and experimental results (bending tests) (3)

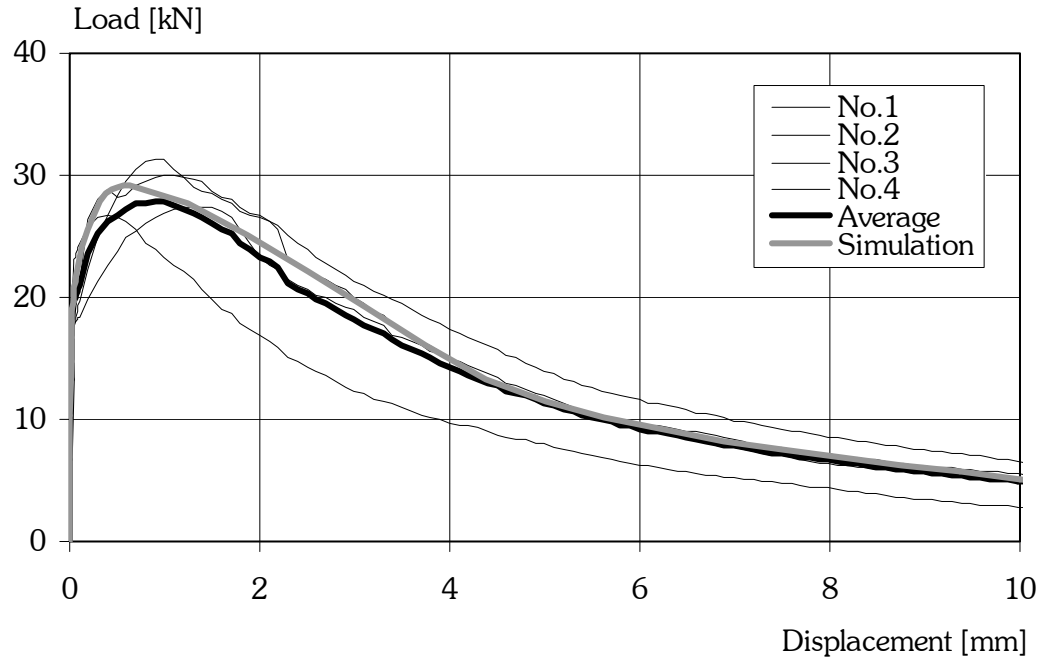


Fig. K5: Bending tests: results, average and simulation (mixture 5: M-R-30-40)

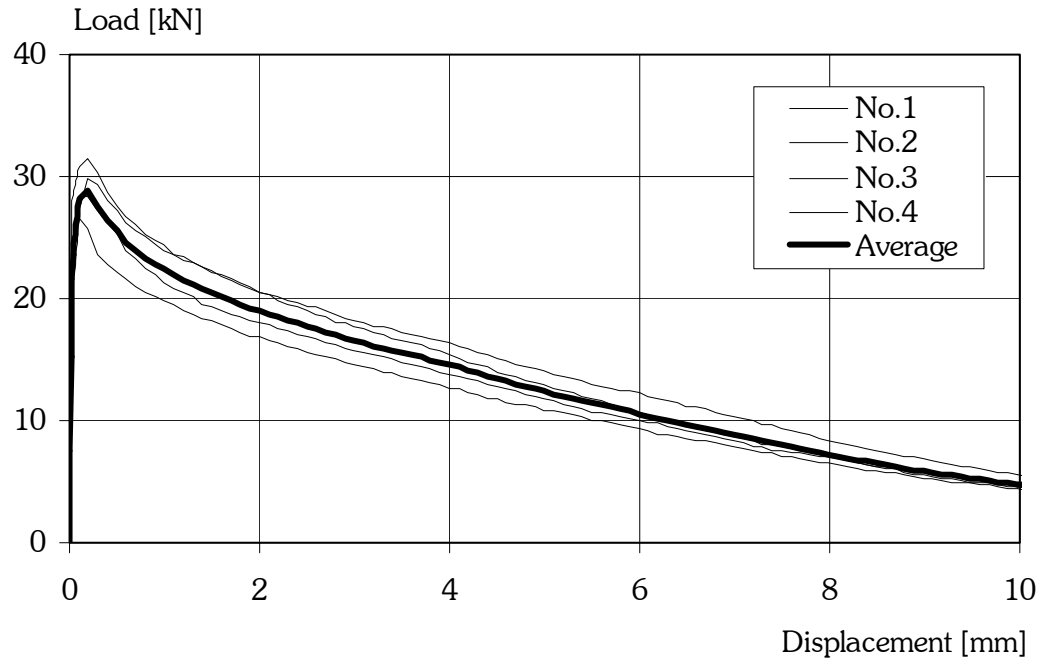


Fig. K6: Bending tests: results and average (mixture 6: M-R-20-60)

Appendix K: Simulations and experimental results (bending tests) (4)

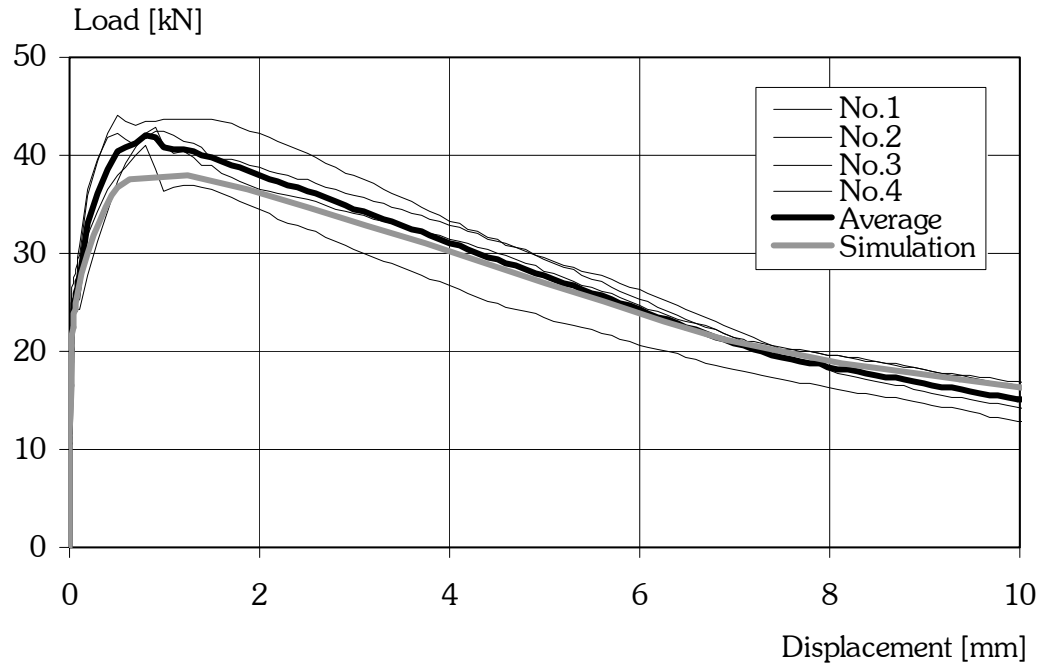


Fig. K7: Bending tests: results, average and simulation (mixture 7: M-R-60-60)

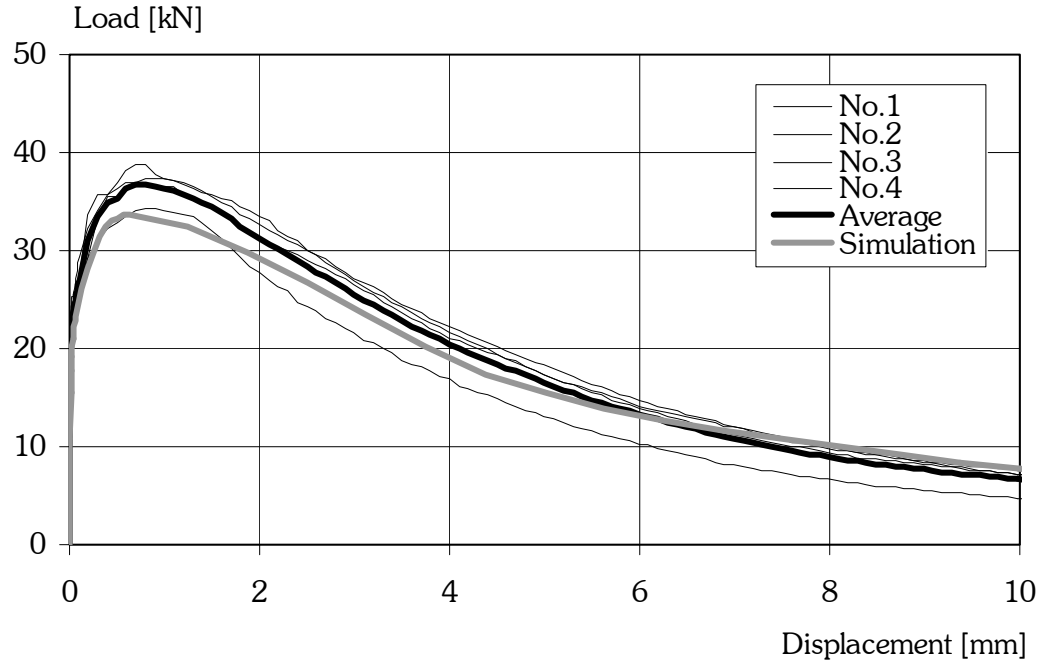


Fig. K8: Bending tests: results, average and simulation (mixture 8: M-R-30-60)

Appendix K: Simulations and experimental results (bending tests) (5)

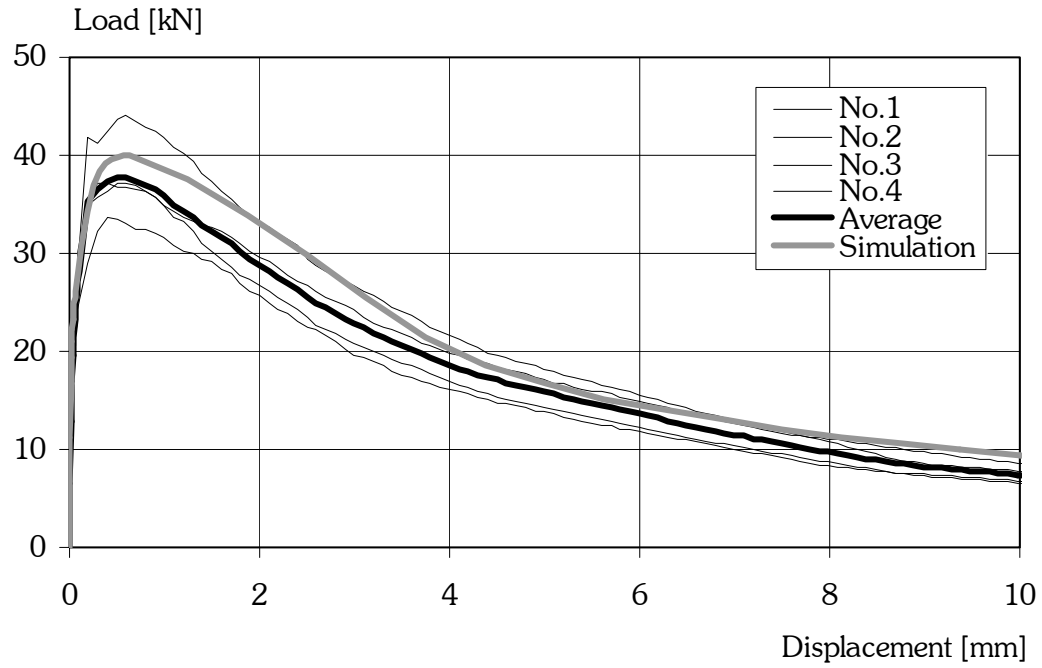


Fig. K9: Bending tests: results, average and simulation (mixture 9: M-R-40-100)

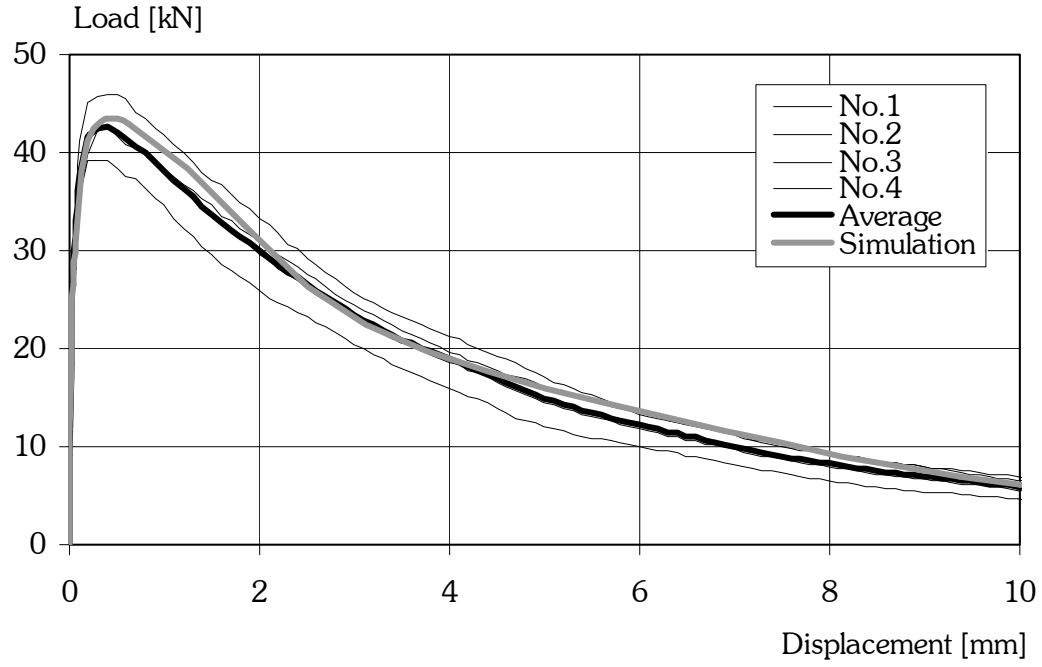


Fig. K10: Bending tests: results, average and simulation (mixture 10: M-R-30-140)

Appendix K: Simulations and experimental results (bending tests) (6)

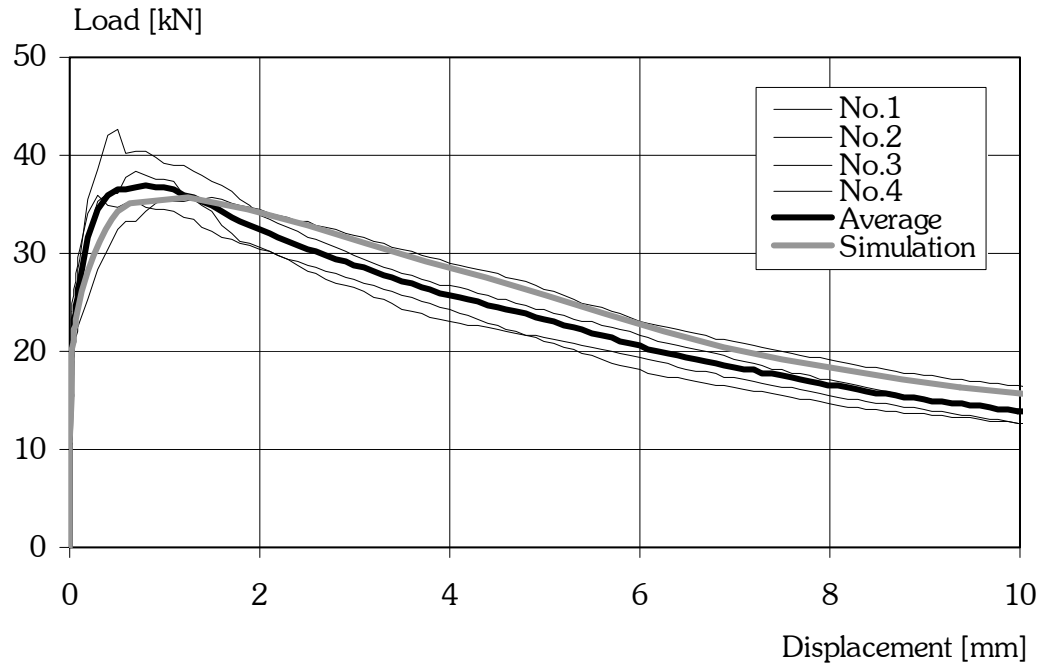


Fig. K11: Bending tests: results, average and simulation (mixture 11: M-F-60-60)

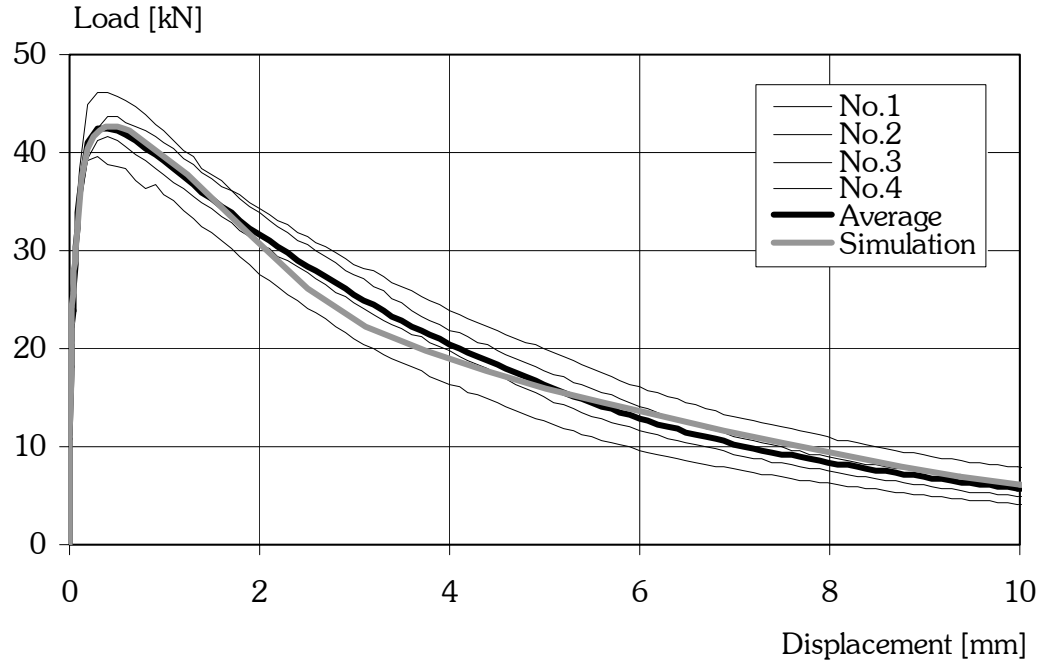


Fig. K12: Bending tests: results, average and simulation (mixture 12: M-F-30-140)

Appendix K: Simulations and experimental results (bending tests) (7)

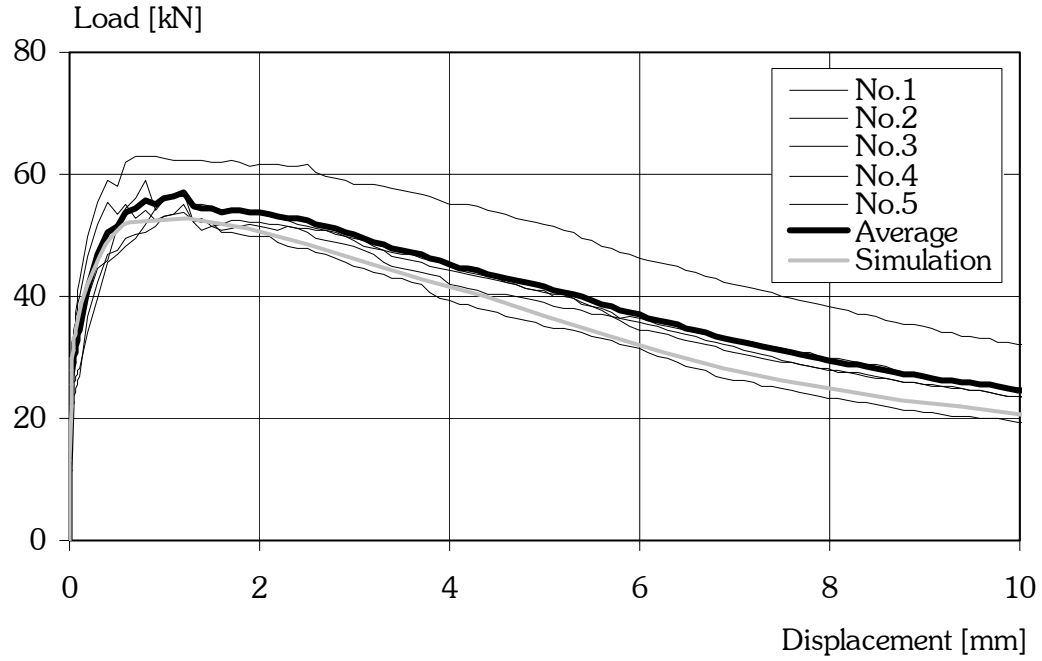


Fig. K13: Bending tests: results, average and simulation (mixture 13: H-R-60-60)

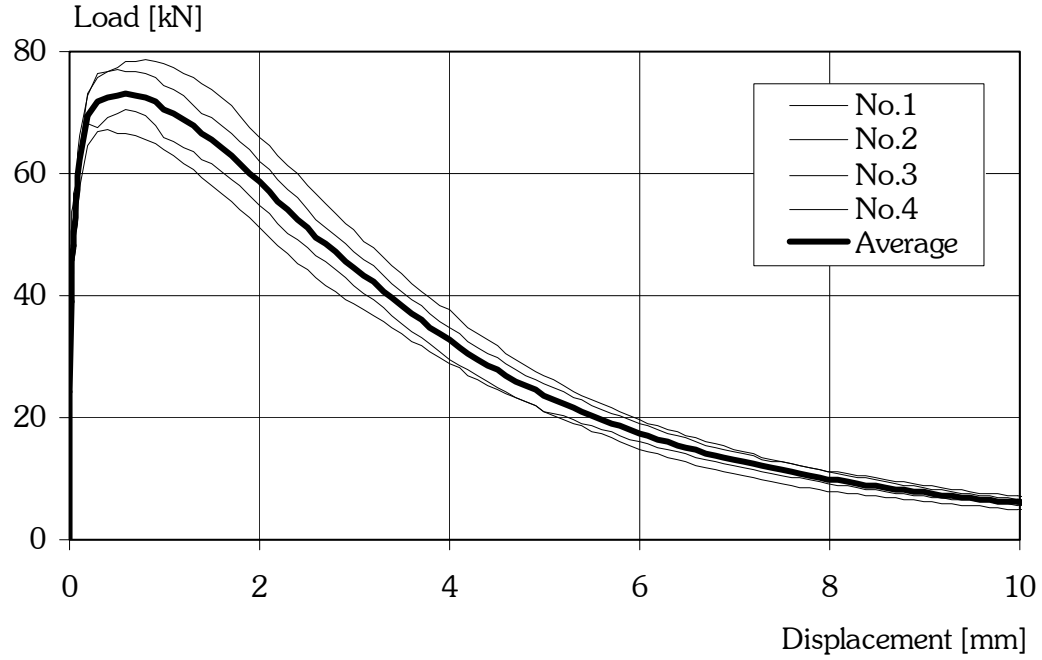


Fig. K14: Bending tests: results and average (mixture 14: H-R-13-125)

Appendix K: Simulations and experimental results (bending tests) (8)

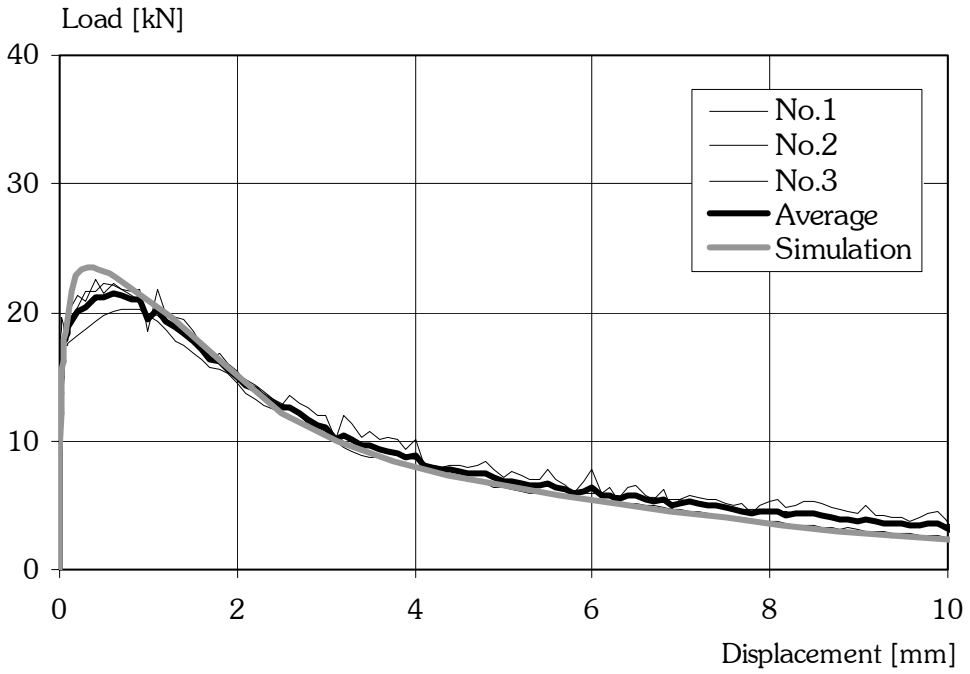


Fig. K15: Bending tests: results, average and simulation (mixture 15: P1)

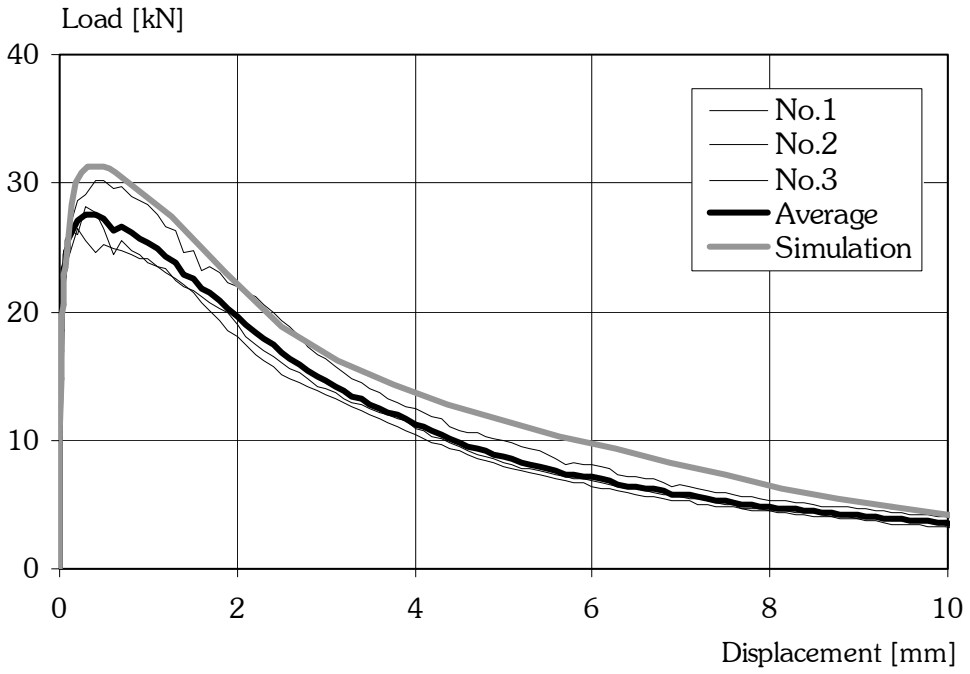


Fig. K16: Bending tests: results, average and simulation (mixture 16: P2)

Appendix K: Simulations and experimental results (bending tests) (9)

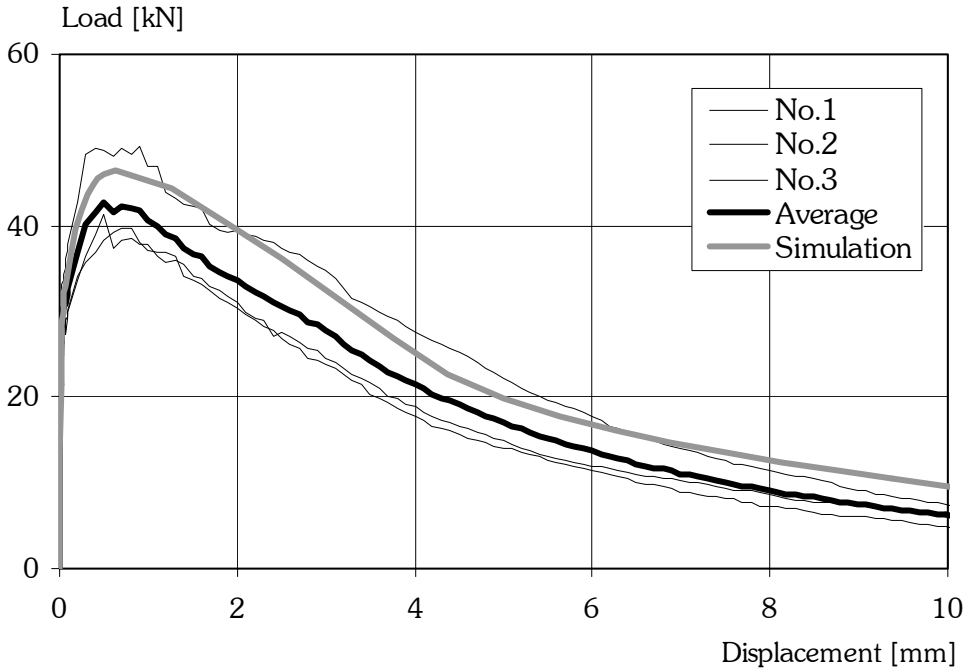


Fig. K17: Bending tests: results, average and simulation (mixture 17: P3)

Notations and symbols

Capital roman letters

A_f	= area of the cross-section of a single fibre	[mm^2]
A_{lig}	= effective cross-section of beam [(h-a)·b]	[mm^2]
B	= width of the tunnel mould	[m]
BD	= blocking diameter (depends on fibres' diameter)	[-]
BF	= blocking factor of SCFRC	[-]
CMOD	= crack mouth opening displacement	[mm]
D_{af}	= diameter of an aggregate fraction	[mm]
D_{pi}	= diameter of grain group i	[mm]
E_{fc}	= Young's modulus of a fibre reinforced cementitious composite	[MPa]
FEF	= fibre efficiency factor	[-]
FT_p	= flow-time mortar funnel	[s]
G_F	= fracture energy bending test	[kN/mm]
$G_{F,2mm}$	= fracture energy bending test at 2 mm	[kN/mm]
$G_{F,10mm}$	= fracture energy bending test at 10 mm	[kN/mm]
K	= compaction index	[-]
K_c'	= contribution of cement (or powders) to the compaction index	[-]
K_i	= contribution of grain group i to the compaction index	[-]
K_i'	= contribution of grain fraction i to the compaction index	[-]
L	= inner length of the tunnel mould (at the bottom)	[m]
L_{EL}	= length of the fibre hook	[mm]
L_f	= fibre length	[mm]
$L_{f,act}$	= actual fibre length in a plane	[mm]
L_f/d_f	= aspect ratio	[-]
L_{fe}	= embedded fibre length	[mm]
LVDT	= Linear Variable Displacement Transducer	[-]
IF	= influence factor slump flow	[1/s]
M	= moment	[Nmm]
MFC	= maximum fibre content volume	[-]
MFF	= mechanical fibre factor	[MPa]
M_i	= upper sieve dimension of aggregate	[mm]
M_{i-1}	= lower sieve dimension of aggregate	[mm]
MS	= mini-slump flow	[mm]
N_f	= number of steel fibres per unit area	[$1/mm^2$]
N_{sf}	= number of steel fibres	[-]
P	= applied load on specimen	[kN]
P^i	= pullout load	[N]
P_c	= computed load on specimen	[kN]
P_e	= excess paste volume	[mm^3]
P_{max}	= average maximum flexural load	[kN]
PD	= packing density	[-]
PD_g	= packing density of the granular skeleton	[-]
PD_p	= packing density of paste	[-]
$P_{f,fric}$	= frictional pull-out force (displacement > L_{EL})	[N]
$P_{f,hook}$	= average pull-out force (displacement < L_{EL})	[N]
$P_{f,max}$	= maximum pull-out force	[N]
P_m	= measured load on specimen	[kN]
P/P^*	= content superplasticiser compared with the saturation dosage	[-]
PVF	= plastic viscosity factor	[-]
PV_{SCFRC}	= plastic viscosity of SCFRC	[Pa·s]
PV_{WF}	= plastic viscosity with fibres, RPL thinner compared with SCC	[Pa·s]
ROB	= risk of blocking	[-]

$ROB_{(BS)}$	= risk of blocking (depends on the chosen bar spacing)	[-]
RPL	= relative paste layer thickness	[-]
RWL	= relative water layer thickness	[-]
SFF	= slump flow factor	[mm]
SFS	= slump flow slope	[-]
SI	= segregation index	[-]
S/M	= sand content of mortar	[Vol.-%]
V_{abi}	= blocking volume of aggregate group i	[m^3]
V_{ai}	= aggregate volume of group i	[m^3]
V_e	= volume of excess fluid to surround the grains	[Vol.-% or mm^3]
V_f	= fibre content (volume)	[Vol.-%]
V_f	= fibre content (mass)	[kg/m^3]
$V_f \cdot L_f/d_f$	= fibre factor	[-]
Vol_C	= volume of the container	[dm^3]
V_{fluid}	= volume of fluid [paste (incl. air) or water (excl. air)] [Vol.-%]	[Vol.-%]
V_{solid}	= solid content	[Vol.-%]
V_t	= total volume of the concrete mix	[m^3]
W	= section modulus	[mm^3]
W_B	= weight of solids in a container	[kg]
W_0	= area under the load-displacement curve	[kN/mm]

Small roman letters

a	= notch depth of the specimen	[mm]
a_f	= longer side of a rectangular cross-section of a fibre	[mm]
a_{ij}	= loosening effect of grains of group j on group i	[-]
b	= width of the specimen	[mm]
b_f	= shorter side of a rectangular cross-section of a fibre	[mm]
b_{ij}	= wall-effect of grains of group j on group i	[-]
c	= clear spacing between reinforcement	[mm]
c_B	= minimum bar spacing with $\Delta h \geq 10$ mm	[mm]
c_f	= correction factor in Kooiman's model to obtain $f_{fctm,eq,bil}$	[-]
c/L_f	= normalised bar spacing to the length of the fibre	[-]
c_{NB}	= maximum bar spacing with $\Delta h < 10$ mm (non-blocking)	[mm]
d_f	= fibre diameter	[mm]
$d_{f,i}$	= equivalent diameter of fibre i	[mm]
d_g	= geometrical diameter	[mm]
$d_{g,i}$	= diameter of grain group i	[mm]
$d_{g,max}$	= maximum grain size	[mm]
d_i	= geometrical diameter of grain group i	[mm]
d_j	= geometrical diameter of grain group j	[mm]
d_p	= equivalent packing diameter	[mm]
d_s	= diameter of a sphere having the same surface area as the particle	[mm]
d_v	= diameter of a sphere having the same volume as the particle	[mm]
e	= exponent Herschel-Bulkley model	[-]
$f_{ccm,cyl}$	= mean cylinder compressive strength of plain concrete	[MPa]
$f_{ctm,spl}$	= mean splitting tensile strength of plain concrete	[MPa]
f_{fccm}	= mean compressive strength of SFRC of SCFRC	[MPa]
$f_{fccm,cyl}$	= mean cylinder compressive strength of SFRC	[MPa]
$f_{ct,ax}$, $f_{fct,ax}$	= axial tensile strength of concrete	[MPa]
$f_{fct,eq,bil}$	= equivalent post-cracking strength in a bilinear softening relationship	[MPa]
$f_{fctm,ax}$	= mean axial tensile strength of SFRC or SCFRC	[MPa]
$f_{fctm,eq,bil}$	= mean equivalent post-cracking strength	[MPa]
$f_{fctm,fl}$	= mean flexural strength of SFRC or SCFRC	[MPa]
$f_{fctm,spl}$	= mean splitting tensile strength of SFRC of SCFRC	[MPa]

g	= acceleration due to gravity (9.81 kg/s^2)	[kg/s^2]
h	= height of the specimen	[mm]
h_{lig}	= effective height of beam (h-a)	[mm]
k_F	= wall-effect fibres, concept 'perturbed zone'	[-]
k_{SF}	= wall-effect of a steel fibre (experimental result)	[-]
k_W	= wall-effect aggregates	[-]
l	= span of the beam	[mm]
l_{cb}	= crack band width	[mm]
l_i	= influence length	[mm]
m	= $m = m_1 + m_2$	[kg]
m_1	= weight of the beam between the supports	[kg]
m_2	= weight of the part of machine that is not attached to machine	[kg]
m_f	= fibre content (mass)	[kg/m^3]
n_{abi}	= blocking volume ratio of group i	[-]
n_{ai}	= aggregate contribution of group i to blocking	[-]
$n_{a,mfi}$	= maximum fibre volume ratio	[-]
$n_{f,i}$	= number of fibres of type i	[-]
$n_{g,i}$	= number of grains of group i	[-]
n_i	= number of aggregates of group I	[-]
o	= German flow spread	[cm]
s	= percentage of splitting tensile strength at which the stiffness changes	[%]
$s{\cdot}f_{fctm,ax}$	= mean axial tensile strength of SCFRC at first cracking	[MPa]
$s_{f,i}$	= surface area of a single fibre of type i	[mm^2]
$s_{g,i}$	= surface area of grain of group i corrected by the sphericity factor	[mm^2]
s_i	= surface area of the aggregate grains in group i	[mm^2]
v_p	= perturbed volume in a container	[Vol.-%]
y_j	= volume fraction group j relative to the total solid volume	[-]
w	= crack width	[mm]
w/b	= water-binder ratio [CUR-Recommendation 70, 1999]	[-]
w/c	= water-cement ratio	[-]
w_c	= characteristic crack width	[mm]
$w_{c,50}$	= characteristic crack width at 50% of the peak stress	[mm]
w_0	= critical crack width	[mm]

Capital greek letters

Γ	= relative thickness of the surrounding fluid	[-]
Δh	= height difference J-ring	[mm]
Δ_{SF}	= difference of the relative slump flow due to the fibres' addition	[-]
Φ	= solid volume of a granular mix, in a unit total volume	[-]
$\overline{\Phi}$	= mean packing density of granular (affected by container size)	[-]

Small greek letters

$\overline{\alpha}$	= mean packing density (affected by the container size)	[-]
α	= unperturbed packing density	[-]
α_f	= bond factor	[MPa]
β	= virtual packing density of a monodisperse mix	[-]
β_f	= factor incorporating the difference in shear stress of different fibre types	[MPa]
β_i, β_j	= residual packing density of a monodisperse mix of group i (j)	[-]
γ	= virtual packing density of a polydisperse mix	[-]
γ_i	= virtual packing density of a polydisperse mix (group i dominant)	[-]
$\dot{\gamma}$	= shear rate	[1/s]

δ	= displacement (elastic + post-cracking regime) at the notch tip	[mm]
δ_m	= average displacement	[mm]
δ_f	= fibre-end displacement in pullout test	[mm]
δ_{max}	= crack opening displacement at maximum bending load (average)	[mm]
δ_{notch}	= crack opening displacement at the notch tip	[mm]
δ_0	= deformation at the final failure of the beam	[mm]
ε_{cc}	= compressive strain	[‰]
$\varepsilon_{ct,fibre}$	= reduced elastic strain of SCFRC in tension	[‰]
$\varepsilon_{cc,elastic}$	= compressive strain at compressive strength	[‰]
$\varepsilon_{cc,max}$	= maximum compressive strain	[‰]
$\varepsilon_{fccm,elastic}$	= mean compressive strain of SCFRC at compressive strength	[‰]
$\varepsilon_{0d,cyl}$	= dense (experimental) packing density of fibres	[-]
$\varepsilon_{fct,elastic}$	= linear elastic strain limit of SCFRC in tension	[‰]
$\eta_{f,fric}$	= efficiency of the fibre (displacement > L_{EL})	[-]
$\eta_{f,hook}$	= efficiency of the fibre (displacement < L_{EL})	[-]
η_φ	= orientation number	[-]
$\eta_{\Theta,ave}$	= average theoretical orientation number	[-]
$\eta_{\Theta 2D}$	= theoretical number of random oriented fibres in a plane	[-]
$\eta_{\Theta 3D}$	= theoretical number of random oriented fibres in 3D-space	[-]
μ	= plastic viscosity	[Pa·s]
μ_F	= plastic viscosity of SCFRC	[Pa·s]
μ_{SCC}	= plastic viscosity of SCC without fibres	[Pa·s]
ρ	= mean specific gravity of the solids	[kg/dm^3]
σ_{cc}	= compressive stress	[MPa]
σ_{ct}	= tensile stress	[MPa]
τ	= shear stress	[Pa]
τ_{avg}	= average bond strength	[MPa]
τ_{fric}	= frictional shear stress	[MPa]
τ_0	= yield value	[Pa]
$\tau_{0,SCC}$	= yield stress SCC without fibres	[Pa]
$\tau_{0,SCFRC}$	= yield stress SCC with fibres	[Pa]
φ	= inclination of a fibre relative to the plane of consideration	[-]
ϕ	= solid content	[-]
ϕ_f	= percentage of fibres of the granular skeleton	[-]
ϕ^*	= packing density, space occupied by the solids	[-]
ϕ/ϕ^*	= normalised solid content	[-]
$(\phi/\phi^*)_p$	= normalised paste content	[-]
$(\phi/\phi^*)_g$	= normalised solid content (fibres and aggregates)	[-]
ϕ_p/ϕ^*	= ratio of paste content (incl. air) to packing density of the aggregates	[-]
ψ	= sphericity	[-]

Curriculum Vitae

Steffen Grünewald

Born:	13 March 1971 in Rheinfelden (Germany)
Academic Education:	Civil Engineer (Diplom-Ingenieur; 1992-1999) Darmstadt University of Technology (Germany)
Main Disciplines:	Concrete Structures, Steel Structures, Project Management
Exchange year:	European Erasmus Program (1995-1996) Delft University of Technology (The Netherlands)
PhD-Research:	Research Assistant (1999-2003) Delft University of Technology (The Netherlands) Department of Structural and Building Engineering
Projects:	Member of the Dutch CUR-Committee B79 'Self-Compacting Concrete' (1999-2002)
	Brite Euram project 'Testing SCC' (2001-2004) Task leader of the workgroup on test methods for filling ability
	Post-doctoral research 'Viscosity Agents in Self-Compacting Concrete' Delft University of Technology (The Netherlands) Department of Structural and Building Engineering (since January 2004)